RÉSUMÉ

Les composés nitroaromatiques sont des contaminants environnementaux associés à des activités anthropiques. Le p-nitroaniline (PNA) est l'un des composés important de cette classe. C'est une substance chimique brute extrêmement importante qui occupe une place non substituable dans la synthèse d'une grande variété de produits chimiques, notamment divers colorants organiques, des pesticides, des médicaments, des agents antivieillissement, des photo-stabilisateurs, des antioxydants et des agents de développement. Cependant, le PNA est fortement toxique, comparable au trinitrotoluène (TNT) et trinitrophénol (TNP), et peut être rejeté dans l'environnement directement sous forme de déchets industriels ou indirectement sous forme de produits de dégradation des herbicides et des pesticides. En raison de la présence de puissants groupes attracteurs d'électrons, le PNA est peu biodégradable dans l'environnement, il pénètre facilement dans le sol et contamine les eaux souterraines. Les recherches scientifiques, ont montré qu'il peut causer des dommages aux humains et aux systèmes aquatiques. Ainsi, les capteurs hautement sensibles et sélectifs permettant une détection rapide et efficace de PNA constituent une question extrêmement urgente concernant la sécurité intérieure, la protection de l'environnement et les préoccupations humanitaires. Ces dernières années, les électrodes chimiquement modifiées ont été utilisées pour la quantification voltampérométrique de diverses espèces organiques et inorganiques après accumulation en circuit ouvert. De nombreux travaux dans ce domaine ont été consacrés à l'exploitation de la réactivité chimique du modificateur envers un analyte cible à des fins électrocatalytiques et électroanalytiques. De nombreux agents modificateurs ont été utilisés soit comme revêtement sur la surface d'électrodes solides, soit dispersés dans une matrice conductrice. Les électrodes modifiées sont fréquemment utilisées dans la détermination voltampérométrique des composés organiques en raison de leur efficacité, de leur sélectivité et de leur sensibilité. Dans ce contexte, le présent travail décrit l'utilisation de diverses électrodes synthétiques à pâte de carbone à base d'argent pour la quantification voltampérométrique de PNA.

La première partie de ce travail a été dédiée à l'étude de l'efficacité catalytique de l'argent pour la réduction de PNA à l'aide d'une électrode en argent métallique, après comparaison de ses performances avec d'autres électrodes, notamment en or, en graphite et en carbone vitreux. En effet, ce matériau possède des propriétés électrochimiques supérieures pour l'étude du comportement électrochimique de PNA et sa détermination. La mise en évidence de cette méthode a été évaluée en utilisant la voltampérométrie cyclique, la chronoamperométrie, les courbes de Tafel et la spectroscopie d'impédance électrochimique.

Dans la deuxième partie, la modification chimique des surfaces d'électrodes par dépôt thermique et électrochimique pour des applications électroanalytiques a ensuite été utilisée, ouvrant de nouvelles voies dans le domaine de la détection en permettant un meilleur contrôle du comportement de la surface des électrodes et en résolvant divers problèmes liés soit à l'électrocatalyse, soit à l'électroanalyse liés aux surfaces non modifiées. Ces modifications ont permis d'améliorer considérablement la sensibilité, la reproductibilité, la stabilité et la sélectivité. La morphologie et la distribution de l'argent sur la surface de l'électrode ont été évaluées par diffraction des rayons X et par microscopie électronique à balayage. La surface électro-active des électrodes préparées a été estimée en utilisant [Fe(CN)6]3-/4- comme une sonde d'oxydoréduction par voltampérométrie cyclique. En outre, la détermination analytique de PNA a été effectuée pour les deux méthodes proposées en utilisant la voltampérométrie à impulsions différentielles. Il a été constaté que l'intensité du courant du pic de réduction de PNA par dépôt thermique est très faible par rapport au dépôt électrochimique ; cela peut confirmer la formation d'oxyde d'argent à la surface des électrodes à pâte de carbone. Enfin, l'électrode modifiée par déposition électrochimique a été appliquée avec succès pour la détermination de PNA dans les échantillons d'eau potable. La simplicité de la préparation, la bonne reproductibilité et le faible coût de l'électrode modifiée, la surface active élevée ainsi que la large gamme de concentration linéaire, la faible limite de détection et la bonne répétabilité constituent les principaux avantages pour la détermination de PNA.

Dans la troisième partie, un matériau composé de nanoparticules d'argent stabilisées au chitosane sur l'électrode à pâte de carbone (CS@AgNPs-CPE) est utilisé pour la détermination électrochimique de PNA. Un procédé chimique est utilisé pour synthétiser des nanoparticules d'argent stabilisées par Chitosane dans de l'acide acétique (2%) en utilisant du borohydrure de sodium comme agent réducteur. La caractérisation du produit final par la spectroscopie UV-Vis a permis de vérifier la présence de nanoparticules d'argent. L'analyse par diffraction des rayons X a montré que les nanoparticules d'argent avaient une taille moyenne de 50 nm. La caractérisation électrochimique a prouvé que les CS@AgNPs-CPE présentent une activité électrocatalytique et électroanalytique élevée qui peut être exploitée pour la construction de capteurs et les applications correspondantes. Le capteur développé a révélé une limite de détection inférieure de 5 nM envers la réduction du PNA dans la gamme allant de 7 nM à 1 µM (R2 = 0,986). Le CS@AgNPs-CPE a ensuite été étendu pour la détermination de PNA dans des échantillons réels tels que les eaux usées. Toutes ces études ont confirmé que les nanoparticules d'argent à la surface de l'électrode à pâte de carbone constituent des alternatives prometteuses pour la détection électrochimique.

Mots clés :

Composés nitroaromatiques, p-nitroaniline, argent, déposition thermique, déposition électrochimique, nanoparticules, détermination électrochimique, électrocatalyse.

UNIVERSITE SULTAN MOULAY SLIMANE

Faculté des Sciences et Techniques

Béni-Mellal

Centre d'Études Doctorales : Sciences et Techniques
Formation Doctorale : Ressources Naturelles, Environnement et Santé (RNES)

THÈSE

Présentée par

FATH-ELLAH LAGHRIB

Pour l'obtention du grade de

DOCTEUR

Spécialité: Chimie Physique

Option: Electrochimie Analytique

Elaboration des capteurs électrochimiques à base d'argent et de chitosane pour l'analyse du paranitroaniline dans l'eau

Soutenue publiquement le **25 Septembre 2020** devant la commission d'examen:

M. Bakasse	Professeur, Faculté des Sciences, El Jadida, Maroc	Président
N. Labjar	Professeur, Ecole Normale Supérieure d'Enseignement Technique, Rabat, Maroc	Rapporteur
M. Siniti	Professeur, Faculté des Sciences, El Jadida, Maroc	Rapporteur
S. El Hajjaji	Professeur, Faculté des Sciences, Rabat, Maroc	Examinateur
M. Khouili	Professeur, Faculté des Sciences et Techniques, Béni-Mellal, Maroc	Examinateur
S. Lahrich	Professeur, Faculté Polydisciplinaire, Khouribga, Maroc	Invité
M. A. El Mhammedi	Professeur, Faculté Polydisciplinaire, Khouribga, Maroc	Directeur de thèse

N° d'ordre :268/20

Elaboration des capteurs électrochimiques à base d'argent et de chitosane pour l'analyse du paranitroaniline dans l'eau

FATH-ELLAH LAGHRIB

SULTAN MOULAY SLIMANE UNIVERSITY

Faculty of Science and Techniques

Beni-Mellal

Center for Doctoral Studies: Sciences and Techniques
Doctoral Training: Natural Resources, Environment and Health (NREH)

THESIS

Presented by

FATH-ELLAH LAGHRIB

To obtain the degree of

DOCTOR

Specialty: Physical Chemistry
Option: Analytical Electrochemistry

Elaboration of silver and chitosane-based electrochemical sensors for paranitroaniline analysis in water

Public defence on **September 25, 2020**

M. Bakasse	Professor, Faculty of Sciences, El Jadida, Morocco	President
N. Labjar	Professor, Higher Normal School of Technical Education, Rabat, Morocco	Reviewer
M. Siniti	Professor, Faculty of Sciences, El Jadida, Morocco	Reviewer
S. El Hajjaji	Professor, Faculty of Sciences, Rabat, Morocco	Examiner
M. Khouili	Professor, Faculty of Science and Techniques, Beni-Mellal, Morocco	Examiner
S. Lahrich	Professor, Polydisciplinary Faculty, Khouribga, Morocco	Invited
M. A. El Mhammedi	Professor, Polydisciplinary Faculty, Khouribga, Morocco	Supervisor

Acknowledgements

Obviously, I did not do this work alone; the research is indeed the result of teamwork. I would therefore like to thank most sincerely all the people who made it possible for me to carry out this work.

➡ **<u>My apologies to all those that I would have forgotten</u>**

I am grateful towards my parents for their unwavering support throughout my studies and research; they are my greatest mentors and supporters.

Abstract

Nitroaromatic compounds are environmental contaminants associated with anthropogenic activities. One important compound of this class is p-nitroaniline (PNA). PNA is an extremely important raw chemical that holds a non-substitutable place in the synthesis of a great variety of chemical products, including various organic dyes, pesticide, medicines, antiaging agents, photo-stabilizers, antioxidants and developing agents. However, PNA is strongly toxic comparable totrinitrotoluene (TNT) and trinitrophenol (TNP) and can be released into the environment directly as industrial waste or indirectly as breakdown products of herbicides and pesticides. Due to the strong electron-withdrawing groups, PNA is poorly biodegradable in the environment. Furthermore, PNA exists in natural world with readily permeating through soil and contaminates groundwater. Research showed that PNA can cause damage to humans and aquatic systems. So, the highly sensitive and selective sensors for rapid and effective detection of PNA are an extremely urgent issue concerning homeland security, environmental protection, and humanitarian concerns. In recent years, chemically modified electrodes (CMEs) have been used in the voltammetric quantification of various organic and inorganic species after open-circuit accumulation. Much work in this field has been directed to exploit the chemical reactivity of the modifier towards a target analyte for both electrocatalytic and electroanalytical purposes. Many modifying agents have been used either as coatings on solid electrode surfaces or dispersed within a conductive matrix. Modified electrodes are frequently used in the voltammetric determination of organic compounds because of their efficiency, selectivity, and sensitivity, which is equivalent to that reached in anodic and cathodic stripping. In this context, the present research work describes the use of various synthetic silver-based carbon paste electrodes for the voltammetric quantification of PNA.

The first part of this work was devoted to study the catalytic efficiency of metallic silver electrode in the reduction of PNA by comparing its performance with other electrodes including gold, graphite and glassy carbon. This material has superior electrochemical properties for the study of the electrochemical behavior of PNA and its determination. The demonstration of this method was evaluated by using cyclic voltammetry, chronoamperometry, Tafel plots, and electrochemical impedance spectroscopy.

In the second part, chemical modification of electrode surfaces using thermal and electrochemical deposition for electroanalytical applications was subsequently used, opening new avenues in the field of detection by allowing better control of electrode surface behavior and solving various problems either electrocatalytic or electroanalytic related to unmodified surfaces. These modifications have made it possible to greatly in enhancing sensitivity, reproducibility, stability, and selectivity. The morphology and the distribution of silver on the electrode surface were evaluated by XRD and Scanning electron microscopy. The electroactive surface area of the as-prepared electrodes was estimated using $[Fe(CN)_6]^{3-/4-}$ as redox probe by cyclic voltammetry. In addition, the analytical determination of PNA was performed for both proposed methods using differential pulse voltammetry (DPV). It was found that the current height of the PNA reduction peak by thermal deposition is very low compared to electrochemical deposition; this may confirm the formation of silver oxide on the surface of carbon paste electrodes. Finally, the modified electrode by electrochemical deposition has been successfully applied for the determination of PNA in drinking water samples. Simplicity of preparation, good reproducibility and low cost of the modified electrode, high active surface area as well as wide linear concentration range, low detection limit and good repeatability for PNA determination are the important advantages.

In the third part, a material comprised of chitosan stabilized silver nanoparticles on the carbon paste electrode (CS@AgNPs-CPE) is used as an electrochemically active material for the determination of PNA in neutral medium. A chemical process is used to synthesis silver nanoparticles protected with Chitosan in acetic acid (2%) using sodium borohydride as reducing agent at room temperature. Characterization of the end product using UV-Vis spectroscopy verified the presence of silver nanoparticles. The silver nanoparticles were shown to have an average size of 50 nm by X-ray diffraction analysis. The electrochemical characterization showed that the CS@AgNPs-CPE exhibits high electrocatalytic and electroanalytic activity that can be harnessed for sensor construction and related applications. The as developed sensor exhibited a lower detection limit of 5 nM towards the PNA reduction in the linear range of 7 nM - 1 μM (R^2= 0.986). The CS@AgNPs-CPE was then extended for the determination of PNA in real samples such as wastewater. All these studies confirmed that the chitosan stabilized silver nanoparticles on the carbon paste electrode are potential alternatives in the field of electrochemical sensing.

Keywords: Nitroaromatics compounds, p-nitroaniline, silver, thermal deposition, electrochemical deposition, nanoparticles, electrochemical determination, electrocatalysis.

Résumé

Les composés nitroaromatiques sont des contaminants environnementaux associés à des activités anthropiques. Le p-nitroaniline (PNA) est l'un des composés important de cette classe. C'est une substance chimique brute extrêmement importante qui occupe une place non substituable dans la synthèse d'une grande variété de produits chimiques, notamment divers colorants organiques, des pesticides, des médicaments, des agents antivieillissement, des photo-stabilisateurs, des antioxydants et des agents de développement. Cependant, le PNA est fortement toxique, comparable au trinitrotoluène (TNT) et trinitrophénol (TNP), et peut être rejeté dans l'environnement directement sous forme de déchets industriels ou indirectement sous forme de produits de dégradation des herbicides et des pesticides. En raison de la présence de puissants groupes attracteurs d'électrons, le PNA est peu biodégradable dans l'environnement, il pénètre facilement dans le sol et contamine les eaux souterraines. Les recherches scientifiques, ont montré qu'il peut causer des dommages aux humains et aux systèmes aquatiques. Ainsi, les capteurs hautement sensibles et sélectifs permettant une détection rapide et efficace de PNA constituent une question extrêmement urgente concernant la sécurité intérieure, la protection de l'environnement et les préoccupations humanitaires. Ces dernières années, les électrodes chimiquement modifiées ont été utilisées pour la quantification voltampérométrique de diverses espèces organiques et inorganiques après accumulation en circuit ouvert. De nombreux travaux dans ce domaine ont été consacrés à l'exploitation de la réactivité chimique du modificateur envers un analyte cible à des fins électrocatalytiques et électroanalytiques. De nombreux agents modificateurs ont été utilisés soit comme revêtement sur la surface d'électrodes solides, soit dispersés dans une matrice conductrice. Les électrodes modifiées sont fréquemment utilisées dans la détermination voltampérométrique des composés organiques en raison de leur efficacité, de leur sélectivité et de leur sensibilité. Dans ce contexte, le présent travail décrit l'utilisation de diverses électrodes synthétiques à pâte de carbone à base d'argent pour la quantification voltampérométrique de PNA.

La première partie de ce travail a été dédiée à l'étude de l'efficacité catalytique de l'argent pour la réduction de PNA à l'aide d'une électrode en argent métallique, après comparaison de ses performances avec d'autres électrodes, notamment en or, en graphite et en carbone vitreux. En effet, ce matériau possède des propriétés électrochimiques supérieures pour l'étude du comportement électrochimique de PNA et sa détermination. La mise en évidence de cette méthode a été évaluée en utilisant la voltampérométrie cyclique, la chronoamperométrie, les courbes de Tafel et la spectroscopie d'impédance électrochimique.

Dans la deuxième partie, la modification chimique des surfaces d'électrodes par dépôt thermique et électrochimique pour des applications électroanalytiques a ensuite été utilisée, ouvrant de nouvelles voies dans le domaine de la détection en permettant un meilleur contrôle du comportement de la surface des électrodes et en résolvant divers problèmes liés soit à l'électrocatalyse, soit à l'électroanalyse liés aux surfaces non modifiées. Ces modifications ont permis d'améliorer considérablement la sensibilité, la reproductibilité, la stabilité et la sélectivité. La morphologie et la distribution de l'argent sur la surface de l'électrode ont été évaluées par diffraction des rayons X et par microscopie électronique à balayage. La surface électro-active des électrodes préparées a été estimée en utilisant $[Fe(CN)_6]^{3-/4-}$ comme une sonde d'oxydoréduction par voltampérométrie cyclique. En outre, la détermination analytique de PNA a été effectuée pour les deux méthodes proposées en utilisant la voltampérométrie à impulsions différentielles. Il a été constaté que l'intensité du courant du pic de réduction de PNA par dépôt thermique est très faible par rapport au dépôt électrochimique ; cela peut confirmer la formation d'oxyde d'argent à la surface des électrodes à pâte de carbone. Enfin, l'électrode modifiée par déposition électrochimique a été appliquée avec succès pour la détermination de PNA dans les échantillons d'eau potable. La simplicité de la préparation, la bonne reproductibilité et le faible coût de l'électrode modifiée, la surface active élevée ainsi que la large gamme de concentration linéaire, la faible limite de détection et la bonne répétabilité constituent les principaux avantages pour la détermination de PNA.

Dans la troisième partie, un matériau composé de nanoparticules d'argent stabilisées au chitosane sur l'électrode à pâte de carbone (CS@AgNPs-CPE) est utilisé pour la détermination électrochimique de PNA. Un procédé chimique est utilisé pour synthétiser des nanoparticules d'argent stabilisées par Chitosane dans de l'acide acétique (2%) en utilisant du borohydrure de sodium comme agent réducteur. La caractérisation du produit final par la spectroscopie UV-Vis a permis de vérifier la présence de nanoparticules d'argent. L'analyse par diffraction des rayons X a montré que les nanoparticules d'argent avaient une taille moyenne de 50 nm. La caractérisation électrochimique a prouvé que les CS@AgNPs-CPE présentent une activité électrocatalytique et électroanalytique élevée qui peut être exploitée pour la construction de capteurs et les applications correspondantes. Le capteur développé a révélé une limite de détection inférieure de 5 nM envers la réduction du PNA dans la gamme allant de 7 nM à 1 µM ($R^2 = 0,986$). Le CS@AgNPs-CPE a ensuite été étendu pour la détermination de PNA dans des échantillons réels tels que les eaux usées. Toutes ces études ont confirmé que les nanoparticules d'argent à la surface de l'électrode à pâte de carbone constituent des alternatives prometteuses pour la détection électrochimique.

Mots Clés : Composés nitroaromatiques, p-nitroaniline, argent, déposition thermique, déposition électrochimique, nanoparticules, détermination électrochimique, électrocatalyse.

– List of abbreviations –

Ag$_{ED}$-CPE	Silver modified carbon paste electrode using electrochemical deposition
Ag$_{Imp}$-CPE	Silver modified carbon paste electrode using thermal deposition
Al$_2$O$_3$	Aluminum oxide
ASV	Adsorption-stripping voltammetry
Au	Gold electrode
B-R	Britton Robinson
CE	Counter electrode
CMEs	Chemically modified electrodes
CPEs	Carbon paste electrodes
CS	Chitosan
CS@AgNPs	Chitosan-silver nanoparticles
CS-CPE	Chitosan modified carbon paste electrode
CTAB	Cetyl trimethylammonium bromide
CV	Cyclic voltammetry
DDA	Degree of deacetylation
DHCBAQS	7-[(2,4- dihydroxy-5-carboxybenzene)azo]-8-hydroxyquinoline-5-sulfonic acid
DLS	Dynamic light scattering
DNA	Deoxyribonucleic acid
DPV	Differential pulse voltammetry
E	Potential
EDTA	Ethylene-diamine-tetra-acetic-acid
EIS	Electrochemical impedance spectroscopy
Emf	Electromotive force
FT-IR	Fourier transform infrared spectroscopy
FWHM	Full width at half of the peak maximum height
GC	Glassy carbon

Gr	Graphite electrode
IUPAC	International Union of Pure and Applied Chemistry
LD	Limit of detection
LQ	Limit of quantification
LSV	Linear Sweep Voltammetry
MTPs	Multiply twinned particles
NHE	Normal hydrogen electrode
NiO	Nickel oxide
NPs	Nanoparticles
O	Oxidized species
OCP	Open circuit potential
o-PDA	o-phenylenediamine
p-AP	p-aminophenol
PBS	Phosphate buffer solution
PEG	Poly(ethylene glycol)
PNA	p-nitroaniline
PVP	poly(vinylpiridine)
R	Reduced species
RE	Reference electrode
RSD	Relative standard deviation
SCE	Saturated calomel electrode
SDS	Sodium dodecyl sulfate
SEM	Scanning electron microscopy
SHE	Standard Hydrogen Electrode
SMSI	Strong metal−support interaction
SPCE	Screen printed carbon electrodes
SPR	Surface plasmon resonance

SWNT	Single-walled carbon nanotube
SWV	Square wave voltammetry
WE	Working electrode
XRD	X-Ray diffraction
ΔG	Gibbs free energy change

– List of figures –

–Chapter 1–

Figure 1: Pathway of a general electrode reaction.

Figure 2: Schematic representation of the composition of the electrode | solution interface.

Figure 3: The three modes of mass transport.

Figure 4: Potential–time excitation signal in a cyclic voltammetric experiment.

Figure 5: Schematic of the EC' catalytic reaction mechanism.

Figure 6: A typical plot of peak potential, E_P versus pH.

Figure 7: Cyclic voltammetric response for the reversible reaction of an adsorbed species.

Figure 8: The typical Nyquist plot of an electrochemical cell containing working electrode into the electrolyte containing electroactive species and inset is the Randles' equivalent circuit.

Figure 9: Schematic representation of an electrochemical cell for CV experiments.

Figure 10: Schematic illustration of the mechanical polishing procedure.

Figure 11: Geometric and electronic structures of single atom, clusters, and nanoparticles.

Figure 12: Description of different stabilizing agents in colloidal plasmonic nanoparticles preparations and related functions/characteristics. Sizes of the nanoparticles and ligands/shells are not drawn to scale.

Figure 13: Schematic of the formation of nanomaterials processes.

Figure 14: Reduction of nitro compounds to the corresponding amines using catalytic process

–Chapter 2–

Figure1: Illustration of the impregnation process of silver on carbon paste electrode (Ag_{Imp}-CPE).

Figure 2: Illustration of the electrodeposition process of silver on carbon paste electrode.

Figure 3: Construction process of chitosan modified carbon electrode CS-CPE.

Figure 4: The mechanism of formation of chitosan-Ag nanoparticles.

Figure 5: The modification process of carbon paste electrodes.

−Chapter 3−

Figure 1: (A) CV of 1.0×10^{-3} mol L^{-1} PNA for Ag, Gr, GC and Au at scan rate 100 mV s^{-1} in 1.0×10^{-1} mol L^{-1} BR buffer (pH 2). Inset blank solution. (B) Chronoamperograms obtained in 0.1 mol L^{-1} BR buffer (pH 2.0) of PNA at reduction potential (-0.3 V) using different electrodes. (C) EIS Nyquist plots obtained for Ag, GC and Gr in 0.1 mol L^{-1} BR buffer containing 1.0×10^{-3} mol L^{-1} of PNA.

Figure 2: CVs of 1.0×10^{-3} mol L^{-1} PNA in 0.1 mol L^{-1} BR buffer (pH 2.0); (A) CVs at scan rates of 1, 10, 20, 50, 80, 100, 150, 200, 300, 400 mV s^{-1}; (B) Variations of Ip with root of scan rate;(C) variation of the scan rate normalized peak current (Ip $v^{-1/2}$) versus scan rate; (D) Variations of Ep with logarithm of scan rate.

Figure 3: (A) CVs (at 50 mV s^{-1}) of 1.0×10^{-3} mol L^{-1} PNA at different values of buffered pH. (B) Plot of *Ep* versus pH.

Figure 4: (A) Chronoamperograms obtained for PNA concentrations at Ag electrode of 1 (1), 0.5 (2), 0.1 (3), 0.05 (4) and 0.01 (5) mmol L^{-1}. (B) Plots of I versus $t^{-1/2}$ obtained from chronoamperograms (1) to (5). (C) Plot of slopes of straight lines against PNA concentration and (D) dependence of I_C/I_L on $t^{1/2}$.

Figure 5: (A) Tafel plots at various PNA concentrations (a: 1.0×10^{-3}; b: 5.0×10^{-4}; c: 1.0×10^{-4} and d: 1.0×10^{-5} mol L^{-1}) in B-R buffer solution (pH 2.0) with scan rate 50 mV s^{-1}. (B) Double logarithmic plot of current as a function of PNA concentrations at constant potential.

Figure 6: DPVs of PNA in 0.1 mol L^{-1} B-R (pH 2.0) 1.0×10^{-3}; 8.0×10^{-4}; 5.0×10^{-4}; 2.0×10^{-4}; 1.0×10^{-4}; 5.0×10^{-5}; 1.0×10^{-5}; 5.0×10^{-6}; 8.0×10^{-7}; 4.0×10^{-7}; 2.0×10^{-7}; 1.0×10^{-7}; 5.0×10^{-8}; 1.0×10^{-8}

and 8.0×10^{-9} mol L^{-1}. Inset: plots of electrocatalytic peak current as a function of PNA concentration.

−Chapter 4−

Figure 1: X-ray diffraction (XRD) patterns of (A) carbon paste and $Ag_{ED}CP$ after electrodeposition step. (B) Silver microparticles impregnated onto CPE heated at 200°C at different percentages of $AgNO_3$.

Figure 2: SEM images of (A) Ag_{Imp}-CPE, and (B) Ag_{ED}-CPE.

Figure 3: (A) CV profile resulting from CPEs modified with different amounts of silver in 0.1 KCl containing 1mM of $K_4Fe(CN)_6$ and 1mM $K_3Fe(CN)_6$ (1:1) at dE/dt = 100 mV s^{-1}. (B) Nyquist plots of $[Fe(CN)_6]^{3-/4-}$ species resulting from CPEs modified by different amount of silver, 2% (i), 9% (ii), 10% (iii) and 15% (iv). Inset represent Simple equivalent circuit model. (C) Bode plots of phase angle vs. logarithm of frequency for the CPEs modified by different amount of silver, 2% (i), 9% (ii), 10% (iii) and 15% (iv) performed between 100 mHz and 1 kHz using amplitude of 10 mV in 0.1 KCl containing 1mM of $K_4Fe(CN)_6$ and 1mM $K_3Fe(CN)_6$. (D) CV profile of Ag_{Imp}-CPE and Ag_{ED}-CPE in 0.1M KCl containing 1mM $[Fe(CN)_6]^{3-/4-}$. (dE/dt) = 50 mV s^{-1}.

Figure 4: Blank for Ag_{Imp}-CPE, 1.0×10^{-3} mol L^{-1}PNA for CPE and for Ag_{Imp}-CPE at scan rate of 100 mV s^{-1} in 1.0×10^{-1} mol L^{-1} B-R (pH 2).

Figure 5: CVs of 1.0×10^{-3}mol L^{-1}PNA in 0.1 mol L^{-1} B-R buffer (pH 2.0); (A) CVs at scan rates of 10, 30, 50, 100, 150, 200, 300, 400 mV s^{-1}. (B) Variations of Ip vs. square root of scan rate.

Figure 6: (A) CVs (at 50 mV s^{-1}) of 1.0×10^{-3} mol L^{-1} PNA at different values of buffered pH. (B) Plot of E versus pH.

Figure 7: (A) Chronoamperograms obtained for PNA concentrations at Ag_{Imp}-CPE of 1 (1), 0.1 (2), 0.05 (3), 0.01 (4) and 0.001(5) mmol L^{-1} at reduction potential (-0.5 V). (B) Insets; plots of I versus $t^{-1/2}$ obtained from chronoamperograms (A) and (C) dependence of I_C/ I_L on $t^{1/2}$.

Figure 8: (A) DPVs for different PNA concentrations in 0.1 mol L^{-1} B-R buffer (pH 2). (B) Plot of electrocatalytic peak current as a function of PNA concentration.

Figure 9: (A) Calibration curve of PNA in drinking water in the concentration range of 1.0×10^{-6} mol L^{-1} to 1.0×10^{-5} mol L^{-1} using DPV method at Ag$_{ED}$-CPE. (B) Plot of peak current as a function of PNA concentration.

−Chapter 5−

Figure 1: (A) UV-Vis absorption spectra of freshly prepared CS@AgNPs solution. Inset photographic images. (B) Photographic images of CS@Ag NPs solution at different amount of NaBH$_4$. (C) UV-Vis absorption spectra of freshly prepared CS@AgNPs solution at different concentration of AgNO$_3$ and (D) UV-Vis absorption spectra of freshly prepared CS@AgNPs solution at different quantity of NaBH$_4$.

Figure 2: (A) XRD pattern of synthesized CS@AgNPs (B) SEM images of synthesized chitosan-AgNPs and (C) The FTIR spectra of synthesized CS@AgNPs.

Figure 3: EIS spectra of unmodified **(i)** chitosan modified carbon CS-CPE **(ii)** and CS@AgNPs-CPE **(iii)** in 0.1M KCl containing 5mM [Fe(CN)$_6$]$^{3-/4}$performed between 100 MHz and 1 kHz using amplitude of 10 mV.

Figure 4: CVs voltammograms of CPE (A), chitosan modified carbon CS/CPE (B) and CS@AgNPs-CPE(C) in 0.1M KCl containing 5mM [Fe(CN)$_6$]$^{3-/4-}$ at scan rate 50 mV s^{-1}.
Figure 5: DPV voltammograms of unmodified CPE and CS-CPE at 0.1 mM PNA containing 0.1 M PBS pH 7.0.

Figure 6: Optimization of the experimental parameters (A) Chitosan percentage (%), (B) Accumulation time, and (C) pH of buffer solution recorded by DPV technique in 55 μM PNA containing 0.1 M PBS pH 7.0.

Figure 7: (A) DPV voltammograms obtained at CS@CPE for different concentrations of PNA. (B) Calibration curve and (Inset B) Zoom of calibration curve at lower concentration.

Experimental conditions: 0.1 M PBS pH 7; 10 mVs^{-1}, 170 ms, 450 mV and 500 ms for step, pulse, width and period, respectively.

Figure 8: CV voltammograms of CS@AgNPs-CPE (a) and CPE (b) at 1.0 mM PNA containing 0.1 M B-R pH 2.0.

Figure 9: (A) CVs of CS@AgNPs in 0.1 M B-R pH 2.0 containing 1.0 mM PNA different scan rates between 5 mV s^{-1} and 500 mV s^{-1}. (B) Plot of the linear relationship between current and square root of scan rate and (C) Plot between peak potential (Ep) and log v.

Figure 10: (A) Plot of I vs. t$^{-1/2}$ of CS@AgNPs-CPE obtained from chronoamperogrammes at various PNA concentrations by setting reduction potential at -300 mV. Slopes of straight lines against PNA concentration showed in insert. (B) Plot of current vs. t$^{-1/2}$ of CS@AgNPs-CPE derived from the data chronoamperogrammes at various PNA concentrations.

Figure 11: (A) DPV voltammograms of the concentration of the Ag^{+} ions on the reduction peak of PNA. (B) Preconcentration time effect on the reduction peak of PNA.

Figure 12: (A) DPV voltammograms obtained at CS@AgNPs-CPE for different concentrations of PNA in the range from $7.0{\times}10^{-9}$ to $7.0{\times}10^{-6}$. (B) Calibration curve. Experimental conditions: 0.1 M PBS pH 7.0; 12 mV s^{-1}, 170 ms, 450 mV and 500 ms for step, pulse, width and period, respectively.

Figure 13: (A) DPV voltammograms obtained at CS-AgNPs-CPE for different concentrations of PNA in wastewater within the range 0.1μM – 10 μM. (B) Calibration curves. Experimental conditions: 12 mV s^{-1}, 170 ms, 450 mV and 500 ms for step, pulse, width and period, respectively.

– List of tables –

−Chapter 1−

Table 1: General classification of electrochemical dynamic methods.

Table 2: Variation of ΔEp with ψ at 25 °C.

Table 3: Synthesis of Ag nanoparticles with different shapes through chemical, physical and biological methods.

−Chapter 3−

Table 1: Influence of coexisting substances on the determination of 1.0×10^{-5} mol L^{-1} of PNA (n = 3).

Table 2: Obtained results for the determination of PNA in drinking and wastewater samples.

−Chapter 4−

Table 1: Summary of calculated EIS parameters obtained for the different electrodes.

Table 2: Some of the reported electrochemical sensors for PNA detection.

−Chapter 5−

Table 1: Results of PNA determination at CS-CPE and CS@AgNPs-CPE in wastewater samples.

Contents

– Chapter 1 –

Literature Review

– Chapter 2 –

Preparation and characterization of silver-based materials as carbon paste electrode modifiers

– Chapter 3 –

Electrochemical evaluation of catalytic effect of metallic silver electrode towards the reduction of p-nitroaniline

– Chapter 4 –

Thermal and electrochemical deposition of Ag catalysts for the electrochemical reduction of p-nitroaniline

– Chapter 5 –

Silver nanostructured electrodes for direct electrocatalysis and electroanalysis of p-nitroaniline

– Introduction –

Nitro-aromatic compounds are organic materials used as precursors for the manufacturing of organic products such as pharmaceuticals, pesticides, explosives, and other industrial chemicals [1]. However, the presence of nitro-aromatic compounds such as PNA and m-nitroaniline in water would be dangerous to aquatic life and human health because of their toxicity, potentially carcinogenic and mutagenic effects. Recently, reports suggested that the presence of even low concentrations of PNA in water has resulted in environmental contamination and public health problems [2–4]. In particular, PNA is a notorious industrial pollutant exhibiting high solubility and stability in water. It is therefore important to develop effective methods for their removal. To date, various processes have been developed for the disposal of these nitro-compounds including microbial degradation, photocatalytic degradation, microwave-assisted catalytic oxidation, electro-Fenton method, electrocoagulation, and electrochemical treatment [5–7]. However, the reduction of nitro group to amino group is considered to be the most efficient, green, and economical approach to dispose nitro-compounds [8], and the reduction products namely, p-aminophenol (p-AP) and o-phenylenediamine(o-PDA) can be reused because they are important intermediates for the synthesis of drugs and dyes [9, 10]. Therefore, the development of low-cost, stable, and highly effective catalysts for the reduction of nitro-compounds in aqueous solutions under mild conditions is highly desirable. Several works have explored its determination using voltammetric methods that exhibit low cost per analysis, possibility of multi-analyte detection, easy miniaturization, and high sensitivity when compared to other methods of determination, such as, e.g., chromatographic and fluorescence methods [11-13]. Electrochemical methods offer the possibility to study this process directly by determining the number of electrons involved.

Electrochemical techniques provide efficient tools for surface modifications. Very simple experiments can be performed where species from solution can be physically adsorbed, electropolymerized, or covalently attached onto the electrode surface at a certain controlled potential.

The fundamental process of electrochemistry is the transfer of electrons between the electrode surface and the molecules in the interfacial region, either in solution or immobilized on the electrode surface. The kinetics of this heterogeneous process can be significantly affected by the microstructure and roughness of the electrode surface, the blocking of active sites on the

electrode surface by adsorbed materials, and the nature of the functional groups (e.g., oxides) present on the electrode surface [14, 15]. Hence, chemically modified electrodes (CMEs) have attracted great attention in recent years and many interesting studies have been carried out in this field. In detail, chemically modified electrodes comprise an approach to electrode system design. They showed great interest in a wide spectrum of basic electrochemical investigations, including the relationship of heterogeneous electron transfer and chemical reactivity of electrode surface chemistry, electrostatic phenomena at electrode surface, and electron as well as ionic transport phenomena in polymers.

There has been an increasing interest in the creation of modified electrode surfaces that differ from the corresponding bare surfaces and produce an electrode that generates a reproducible result, which has been particularly important to electroanalytical chemistry [16, 17]. Modification has provided routes to providing selectivity, resisting fouling, concentrating species, improving electrocatalytic properties [18] and limiting access of interferences in a complex sample [19], such as a biological fluid, but has also had major impact for research into energy conversion [20, 21] and storage, corrosion protection [22], molecular electronics [23–25], electrochromic devices [26] and fundamental research into phenomena that influence electrochemical processes [23]. In recent years, this revolution in adapting electrode surfaces so that the electrode has unique properties has continued at an even faster pace, with unprecedented control of the modification process through advances in nanofabrication. Taken in their broadest context, nanostructured electrodes can be seen to control electrode architecture at the nanoscale, whether it is the use of nanomaterials, modeling methods, modification of electrode surfaces by polymers, or composites and nanomaterials. These different electrode modification strategies offer the possibility of imparting a unique range of properties to electrode surfaces, from ultra-high surfaces obtained with model electrodes to electrocatalytic properties with metal nanoparticles, strategies to perform electrochemistry in places too small for conventional electrodes, and to give electrodes with switchable properties.

The work covered by this thesis aims at controllably modifying the properties of carbon surfaces so that these surfaces can be used for the desired sensor applications. Carbon was chosen because it is highly conductive and has a large potential window. Structurally stable, relatively inexpensive and stable modifier layers can be attached to the surface in a controllable manner. In

this thesis, carbon powder was selected and was applied to study the electrochemical properties of the selected hazardous nitro-compound PNA and the process taking place a cross the interface of the electrode surface and the electrolyte. A species capable of undergoing electron transfer process is called an electroactive species. In order to carry out electron transfer process with the electrode, the electroactive species comes from the bulk solution and approaches the electrode surface. Hence, the electron transfer plays a fundamental role in governing the pathways of chemical reactions. Measuring the rate of the electron transfer process and the number of electrons involved is difficult in traditional experimental methods such as spectral and chromatographic methods [27]. Consequently, knowledge of the driving force of many reactions remains elusive.

The effect of silver-based modified carbon paste electrodes on the reduction properties of PNA in aqueous media has also been studied. Firstly, the catalytic efficiency of silver in the reduction of PNA was studied using a metallic silver electrode following comparison of its performance against other electrodes including gold, graphite and glassy carbon. This material has superior electrochemical properties for the study of the electrochemical behavior of PNA and its determination. Chemical modification of electrode surfaces for electroanalytical applications was subsequently used, opening new avenues in the field of detection by allowing better control of electrode surface behavior and solving various problems either electrocatalytic or electroanalytic related to unmodified surfaces. These modifications have made it possible to greatly in enhancing sensitivity, reproducibility, stability, and selectivity.

This thesis is presented in five roughly chapters. The first chapter is devoted to fundamental aspects of electrode reactions and the structure of the interfacial region. The objective is to provide a sound understanding of the fundamentals of electrode reactions and the principles of electrochemical methods and to demonstrate their potential for solving real-life analytical problems. Then, there are discussions of thermodynamics and potential, electron-transfer kinetics, and mass transfer. Next are discussions of electrodeposition and impregnation. Special attention is paid for nanoparticles, focuses on the roles and effects of stabilizing agents such as surfactants, silica, biomolecules, and polymers. Possible methods for the synthesis of silver nanoparticles with specific shapes are also discussed.

The second chapter aims for providing a detailed overview of different chemicals and procedures, which were used to carry out the present work. Experimental section is divided into different parts comprising of detailed list of chemicals, electrodes, and their preparation, protocols for electrodes modification and electrochemical setup, and analytical techniques used in this study.

The third chapter devoted to the electrocatalytic effect of metallic silver electrode towards the reduction of PNA and their sensitive determination in aqueous medium. Emphasis was put on the comparison of the performances of metallic silver electrode with different other electrodes including gold, graphite and glassy carbon. Reported research works on electrochemical application of unmodified/modified electrodes for the determination of PNA are considered.

In the fourth chapter, our approach is the modification of carbon paste electrode with silver using thermal and electrochemical deposition, emphasizing there electrocatalytic activity towards the reduction of PNA with determination of kinetic parameters. The effect of electro-active surface area and particle size are also discussed.

The fifth chapter seeks to emphasize how the modification of carbon paste electrodes with silver nanoparticles offers the possibility of gaining higher electrocatalytic activities, sensitivities, and selectivity's in reducing PNA. Eventually, a chemical process has been used to synthesis silver nanoparticles. Through this chapter, the relationship between the kinetics of the reaction and the concentration of Ag^+ ions and the concentration of $NaBH_4$ is discussed. The effect of silver nanoparticles as modifier was treated separately with chitosan modified carbon paste electrode in such a way that it provides a comparative view of the responses of both electrodes.

References

[1]   Guo, P., Tang, L., Tang, J., Zeng, G., Huang, B., Dong, H., & Tan, S. (2016). Catalytic reduction–adsorption for removal of p-nitrophenol and its conversion p-aminophenol from water by gold nanoparticles supported on oxidized mesoporous carbon. Journal of colloid and interface science, 469, 78-85.

[2]   Farooqi, Z. H., Naseem, K., Begum, R., & Ijaz, A. (2015). Catalytic reduction of 2-nitroaniline in aqueous medium using silver nanoparticles functionalized polymer microgels. Journal of Inorganic and Organometallic Polymers and Materials, 25(6), 1554-1568.

[3]   Li, K., Zheng, Z., Huang, X., Zhao, G., Feng, J., & Zhang, J. (2009). Equilibrium, kinetic and thermodynamic studies on the adsorption of 2-nitroaniline onto activated carbon prepared from cotton stalk fibre. Journal of hazardous materials, 166(1), 213-220.

[4]   Dong, Z., Le, X., Li, X., Zhang, W., Dong, C., & Ma, J. (2014). Silver nanoparticles immobilized on fibrous nano-silica as highly efficient and recyclable heterogeneous catalyst for reduction of 4-nitrophenol and 2-nitroaniline. Applied Catalysis B: Environmental, 158, 129-135.

[5]   Oturan, M. A., Peiroten, J., Chartrin, P., & Acher, A. J. (2000). Complete destruction of p-nitrophenol in aqueous medium by electro-Fenton method. Environmental Science & Technology, 34(16), 3474-3479.

[6]   O'Connor, O. A., & Young, L. Y. (1989). Toxicity and anaerobic biodegradability of substituted phenols under methanogenic conditions. Environmental Toxicology and Chemistry: An International Journal, 8(10), 853-862.

[7]   Dieckmann, M. S., & Gray, K. A. (1996). A comparison of the degradation of 4-nitrophenol via direct and sensitized photocatalysis in TiO2 slurries. Water Research, 30(5), 1169-1183.

[8]   Mohamed, M. M., & Al-Sharif, M. S. (2013). Visible light assisted reduction of 4-nitrophenol to 4-aminophenol on Ag/TiO2 photocatalysts synthesized by hybrid templates. Applied Catalysis B: Environmental, 142, 432-441.

[9]   Zhang, Y., Yuan, X., Wang, Y., & Chen, Y. (2012). One-pot photochemical synthesis of graphene composites uniformly deposited with silver nanoparticles and their high

catalytic activity towards the reduction of 2-nitroaniline. Journal of Materials Chemistry, 22(15), 7245-7251.

[10] Saha, S., Pal, A., Kundu, S., Basu, S., & Pal, T. (2010). Photochemical green synthesis of calcium-alginate-stabilized Ag and Au nanoparticles and their catalytic application to 4-nitrophenol reduction. Langmuir, 26(4), 2885-2893.

[11] Tarley, C. R. T., & Kubota, L. T. (2005). Molecularly-imprinted solid phase extraction of catechol from aqueous effluents for its selective determination by differential pulse voltammetry. Analytica chimica acta, 548(1-2), 11-19.

[12] Shkumbatiuk, R., Bazel, Y. R., Andruch, V., & Török, M. (2005). Investigation of 2-[(E)-2-(4-diethylaminophenyl)-1-ethenyl]-1, 3, 3-trimethyl-3H-indolium as a new highly sensitive reagent for the spectrophotometric determination of nitrophenols. Analytical and bioanalytical chemistry, 382(6), 1431-1437.

[13] Wang, S. P., & Chen, H. J. (2002). Separation and determination of nitrobenzenes by micellar electrokinetic chromatography and high-performance liquid chromatography. Journal of Chromatography A, 979(1-2), 439-446.

[14] Kissinger, P., & Heineman, W. R. (1996). Laboratory Techniques in Electroanalytical Chemistry,revised and expanded. CRC press, New York Eds), 1995.

[15] Mc Creery, R.L. (1991). "Electroanalytical Chemistry" Vol.17 (Dekker, New York Eds).

[16] Imisides, M. D., John, R., Riley, P. J., & Wallace, G. G. (1991). The use of electropolymerization to produce new sensing surfaces: a review emphasizing electrode position of heteroaromatic compounds. Electroanalysis, 3(9), 879-889.

[17] Wang, J. (1991). Modified electrodes for electrochemical sensors. Electroanalysis, 3(4-5), 255-259.

[18] Malinauskas, A. (1999). Electrocatalysis at conducting polymers. Synthetic Metals, 107(2), 75-83.

[19] Situmorang, M., Gooding, J. J., & Hibbert, D. B. (1999). Immobilisation of enzyme throughout a polytyramine matrix: a versatile procedure for fabricating biosensors. Analytica chimica acta, 394(2-3), 211-223.

[20] Marković, N. M., & Ross Jr, P. N. (2002). Surface science studies of model fuel cell electrocatalysts. Surface Science Reports, 45(4-6), 117-229.

[21]   Alexander, B. D., Kulesza, P. J., Rutkowska, I., Solarska, R., & Augustynski, J. (2008). Metal oxide photoanodes for solar hydrogen production. Journal of Materials Chemistry, 18(20), 2298-2303.

[22]   Mathiyarasu, J., Pathak, S. S., & Yegnaraman, V. (2006). Review on corrosion prevention of copper using ultrathin organic monolayers. Corrosion Reviews, 24(5-6), 307-322.

[23]   Adams, D. M., Brus, L., Chidsey, C. E., Creager, S., Creutz, C., Kagan, C. R., & Metzger, R. M. (2003). Charge transfer on the nanoscale: current status. The Journal of Physical Chemistry B, 107(28), 6668-6697.

[24]   Ybarra, G., Moina, C., Florit, M. I., & Posadas, D. (2008). Current rectification by mediating electroactive polymers. Electrochimica acta, 53(11), 3955-3959.

[25]   Haick, H., & Cahen, D. (2008). Making contact: Connecting molecules electrically to the macroscopic world. Progress in Surface Science, 83(4), 217-261.

[26]   Mortimer, R. J. (1997). Electrochromic materials. Chemical Society Reviews, 26(3), 147-156.

[27]   Savéant, J. M. (1997). Physical organic chemistry. Electron transier chemistry. Molecular electrochemistry. Pure and applied chemistry, 69(2), 269-272.

– Chapter 1 –

Literature Review

I. Fundamentals in electrochemistry

The word electrochemistry is derived from two words "electricity" and "chemistry". It can be defined as, "the domain of science associated with studies of interactions between chemistry and electricity". The more precise definition for electrochemistry would be "The science that analyses and describes the charge transfer reaction of matter at atomic level carried out by applying electric current or voltage with the help of electronic devices" [1].

The science of electrochemistry is concerned with electron transfer at the solution/electrode interface. Most of the basic principles and relationships, however, were described prior to the discovery of the electron by J. J. Thompson in 1893. In 1800, Alessandro Volta invented the first battery, and then known as a voltaic pile, by alternating stacks of copper and zinc disks separated by paper soaked in acid solutions. With the discovery of a sustainable source of electrical current, the stage was set for the rapid development of the area of science now known as electrochemistry. By 1835, Michael Faraday had already defined the anode, cathode, electrode, electrolyte, and ion: concepts without which any definitive description of electrochemistry is virtually impossible. The positive and negative mathematical convention for electrical charge is attributed to Benjamin Franklin [2]. Charles-François de Cisternay du Fay had earlier theorized the existence of only two types of electrical charge. Du Fay had named the charge generated by rubbing a glass rod as "vitreous," while the equivalent charge generated by rubbing amber, or resin, as "resinous." Franklin, however, envisioned electrical charge as being attributed to the level of a single invisible fluid present inside objects (i.e., a negatively charged object had a lesser amount of this fluid and a positively charged one had an excess amount). Franklin accordingly renamed resinous charge as negative and vitreous charge positive, thereby establishing the convention that would eventually demand the electron to be defined as a negative charge.

I.1. Potential conventions

Although the work of Faraday had established early on the relationship between the current generated during electrolysis and the amount of generated species, the dependence of cell potential on the concentration of electroactive species remained theoretically elusive until the advent of thermodynamics. Let us consider the following reduction reaction (Eq. 1):

$$O + ne^- \rightleftharpoons R \quad (1)$$
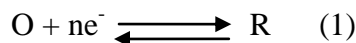
Where O is the oxidized species, R is the reduced species, and n is the number of electrons exchanged between O and R. The relationship between the concentration of oxidized species [O], concentration of reduced species [R], and free energy (ΔG [J mol^{-1}]) is given as (Eq. 2):

$$\Delta G = \Delta G^\circ + RT \ln \frac{[R]}{[O]} \quad (2)$$

where R is the gas constant (8.3145 J mol^{-1} K^{-1}) and T [K] is the temperature. The critical aspect of this equation is that the ratio of reduced/oxidized species can be related to the Gibbs free energy change (ΔG), from which we can then derive the potential (E [V]) (Eq. 3):

$$\Delta G = -nFE \quad (3)$$

Here E is the maximum potential between two electrodes, also known as the open-circuit potential (OCP) or the equilibrium potential, which is present when no current is flowing through the cell, and F is Faraday's constant (1F = 96,485.3 C mol^{-1}). If the reactant and product have unit activity, and E is for the reaction in the direction of reduction (left to right in equation (1)), then equation (3) can be written as (Eq. 4):

$$\Delta G^\circ = -nFE^\circ \quad (4)$$

In this case, the potential is known as the standard electrode potential (E°[V]) or the standard potential and it relates to the standard Gibbs free energy change (ΔG° [J mol^{-1}]). It should be noted here that due to the minus sign in equation (4), all spontaneous reactions (i.e., with $\Delta G^\circ < 0$) will have a positive standard electrode potential (E° > 0). The mathematical expression describing the correlation between potential and concentration for a cell reaction is a central tenant of electrochemistry and is known as the Nernst equation (obtained by combining equations (2)–(4)):

$$E = E^\circ + \frac{RT}{nF} \ln \frac{[R]}{[O]} \quad (5)$$

In addition to the use of the standard potential (E^0), reaction potentials may also be reported with the convention of electromotive force (emf or E [V]). The convention of emf was adopted to make the calculation of cell potentials, from the combination of two half reactions, more straightforward.

I.2. Thermodynamic functions and electrode potential

The well-known tools of chemical thermodynamics are used in electrochemical systems to describe equilibrium and processes, but some special features arising from the presence of charged particles and potential differences between the phases must be taken into account. Electrochemical systems are usually discussed under conditions of constant temperature T and pressure p [1,2]. Under these conditions, the most convenient thermodynamic functions are the Gibbs energy G, given by U + PV - TS, and the enthalpy H, given by U + PV (where U is the internal energy, V is the volume, and S is the entropy).

The values of these functions change when thermodynamic processes take place. Processes in which the Gibbs energy decreases (i.e., for which $\Delta G < 0$), will take place spontaneously without specific external action. The Gibbs energy is minimal in the state of equilibrium, and the conditions for equilibrium are given as (Eq. 6):

$$\Delta G = 0 \text{ or } dG = 0 \quad (6)$$

In systems with different components, the values of the thermodynamic functions depend on the nature and number of these components. One distinguishes components forming independent phases of constant composition (the "pure" components) from the components that are part of mixed phases of variable composition (e.g., solutions) [1].

The thermodynamic conditions of equilibrium for an isolated biphasic system include the equality of the chemical potential in the two phases. The conventional thermodynamic definition of chemical potential of a component (i) in a macroscopic system is (Eq. 7):

$$\mu i = \frac{\partial G}{\partial Ni} \quad (7)$$

where N is the quantity of species i in moles, G the Gibbs free energy, and the derivative is taken under the conditions that T, p and the concentrations of the other components are kept constant. According to this definition, μi corresponds to the partial molar Gibbs free energy [1,2]. In practice, μ_i is the change in Gibbs free energy when one mole of this component is added to a large amount of the mixture, so that the concentration of the other components is unchanged. It is usually assumed that μi depends on the thermodynamic activity (ai) of the species i as (Eq. 8):

$$\mu i = \mu i(0) + RT \ln ai \quad (8)$$

μi maintains its physical meaning only in the absence of electric fields.

When dealing with charged species, which always appear in electrochemistry, a more convenient quantity is introduced, namely the electrochemical potential $\underline{\mu_i}$ defined as (Eq. 9):

$$\underline{\mu i} = \mu i + zF\varphi \quad (9)$$

The second term on the right side represents the work done against a potential difference φ when transferring the charged species from infinity to inside the solution ("Galvani potential").

When the two phases (i.e. the metallic electrode and the solution) are in thermodynamic equilibrium their electrochemical potentials are equal (Eq. 10):

$$\mu1 + zF\,\varphi1 = \mu2 + zF\,\varphi2 \quad (10)$$

Inversely, the electrochemical equilibrium is attained when the electrochemical potentials are equal. This implies that (Eq. 11)

$$zF\,\Delta\varphi1^2 = \mu2 - \mu1 \quad (11)$$

where the μi are the chemical potentials in the two phases. The symbol $\Delta\varphi_{12}$ denotes the potential drop between the two phases, otherwise called Galvani potential difference. In general, the Galvani potential difference between two phases is determined by the difference of chemical

potentials of the ions and/or electrons in the metal and in the electrolyte; the thermodynamic equilibrium in fact must be attained both for ions and electrons.

It is impossible to experimentally measure the Galvani potential between liquid and solid phases. In fact, if we were to perform this measurement, we would need to immerse another metallic electrode in the liquid, effectively introducing an additional interface. For this reason the potential of the solid electrode is conventionally measured with reference to some other electrode which has a strictly defined Galvani potential relative to the solution. Such a measurement gives the emf generated by the electrochemical cell consisting of this reference electrode and the electrode under study. By using this method the solution drops out of the problem because the voltage measurement can now be performed between two metallic phases [1,2].

The second electrode is termed reference electrode. Many types of electrodes are feasible as reference electrodes; the most important property of a good reference electrode is the stability over time and reproducibility of its potential. Calomel and silver chloride electrodes are used most often in practice. Due to its unequaled stability and precision, the Standard Hydrogen Electrode (SHE) is chosen as the standard reference. This electrode consists of a platinized platinum surface immersed in an acidic solution having a hydrogen ion activity a $(H^+) = 1$ in contact with hydrogen gas at atmospheric pressure. The Galvani potential difference of this electrode is set equal to zero at any temperature. This electrode configuration allows formulation of the following definition for the electrode potential: Electrode potential E is the EMF of the electrochemical cell consisting of the SHE and the electrode of interest, at which the redox process takes place.

Just like the emf values of galvanic cells, the electrode potentials depend on the composition of the electrolyte and other phases of variable composition. The electrode potential corresponds to the Galvani potential of the electrode-electrolyte interface, up to a constant term $E = \varphi_G + const$. Such an objective is accomplished by monitoring the transfer of electron(s) during the redox process of the analyte (Eq. 12):

$$E = E^\circ + \frac{RT}{nF}\left(\sum_{ox} vj \ lnC_j - \sum_{red} vj \ lnC_j\right) \quad (12)$$

The partial pressures pj will appear here for gaseous substances instead of concentrations C_j.

E° is a constant that depends on the nature of the electrode reaction; it is equal to the electrode potentials for values $c_j=1$. The value of the electrode potential E depends primarily on the value of this constant, since the second term of this equation, which is the correction term for concentrations, is relatively small, although in certain cases it becomes the major term. The components that are involved in the electrode reaction and therefore influence the value of the electrode potential are called potential-determining substances. It follows from this equation that the potential will shift in the positive direction when the concentration of the oxidizing agent or components entering the reaction together with it is raised, but it will shift in the negative direction when the concentration of the reducing agent or components entering the reaction together with it is raised.

The combination of constants RT/F often appears in electrochemical equations; it has the dimensions of voltage. At 25°C (298.15 K) it has a value of 0.02569 V (or roughly 25 mV). When including the conversion factor for changing natural to common logarithms, we find a value of 0.05916 V (about 59 or 60 mV) for 2.303 (RT/F) at 25°C. Values for other temperatures can be found by simple conversion, since this parameter is proportional to the absolute temperature.

At an electrode which is brought about through the application of a suitability negative potential to the electrode. Note that a second electrode will be needed somewhere in the solution to facilitate the passage of the required electrical current through the solution and a reference electrode will also be required.

I.3. Factors affecting electrode reaction rate and current

Consider an overall electrode reaction, O + ne- $\rightleftharpoons$ R, composed of a series of steps that cause the conversion of the dissolved oxidized species, O, to a reduced form, R, also in solution (Fig. 1). In general, the current (or electrode reaction rate) is governed by the rates of processes such as (1, 2):

1. Mass transfer (e.g., of O from the bulk solution to the electrode surface).
2. Electron transfer at the electrode surface.

3. Chemical reactions preceding or following the electron transfer. These might be homogeneous processes (e.g., protonation or dimerization) or heterogeneous ones (e.g., catalytic decomposition) on the electrode surface.

4. Other surface reactions, such as adsorption, desorption, or crystallization (electrodeposition).
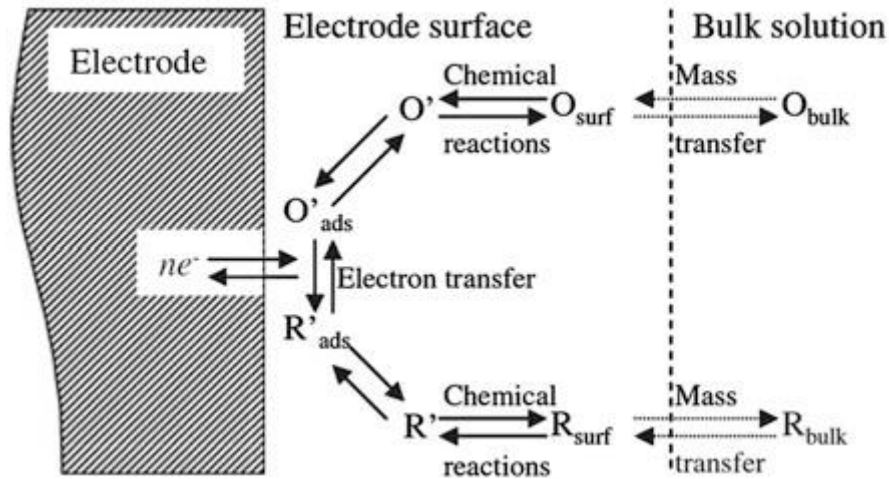
Figure 1: Pathway of a general electrode reaction.

The rate constants for some of these processes (e.g., electron transfer at the electrode surface or adsorption) depend upon the potential [3-10].

The simplest reactions involve only mass transfer of a reactant to the electrode, heterogeneous electron transfer involving nonadsorbed species, and mass transfer of the product to the bulk solution. This general electrochemical process shows that the observed electrode current is dependent upon mass transport, which usually occurs in series with other processes, such as chemical reactions, adsorption/desorption and also the heterogeneous rate constant for the electron transfer reaction. The working electrode is immersed into an electrolyte usually containing the electroactive species under investigation and a supporting electrolyte salt to achieve the required conductivity and to minimize the IR drop. The electric double layer at the working electrode occurs over a distance of ca. 1 nm. Fig. 2 shows a schematic representation of the composition of the solution phase close to the (working) electrode surface where the compact layer is also termed the ''inner Helmholtz'' layer that is closest to the surface in which the distribution of charge, and hence potential, changes linearly with the distance from the electrode

surface and the diffuse layer, known as the ''Gouy-Chapman'' layer, in which the potential changes exponentially.
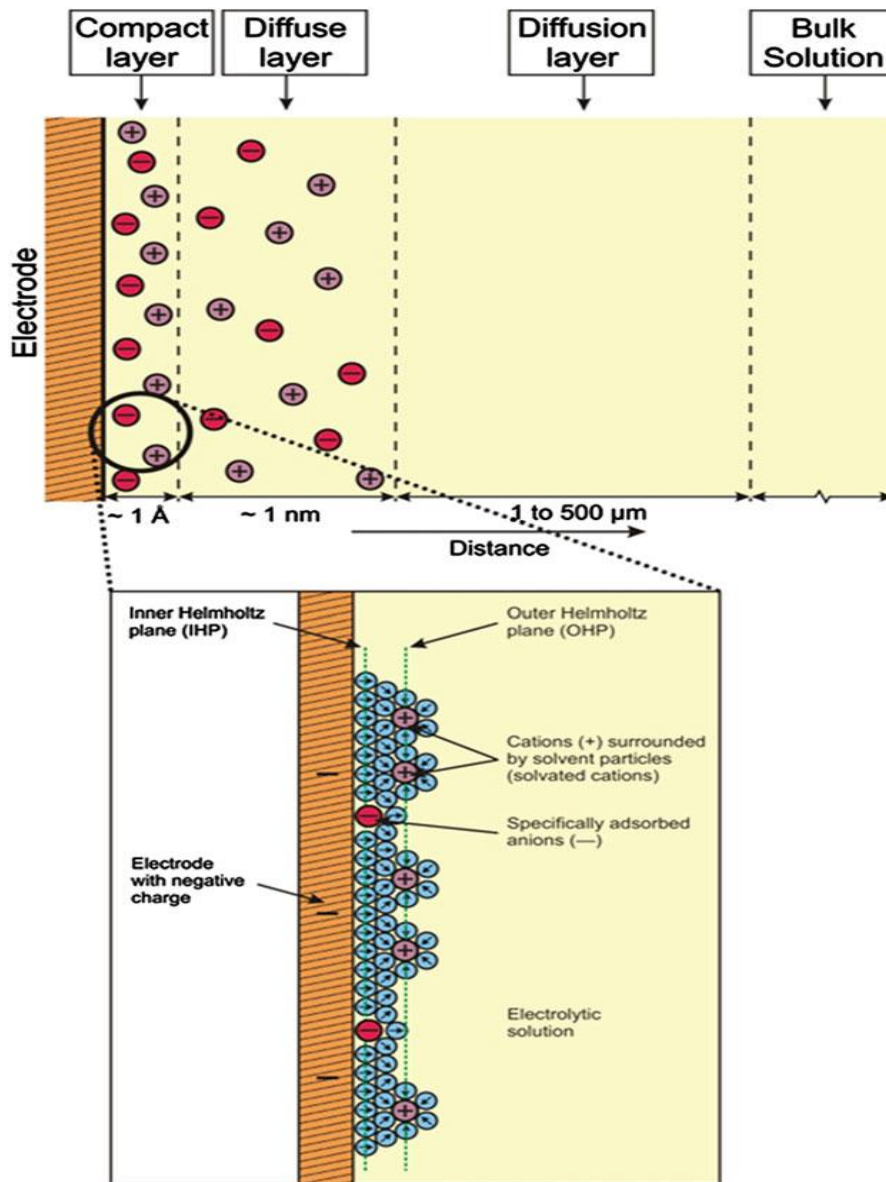
Figure 2: *Schematic representation of the composition of the electrode | solution interface*

The solvated ions are nonspecifically adsorbed and are attracted to the surface by long range coulombic forces. Both Helmholtz layers represent the compact layer. Such a compact layer of charges is strongly held by the electrode and can survive even when the electrode is pulled out of the solution. The Helmholtz model does not take into account the thermal motion of ions, which loosens them from the compact layer [11].

Reversibility also can affect the rate of the reaction. Reversibility is a key concept when dealing with electrochemical reaction mechanisms. An electrochemical cell is considered chemically reversible if reversing the current through the cell reverses the cell reaction and no new reactions or side products appear. An electrochemical cell is considered chemically irreversible if reversing the current leads to different electrode reactions and new side products. This is often the case if a solid fall out of solution or gas is produced, as the solid or gaseous product may not be available to participate in the reverse reaction.

The concept of thermodynamic reversibility is theoretical; it applies to adiabatic changes, where the system is always at equilibrium. An infinitesimal change causes the system to move in one particular direction, resulting in an infinitesimal response; the analogy in electrochemistry is that a small change in potential could result in the reversal of the electrochemical process. In electrochemistry, the researcher is concerned with practical reversibility. In reality, electrochemical processes occur at finite rates, and as long as the experimental parameters are set in a manner that allows for the reversal of the reaction to regenerate the original species, the processes are deemed practically reversible [12].

I.4. Mass transport-Controlled reaction

The faradaic current that flows at any time is a direct measure of the rate of the electrochemical reaction taking place at the electrode. Further, the current itself is dependent upon two things:

1. The rate at which material gets from the bulk of solution to the electrode, known as mass transport;
2. The rate at which electrons can transfer across the interface, or charge transfer kinetics.

Mass transport occurs by three different modes [13]:

- *Diffusion*—the spontaneous movement under the influence of concentration gradient, from regions of high concentrations to regions of lower ones, aimed at minimizing concentration differences.
- *Convection*—transport to the electrode by a gross physical movement; the major driving force for convection is external mechanical energy associated with stirring or flowing the solution or rotating or vibrating the electrode (i.e., forced convection). Convection can also occur naturally as a result of density gradients.

- *Migration*—movement of charged particles along an electrical field (i.e., where the charge is carried through the solution by ions according to their transference number). These modes of mass transport are illustrated in Fig. 3.
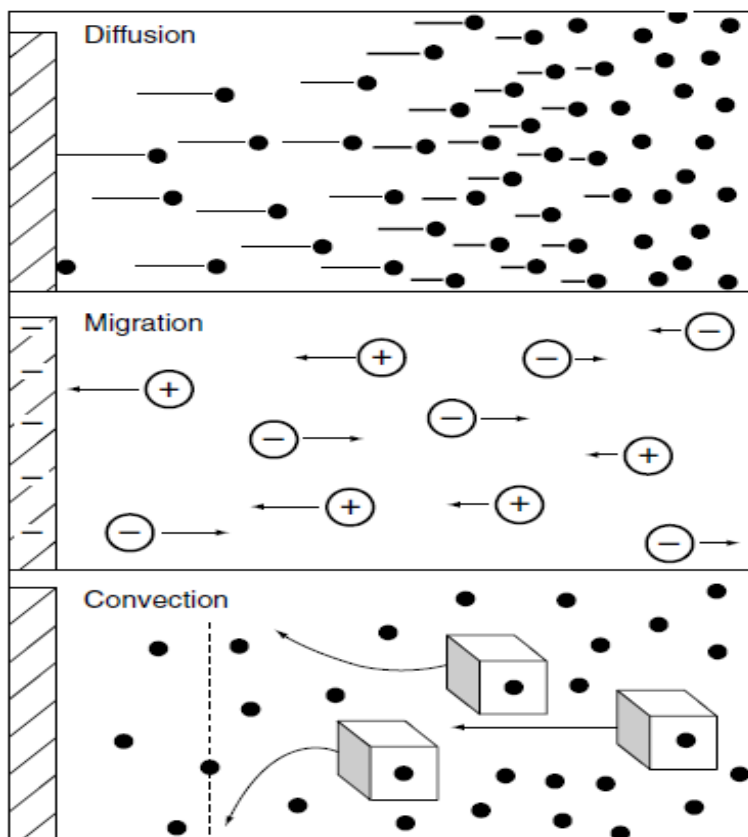
Figure 3: *The three modes of mass transport.*

II. Overview of electrochemical experiments

II.1. Electrochemical techniques

The electrochemical techniques can be divided into two major groups: static ($i=0$) and dynamic ($i\neq0$) [14]. Potentiometry is a static method, and it measures the rest potential vs. time; the most common applications in potentiometry are the use of ion-selective electrodes and pH meters. The dynamic methods comprise mostly all the other electrochemical techniques [15]. Table 1 lists the most commonly used methods.

Table 1: *General classification of electrochemical dynamic methods*

Controlled potential	Potential step	Amperometry	Chronoamperometry Double Potential Step Chronoamperometry	
		Chronocoulometry; Double Potential Step Chronocoulometry		
		Sampled Current Voltammetry; Differential Pulse Voltammetry; Square Wave Voltammetry		
	Potential sweep	Voltammetry	Stationary	Linear Scan Voltammetry
				Cyclic Voltammetry
			Hydrodynamic	Stirred Solution/ Flow Cell
				Rotating Disk Electrode; Rotating Ring-Disk Electrode
	Constant Potential	Bulk Electrolysis	Stirred Solution	
			Flow Electrolysis	
Controlled current	Chronopotentiometry		Constant-Current	
			Linearly Increasing Current	
			Current Reversal	
	Coulometry		Coulometric Titrations	
	Electrolysis			
Controlled Charge	Charge Step	Coulostatic Methods		
Impedance Techniques	ac Voltammetry (ac Polarography)			
	Electrochemical Impedance Spectroscopy			

The distinction between various electroanalytical techniques reflects the type of electrical signal used for the quantitation. The two principal types of electroanalytical measurements are potentiometric and potentiostatic. Both types require at least two electrodes (conductors) and a contact sample solution (electrolyte), which make up the electrochemical cell. The surface is therefore a junction between an ion conductor and an electronic conductor.

One of the two electrodes responds to the target analyte(s) and is therefore called the indicator (or working) electrode. The second, called the reference electrode, is at a constant potential (i.e. independent of the properties of the solution). Electrochemical cells can be classified as electrolytic (when they consume electricity from an external source) or galvanic (when they are used to produce electrical energy).

Potentiometry, which is of great practical importance, is a static (zero-current) technique in which the information about the sample composition is obtained from measurement of the potential established across a membrane. Different types of membrane materials, possessing different ion recognition processes, have been developed to impart high selectivity. The resulting potentiometric probes have thus been widely used for several decades for direct monitoring of ionic species.

Controlled-potential (Potentiostatic) techniques deal with the study of charge transfer processes at the electrode–solution interface and are based on dynamic (non-zero-current) situations. Here, the electrode potential is being used to derive an electron transfer reaction and the resultant current is measured. The role of the potential is analogous to that of the wavelength in optical measurements. Such a controllable parameter can be viewed as "electron pressure," which forces the chemical species to gain or lose an electron (reduction or oxidation, respectively). Accordingly, the resulting current reflects the rate at which electrons move across the electrode–solution interface. Potentiostatic techniques can thus measure any chemical species that are electroactive, that is, that can be made to reduce or oxidize. Knowledge of the reactivity of a functional group in a given compound can be used to predict its electroactivity. Nonelectroactive compounds may also be detected in connection with indirect or derivatization procedures [16, 17]. The advantages of controlled-potential techniques include high sensitivity, selectivity toward electroactive species, a wide linear range, portable and low-cost instrumentation, speciation capability, and a wide range of electrodes that allow assays of unusual environments.

II.1.1. Linear sweep voltammetry and cyclic voltammetry

Linear Sweep Voltammetry (LSV) and Cyclic Voltammetry (CV) were the first reported in 1938 and described theoretically in 1948 by Randles and Sevick. In effect rather than monitoring the response of an electrochemical system to a small amplitude periodic potential change, as AC impedance, in LSV and CV, a large periodic potential change is imposed on the system. Cyclic voltammetry is the most widely used technique for acquiring qualitative information about electrochemical reactions. The power of cyclic voltammetry results from its ability to rapidly provide considerable information on the thermodynamics of redox processes and the kinetics of heterogeneous electron transfer reactions and on coupled chemical reactions or adsorption processes. CV is often the first experiment performed in an electroanalytical study. In particular, it offers a rapid location of redox potentials of the electroactive species and convenient evaluation of the effect of media on the redox process. CV consists of linearly scanning the potential of a fixed working electrode (in a non-stirred solution), using a triangular potential waveform (Fig. 4). Depending on the information sought, single or multiple cycles can be used. During the potential sweep, the potentiostat measures the current resulting from the applied potential. The resulting current–potential plot is termed a cyclic voltammogram. The cyclic voltammogram is a complicated, time-dependent function of a large number of physical and chemical parameters.
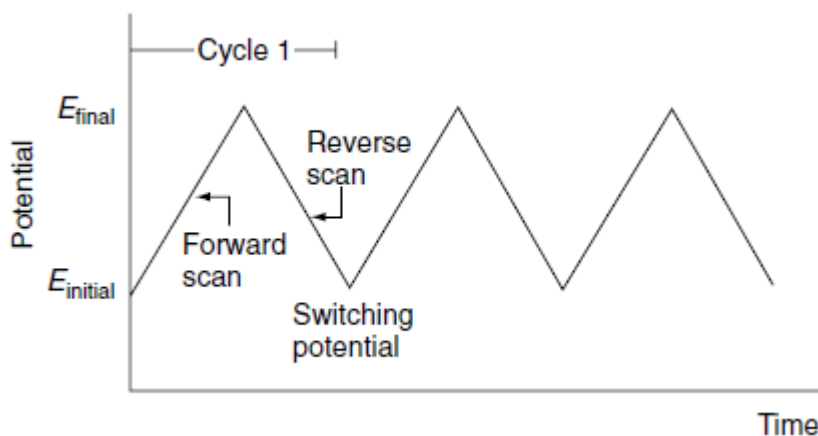
Figure 4: Potential–time excitation signal in a cyclic voltammetric experiment.

The cyclic voltammogram is characterized by several important parameters. Four of these observables, the two peak currents and the two peak potentials, form the basis of the diagnostics developed by Nicholson and Shain [18] for the analysis of the cyclic voltammetric response. The

cyclic voltammetric response can be discovered by solving the transport equations (in three-dimensions, x, y and x) [19]:

$$\frac{\partial [A]}{\partial t} = D_A \nabla^2 [A] \qquad (17)$$

and

$$\frac{\partial [B]}{\partial t} = D_B \nabla^2 [A] \qquad (18)$$

with D_A and D_B are the diffusion coefficients of A and B, respectively.

It is important to note that in the plotting of voltammetric data, i.e. current versus potential, there are a number of different axis conventions. In the conventional (or polarographic convention using mercury), negative potentials are plotted in the positive "x" direction, so the cathode currents (due to reductions) are positive. In the IUPAC convention, the opposite applies where positive potentials are plotted in the positive ''x'' direction, thus anodic currents (due to oxidations) are positive (in other conventions, current is plotted along the axis and/or a logarithmic current scale is used). In reality, the plotting is dictated by the software that is installed on your potentiostat and your geographic location (for example the USA and related countries favor the classical convention). However, one needs to become familiar with this concept as the literature presents voltammograms in mixed styles and one should ensure on first encountering a voltammogram that clarification is sought upon which potential sweep has been applied and understand which currents are anodic and which are cathodic.

In the 'reversible' limit the electrode kinetics are so 'fast' (relative to the rate of mass transport) that Nernstian equilibrium is attained at the electrode surface throughout the voltammogram with concentrations of A and B at the electrode surface governed by the Nernst equation (Eq. 19):

$$E = E_f^\circ(A/B) + \frac{RT}{F} \ln \frac{[B]}{[A]} \qquad (19)$$

where E is now the applied potential which defines the ratio of the surface concentrations $[A]_0$ and $[B]_0$ once $E_f^\circ(A/B)$ is specified.

In the case of an electrochemically reversible process with fast electron transfer, the peak-to-peak separation $\Delta Ep = (E_p^{ox} - E_p^{red})$ is relatively small at the reversible limit, where $\Delta Ep = 2.218RT/nF$, corresponding to a value of ca. 57 mV (at 298 K where n = 1). For the case of n electrons, the wave-shape of the voltammogram can be characterized by (Eq. 20):

$$E_p - E_{1/2} = 2.218 \frac{RT}{nF} \qquad (20)$$

Where $E_{1/2}$ corresponds to the potential at which half the peak current is observed. The magnitude of the voltammetric current Ip^{Rev} observed at a macroelectrode is governed by the following Randles–Ševc´ik equation (Eq. 21):

$$I_p^{Rev} = \pm 0.446\, nFAC(nFDv/RT)^{\frac{1}{2}} \qquad (21)$$

where the $\pm$ sign is used to indicate oxidation or reductive process respectively though the equation is usually devoid of such sign. The voltammetric diagnosis that the electrochemical process is undergoing a reversible heterogeneous charge transfer process is given by Equation 21 where ΔEp is independent of the applied voltammetric scan rate and: $I_p^{ox} / I_p^{Red} = 1$.

The question is; how can you determine if your observed voltammetry corresponds to this range? A key diagnostic is a scan rate study. As shown in Equation 21, the peak height (IP) is proportional to the applied voltammetric scan rate and a plot of I_p^{Rev} against $v^{1/2}$ should be linear [3-10].

It is important to note that when the position of the current maximum occurs at the same potential; this peak maximum, which does not shift in potential with scan rate, is characteristic of electrode reactions that exhibit rapid electron transfer kinetics, usually termed reversible electron transfer reactions.

The formal potential can be found as the mid-way between the two voltammetric peaks comprising the voltammogram (Eq. 22):

$$E_f^0 = \frac{\left(E_p^{Ox} + E_p^{red}\right)}{2} \qquad (22)$$

Assuming that the diffusion coefficient of the reagent and the product are equal, the cyclic voltammetric response for an irreversible electrochemical couple (in which the ΔE_P is larger than that observed for the reversible and quasi-reversible case) where appreciable over-potentials are required to drive the reaction, as evidenced by the peak height (maxima) occurring at a greater potential than that seen for the reversible case. It is evident that as the standard electrochemical rate constant, $k°$, is either fast or slow, termed 'electrochemically reversible' or 'electrochemically irreversible' respectively, changes in the observed voltammetry are striking. Since the electrochemical process, that is reversible or irreversible, reflects the competition between the electrode kinetics and mass transport, $(k° << m_T)$ indicating electrochemical irreversibility. Where m_T is the rate of mass transport and given by Eq. 23:

$$m_{T=}\sqrt{D(RT/Fv)} \quad (23)$$

The distinction between fast and slow electrode kinetics relates to the prevailing rate of mass transport given by '$k° \gg mT$' indicating electrochemical reversibility or '$k° \ll m_T$' indicating electrochemical irreversibility. Matsuda and Ayabe [20] introduce the parameter, ξ, given by Eq. 24:

$$\xi = k° \ (FDv \ /RT)^{1/2} \quad (24)$$

where the following ranges are identified at a stationary macroelectrode: $\xi \geq 15$ corresponds to the reversible limit '$15 > \xi > 10^{-3}$' corresponds to the quasi-reversible limit and '$\xi \leq 10^{-3}$' corresponds to the irreversible limit.

Reversible, quasi-reversible, and irreversible, all of which are linked to the mass transport rate. In reversible reactions, the electron transfer rate at all potentials is higher than the mass transport rate and the peak potential is independent of the applied voltammetric scan rate. In the case of quasi-reversible, the electron transfer rate becomes comparable to the mass transport rate. In this regime, the peak potentials increase with the scan rate applied. Finally, it is obvious that for the irreversible case, the electron transfer rates are lower than the mass transport rate; the summary by Matsuda and Ayabe is extremely useful [20]. The above conditions given by Matsuda and Ayabe show that the observed electrochemical behavior depends on the applied voltammetric

scan rate. In applying various scan rates the diffusion layer thickness dramatically changes, in the case of slow scan rates, the diffusion layer is very thick while at faster scan rates the diffusion layer is relatively thinner. Since the electrochemical process, that is, reversible or irreversible, reflects the competition between the electrode kinetics and mass transport, faster scan rates will encourage greater electrochemical irreversibility.

At macroelectrodes the Nicholson method is routinely used to estimate the observed standard heterogeneous electron transfer rate constant (k^o, cm s^{-1}) for quasi-reversible systems using the following equation (Eq. 24) [21];

$$\Psi = K^{\circ}[\pi D n \upsilon F / (RT)]^{-1/2} \quad (25)$$

Where Ψ is a kinetic parameter, D is the diffusion coefficient, n is the number of electrons involved in the process, F is the Faraday constant, R is the gas constant and T is the temperature (K). The kinetic parameter (Ψ) is tabulated as a function of peak-to-peak separation ($\Delta Epc \times n$) at a temperature (298 K) for a one electron process (where the charge transfer coefficient, $\alpha = 0.5$). A plot of Ψ against $[\pi D n \upsilon F / (RT)]^{-1/2}$ allows the standard heterogeneous rate transfer constant, k^o to be readily deduced.

The kinetic parameter was deduced as a function of ΔEpc by utilizing the Nicholson method. Note that there are some restrictions, in that the above method is based on the assumption that electron transfer kinetics are described by the Butler–Volmer formalism, α is 0.5, that the switching potential is 141 mV above the reversible $E_{1/2}$ and that the temperature is 298 K. Failure to strictly observe most of these factors will result in only minor errors. However, there is one experimental problem that can be serious: incomplete compensation of the solution resistance. Thus, the measurement error will be small at slow scanning speeds where currents and IR errors are generally low; however, potentiostats help to overcome this problem.

Table 2: *Variation of ΔEp with ψ at 25 °C* [21]

Ψ	$\Delta Ep \times n$ /mV
20	61
7	63
6	64
5	65
4	66
3	68
2	72
1	84
0.75	92
0.50	105
0.35	121
0.25	141
0.10	212

Beyond the limits of the Nicholson method, that is where the ΔEP is >200 mV (see Table 2), a suitable relationship has been reported by Klingler and Kochi [22]:

$$K° = 2.18 \sqrt{\left[\frac{D\alpha nvF}{RT}\right] \exp\left[-\left(\frac{\alpha^2 nF}{RT}\right)\left(E_p^{Ox} - E_p^{red}\right)\right]} \quad (26)$$

Thus two procedures are available for different ranges of ΔEP × n values, that is for low (Nicholson) and high values (Klingler and Kochi). Lavagnini et al. [23] proposed the following function of ψ (ΔEP), which fits Nicholson's data, for practical usage (rather than producing a working curve) (Eq. 27):

$$\Psi = (-0.6288 + 0.021X) / (1 - 0.017X) \quad (27)$$

Where X = ΔEp in mV used to determine the Ψ as a function of ΔEp.

The Randles–Ševc´ik equation for a quasi-reversible system (at 298 K) is given by Eq. 28:

$$I_p^{quasi} = \pm(2.65 \times 10^5)n^{3/2} ACD^{1/2} v^{1/2} \qquad (28)$$

For an irreversible system (those with slow electron exchange), the individual peaks are reduced in magnitude and widely separated. Totally irreversible systems are quantitatively characterized by a shift in the peak potential with scan rate as given by Eq. 29:

$$E_{p,c} = E_f^0 - \frac{RT}{\alpha n'F}\left[0.78 + ln\frac{D^{\frac{1}{2}}}{K^\circ} + 0.5\,ln(\frac{\alpha n'Fv}{RT})\right] \quad (29)$$

where a is the transfer coefficient, n' is the number of electrons transferred per mole before the rate determining step and where E_f^0 is the formal potential. Hence, E_P occurs at potentials higher than E_f^0, with the over-potential related to k° and α (the voltammogram becomes increasingly 'drawn out' as αn decreases). For the case of a fully irreversible electron transfer process, the Randles–Ševc´ik equation is Eq. 30:

$$I_p^{irev} = \pm 0.496\,(\alpha n')^{\frac{1}{2}}nFAC(nFDv/RT)^{\frac{1}{2}} \qquad (30)$$

where A is the geometric area of the electrode (cm^2), a is the transfer coefficient (usually assumed to be close to 0.5), n is the total number of electrons transferred per molecule in the electrochemical process and *n'* is the number of electrons transferred per mole before the rate determining step.

II.1.1.1. Study of reaction mechanisms
One of the most important applications of cyclic voltammetry is the qualitative diagnosis of the chemical reactions that precede or follow the redox process [18]. To classify these reaction mechanisms, the letters E and C (for redox and chemical steps, respectively) are generally used in the order of the steps in the reaction scheme. The occurrence of such chemical reactions, which directly affect the available surface concentration of electro active species, is common to the redox processes of many important organic and inorganic compounds. Changes in the shape of the cyclic voltammograms, resulting from chemical competition for the reagent or

electrochemical product, can be extremely useful in elucidating these reaction pathways and in providing reliable chemical information on reactive intermediates. For example, when the redox system is perturbed by a following chemical reaction using the notation of Testa and Reinmuth [24] this is described as EC mechanism (Eq. 31).

$$O + ne^- \rightleftharpoons R \longrightarrow Z \qquad (31)$$
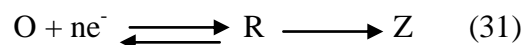
The cyclic voltammogram will display a smaller reverse peak (because the product R is chemically removed from the surface). The peak ratio of the forward and reverse peaks will thus be less than 1 (not equal); the exact value can be used to estimate the rate constant of the chemical step. In some (extreme) cases, the chemical reaction may progress so rapidly that all of R is converted to Z, resulting in no reverse wave being observed. Note that by varying the scan rate, further information on the rates of these coupled reactions can be obtained. In particular, the scan rate controls the time spent between the switching potential and the peak potential (during which time the chemical reaction occurs).

A specific example worth exploring is the EC' reaction defined as (Eqs. 32, 33):

$$A + e^- \rightleftharpoons B \qquad (32)$$

$$B + X \xrightarrow{K_2} A + P \qquad (33)$$
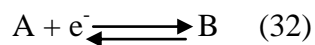
It is known that under certain conditions, a cyclic voltammogram of an EC' system will show two distinct peaks in the forward sweep [25]. This typically occurs when the initial concentrations of species 'A' and species 'X' are similar and when the second-order rate constant, K_2, is above a certain value. For low K_2, the voltammetry is similar to that observed for a simple one-electron reduction (the E mechanism) [26], as expected; however, as the rate constant increases, so too does peak current response. The explanation is as follows: a faster rate constant means a more rapid regeneration of 'A' within the diffusion layer and hence greater current. As K_2 is increased further, the waveform begins to split into two distinct peaks with greater K_2, resulting in a more obvious separation.

For a fast scan rate, this also leads to a decrease in peak height with increasing peak-to-peak separation, although the peak currents tend toward limiting values as K_2 increases and the peaks become more distinct. As illustrated in Fig.5.
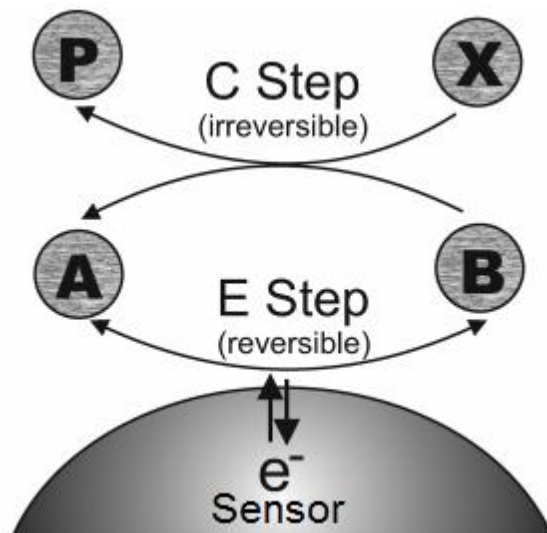
Figure 5: *Schematic of the EC' catalytic reaction mechanism.*

The net result of the process is the transformation of reactant species 'X' to product species 'P', catalyzed by species 'A' (which is regenerated). It is important to distinguish this form of catalysis from the case where the particle catalyzes the electron transfer 'A + e$^-$ $\longleftrightarrow$ B'; rather in this case, the A/B redox couple catalyzes the transformation of X to P. A series of papers by Saveant et al. [27-32] examining the 'homogeneous catalysis of electrochemical reactions' explored systems similar to the EC' mechanism resulting from a high second-order rate constant in experiment [30]. Following this, Compton et *al.* studied the EC' mechanism theoretically and experimentally at the channel electrode [33, 34] and at the rotating disk electrode [35-37]. Additionally, Dimarco et *al.* [38] studied the second-order EC' reaction on a planar surface. An example of such a catalytic EC process is the oxidation of dopamine in the presence of ascorbic acid [39]. The dopamine quinone formed in the redox step is reduced back to dopamine by the ascorbate ion. The peak ratio for such a catalytic reaction is always unity. Some other reaction mechanisms can be elucidated in the same way. For example, for a CE mechanism, where a slow chemical reaction precedes the transfer of electrons, the current ratio is generally greater than one, and approaches unity as the scan rate decreases. The reverse peak is rarely affected by the

coupled reaction, while the forward peak is no longer proportional to the square root of the scan rate [40]. ECE processes, with a chemical step being interposed between electron transfer steps.

Many anodic oxidations involve an ECE pathway [41]. For example, the electrochemical oxidation of aniline is another classical example of an ECE pathway [42]. The cation radical thus formed rapidly undergoes a dimerization reaction to yield an easily oxidized p-aminodiphenylamine product. Another example (of industrial relevance) is the reductive coupling of activated olefins to yield a radical anion, which reacts with the parent olefin to give a reducible dimer [43]. If the chemical step is very fast (in comparison to the electron transfer process), the system behaves as an EE mechanism (of two successive charge transfer steps). Powerful cyclic voltammetric computational simulators, exploring the behavior of virtually any user-specific mechanism have been developed [44]. Such simulated voltammograms can be compared with and fitted to the experimental ones. The new software also provides "movie" like presentations of the corresponding continuous changes in the concentration profiles.

II.1.1.2. Effect of pH

Consider the following process involving the uptake of m-protons and consumption of n-electrons (Eq. 24):

$$A + mH^+ + ne^- \rightleftharpoons B \qquad (34)$$
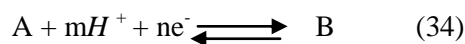
The limiting cases correspond to those of electrochemical reversibility and irreversibility. Here we consider the electrode process being fully electrochemically reversible, thus for the relevant Nernst equation we can write [45]:

$$E = E_f^0\left(^A/_B\right) + \frac{RT}{nF} \ln \frac{[A][H^+]^m}{[B]} \qquad (35)$$

$$E = E_f^0\left(^A/_B\right) + \frac{RT}{nF} \ln [H^+]^m - \frac{RT}{nF} \ln \frac{[B]}{[A]} \qquad (36)$$

$$E = E_f^0\left(^A/_B\right) - 2.303 \frac{RTm}{nF} pH - \frac{RT}{nF} \ln \frac{[B]}{[A]} \qquad (37)$$

Leading to:

$$E = E_f^0\left(A/B\right) - 2.303\,\frac{RTm}{nF}pH - \frac{RT}{nF}\ln\frac{[B]}{[A]} \quad (38)$$

$$E_{f,eff}^0 = E_f^0\left(A/B\right) - 2.303\,\frac{RTm}{nF}pH \quad (39)$$

where $E_{f,eff}^0$ is an effective formal potential. Provided $D_A = D_B$ the potential midway between the peaks for the reduction of (A) and the oxidation of (B) corresponds to $E_{f,eff}^0$ with the shape of the voltammogram being otherwise unaffected.Accordingly the midpoint potential varies by an amount of $2.303\,\frac{RTm}{nF}$ per pH unit. In the commonly seen case where m = n, this corresponds to ca. 59 mV per pH unit at 25 °C as in the following case. Experimentally, the cyclic voltammetric response is recorded over a range of pH's with the $E_{f,eff}^0$ (or more commonly 'peak potential') plotted as a function of pH. Fig.6 shows a typical response where the deviation from linearity is due to the pKa of the target analyte and the gradient from the linear part allows information on the number of electrons and protons transferred in the electrochemical process.
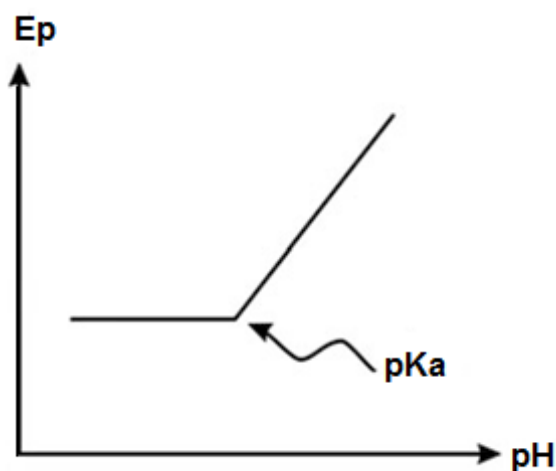
Figure 6: *A typical plot of peak potential, E_P versus pH.*

A real example reported by Laghrib et *al*. which utilizes a metallic silver electrode for the electrocatalytic reduction of PNA in 0.1 M Britton Robinson (B-R) buffer solution pH 2.0 [10]. The effect of buffer pH on cyclic voltammetric responses of the silver electrode was further

investigated in the pH range from 1.07 to 11.8. It was found that with the decrease of buffer pH bellow 2.0, the reduction peak potential shifted to the positive direction, implying that protons were involved in the electrode process. Once the pH of the solution exceeds pH 2.48, the peak potential of PNA reduction returns to its initial position -0.8 V obtained at carbon paste electrode (i.e. no catalytic effect of silver towards the reduction of PNA was observed). It is evident that there are two slopes; the first corresponds to 176.3 mV/pH over the pH range of 1–2.48 which is higher than the theoretical value of -59 mV/pH at 25 °C and elucidated that the transfer-electron numbers were fewer than those of the proton numbers taking part in this reaction [8]. The second slope is evident in the pH range of 2.48—7; a slope of 35 mV/pH is obtained which is very close to the Nernstian value. Additionally, it has been reported that a gradual decrease in the peak currents in this pH range which they attribute to the deprotonation of PNA molecules, which leads to an increase in the charge on the PNA molecules where the charged species is more soluble than the former species. Clearly, the use of pH measurements can help provide insights into electrochemical mechanisms.

II.1.1.3. Adsorption

In some instances, rather than having the analyte under investigation undergoing simply diffusional processes, the species of interest might adsorb onto the electrode surface and will give rise to different voltammetry. Fig. 9 shows a typically voltammetric profile where a unique shape is observed. Since the adsorbed species does not have to diffuse to the electrode surface, the observed voltammogram is symmetrical. The peak current can be related directly to the surface coverage ($\acute{\Gamma}$) and potential scan rate for a reversible process (Eq. 40):

$$I_P \frac{n^2 F^2 \acute{\Gamma} A v}{4RT} \quad (40)$$

Recall that a Nernstian behavior of diffusing species yields $v^{1/2}$ dependence. In practice, the ideal behavior is approached for relatively slow scan rates, and for an adsorbed layer that shows no intermolecular interactions and fast electron transfers. The peak area at saturation (i.e., the quantity of charge consumed during the reduction or adsorption of the adsorbed layer) can be used to calculate the surface coverage (Eq. 41):

$$Q = nFA\acute{\Gamma} \qquad (41)$$

This can be used for calculating the area occupied by the adsorbed molecule and hence to predict its orientation on the surface.
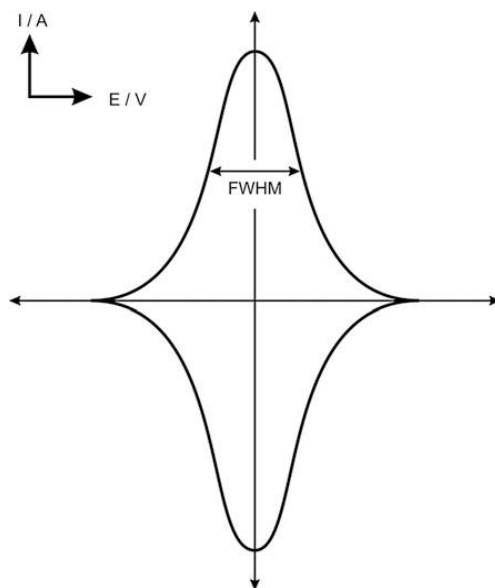
Figure 7: Cyclic voltammetric response for the reversible reaction of an adsorbed species

As shown in Fig. 7, the full width at half of the peak maximum height (FWHM) is given by (Eq. 42):

$$FWHM = 3.53RT/nF \qquad (42)$$

The diagnosis of an adsorbed species is to explore the effect of scan rate on the voltammetric response, which should yield a linear response for the case of *Ip versus* scan rate v. In real situations, the absorbed species may be weakly or strongly absorbed. In these contexts, one usually refers to the reactants that are adsorbed, but four scenarios can be encountered. Of note is that in the case of a strongly absorbed reactant there is a pre-peak before the solution phase voltammetric peak while in the case that the product is strongly adsorbed, the adsorption wave is seen following the solution phase peak. The effect of varying the voltammetric scan rate can be highly illuminating, for the case of a strongly adsorbed product, where at slow scan rates the

adsorption wave is large relative to the first diffusional peak. As the scan rate is increased, the current of the adsorption peak decreases in magnitude while the diffusional peak current increases. At very high scan rates the adsorption wave is absent [46, 47]. There is also another scenario which can give rise to unique voltammetry. In the context of studying new materials, such as carbon nanotubes and indeed graphene, researchers usually disperse their chosen nanotubes into a non-aqueous solvent and put aliquots onto the working electrode of their choice. This modified surface is allowed to dry to enable the solvent to evaporate leaving the nanotubes immobilized upon the electrode surface, which is now ready to be electrochemically explored (the so called drop-coating method). It has been shown that the nanotube modified electrode exhibits a porous surface where 'pockets' of the electroactive species are trapped in-between multiple layers of nanotubes and the trapped species act akin to that of a thin layer cell [48]. The porous nanotubes layer has a large surface area and the electrode is thought to be in contact with a finite, 'thin-layer' of solution (the species is trapped within the nanotube structure). In this case, a mixture of diffusional regimes exists.

II.1.1.4. Residual current

While applying a potential sweep, the current flowing through the cell before the charge transfer takes place is called the residual or background current. It is composed of the following components [49].

- **Faradaic Current**

It is generated from the faradaic process which is a non-adsorptive process arising from electron transfer across the metal or electrolyte interface. The redox reaction of solution species that takes place is controlled by Faraday's laws [50], that is, the amount of electricity which is passed (charge) is proportional to the number of moles of reactant converted. Electrode process where Faradaic process takes place is classified as charge transfer electrodes since the extent of reaction depends on the measured charge passing through the electrode surface.

- **Non-Faradaic Current**

It arises when the adsorption and desorption of ions from the electrode surface results in an electric current due to charging of double layer. The interface between the electrolyte and the

working electrode acts as a capacitor. Therefore, a current is required to change the potential applied to the working electrode and this is referred to as non-faradaic current. Since the potential in a CV experiment is constantly changing, there is an approximately constant charging current, which makes a major contribution to the background current. As there is no charge transfer across the double layer, it is not governed by faraday's laws and hence is called non-faradaic current. The charging current is directly proportional to the sweep rate whereas the faradaic current is directly proportional to the square root of scan rate.

II.1.2. Square Wave Voltammetry

Among the various voltammetric techniques, exceptional versatility is found in a method called square wave voltammetry, which was invented by Ramaley and Krause, and developed extensively by the Osteryoungs and their co-workers [12]. It's a differential technique in which potential waveform composed of a symmetrical square wave of constant amplitude is superimposed on a base staircase potential [40, 51]. More significant than each of its two components is the difference between the two, the net current, in the region of the peak which is centered on the half-wave potential. Capacitive contributions can be effectively discriminated before they disappear, since over a small potential range between the forward and reverse pulses, the capacitance is constant and is therefore canceled out by subtraction. It is the plot of the difference in the current measured in forward (if) and reverse cycle (ir), plotted against the average potential of each waveform cycle. In this technique, the peak potential occurs at the $E_{1/2}$ of the redox couple because the current function is symmetrical around the potential [52, 53].

Detection limits of ca. 10^{-8} M or lower are readily achievable under optimum conditions. The advantages over cyclic voltammetry are as follows: faster scan rates are possible (faster reactions can be studied), higher sensitivity (lower concentrations can be used) and a higher dynamic range (a larger range of concentrations can be investigated). Usually, in electrochemistry, solutions are vigorously degassed with; for example, nitrogen to remove oxygen which is electrochemically reduced and can interfere with the voltammetric measurement under investigation. A different way of greatly diminishing or eliminating the interference of oxygen, with no need for its removal, is by the use of the high frequencies employed in SWV. In fact, due to the irreversibility of oxygen reduction, the increase of its signal with frequency is small at high frequencies, and becomes negligible eventually, when compared with the response of the determinant [54].

II.1.3. Differential pulse voltammetry

As introduced earlier, voltammetry so far has been concerned with applying a potential step where the response is a pulse of current which decays with time as the electroactive species near the vicinity of the electrode surface are consumed. This Faradaic process (IF) is superimposed with a capacitative contribution (IC) due to double layer charging which dies away much more quickly, typically within microseconds. This technique was proposed by Barker and Gardner [55]. In pulse techniques such as differential pulse and square wave voltammetry, the capacitative contribution is eliminated via subtraction. Differential pulse voltammetry (DPV) measures the difference between two currents just before the end of the pulse and just before its application.

DPV is useful due to eliminations in the contribution of non-faradaic (capacitive) processes, which are effectively subtracted out. Additionally, DPV is useful for resolving the voltammetric signals due to two species with close half-wave potentials, producing easily quantifiable peak shaped responses.

II.1.4. Chronoamperometry

Chronoamperometry is commonly used either as a single potential step, in which only the current resulting from the forward step (as described above) is recorded, or double potential step, in which the potential is returned to a final value following a time period, usually designated as s, at the step potential. The electrochemical technique of chronoamperometry involves stepping the potential applied to the working electrode, where initially it is held at a value at which no Faradaic reactions occur before jumping to a potential at which the surface concentration of the electroactive species is zero, where the resulting current-time dependence is recorded. In this method, a pulse potential is applied to a working electrode and the current passing through the cell is determined versus time [56]. Changes in the current appear in response to rises or decreases in the diffuse layers of the analyte at the surface of the working electrode. According to the definition by the IUPAC, the diffuse layer is equal to the surrounding region of an electrode in which analyte concentrations are different from those in the bulk solution. By applying an appropriate potential to the system, the local concentration of the analyte drops to zero. Under these conditions, a concentration gradient is generated that provides analyte transfer through diffusion from a higher concentration section (bulk solution) to the electrode surface [57].

Chronoamperometric experiments are performed in either of two general forms: a single potential step (applying a forward potential step and recording the resulting current) or a double potential step (applying a forward potential and returning the potential to the initial value during a given period of time). Cottrell's equation captures the current obtained at each point in time after a high single potential step (or large overpotential) is applied in a reversible redox reaction (Eq. 43) [58]:

$$Ip = \frac{nFAC * \sqrt{D}}{\sqrt{\pi}\sqrt{t}} \quad (43)$$

where n is the stoichiometric number of the electrons transferred in the redox reaction, F is the Faraday's constant (96,485 C/equivalent), A denotes the electrode surface area (cm), and C and D are the concentration (mol cm^{-1}) and diffusion constant, respectively, of the electroactive species (cm s^{-1}) in the solution [58].

II.1.5. Electrochemical impedance spectroscopy

Electrochemical impedance spectroscopy (EIS) or alternative impedance method has seen a considerable increase in its popularity in recent years [59]. We call impedance when current flow a circuit containing resistors, capacitors or inductors or any combination of these. Among the most attractive aspects of (EIS) as a contrivance for investigating the electrical and electrochemical properties of materials and systems is the direct connection that frequently exists between the behavior of a real system and that of an idealized model circuit consisting discrete electrical components [60]. The investigator generally compares or corrects the impedance data to an equivalent-circuit, which is representative of the physical processes taking place in the system being investigated. This method studies the response of the system to the application of a low amplitude periodic AC signal. The measures are performed at different AC frequencies. The analysis of the system response contains information about the interface, its structure and the reactions that occur there. EIS at first applied to the determination of the double-layer capacitance [61–63] and in ac polarography [64–66]. It is also useful to investigate the kinetics of surface reactions [67]. This technique considered that it is non-invasive and can be applied in-situ [68]. Moreover, the frequency response tests are simple to perform and can be easily turned for greater

accuracy, using readily available sinusoidal generators and accurate measurement equipment. Impedance is basically the time-dependent resistance Z= V (t)/I (t) and contains both a real and imaginary part (Eq. 44):

$$Z\left(\omega\right) = Z_{Re} - j\, Z_{im} \quad \text{with } j = j = \sqrt{-1} \qquad (44)$$

Usually, the impedance varying with frequency is of interest and can be displayed in various ways. In a Bode phase plot, while, the phase angle (ϕ) is plotted as a function of the logarithm of the frequency ($\omega = 2\pi f$). The phase angle is the difference between the sinusoidal current and the potential response of the system.
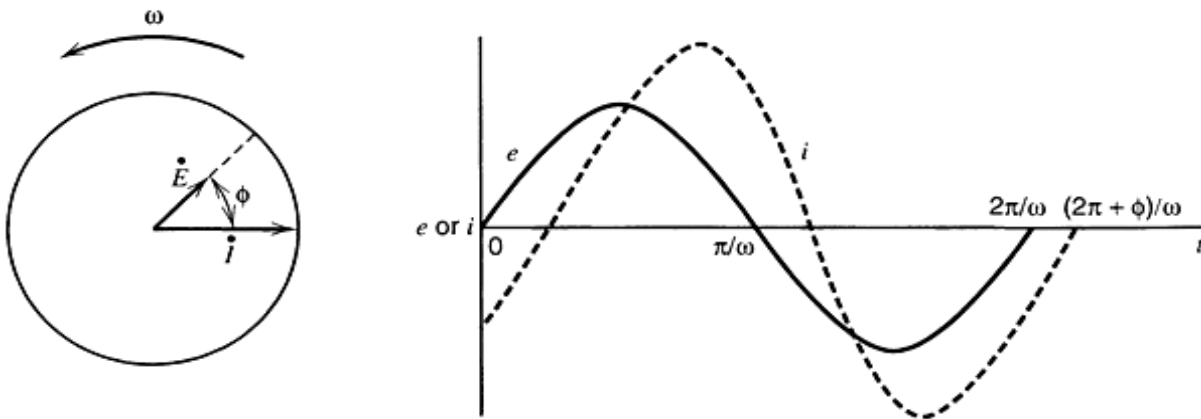
The most common plot is called a Nyquist plot, which displays Z_{Re} on the x-axis and $-Z_{Im}$ on the y-axis for different frequency values.

38
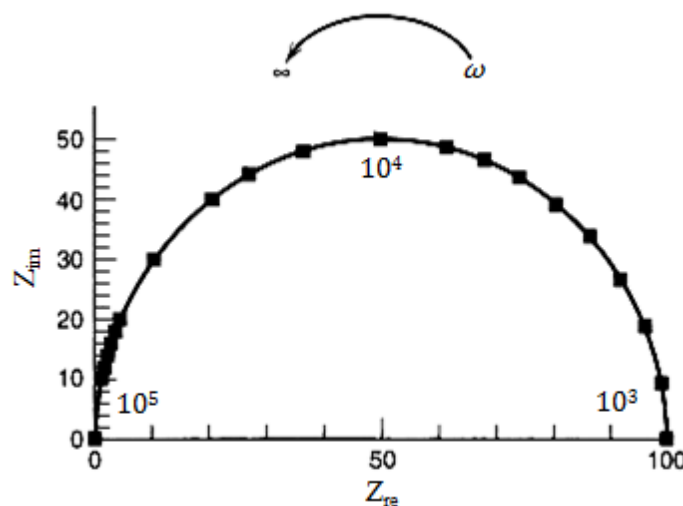
With reference to the Nyquist, the frequency is highest to the left and lowest to the right. The intercept with the x-axis gives the resistance. If the system was purely a resistor, the Nyquist plot would just be a dot on the x-axis at the resistance value - and consequently. The four elements of ohmic resistance, capacitance, constant phase element, and Warburg impedance (W) are used in the EIS analysis of electrolyte-based systems.
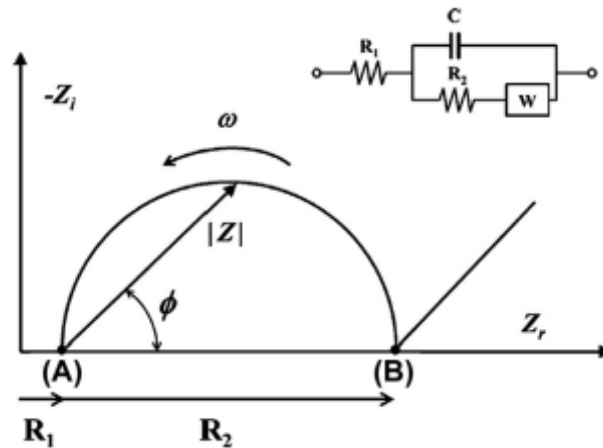
Figure 8: The typical Nyquist plot of an electrochemical cell containing working electrode into the electrolyte containing electroactive species and inset is the Randles' equivalent circuit.

To investigate the impedance behavior of each particular system, it is necessary to select an appropriate equivalent circuit.

Equivalent circuits are useful tools for approximating experimental impedance data, as they provide good descriptions of impedance components in parallel and/or in series. Randles circuit is most commonly used for electrodes immersed in electrolytes; it includes solution resistance (Rs), charge (electron) transfer resistance (Rct), capacitance of double layer (Cdl), and mass transfer element, shown as Warburg impedance (W) [15].

As seen in Fig. 8, in a typical Nyquist plot, the equation $\omega = 2\pi f = 1/R_{ct} C_{dl}$ is used to calculate the double-layer capacitance based on the frequency on the maximum point of the semicircle. A line at an angle of 45 degrees represents the Warburg limited behavior, which can be extrapolated from the real axis. Also, the intercept at this section is equal to Rs + R_{ct} –2σC_{dl}, in which s

represents the diffusion coefficient whose value can be subsequently calculated. In this method, Rs and Rct can be straightforwardly obtained from the points (A) and (B), respectively.

AC alternative impedance method is an analytical method frequently used in applied and fundamental electrochemical studies [69-70] as well as in some other domains [72]. The powerful aspect of the technique can be attributed to its ability to distinguish interfacial processes with different time constants [73]. It is a widespread and useful technique for characterizing electrode surfaces [74-78]. EIS has been widely used to investigate the procedures for biosensor fabrication. It also plays an essential role in the study of such different kinds of bioanalytical species as whole cells, proteins, microorganisms, nucleic acids, antigens, and antibodies [79-81].

Ismail et *al.* [82] used the EIS technique to examine clustered mineral ions. In the pathological calcification of the cardiovascular system, this agent is known to be a cause of high mortality. Inhibition of ectopic calcification is based on two modes: (1) formation of various acidic serum proteins, calciprotein particles, nanospherical complexes of calcium phosphate mineral, and fetuin-A and (2) stability of calcium phosphate prenucleation clusters using a fetuin-A monomer [82, 83] designed a monoclonal antibody immunosensor based on AgNPs to determine the presence of doxorubicin, an important anticancer drug, in human serum samples using the EIS-based technique. The results indicate that the immunosensor served as a useful tool in a clinical laboratory for screening picogram quantities of doxorubicin [83].

II.2. Introduction to electrochemical cells

The vessel used for a cyclic voltammetry experiment is called an electrochemical cell. A schematic representation of an electrochemical cell is shown in Fig.9. The cell is usually a covered beaker of 5–50mL volume, and contains the three electrodes (working, reference, and auxiliary), which are immersed in the sample solution. The exact cell design and the material used for its construction are selected according to the experiment at hand and the nature of the sample. The various designs differ with respect to size, temperature control capability, stirring requirement, shape, or number of cell compartments. The following sections describe the role of each component and how to assemble an electrochemical cell to collect data in voltammetry experiments.
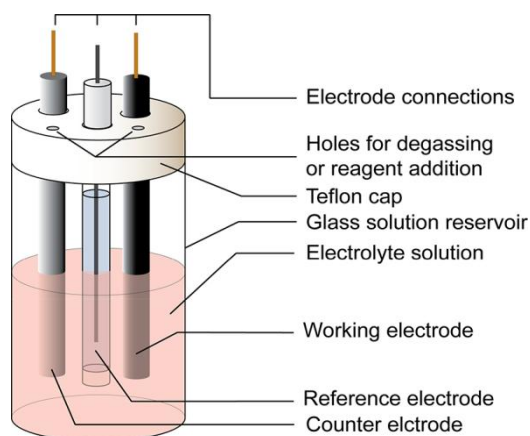
Figure 9: *Schematic representation of an electrochemical cell for electrochemical experiments.*

II.2.1. Supporting electrolytes

All ionic salts or ionisable compounds in a solvent are defined as supporting electrolytes. It is very important to realize that they can influence the electrochemical processes in a number of ways. These electrolytes impart conductivity to the solvent and hence enable continuous current flow in solution. The salient features of supporting electrolyte are, they must remain electroactive in the potential region of interest, the concentration of the supporting electrolyte should be very high, in order that they do not form space charges near the surface and hence the space charge potential do not influence the charge transfer kinetics. They should not get adsorbed on the surface, in which case they can catalyze or inhibit other reactions. They should neither form ion pairs with anion radicals formed in the electrode process nor form complexes with the reactants or products. Supporting electrolytes are required in controlled-potential experiments to decrease the resistance of the solution, eliminate electromigration effects, and maintain a constant ionic strength (i.e., "swamping out" the effect of variable amounts of naturally occurring electrolyte) [84]. H_2SO_4, $HClO_4$, and HCl are normally employed for studies in acidic aqueous solutions and NaOH or KOH are employed for alkaline media. In neutral region, if buffering is important, acetate, citrate, pyrophosphate and phosphate buffers are usually employed. B-R buffer is used over a wide pH range. If the redox process does not involve acid-base reactions, no buffer is needed and any electrolyte may be used. Buffer systems are used when a pH control is essential. The composition of the electrolyte may affect the selectivity of voltammetric measurements. For example, the tendency of most electrolytes to complex metal ions can benefit the analysis of

mixtures of metals. In addition, masking agents [such as ethylene-diamine-tetra-acetic-acid (EDTA)] may be added to "remove" undesired interferences [85]. The supporting electrolyte should be prepared from highly purified reagents, and should not be easily oxidized or reduced (hence minimizing potential contamination or background contributions, respectively). The usual electrolyte concentration range is 0.1–1.0 M, i.e., in large excess of the concentration of all electroactive species.

II.2.2. Type of electrodes

The advent of modern electrochemistry has created the need for new electrodes and electrode setups. The most common arrangement today is the electrochemical cell with three different electrodes: a working electrode (WE), a counter electrode (CE), and a reference electrode (RE). While the current flows between the working electrode and the counter electrode, the reference electrode is used to accurately measure the applied potential relative to a stable reference reaction.

II.2.3. Reference Electrode

A reference electrode has a well defined and stable equilibrium potential. It is used as a reference point against which the potential of other electrodes can be measured in an electrochemical cell. The applied potential is thus typically reported as "versus" a specific reference.

There are a few commonly used (and usually commercially available) electrode assemblies that have an electrode potential independent of the electrolyte used in the cell. Some common reference electrodes used in aqueous media include the saturated calomel electrode (SCE), standard hydrogen electrode (SHE), and the AgCl/Ag electrode. These reference electrodes are generally separated from the solution by a porous frit. It is best to minimize junction potentials by matching the solvent and electrolyte in the reference compartment to the one used in the experiment.

At 25°C, the formal potential for the SCE half reaction lies 0.2415 volts more positive than the SHE reference electrode. A potential measured against using an SCE can be reported versus the SHE simply by adding 0.2415 volts to it. For work in aqueous systems, the "silver-silver chloride" or "Ag/AgCl" reference is quite popular. The half reaction for this reference electrode is as follows (Eq. 45):

$$\text{AgCl}_{(s)} + e^- \ \text{---} \!\!\!\rightarrow \ \text{Ag}_{(s)} + Cl^-_{(aq)} \qquad (45)$$

The actual potential assumed by an Ag/AgCl reference depends only on the activity of the chloride anion. (The other two species appearing in the half reaction are solids which always have unit activity.). To serve as a reference, the chloride activity needs to be held constant. To accomplish this, a silver wire (coated with a layer of silver chloride) is immersed in an internal solution saturated with potassium chloride. The chloride ion concentration remains fixed at the saturation limit. The shorthand notation for this reference electrode half cell is given below (Eq. 46):

$$\text{Ag}_{(s)} / \text{AgCl}_{(s)} / \text{KCl } (aq, sat'd), \text{ AgNO}_{3\,(aq)} // \qquad (46)$$
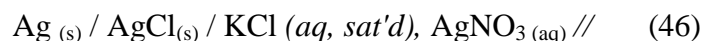
Electrical contact is made by a direct connection to the silver wire, and the internal electrode solution is placed in ionic contact with the test solution via a salt bridge or porous glass frit.

II.2.4. Counter Electrode

In traditional two electrode cells that have only a working electrode and a reference electrode, current is necessarily forced to flow through the reference electrode whenever a measurement is made. If enough current flows through a reference electrode, its internal chemical composition may be significantly altered, causing its potential to drift away from the expected standard value. For this and other reasons, it is desirable to make electrochemical measurements without current flowing through the reference electrode. Modern three and four electrodes potentiostats use a feedback circuit to prevent this from happening, but this feedback circuit requires that an additional auxiliary electrode be introduced into the electrochemical cell. This auxiliary (or counter) electrode provides an alternate route for the current to follow, so that only a very small current flows through the reference electrode.

Because current flows at the auxiliary electrode, electrochemical processes will also occur there. If the working electrode is reducing something, then the auxiliary electrode must oxidize something and vice versa. The products generated at the auxiliary electrode, if allowed to diffuse to the working electrode, may interfere with the experimental measurement. When this is a problem, the auxiliary electrode is placed in a separate compartment containing an electrolyte

solution that is in ionic contact with the main test solution via a glass frit. In most cases, however, the auxiliary can be placed right in the test solution along with the reference and working electrodes.

When studying a reduction at the WE, oxidation occurs at the CE. As such, the CE should be chosen to be as inert as possible. Counter electrodes can generate byproducts depending on the experiment; therefore, these electrodes may sometimes be isolated from the rest of the system by a fritted compartment [86].

II.2.5. Working Electrode

The working electrode carries out the electrochemical event of interest. A potentiostat is used to control the applied potential of the working electrode as a function of the reference electrode potential. The most important aspect of the working electrode is that it is composed of redox inert material in the potential range of interest. The type of working electrode can be varied from experiment to experiment to provide different potential windows or to reduce/promote surface adsorption of the species of interest.

The ideal working electrode is very clean metal surface with a well-defined geometry that is in direct contact with an electrochemical test solution. Working electrodes intended for general purpose work are usually made from a metal that is electrochemically inert over a wide range of potentials. The most widely used metals are mercury, platinum, gold, and various forms of carbon. Solid metals are typically fashioned into disks surrounded by a chemically inert shroud made from Teflon, glass, or epoxy. Mercury, being a liquid, tends to be used as a spherical droplet in contact with the solution. For cleaning electrodes, the polishing procedure varies according to the type of electrode and may vary from one laboratory to another. When using electrodes such as glassy carbon or platinum; clean electrode surfaces can be prepared by mechanical polishing (Fig. 10). To remove particles, the electrode is then sonicated in high-purity water [87]. It is often necessary to perform several CV scans in a single electrolyte through a large potential window to remove any remaining adsorbed species from the polishing procedure. This can be repeated until the scans overlap and no peaks are observed. This procedure is sometimes referred to as "pre-treatment" of the electrode [88].
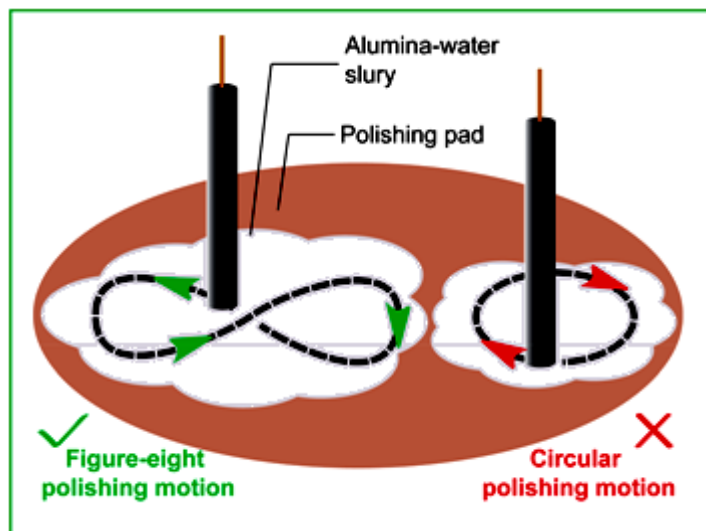
Figure 10: *Schematic illustration of the mechanical polishing procedure*

It is necessary to polish the electrode prior to measurements, and often, electrodes need to be repolished between measurements over the course of an experiment because some analytes are prone to electrode surface adsorption. To determine if an analyte is adsorbed to the electrode surface, a simple rinse test can be performed: after recording a voltammogram, the WE is rinsed and then transferred to an electrolyte-only solution. If no electrochemical features are observed by CV, this rules out strong adsorption (although not weak adsorption). Since electrodes are capable of adsorbing species during an experiment, it is good practice to polish them after every experiment. Ideally, separate polishing pads are used before and after experiments to avoid contamination. The size and shape of the electrode surface also affects the voltammetric response of the electrode. Different electrode materials can also lead to varying electrochemical responses, such as when electron transfer kinetics differ substantially between electrode types, when adsorption occurs strongly on only certain electrode materials, or when electrode specific reactivity with substrates occurs. As such, changing the electrode material is a good first step to diagnose and assess these issues [89].

II.2.5.1. Mercury Electrodes

For many years, mercury electrodes have been considered preferred electrodes because of their wide range of cathodic electroactivity, reproducibility and high sensitivity, allowing the detection of a high number of trace elements with long term unmatched performance [90-92]. However,

these electrodes are mechanically unstable, which proves to be very limiting, particularly for redissolution voltammetry analyses during which they are subjected to convection forces (agitation, ultrasound, etc.) [93, 94]. Furthermore, these electrodes have a restricted anodic range which excludes the analysis of certain metals. With regard to the toxicity caused by mercury, mercury electrodes have been subjected to restrictions by health organizations and their use is now undesirable, even in reduced quantities.

II.2.5.2. Platinum Electrodes

The platinum electrode is very frequently used because it has a high resistance to oxidation. In aqueous solution, in the absence of dissolved oxygen, the platinum electrode can work, depending on the pH, from -1.1 V to +1 V (compared to the normal hydrogen electrode, (NHE). It overlaps at positive potentials (E > 1 V/NHE) with platinum oxide which only redissolves below 0.65 V / ENH. In addition, it can adsorb many substances, which leads to a high residual current and surface blocking phenomena. Some applications for platinum electrodes include the determination of cadmium [95], silver ions [96] and mercury [97].

II.2.5.3. Gold Electrodes

The Gold working Electrode has similar properties to the Platinum Electrode but is more inert at positive potentials and allows slightly more negative potentials to be reached than those reached by the Platinum Electrode. The gold electrode currently occupies an important place in the electroanalytical field due to its electrochemical performance in organic and inorganic analysis [98]. Several researchers have shown that the gold electrode can be used as a carrier for a thin film of mercury for the simultaneous determination of lead, cadmium, and copper [99, 100].

II.2.5.4. Carbon Electrodes

Solid electrodes based on carbon are currently in widespread use in electroanalysis, primarily because of their broad potential window, low background current, rich surface chemistry, low cost, chemical inertness, and suitability for various sensing and detection applications. In contrast, electron transfer rates observed at carbon surfaces are often slower than those observed at metal electrodes. Electron transfer reactivity is strongly affected by the origin and history of the carbon surface [101, 102].

Numerous studies have thus been devoted for understanding the structure–reactivity relationship at carbon electrodes [101]. The type of carbon, as well as the pretreatment method, thus has a profound effect on analytical performance. The most popular carbon electrode materials are those involving glassy carbon, carbon paste, carbon fiber, screen-printed carbon strips, carbon films, or other carbon composites (e.g., graphite epoxy, wax-impregnated graphite, Kelgraf). The surface of a carbon electrode usually needs to be polished quite frequently, and the surface sometimes has to be "activated" by various empirical methods in order to obtain maximal performance from the electrode.

II.2.5.5. Chemically Modified Electrodes

Chemically modified electrodes (CMEs) represent a modern approach to electrode systems. These electrodes rely on the placement of a reagent onto the surface, to impart the behavior of that reagent to the modified surface. Such deliberate alteration of electrode surfaces can thus meet the needs of many electroanalytical problems and may form the basis for new analytical applications and different sensing devices. Such surface functionalization of electrodes with molecular reagents has other applications, including energy conversion, electrochemical synthesis, and microelectronic devices. There are different directions by which CMEs can benefit analytical applications. These include acceleration of electron transfer reactions, preferential accumulation, or selective membrane permeation. Such steps can impart higher selectivity, sensitivity, or stability on electrochemical devices. These analytical applications and improvements have been extensively reviewed [103–105]. Many other important applications, including electrochromic display devices, controlled release of drugs, electrosynthesis, fuel cells, and corrosion protection, should also benefit from the rational design of electrode surfaces.

In the last 30 years, considerable progress has been made in the development of 'tailor-made' electrode surfaces by chemical modification [106–110, 103, 111–113] of electrodes surfaces with electroactive polymer films. A comprehensive description of electroactive polymer-modified electrodes can be found in the book edited by M. Lyons [114]. The redox groups can be introduced by coordination, electrostatic binding or covalent attachment to the polymer backbone. Many of these systems employ charged polymers or polyelectrolytes that confer on them particular properties due to the existence of electrical charges in the polymer structure. Oyama and Anson [115, 116] introduced polyelectrolytes at electrode surfaces by using

47

poly(vinylpiridine), PVP, and poly-(acrylonitrile) to coordinate metal complexes via the pyridines or nitrile groups pending from the polymer backbone. Thomas Meyer's group at North Carolina [117] also employed poly(vinylpyridine) to coordinate Ru, Os, Re and other transition-metal complexes by generating an open coordination site on the precursor-metal complex.

Oyama and Anson [118] introduced in 1980s ion-exchange polymers on electrodes by incorporating redox-active counter ions to an electrode modified with polyelectrolytes by 'electrostatic binding'. The polycation poly(vinylpyridine) (PVP) was used to bind $Fe(CN)_6^{3/4}$ and deprotonated poly(acrylic acid) to bind $Ru(NH_3)_6^{2/3+}$ [118]. Other cationic polyelectrolytes besides poly(vinylpyridine) such as poly(lysine) and several anions with multiple charges like $Fe(CN)_6^{3/4}$, $IrCl_6^3$, $Mo(CN)_8^4$, and so on were employed. Among the polyanions, poly(styrene sulfonate), PSS was one of the first choices with redox-active cations such as $Ru(bpy)_3^{3/2+}$ and, $Co(bpy)_3^{3+}$. Of special interest is the use of perfluoro sulfonated poly(ethylene), Dupont de Nemours' Nafion, with fluorocarbon hydrophobic backbone and sulfonates that provide hydrophilic environment. The third approach has been to graft the redox couple by means of a covalent bond to the polyelectrolyte backbond as described early in 1965 in the book of Cassidy and Kun [119]. Several of these systems are charged polymers in at least one oxidation state, like poly(viologen), poly(vinylferrocene), and so on. Examples of polyelectrolytes like polyacrylic acid with covalently bound viologen were reported by Fernandez, Katz and coworkers [120], hydroquinone [121] and Anson et al. with bound ferrocene [122].

The latter method offers precise control of the film thickness (and often the morphology) and is particularly attractive in connection with miniaturized sensor surfaces. These materials may also include other additives, such as DNA, polysaccharide, activated carbon, phosphate-based materials, clay, and metal or metal oxide particles, among others, to gain sensitivity and selectivity toward the desired analyte. In general, the resulting materials are usually packed into polypropylene syringes, Teflon, plastic, or glass tubes. The electrical contact is made through a copper wire inserted in the paste or a stainless steel screw, and the surface is renewed by expelling an excess of paste and then polishing it into a soft paper. Surfactants, such as sodium dodecyl sulfate (SDS) and Triton X-100, have been lately used as binders, since the latter improve the conductivity of the paste material and, depending on the molecular structure, can also provide catalytic properties or selectivity toward certain compounds. The electrodes can be

modified by immersion, drop coating, impregnation, electrodeposition of different molecules, polymers, biomolecules or metals, or using metals nanoparticles.

III. Surface modification methods

III.1. Electrodeposition

Electrodeposition is a technology for the production of metals, alloys or composite films, characterized by a unique simplicity of implementation, low capital cost, and high versatility. This technique has been in use since the nineteenth century for the deposition of decorative films, as well as coatings that impart better corrosion resistance, or improved mechanical or wear properties [123, 124].

However, over the past 40 years, electrodeposition has been applied to various aspects of manufacturing in electronics, leading to revolutionary advances; with an increased understanding of its fundamentals, it is being utilized today in an ever wider set of applications.

Electrodeposition refers to a film growth process which consists in the formation of a metallic coating onto a base material occurring through the electrochemical reduction of metal ions from an electrolyte. The corresponding technology is often known as electroplating. Besides the production of metallic coatings, electrochemical metal reduction is also used for the extraction of metals starting from their ores (electrometallurgy) or for the reproduction of molds to form objects directly in their final shape (electroforming). In most cases, the metallic deposit thus obtained is crystalline; this process can therefore be called also electrocrystallization [124]. In principle, metal deposition is possible from simple solutions of some salt or other soluble compound containing the metal in the form of cation, anion or complex (electrically charged or uncharged). One component solutions are however rarely used in practice since they do not provide high-quality deposits. Electrolytes used in practice do contain some additional compounds, each playing a specific role. To increase the electrical conductivity of the solution, inorganic acids or alkali are added; more conductive electrolytes permit to decrease voltage (and therefore save energy) and to increase the uniformity of deposit thickness. Substances taking no part in electrode processes are called "supporting electrolytes". Moreover, acids and alkali are also used for adjusting pH; the standard recipes of plating solution compositions indicate optimum pH values. Acidity has to be stable and constant throughout the entire bath (the cell

volume) including the region near the electrode; this is achieved by addition of buffering agents (e.g. boric acid in nickel deposition). Buffering is especially necessary when hydrogen evolution occurs because the latter leads to higher pH near the electrode as a consequence of H+ consumption, resulting eventually in metal hydroxide precipitation. The value of acidity near the electrode can differ from that of the bulk by several pH units [123, 124].

Along with these most important components, so-called 'additives' are also widely used in practice. Examples of this sort of substances are surfactants added to the solution to decrease the surface energy of the electrode and facilitate the detachment of hydrogen bubbles from the surface. Adhesion of hydrogen bubbles to the electrode leads to undesirable 'pitting, which is the occurrence of macroscopic point defects (pits or pores) at the plated surface [125].

The selection of the most appropriate material to be used in the electrodeposition of the coating of interest is based first of all on the functional requirements imposed on the coating; in some cases, a unique material is suitable to perform the function sought for, while in other cases alternatives may exist. For any metal or alloy that can be deposited from aqueous solutions, there usually exist several types of electrolytes that permit to obtain a deposit with a suitable microstructure and properties. This raises the question of selection of the optimum solution.

Common rules in this respect do not exist so we shall restrict our consideration to some typical examples. In choosing a particular deposition process, we must start from the distinction between acid and alkaline electrolytes. Acidic solutions allow very high current densities to be used and can therefore produce thick coatings in a short time; however, they generally have a low power of attraction and are therefore only satisfactory for simple shaped articles.

From the point of view of alkaline cyanide or ammonia electrolytes, they tend to be much better. In most cases, cyanide solutions give more uniform and protective deposits. Cyanide solutions, on the other hand, have several disadvantages that discourage their use. Most importantly, these solutions are highly toxic and their use is strongly discouraged and regulated by law. In addition, the deposition rate and current efficiency are much lower than those of other electrolytes. Finally, cyanide and non-cyanide alkaline solutions contain organic additives in the presence of which hydrogenation of steel can occur.

III.1.1. Chemical and Electrochemical Degreasing

In the preliminary cleaning process, various operations are carried out to remove greasy compounds and oxide films from the surface to be metalized, which can prevent adhesion and affect the appearance of the deposit. Indeed, the metal may only be successfully deposited on a sufficiently clean surface, which in practice is contaminated by several types of greases, namely fatty compounds (oils and fats of vegetable or animal origin) and mineral oils. A metal surface is also covered with oxide layers or scale that must also be removed. Overall, the type and amount of foreign matter usually present on the surface depends on the history of the item.

In order to clean the surfaces, degreasing, which may be chemical or electrochemical, must first be carried out.

- *Chemical Degreasing*—alkaline degreasing is done in an aqueous solution of an alkaline degreasing agent, usually with a mixture of surfactants. The main components of alkaline agents are sodium hydroxide and potassium phosphate. The degreasing action consists of the dissolution of the grease and its emulsification. In order to obtain the effectiveness of the degreasing, the temperature of the degreasing bath must be maintained above 50°C. This method of degreasing therefore has a high energy demand.

  During its service life, the bath gradually fills up with emulsified grease and when a certain level of saturation has been reached, it is then filled with emulsified grease. Alkaline degreasing should always be followed by rinsing to avoid damage to the acid pickling bath. Acid degreasing is becoming increasingly popular. Commonly used agents that also utilize surfactants usually involve the action of phosphoric acid in a mixture with nitric, sulfuric or hydrochloric acid. Acidic degreasing agents work at the ambient temperature; thus they do not require costly heating and reduce the production of hazardous waste. However, they may have lower efficiency than alkaline agents.

- *Electrochemical Degreasing*— (Both cathodic and anodic) is very effective and widely used along with chemical cleaning. The solutions are the same as with chemical degreasing (with the exception of sodium silicate). These processes are characterized by the evolution of gas bubbles—hydrogen or oxygen, respectively— whereby the bubbles capture the impurities when they separate from the surface.

These processes are carried out at 70°C, and using cathodic or anodic current densities of 3–6 A/dm^2. The duration of cathodic degreasing is about 1min; that of the anodic process 5–20s. (In the case of steel up to 5min). Electrochemical degreasing however presents some drawbacks [123, 124, 126].

- *Pickling*—oxides and some other compounds present at the surface and capable to reduce adhesion of a deposit, or even to prevent deposition, cannot be removed with cleaning procedures. These substances can form either a thick scale or a thin tarnishing film, which are usually removed by pickling in a sufficiently acidic or sometimes alkaline solution. This is often done in combination with mechanical removal methods: grinding, brushing, etc [123]. The specific process to be used depends to a large extent on the substrate material but the majority of solutions consist of a mixture of acids (H_2SO_4, HCl, HNO_3, H_3PO_4, and HF) or NaOH. The acidic solutions are usually preferred but the alkaline ones may be used for a previous treatment of heavily oxidized surfaces, in order to loosen the oxide layer. Furthermore, the addition of inhibitors, which do not affect the rate of oxide dissolution while simultaneously inhibiting chemical dissolution of the metal, is very useful [124].

III.2. Impregnation

The term impregnation can be defined as the distribution of chemicals and or/metals in the pores of electrodes. Recently, the impregnation of metals is one of emerging fields of research. In the impregnation method, the chemicals species are blended inside the pores physically to modify the surface. The preparation technique is simple and generally carried out in two steps. Reported research works on the impregnation of carbon pate electrode with silver [9, 127], alumina oxide [128], and nickel oxide [129] are gaining wide interest because of their significantly high sensitivity and electrocatalytic capacity towards nitroaromatics, phenolic, and pharmaceutical compounds, and pesticides. Impregnation can be made by different methods:

II.2.1. Impregnation by soaking, or with an excess of solution

Excess liquid is eliminated by evaporation or by draining. Deposition of the active element is never quantitative. The quantity deposited depends on the solid/liquid ratio. Deposition is slow,

requiring several hours or days. Extensive restructuring of the surface (loss of surface area, etc.) may occur. However, the method allows the distribution of the species to be very well controlled and high dispersions may be obtained. The method works best if ion/solid interactions are involved.

II.2.2. Dry or pore volume impregnation

The required amounts of components are introduced in the volume corresponding to the pore volume of the support. The method is best suited to deposition of species which interact very weakly with the surface, and for deposition of quantities exceeding the number of adsorption sites on the surface. If the number of species which can adsorb on the surface is smaller, a chromatographic effect may occur, i.e. attachment to the mouth of the pores. Redistribution inside the pores is very slow.

II.2.3. Incipient wetness impregnation

A procedure similar to dry impregnation, but the volume of the solution is more empirically determined to correspond to that beyond which the catalyst begins to look wet.

II.2.4. Solid-Solid reactions

In certain cases it is possible to use a solid salt of the active element, e.g. a nitrate, to impregnate the support. This is done by dry mixing. The method is well adapted to industrial production but is difficult to use reproducibly in a laboratory.

III.3. Noble metal nanoparticles

The real explosion of work on nanosciences, particularly on nanomaterials, does not prevent us from going back in time and observing that nanomaterials were previously prepared and regularly used for heterogeneous catalysis more than 60 years ago [130−132]. Effectively, the supported metal catalysts were based on near-nanometer size metal crystallites, and catalytic reactions with zeolite materials occurred in nanopores smaller than 1 nm, where strong confinement effects had an impact on reactivity [133, 134]. The structure-reactivity correlations for metallic catalysts have already been established by previous researchers using available techniques such as transmission electron microscopy and gas chemisorption.

The relative activities of the metal atoms on the edges, corners, and facets of crystals during different catalytic reactions were then investigated, and the reactions on the metal catalysts were classified into structure-sensitive and non-structure-sensitive reactions [135]. These studies showed that it was possible to rationalize the impact of the size of the supported metal nanoparticles on their catalytic reactivity [136]. With the characterization techniques available at that time, it was obvious that it was not possible to visualize metal particles below 1 nm. Nevertheless, the electronic properties of metal particles are expected to change significantly when they fall below 1 nm (see Fig. 11). Therefore, subnanometric metal particles could be expected to interact differently with reagents, showing distinct reactivity to larger nanoparticles [137].

The most frequently and widely used metals are silver and gold nanoparticles (AgNPs and AuNPs), though metal plasmonic nanoparticles can also be fabricated from aluminum, copper, palladium, and platinum [138]. On the basis of the dielectric properties, copper should also have good performance, but its propensity to oxidize limits the use of copper nanoparticles. Typically, the surface plasmonic qualities of transition metals, such as titanium, cobalt, and nickel, are less compelling than those of the coinage metals [139].

There are multiple reasons for the dominance of AgNPs and AuNPs in plasmonic nanoparticle research. AgNPs and AuNPs can be tuned to absorb and scatter light throughout the visible and near-infrared regions (i.e., Ag LSPRs can range from 300 to 1200 nm). AuNPs are chemically inert, oxidation-free, and show high biocompatibility, which is critical for biomedical applications [140]. Moreover, various synthetic strategies to produce different shapes and sizes of AuNPs and AgNPs have been explored, thereby addressing their application in the areas of energy, catalysis, sensing, and biotherapy [141−146].
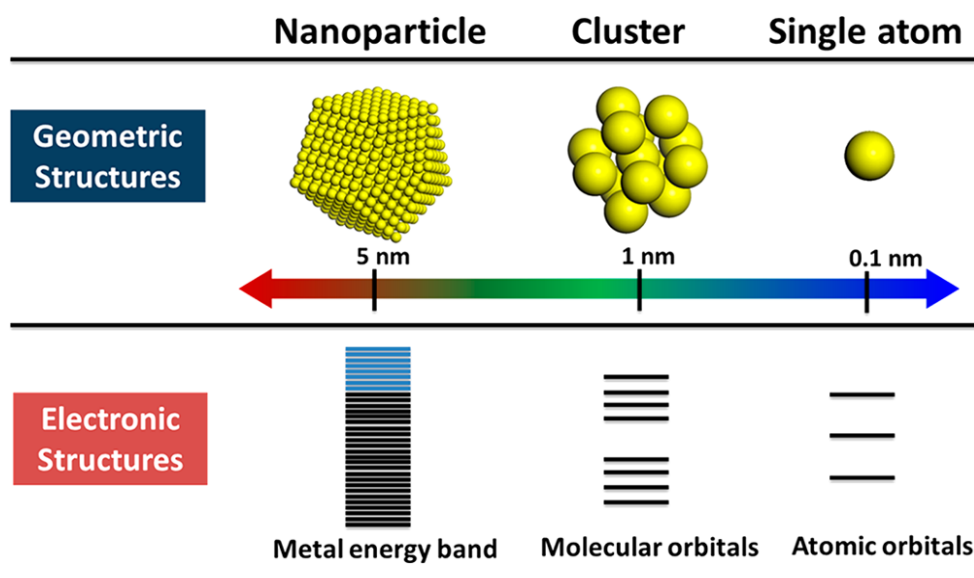
Figure 11: *Geometric and electronic structures of single atom, clusters, and nanoparticles.*

The life of nanoparticles, including plasmonic nanomaterials, can be divided into three stages: preparation, storage, and application. Especially for plasmonic nanoparticles, whose size, morphology, and chemical stability determine the overall level of plasmonic and application performance; conservation of particles' physical and chemical characteristics is critical and must be carefully controlled. In most cases, how the nanoparticles are prepared is deeply associated with how the nanoparticles are stabilized. The methods for generating Ag and AuNPs can be categorized into two major classes: wet chemical synthesis and lithographic fabrication.

Nanoparticles in the wet chemical synthesis method can be adjusted in size and morphology by various reaction parameters, such as choice of precursor chemical, temperature, pH, or reaction time. To provide colloidal stability to the nanoparticles, stabilizing agents should be present during and after nucleation and growth. Without suitable stabilizers, neither Ag nor AuNPs can maintain their structures and will aggregate or dissolve, resulting in loss of plasmonic functionality [147−151]. These initial stabilizing agents can be replaced by other more robust stabilizers specific to an application's needs. Choosing appropriate protecting materials is especially important for in vivo applications, where the nanoparticles must maintain their plasmonic properties until the nanoparticle arrives at a site of action and performs the desired function within a complex biological matrix. In current research, many studies exploit more than one stabilizing approach to set up a platform that can maximize the nanoparticles' plasmonic

abilities and perform other critical functions (Fig. 12). In lithographic fabrication, metal nanoparticles are usually deposited using various patterning methods, under vacuum, [150] and immobilized on supporting substrates to form nanoparticle arrays. Different from colloidally synthesized Ag or AuNPs, these plasmonic nanoparticle arrays do not always require stabilizing agents during the preparation step, but their stability during long-term storage and use is still important.
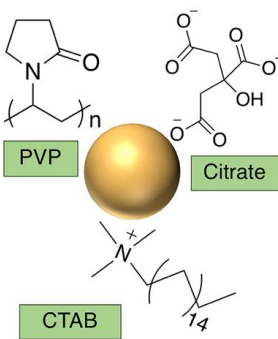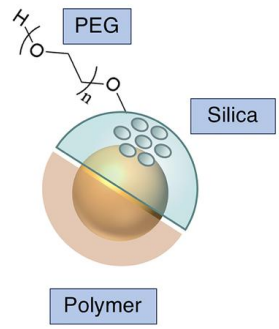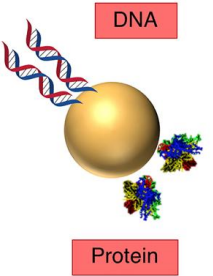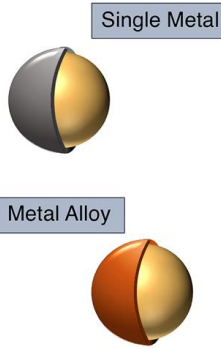
Conventional Surfactants and Ligands	Organic/Inorganic Shells	Biomolecular Ligands	Metal Shells
PVP Citrate CTAB	PEG Silica Polymer	DNA Protein	Single Metal Metal Alloy
• Reversibility • Morphology guide	• High colloidal stability • Facile functionalization	• High biocompatibility • Programmable assembly	• Core-shell chemical interaction

Figure 12. Description of different stabilizing agents in colloidal plasmonic nanoparticles preparations and related functions/characteristics. Sizes of the nanoparticles and ligands/shells are not drawn to scale.

III.3.1. Synthesis of nanoparticles and Stabilization

The importance of controlled synthesis and fabrication of nanostructures has grown along with development of increased applications for nanomaterials. It is now well-appreciated that the plasmonic properties and, thus, the performance in various applications are largely determined by the size, shape, and composition of nanoparticles. Solution phase synthesis of Ag and AuNPs is the most common way to generate monodisperse particles with intentionally varied size and shape [138, 152]. In this variety of solution-phase synthesis methods (Figure 13), the stabilizer (also known as the capping agent) must be present to control the size and morphology, prevent aggregation, and facilitate long-term storage. Both AgNPs and AuNPs have shared some

common and popular stabilizers for synthesis, and each particle's synthetic history is discussed herein. AuNPs were first introduced into the research field in 1857 when Michael Faraday reported the preparation of colloidal AuNPs by the reduction of chloroauric acid by phosphorus [153]. Since that discovery, 20th-century scientists have made large efforts to control nanoparticle size and shape with tailored synthetic designs. Through the work of Turkevitch and Frens, who have been among the most important in the field of AuNP synthesis, the reduction of HAuCl4 in citrates has been improved [154, 155]. For the synthesis of colloidal gold nanomaterials, this method is very often used, in which citrate acts both as a reducing agent and a stabilizer. In 1993, Mulvaney and Giersing reported the stabilization of AuNPs with alkenethiols of various chain lengths [156]. This two-phase, thiolate-stabilized method was more clearly illustrated by the Schiffrin group in 1994 [157], to allow researchers to synthesize AuNP at lower temperatures with relatively high stability and easy size control.
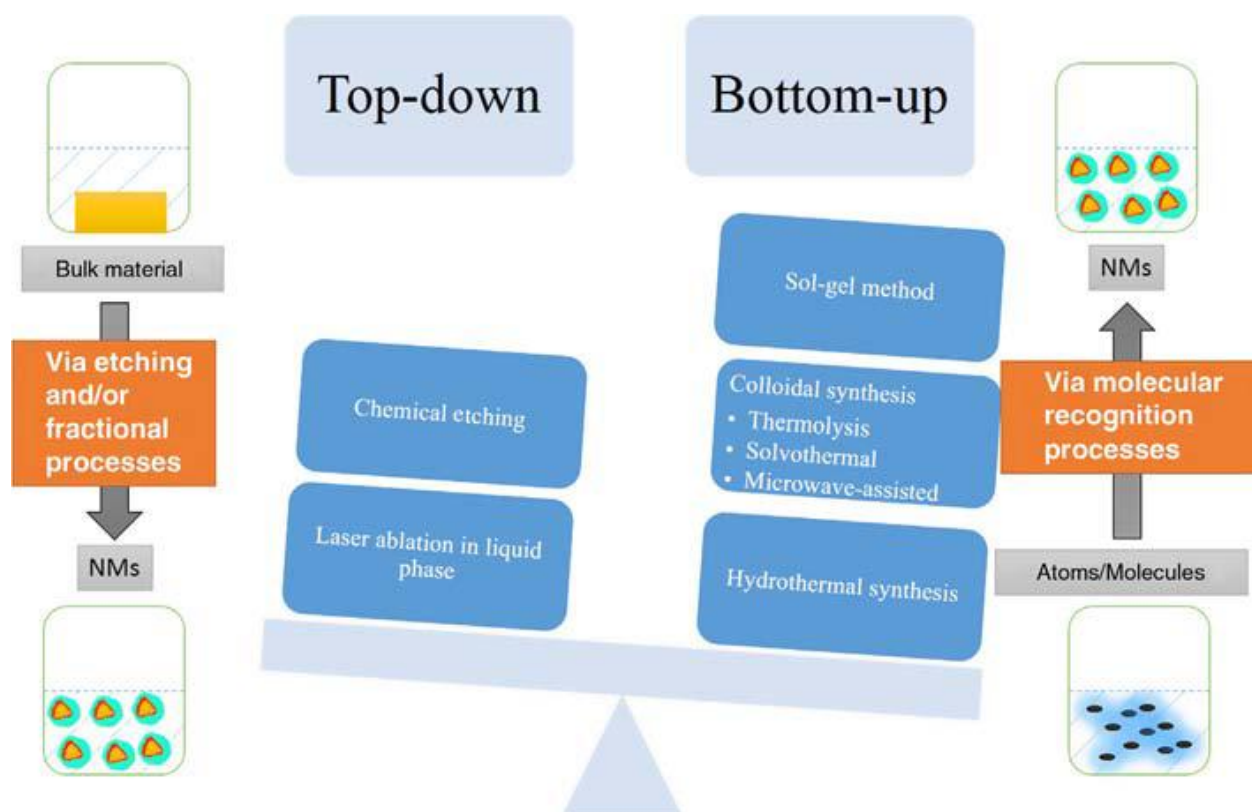
Figure 13: *Schematic of the formation of nanomaterials processes.*

In the same year, Reetz et *al*. also reported an electrochemical synthetic strategy for metal nanoparticles [158]. This electrochemical technique involves non-aqueous media where the dissolved metals from the anode and the intermediate metal salts are reduced at the cathode. The stabilizer, usually a tetra-alkyl-ammonium salt, is required to avoid indiscriminate aggregation in solution as well as to prevent all particles from plating at the surface of the cathode [159]. Electrochemical synthesis of metallic nanoparticles is an important avenue to keep in mind because of the advantages of low cost, modest equipment, and the ease of controlling the yield and size of the nanoparticles by adjusting the current density [160−164].

In colloidal synthesis, also commonly called chemical synthesis, of AgNPs, the basic synthetic approach is similar to that of AuNPs. The synthesis of AgNPs generally requires three chemical functional compounds: a silver precursor, solvent, and a reducing/stabilizing agent. As the synthesis of AuNPs, the reduction of AgNO3 with citrate in water was first reported in 1982 [165]. However, relying on citrate-stabilized AgNPs synthesis usually produces nanoparticles with poor control of size and shape [138]. Rather than this citrate reduction method, the reduction of the silver precursor in multivalent alcohols-so-called polyols is a more popular chemical approach to synthesize various shapes of mono-disperse silver nanoparticles [166]. In a typical synthetic process, ethylene glycol (EG), AgNO3, and poly(vinylpyrrolidone) (PVP) serve as the solvent/reducing agent, silver precursor, and stabilizing/capping agent, respectively. This polyol method can achieve a high degree of control over the morphology of the final products by controlling the types and amounts of capping agents and oxidative etchants, the availability of Ag+ ions, or reaction kinetics with temperature [167]. Other methods, such as seed-mediated growth or light-mediated growth, have received great attention as well [168−171].

The general synthetic strategies described above for both AuNPs and AgNPs mainly focus on solution-based synthesis. These are "bottom-up" methods whereby particles are produced by chemical reductions. Furthermore, mechanical grinding of bulk metals, thermal decomposition, and evaporation are other manufacturing methods to produce gold and silver nanoparticles. The solution-based chemical approaches are advantageous due to their low cost, high yield, and ease of production. As described, under these chemical approaches, the metal precursors or seeds are treated with surfactants or other molecules as stabilizing agents during growth, such as citrate, CTAB, and PVP in previous examples. Those loosely bound molecules are somewhat limited in

their ability to maintain the colloidal stability of nanoparticles, so in the final products, these stabilizing agents can still be present in their original role or they can be replaced with other functional groups via substitution. In this section, the roles of those stabilizing surfactants and other replacement stabilizing molecules and ligands will be discussed.

III.3.2. Metal−Support Interaction

The concept of Strong Metal-Support Interaction (SMSI) has been recognized since the 1970s [172]. Unfortunately, it is too complicated to elucidate the fundamental mechanism behind practical metal-supported catalysts. Metal-support interactions have therefore been studied by surface science techniques in order to understand the structures and properties of metal species supported at the atomic level. By depositing metal species on a solid support, their location can be expected to be related to the local surface structure of the support. One of the important roles of the support in supported metal catalysts is to stabilize the sintered metal species, which is a fairly common phenomenon in the preparation and application of metal catalysts. Nevertheless, it is difficult to model the sintering process quantitatively. In past years, on the basis of concepts from surface chemistry, Campbell et al. have studied the influence of particle size on the stability of supported metal species [173, 174]. For metallic species, an increase in particle size from 1 to 6 nm significantly increases thermal stability, i.e. metallic nanoparticles become relatively stable to sintering when the particle size is as large as 6 nm. Using similar concepts, Campell et al. also studied the effects of supports on the thermal stability of metal species [175].

III.3.3. Different Shapes of Nanoparticles Synthesized
III.3.3.1. Synthesis of Cubic Nanoparticles

Sun and Xia could synthesize cubic silver nanoparticles by the reduction of silver nitrate using ethylene glycol in the presence of poly(vinyl pyrrolidone) (PVP) [176]. The results of this study have shown that the morphology of the product is strongly influenced by the reaction conditions such as temperature, AgNO3 concentration and molar ratio of the units of PVP and AgNO3. For example, when the temperature reduced from 161 °C to 120 °C or increased to 190 °C, the shapes of produced silver nanoparticles were irregular. Moreover, the input concentration of AgNO3, as the next effecting factor should be higher than 0.1 M. Otherwise, silver nanowires will be the main product. If the molar ratio of the repeating unit of PVP and $AgNO_3$ increases from 1.5 to 3,

the main product would be multiply twinned particles (MTPs) [177]. Im et *al*. could synthesize uniform silver nanocubes by reduction of silver nitrate using ethylene glycol at 140°C in the presence of poly(vinyl pyrrolidone) (PVP) and HCl [178].

In polyol process, alcohol containing hydroxyl groups such as ethylene glycol and pentanediol act as both solvent and reducing agent. A capping agent, poly(vinyl pyrrolidone) (PVP) was used to build the cubic shape. Finally, molar ratio of the repeating units of PVP and silver ions determines the morphology of the product [164]. High molar ratio is used for nanocubes and low molar ratio is used for nanowires. In addition, very small amounts of chloride ions due to precipitation of the low-solubility of AgCl salt prevents the rapid reduction of metal ions, it eventually leads to the formation of nanocubes [179]. Tao et *al*. have successfully synthesized silver nanocubes using an experimental procedure [164], in which silver nitrate acted as precursor, PVP was used to control the shape, and pentanediol (PDO- 1.5 H) was used as both solvent and reducing agent.

The synthesis of three different forms of silver nanoparticles by the chemical polyol method, in which ethylene glycol (EG) acted both as a solvent and a reducing agent was carried out [180]. The interesting point was that the reduction ratio could be controlled by changing the reaction temperature. In the experiment, PVP acted as a stabilizer to prevent the aggregation of nanoparticles, as a reducing agent and also as a substance to control the shape of nanoparticles. The group was able to synthesize silver nanocubes with controllable corner truncation using Cl$^-$ (NaCl) [180].

III.3.3.2. Synthesis of Nanoprisms

Generally, chemical reduction of metal salts and photochemical growth are two methods which, have been used for the synthesis of silver nanoprisms [181-183]. It is proved that the former chemical reduction method is better than the photochemical method for mass production of silver prisms, which is necessary for industrial applications. Métraux and Mirkin used a unique simple chemical reduction method for the preparation of silver nanoprisms. They used a mixture of AgNO$_3$/NaBH$_4$/polyvinylpyrrolidone(PVP)/trisodium citrate (Na$_3$CA)/H$_2$O$_2$ in an aqueous solution as reagents to prepare silver nanoprisms at room temperature [181]. Darmanin et *al*. could produce high concentrations of silver nanoprisms with controllable size ((height) of the pyramid) and size disparity. In this study, they showed that synthesis of silver nanoprisms can be

performed by careful selection in the parameters of polyol method especially in the reducing agent [184].

III.3.3.3. Synthesis of Spherical Nanoparticles

Li et al. could synthesize spherical silver nanoparticles via convenient (quick and easy) method at room temperature and by chemical reduction method and finally used transmission electron microscopy and UV−visible spectrophotometer in order to observe and investigate the produced nanoparticles. If silver nitrate, polyvinyl pyrrolidone, and sodium borohydride are used as the reagent, stabilizing factor and reducing agents respectively, spherical and monodisperse silver nanoparticles of 9.0 nm sizes are synthesized [185]. As it can be seen in Table 3 for the synthesis of spherical and cubic silver nanoparticles regarding the size range, either physical, chemical or biological methods can be used, but for synthesis of other shapes (nanorods, nanowires, and nanobars) due to the underdevelopment of biological methods, using either chemical or physical methods is inevitable. Although chemical and physical approaches have the high ability to shape-controlled synthesis of nanoparticles, they have some disadvantages using toxic chemicals in the synthesis process and the biological hazards are the main disadvantages of chemical methods and the high cost of equipment to prepare the nanoparticles and also consuming a lot of energy can be mentioned for physical methods. Since the biological methods are cheaper, environmentally friendly, and easy to use, further studies in order to shape-controlled synthesis of silver nanoparticles using biological methods are needed.

Table 3: Synthesis of Ag nanoparticles with different shapes through chemical, physical and biological methods.

Method	Reducing agent or solvent	Stabilizer or surfactant	Particle size (nm)	Shape	Reference
Chemical method	Trisodium citrate	Trisodium citrate	30-60 nm		[186]
	NaBH4	Dodecanoic acid (DDA)	7 nm		[187]
	Ethylene glycol	Polyvinyl pyrrolidone (PVP)	17 nm		[188]
	Parafin	Oleylamine	10-14 nm		[189]
	Hydrazine hydrate	Bis(2-ethylhexyl) (sulfosuccinate AOT)	2-5 nm		[190]
	NaBH$_4$	Chitosan	35 nm	Spherical	[5, 6]
Electrochemical	Electrolysis cathode	Polyvinyl pyrrolidone (PVP)	11		[191]
Physical synthesis	Electrical arc discharge	Sodium citrate	14-27		[192]
	TX-100, UV	TX-100	30 nm		[193]
Biological synthesis	Bacillus sp.	Bacillus sp.	5-15		[194]
	Lactobacillus	Lactobacillus Proteins	6-15.7		[195]
	Shewanella oneidensis	Shewanella oneidensis	2-11		[196]

	Fungus T. viride	Trichoderma viride	5-40		[197]
	Aspergillus niger	Aspergillus niger	1-20		[198]
Chemical method	Ethylene glycol	Polyvinyl pyrrolidone (PVP)	____		[176]
Chemical method	Pentanediol (H-1.5 PDO)	Polyvinyl pyrrolidone (PVP)	____	Cubic	[166]
Chemical method	Ethylene glycol	Polyvinyl pyrrolidone (PVP)	30-50		[199]
Photochemical	Carboxymethylated chitosan (CMCTS)	Carboxymethylated chitosan (CMCTS)	2-8		[200]
Wet-chemical	Sodium borohydride in the presence of sodium citrate	____	4	Nanorods	[201]
Chemical method	Potassium tartaric	PVP	____		[202]
Chemical method (soft, solution-phase)	Ethylene glycol	____	30-40		[177]
Wet chemical	Ascorbic acid	____	30-40	Nanowires	[203]
Microwave technique	Ethylene glycol	PVP	____		[204]
Chemical method (polyol)	Ethylene glycol	PVP	____	Nanobars	[167]

| Chemical reduction | Hydrazine hydrate | PVP | 50-200 | Triangular | [185] |
| Microwave-assisted | Ethylene glycol monoalkyl ethers | PVP | ____ | Nanoprisms | [184] |

III.3.4. Factors affecting the synthesis of nanoparticles

III.3.4.1. Temperature

Temperature is the most common reaction parameter used to control the reaction kinetics for nanoparticle formation. In general, for exothermic reactions, the reaction rate decreases with increasing temperature, whereas the opposite is the case for endothermic reactions. Normally, temperature is not an important parameter for reductions or sol-gel reactions [205] or wire electrical explosions, but it is in fact a very important parameter for thermal decompositions, polymerizations, or precipitation reactions. Generally, higher temperature is required for thermal decomposition reactions, but for exothermic polymerization reactions, a low temperature is much better for the conversion. In the case of precipitation reactions, the situation is little bit different.

For particle formation through precipitation, a reaction can be divided into three different steps: (i) nucleation, (ii) growth, and (iii) agglomeration. As a result, the size of the particles depends on the relative rate of these three different steps. The nucleation process involves the nature of the chemical reaction, whether endothermic or exothermic, whereas the growth process is more complicated and may depend on the nature of the reaction and the diffusion of the atoms or embryo from the mass to the surface of the nuclei. As the temperature rises, the diffusion coefficient of the atoms or embryo increases, or the concentration of the product depends on the nature of the reaction. However, an endothermic reaction is one in which diffusion increases due to an increase in the concentration of the product in the mass since the rate of endothermic reaction increases with temperature and vice versa for exothermic reaction.

III.3.4.2. Reactant concentration

The reactant concentration is another important parameter for the control of core size or shell thickness. To reach equilibrium of the reaction and thus the final particle size, two steps are probably required: (i) reaction between the reactants to form nuclei and (ii) collision between nuclei or diffusion of molecules to the nuclei surface and deposition to create a final particle size [206]. The first step may be considered the reaction step, which is then followed by growth. The first step can be very fast. If the reaction rate is fast, then the result is that the final particle size depends totally on the growth process. There appears to be no particular trend reported in the literature relating to the change in particle size with increasing reactant concentration. On the

other hand, increasing trends, [207-211] decreasing trends [212, 213] or both [214] on particle size are found to be dependent on the types of particles and the synthesis media. In general, an increasing trend is quite common because of increases in the total amount of the product. When there is more than one reactant present, at low reactant concentration, the number of nuclei formed will be less, probably because of the slow reaction rate. The atoms (embryo) formed at a later period will collide with the nuclei that have already formed instead of forming new nuclei; this, in turn, leads to larger sized particles. When the reactant concentration is increased because of an increase in reaction rate, a greater number of nuclei will form. This leads to smaller sized particles [206].

III.3.4.3. Effect of pH

The effect of pH on the particle size depends mainly on the reaction mechanism involved. This is especially true when H+ or OH- ions are directly involved in the reaction. In addition, changes in the pH of the medium also have an important effect on reduction and precipitation reactions. In a redox reaction, the compound with the highest reduction potential is reduced by oxidizing the compound with the lower reduction potential. The half-cell reduction potential of a redox couple depends on the pH of the media. Hence a favorable pH is highly desirable for controlling the reaction. The extent of surface modification can also be controlled by adjusting the pH of the media. When the core is hydrophilic, the surface charge depends on the pH.

III.3.5. Toxicity of nanoparticles

Beside many industrial and medical applications, there are certain toxicities which are associated with NPs and other nanomaterials [215-217] that require basic knowledge for these toxic effects to be properly addressed. Through various human activities, nanoparticles enter the environment surreptitiously through water, soil, and air. However, the application of nanoparticles for environmental treatment deliberately injects or dumps engineered nanoparticles into the soil or aquatic systems. This has led to a growing concern on the part of all stakeholders. The advantages of magnetic NPs such as their small size, high reactivity, and great capacity, could become potential lethal factors by inducing adverse cellular toxic and harmful effects, unusual in micron-sized counter-parts. Studies also illustrated that NPs can enter organisms during ingestion or inhalation and can translocate within the body to various organs and tissues where the NPs

have the possibility to exert the reactivity being toxicology effects. Although some studies have also addressed the toxicological effects of NPs on animal cells and plant cells the toxicological studies with magnetic NPs on plants to date are still limited. The uses of Ag NPs in numerous consumer products lead them to their release to the aquatic environment and become a source of dissolved Ag and thus exert toxic effects on aquatic organisms including bacteria, algae, fish and daphnia. The respiratory system represents a unique target for the potential toxicity of NPs due to the fact that in addition to being the portal of entry for inhaled particles, it also receives the entire cardiac output.

NPs are used in bio-applications widely but despite the rapid progress and early acceptance of nanobiotechnology the potential for adverse health effects due to prolonged exposure at various concentrations levels in human in the environment has not yet been established. However, the environmental impact of NPs is expected to increase in the future. One of the NPs toxicity is the ability to organize around the protein concentration that depends on particles size, curvature, shape and surface characteristics charge, functionalized groups, and free energy.

III.3.6. Applications of nanoparticles

The great current interest in nanoparticles is partly due to the fact that these materials often have unusual physical (structural, electronic, magnetic, and optical) and chemical (catalytic) properties.

Many studies have been conducted on catalysis, which is the most important chemical application of metallic nanoparticles. Transition metals, especially precious metals, show very high catalytic abilities for many organic reactions (See figure 14). These materials present properties of both heterogeneous and homogeneous catalysts. The catalysis takes place on the active sites of the surface of metal nuclei, that is, the mechanism is similar to conventional heterogeneous catalysts. However, nanoparticles perfectly melt in reaction medium as conventional homogeneous catalysts. Another advantage is that nanoparticles can be easily recovered from the reaction medium when the catalysis finishes.

All these properties and those described above make nanoparticles suitable for application in different fields of analytical chemistry, such as optoelectronics or chemicals and biosensing.
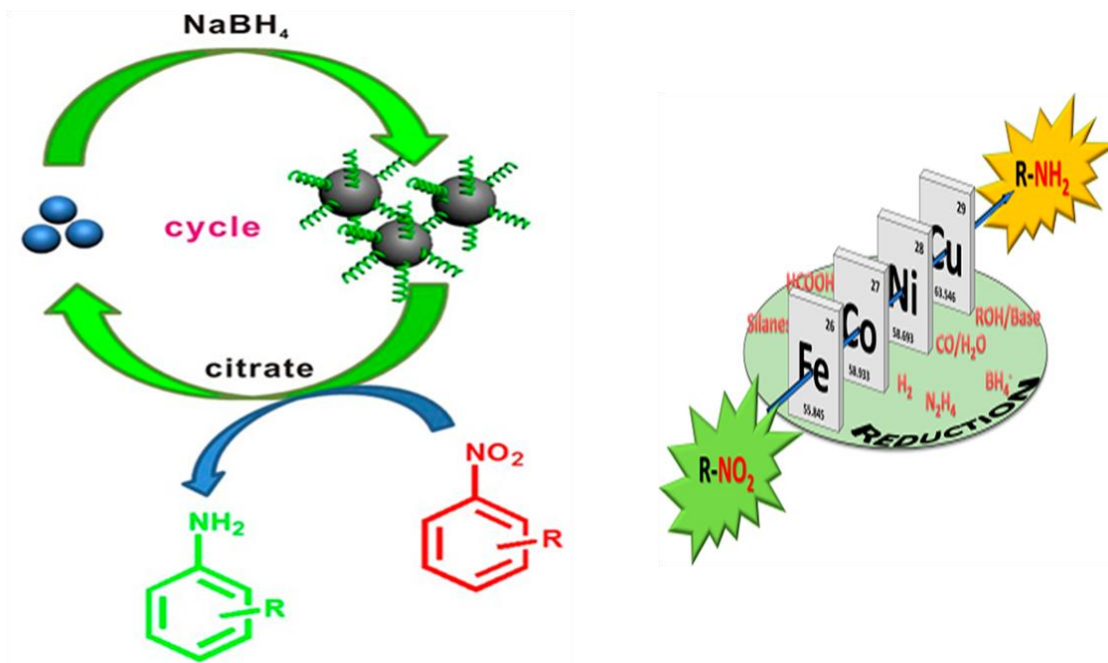
Figure 14*: Reduction of nitro compounds to the corresponding amines using catalytic process*

III.3.6.1. Metal nanoparticles-based sensors

Modifying a solid electrode surface with solid nanoparticles of a different chemical identity can impart additional chemical functionality to the electrode such as electrocatalytic activity. Modifying electrodes with nanoparticles to act as electrocatalysts has the following advantages: i) nanoparticles have a high surface area to volume ratio, hence ii) nanoparticles experience a greater rate of mass transport than bulk materials, iii) the surface properties of the nanoparticles are different to their bulk form and in some cases exhibit enhanced catalytic activity, iv) gives specific control over the electrode environment, and v) can be a more economic method of utilizing catalyst materials.

The most commonly utilized metal nanoparticle electrocatalysts are transition metals such as gold, silver, platinum, copper, and palladium. Carbon is the preferred electrode substrate for the deposition of metal nanoparticles due to its wide potential window, range of hardness commercially available, relative cheapness, and its non-metallic identity. Metals are excellent conductors of electricity and are often described as a rigid network of metallic nuclei bathed in a sea of electrons. When the oxidation number of the metallic nuclei is altered (by oxidation or

reduction) the transport of charge into the material must be compensated for by either the transport of an opposite charge into the material or by the expulsion of an equivalent charge out of the material to maintain electro-neutrality. Hence the issue of charge transport in and out of the material becomes important when considering electron transfer processes. The ease of oxidation and reduction can be limited by the nature of the charge compensating species present in the electrolyte solution surrounding the electrode.

References

[1] Lefrou, C., Fabry, P., & Poignet, J. C. (2012). Electrochemistry: the basics, with examples. Springer Science & Business Media.

[2] Mc Naught, A. D., & Wilkinson, A. (1997). Compendium of chemical terminology. IUPAC recommendations, Blackwell Science: Oxford, England; Malden, MA, USA.

[3] Gileadi, E. (1993). Electrode kinetics for chemists, chemical engineers, and materials scientists. Capstone, VCH: New York.

[4] Laghrib, F., Ajermoun, N., Bakasse, M., Lahrich, S., & El Mhammedi, M. A. (2019). Catalytic effect of silver particles supported on chitosan surface for the electrochemical sensing para nitroaniline at graphite electrode. International Journal of Environmental Analytical Chemistry, 1-16.

[5] Laghrib, F., Farahi, A., Bakasse, M., Lahrich, S., & El Mhammedi, M. A. (2019). Chemical synthesis of nanosilver on chitosan and electroanalysis activity against the p-nitroaniline reduction. Journal of Electroanalytical Chemistry, 845, 111-118.

[6] Laghrib, F., Ajermoun, N., Bakasse, M., Lahrich, S., & El Mhammedi, M. A. (2019). Synthesis of silver nanoparticles assisted by chitosan and its application to catalyze the reduction of 4-nitroaniline. International journal of biological macromolecules, 135, 752-759.

[7] Laghrib, F., Farahi, A., Bakasse, M., Lahrich, S., & El Mhammedi, M. A. (2019). Voltammetric determination of nitro compound 4-nitroaniline in aqueous medium at chitosan gelified modified carbon paste electrode (CS@ CPE). International journal of biological macromolecules, 131, 1155-1161.

[8] Laghrib, F., Ajermoun, N., Hrioua, A., Lahrich, S., Farahi, A., El Haimouti, A., & El Mhammedi, M. A. (2019). Investigation of voltammetric behavior of 4-nitroaniline based on electrodeposition of silver particles onto graphite electrode. Ionics, 25(6), 2813-2821.

[9] Laghrib, F., Lahrich, S., Farahi, A., Bakasse, M., & El Mhammedi, M. A. (2018). Impregnation of silver in graphite carbon using solid reaction: Electrocatalysis and detection of 4-nitroaniline. Journal of Electroanalytical Chemistry, 823, 26-31.

[10] Laghrib, F., Boumya, W., Lahrich, S., Farahi, A., El Haimouti, A., & El Mhammedi, M. A. (2017). Electrochemical evaluation of catalytic effect of silver in reducing 4-nitroaniline: Analytical application. Journal of Electroanalytical Chemistry, 807, 82-87.

[11] Bard, A. J., & Faulkner, L. R. (2000). Fundamentals and applications. Electrochemical Methods, 2nd ed, Wiley: New York.

[12] Zoski, C. G. (Ed.). (2006). Handbook of electrochemistry. Elsevier, 1000 AE Amsterdam, The Netherlands.

[13] Albery, W. J. (1975). Electrode kinetics (Vol. 14). Oxford University Press.

[14] Kissinger, P., & Heineman, W. R. (1996). Laboratory Techniques in Electroanalytical Chemistry revised and expanded. CRC press.

[15] Bard, A. J., & Faulkner, L. R. (2001). Fundamentals and applications. Electrochemical Methods, Wiley: New York, 2(482), 580-632.

[16] Boumya, W., Hammani, H., Laghrib, F., Lahrich, S., Farahi, A., Achak, M., ... & Mhammedi, M. E. (2017). Electrochemical Study of 2, 4-Dinitrophenylhydrazine as Derivatization Reagent and Aldehydes at Carbon Glassy Electrode. Electroanalysis, 29(7), 1700-1711.

[17] Laghrib, F., Lahrich, S., & El Mhammedi, M. A. (2019). Recent Advances in Direct and Indirect Methods for Sensing Carbonyl Compounds Aldehydes in Environment and Foodstuffs. Journal of The Electrochemical Society, 166(15), B1543.

[18] Nicholson, R. S., & Shain, I. (1964). Theory of stationary electrode polarography. Single scan and cyclic methods applied to reversible, irreversible, and kinetic systems. Analytical chemistry, 36(4), 706-723.

[19] Davies, T. J., Banks, C. E., & Compton, R. G. (2005). Voltammetry at spatially heterogeneous electrodes. Journal of solid state electrochemistry, 9(12), 797-808.

[20] Matsuda, H., & Ayabe, Y. (1955). Zur Theorie der Randles-Sevčikschen Kathodenstrahl-Polarographie. Zeitschrift für Elektrochemie, Berichte der Bunsengesellschaft für physikalische Chemie, 59(6), 494-503.

[21] Nicholson, R. S. (1965). Theory and application of cyclic voltammetry for measurement of electrode reaction kinetics. Analytical chemistry, 37(11), 1351-1355.

[22] Klingler, R. J., & Kochi, J. K. (1981). Electron-transfer kinetics from cyclic voltammetry. Quantitative description of electrochemical reversibility. The Journal of Physical Chemistry, 85(12), 1731-1741.

[23] Lavagnini, I., Antiochia, R., & Magno, F. (2004). An extended method for the practical evaluation of the standard rate constant from cyclic voltammetric data. Electroanalysis:

An International Journal Devoted to Fundamental and Practical Aspects of Electroanalysis, 16(6), 505-506.

[24]   Testa, A. C., & Reinmuth, W. H. (1961). Stepwise reactions in chronopotentiometry. Analytical chemistry, 33(10), 1320-1324.

[25]   Compton, R. G., & Banks, C. E. (2011). Understanding voltammetry. World Scientific, 2nd ed.; ICP: London.

[26]   Ward, K. R., Lawrence, N. S., Hartshorne, R. S., & Compton, R. G. (2011). Cyclic Voltammetry of the EC′ Mechanism at Hemispherical Particles and Their Arrays: The Split Wave. The Journal of Physical Chemistry C, 115(22), 11204–11215.

[27]   Andrieux, C. P., Dumas-Bouchiat, J. M., & Saveant, J. M. (1978). Homogeneous redox catalysis of electrochemical reactions: Part I. Introduction. Journal of Electroanalytical Chemistry and Interfacial Electrochemistry, 87(1), 39-53.

[28]   Andrieux, C. P., Dumas-Bouchiat, J. M., & Savéant, J. M. (1978). Homogeneous redox catalysis of electrochemical reactions: Part II. Rate determining electron transfer, evaluation of rate and equilibrium parameters. Journal of Electroanalytical Chemistry and Interfacial Electrochemistry, 87(1), 55-65.

[29]   Andrieux, C. P., Dumas-Bouchiat, J. M., & Savéant, J. M. (1978). Homogeneous redox catalysis of electrochemical reactions: Part III. Rate determining electron transfer. Kinetic characterization of follow-up chemical reactions. Journal of Electroanalytical Chemistry and Interfacial Electrochemistry, 88(1), 43-48.

[30]   Andrieux, C. P., Dumas-Bouchiat, J. M., & Savéant, J. M. (1980). Homogeneous redox catalysis of electrochemical reactions: Part IV. Kinetic controls in the homogeneous process as characterized by stationary and quasi-stationary electrochemical techniques. Journal of Electroanalytical Chemistry and Interfacial Electrochemistry, 113(1), 1-18.

[31]   Andrieux, C. P., Blocman, C., Dumas-Bouchiat, J. M., M'halla, F., & Savéant, J. M. (1980). Homogeneous redox catalysis of electrochemical reactions: Part V. Cyclic voltammetry. Journal of Electroanalytical Chemistry and Interfacial Electrochemistry, 113(1), 19-40.

[32]   Savéant, J. M., & Su, K. B. (1984). Homogeneous redox catalysis of electrochemical reaction. VI: Zone diagram representation of the kinetic regimes. Journal of electroanalytical chemistry and interfacial electrochemistry, 171(1-2), 341-349.

[33]   Compton, R. G., Fisher, A. C., & Spackman, R. A. (1992). Homogeneous catalysis of electrochemical reactions. Channel electrode voltammetry and the EC′ mechanism. Electroanalysis, 4(2), 167-182.

[34]   Fisher, A. C., & Compton, R. G. (1992). The EC′ mechanism: Split waves at the channel electrode. Electroanalysis, 4(3), 311-315.

[35]   Compton, R. G., Spackman, R. A., & Unwin, P. R. (1989). Homogeneous catalysis of electrochemical reactions: Mechanistic resolution via rotating-disc electrode voltammetric wave shape analysis. Journal of electroanalytical chemistry and interfacial electrochemistry, 264(1-2), 1-25.

[36]   Compton, R. G., Day, M. J., Laing, M. E., Northing, R. J., Penman, J. I., &Waller, A. M. (1988). Rotating-disc electrode voltammetry. Journal of the Chemical Society, Faraday Transactions, 84, 2013–25.

[37]   Compton, R., & spackman, R. (1990). Homogeneous catalysis of electrochemical reactions:"Split waves" at the rotating disc electrode. Journal of electroanalytical chemistry and interfacial electrochemistry, 285(1-2), 192, 71–97.

[38]   Dimarco, D. M., Forshey, P. A., & Kuwana, T. (1982, January). Simulation of the cyclic voltammetric characteristics of a 2nd order ec catalytic mechanism. In ACS Symposium Series (Vol. 192, pp. 71-97). 1155 16th st, nw, Washington, DC 20036 USA: Amer. Chemical Soc.

[39]   Gelbert, M. B., & Curran, D. J. (1986). Alternating current voltammetry of dopamine and ascorbic acid at carbon paste and stearic acid modified carbon paste electrodes. Analytical chemistry, 58(6), 1028-1032.

[40]   Wang, J. (2006). Analytical electrochemistry, 3th ed. John Wiley & Sons, Inc. New Jersy.

[41]   Hawley, M. D., Tatawawadi, S. V., Piekarski, S., & Adams, R. N. (1967). Electrochemical studies of the oxidation pathways of catecholamines. Journal of the American Chemical Society, 89(2), 447-450.

[42]   Mohilner, D. M., Adams, R. N., & Argersinger, W. J. (1962). Investigation of the kinetics and mechanism of the anodic oxidation of aniline in aqueous sulfuric acid solution at a platinum electrode. Journal of the American Chemical Society, 84(19), 3618-3622.

[43]   Evans, D. H. (1977). Voltammetry: doing chemistry with electrodes. Accounts of Chemical Research, 10(9), 313-319.

[44] Rudolph, M., Reddy, D. P., & Feldberg, S. W. (1994). A simulator for cyclic voltammetric responses. Analytical chemistry, 66(10), 589A-600A.

[45] Compton, R. G., & Banks, C. E. Understanding Voltammetry 2007. (World Scientific, Singapore).

[46] Wopschall, R. H., & Shain, I. (1967). Effects of adsorption of electroactive species in stationary electrode polarography. Analytical Chemistry, 39(13), 1514-1527.

[47] Wopschall, R. H., & Shain, I. (1967). Adsorption characteristics of the methylene blue system using stationary electrode polarography. Analytical Chemistry, 39(13), 1527-1534.

[48] Streeter, I., Wildgoose, G. G., Shao, L., & Compton, R. G. (2008). Cyclic voltammetry on electrode surfaces covered with porous layers: an analysis of electron transfer kinetics at single-walled carbon nanotube modified electrodes. Sensors and Actuators B: Chemical, 133(2), 462-466.

[49] Parsons, R. (1964). The kinetics of electrode reactions and the electrode material. Surface Science, 2, 418-435.

[50] Faraday, M. (1834). VI. Experimental researches in electricity.-Seventh Series. Philosophical transactions of the royal society of london, (124), 77-122.

[51] Wang, J., Luo, D. B., Farias, P. A., & Mahmoud, J. S. (1985). Adsorptive stripping voltammetry of riboflavin and other flavin analogs at the static mercury drop electrode. Analytical chemistry, 57(1), 158-162.

[52] Osteryoung, J. (1993). Voltammetry for the future. Accounts of chemical research, 26(3), 77-83.

[53] Osteryoung, J. G., & Osteryoung, R. A. (1985). Square wave voltammetry. Analytical Chemistry, 57(1), 101-110.

[54] Barros, A. A., Rodrigues, J. A., Almeida, P. J., Rodrigues, P. G., & Fogg, A. G. (1999). Voltammetry of compounds confined at the hanging mercury drop electrode surface. Analytica chimica acta, 385(1-3), 315-323.

[55] Hibbert, D.A. Introduction to Electrochemistry, (Macmillan, London Eds), 1993.

[56] Kamat, A., Huth, A., Klein, O., Scholl, S., 2010. Chronoamperometric investigations of the electrode-electrolyte interface of a commercial high temperature PEM fuel cell. Fuel Cells 10, 983e992.

[57]   Evans, D.H., Kelly, M.J., 1982. Theory for double potential step chronoamperometry, chronocoulometry, and chronoabsorptometry with a quasi-reversible electrode reaction. Analytical Chemistry 54, 1727e1729.

[58]   Honeychurch, K. C. (2012). Printed thick-film biosensors. In Printed Films (pp. 366-409). Wood head publishing.

[59]   Modern Aspects of Electrochemistry, Number 32, edited by B. E. Conway et al. Kluwer Academic / Plenum Publishers, New York, 1999.

[60]   Grahame, D. C. (1947). The electrical double layer and the theory of electrocapillarity. Chemical reviews, 41(3), 441-501.

[61]   Parsons, R. in Modern Aspects of Electrochemistry, Vol. 1, Plenum, New York, 1954, p. 103.

[62]   Delahay, P. (1965). Double layer and electrode kinetics. John Wiley & Sons Inc.

[63]   Peover, M. E., & Bard, A. J. (1967). Electroanalytical chemistry. by AJ Bard, Marcel Dekker, New York, 2, 1.

[64]   Breyer, B., & Bauer, H. H. (1963). Alternating current polarography and tensammetry (No. 543.85), Interscience Publishers.

[65]   Smith, D. E. in Electroanalytical Chemistry, A. J. Bard, ed., Vol. 1, Marcel Dekker, New York, 1966, p. 1.

[66]   Reeves, R. M. (1980). AM Bond, Modern Polarographic Methods in Analytical Chemistry, Marcel Dekker, New York and Basel (1980), 518 pp., Sfr. 135.00.

[67]   Hassel, A. W., & Mardare, A. I. (2015). Localized electrochemical impedance spectroscopy using a scanning droplet cell microscope. Journal of Electroanalytical Chemistry, 737, 93-99.

[68]   Cruz-Manzo, S., & Chen, R. (2013). A generic electrical circuit for performance analysis of the fuel cell cathode catalyst layer through electrochemical impedance spectroscopy. Journal of Electroanalytical Chemistry, 694, 45-55.

[69]   Ispas, A., Matsushima, H., Bund, A., & Bozzini, B. (2011). A study of external magnetic-field effects on nickel–iron alloy electrodeposition based on linear and non-linear differential AC electrochemical response measurements. Journal of electroanalytical chemistry, 651(2), 197-203.

[70] Wan, Y., Lin, Z., Zhang, D., Wang, Y., & Hou, B. (2011). Impedimetric immunosensor doped with reduced graphene sheets fabricated by controllable electrodeposition for the non-labelled detection of bacteria. Biosensors and Bioelectronics, 26(5), 1959-1964.

[71] Wang, X., Yang, T., Li, X., & Jiao, K. (2011). Three-step electrodeposition synthesis of self-doped polyaniline nanofiber-supported flower-like Au microspheres for high-performance biosensing of DNA hybridization recognition. Biosensors and Bioelectronics, 26(6), 2953-2959.

[72] Macdonald, J. R. Impedance Spectroscopy, Wiley, New York, 1987.

[73] Cachet, C., Ströder, U., & Wiart, R. (1982). The kinetics of zinc electrode in alkaline zincate electrolytes. Electrochimica Acta, 27(7), 903-908.

[74] Gouveia-Caridade, C., & Brett, C. M. (2005). Electrochemical impedance characterization of Nafion-coated carbon film resistor electrodes for electroanalysis. Electroanalysis: An International Journal Devoted to Fundamental and Practical Aspects of Electroanalysis, 17(7), 549-555.

[75] Gouveia-Caridade, C., & Brett, C. M. (2006). The influence of Triton-X-100 surfactant on the electroanalysis of lead and cadmium at carbon film electrodes–an electrochemical impedance study. Journal of Electroanalytical Chemistry, 592(1), 113-120.

[76] Ferreira, A. A. P., Fugivara, C. S., Barrozo, S., Suegama, P. H., Yamanaka, H., & Benedetti, A. V. (2009). Electrochemical and spectroscopic characterization of screen-printed gold-based electrodes modified with self-assembled monolayers and Tc85 protein. Journal of Electroanalytical Chemistry, 634(2), 111-122.

[77] Bonanni, A., Pumera, M., & Miyahara, Y. (2011). Influence of gold nanoparticle size (2–50 nm) upon its electrochemical behavior: an electrochemical impedance spectroscopic and voltammetric study. Physical Chemistry Chemical Physics, 13(11), 4980-4986.

[78] Mandil, A., Pauliukaite, R., Amine, A., & Brett, C. M. (2012). Electrochemical characterization of and stripping voltammetry at screen printed electrodes modified with different brands of multiwall carbon nanotubes and bismuth films. Analytical letters, 45(4), 395-407.

[79] Bonanni, A., & Del Valle, M. (2010). Use of nanomaterials for impedimetric DNA sensors: a review. Analytica chimica acta, 678(1), 7-17.

[80] Guan, J. G., Miao, Y. Q., & Zhang, Q. J. (2004). Impedimetric biosensors. Journal of bioscience and bioengineering, 97(4), 219-226.

[81] Shipway, A. N., Katz, E., & Willner, I. (2000). Nanoparticle arrays on surfaces for electronic, optical, and sensor applications. ChemPhysChem, 1(1), 18-52.

[82] Ismail, A. H., Schäfer, C., Heiss, A., Walter, M., Jahnen-Dechent, W., & Leonhardt, S. (2011). An electrochemical impedance spectroscopy (EIS) assays measuring the calcification inhibition capacity in biological fluids. Biosensors and Bioelectronics, 26(12), 4702-4707.

[83] Rezaei, B., Majidi, N., Rahmani, H., & Khayamian, T. (2011). Electrochemical impedimetric immunosensor for insulin like growth factor-1 using specific monoclonal antibody-nanogold modified electrode. Biosensors and Bioelectronics, 26(5), 2130-2134.

[84] Silva, S. M., & Bond, A. M. (2003). Contribution of migration current to the voltammetric deposition and stripping of lead with and without added supporting electrolyte at a mercury-free carbon fibre microdisc electrode. Analytica chimica acta, 500(1-2), 307-321.

[85] Schwickart, M., Vainshtein, I., Lee, R., Schneider, A., & Liang, M. (2014). Interference in immunoassays to support therapeutic antibody development in preclinical and clinical studies. Bioanalysis, 6(14), 1939-1951.

[86] Elgrishi, N., Rountree, K. J., McCarthy, B. D., Rountree, E. S., Eisenhart, T. T., & Dempsey, J. L. (2018). A practical beginner's guide to cyclic voltammetry. Journal of Chemical Education, 95(2), 197-206.

[87] Ranganathan, S., Kuo, T. C., & McCreery, R. L. (1999). Facile preparation of active glassy carbon electrodes with activated carbon and organic solvents. Analytical chemistry, 71(16), 3574-3580.

[88] McCarthy, B. D., Martin, D. J., Rountree, E. S., Ullman, A. C., & Dempsey, J. L. (2014). Electrochemical Reduction of Brønsted Acids by Glassy Carbon in Acetonitrile：Implications for Electrocatalytic Hydrogen Evolution. Inorganic chemistry, 53(16), 8350-8361.

[89] Hendel, S. J., & Young, E. R. (2016). Introduction to electrochemistry and the use of electrochemistry to synthesize and evaluate catalysts for water oxidation and reduction. Journal of Chemical Education, 93(11), 1951-1956.

[90]   Esteban, M., & Casassas, E. (1994). Stripping electroanalytical techniques in environmental analysis. TrAC Trends in Analytical Chemistry, 13(3), 110-117.

[91]   Bond, A. M. (1981). Developments in polarographic (voltammetric) analysis in the 1980's. Journal of Electroanalytical Chemistry and Interfacial Electrochemistry, 118, 381-394.

[92]   Omanović, D., Peharec, Ž., Pižeta, I., Brug, G., & Branica, M. (1997). A new mercury drop electrode for trace metal analysis. Analytica chimica acta, 339(1-2), 147-153.

[93]   Zen, J. M., & Ting, Y. S. (1996). Square-wave voltammetric stripping analysis of lead (II) at a Nafion®/copper-mercury film electrode. Analytica chimica acta, 332(1), 59-65.

[94]   Gunasingham, H., & Dalangin, R. R. (1991). Anodic stripping voltammetry of lead using a copper-mercury film electrode. Analytica chimica acta, 246(2), 309-313.

[95]   El Mhammedi, M. A., Achak, M., Hbid, M., Bakasse, M., Hbid, T., & Chtaini, A. (2009). Electrochemical determination of cadmium (II) at platinum electrode modified with kaolin by square wave voltammetry. Journal of hazardous materials, 170(2-3), 590-594.

[96]   Zejli, H., de Cisneros, J. H. H., Naranjo-Rodriguez, I., & Temsamani, K. R. (2007). Stripping voltammetry of silver ions at polythiophene-modified platinum electrodes. Talanta, 71(4), 1594-1598.

[97]   Pinilla, J. M., Hernandez, L., & Conesa, A. J. (1996). Determination of mercury by open circuit adsorption stripping voltammetry on a platinum disk electrode. Analytica chimica acta, 319(1-2), 25-30.

[98]   Noh, M. F. M., & Tothill, I. E. (2006). Development and characterisation of disposable gold electrodes, and their use for lead (II) analysis. Analytical and bioanalytical chemistry, 386(7-8), 2095-2106.

[99]   Bonfil, Y., Brand, M., & Kirowa-Eisner, E. (2002). Characteristics of subtractive anodic stripping voltammetry of Pb and Cd at silver and gold electrodes. Analytica chimica acta, 464(1), 99-114.

[100]   Beni, V., Newton, H. V., Arrigan, D. W., Hill, M., Lane, W. A., & Mathewson, A. (2004). Voltammetric behaviour at gold electrodes immersed in the BCR sequential extraction

scheme media: Application of under potential deposition–stripping voltammetry to determination of copper in soil extracts. Analytica chimica acta, 502(2), 195-206.

[101] McCreery, R. L. (1991). Carbon electrodes: structural effects on electron transfer kinetics. Electroanalytical chemistry, 17, 221-374.

[102] Chen, P., & McCreery, R. L. (1996). Control of electron transfer kinetics at glassy carbon electrodes by specific surface modification. Analytical Chemistry, 68(22), 3958-3965.

[103] Murray, R. W., Ewing, A. G., & Durst, R. A. (1987). Chemically modified electrodes. Molecular design for electroanalysis. Analytical Chemistry, 59(5), 379A-390A.

[104] Wang, J. (1991). Modified electrodes for electrochemical sensors. Electroanalysis, 3(4-5), 255-259.

[105] Baldwin, R. P., & Thomsen, K. N. (1991). Chemically modified electrodes in liquid chromatography detection: A review. Talanta, 38(1), 1-16.

[106] Fujihira, M., Rusling, J.F. & Rubinstein, I. (2006) in Encyclopedia of Electrochemistry, 1st edn (ed. A.J. Bard and M. Stratmann), vol. 10, Wiley-VCH, Weinheim.

[107] Moses, P. R., Wier, L., & Murray, R. W. (1975). Chemically modified tin oxide electrode. Analytical Chemistry, 47(12), 1882-1886.

[108] Murray, R. W. (1980). Chemically modified electrodes. Accounts of Chemical Research, 13(5), 135-141.

[109] Murray, R. W., & Bard, I. A. (1984). Electroanalytical chemistry. by AJ Bard, Marcel Dekker, New York, 13, 191.

[110] Murray, R. W. (1992). Introduction to the chemistry of molecularly designed electrode surfaces. Molecular Design of Electrode Surfaces, 22, 1-48.

[111] Lane, R. F., & Hubbard, A. T. (1973). Electrochemistry of chemisorbed molecules. I. Reactants connected to electrodes through olefinic substituents. The Journal of Physical Chemistry, 77(11), 1401-1410.

[112] Lane, R. F., & Hubbard, A. T. (1973). Electrochemistry of chemisorbed molecules. II. Influence of charged chemisorbed molecules on the electrode reactions of platinum complexes. The Journal of Physical Chemistry, 77(11), 1411-1421.

[113] Abruña, H. D. (1988). Coordination chemistry in two dimensions: chemically modified electrodes. Coordination Chemistry Reviews, 86, 135-189.

[114] Lyons, M. E. (1994). Electroactive Polymer Electrochemistry, Part I: Fundamentals, Plenum Press, New York.

[115] Oyama, N., & Anson, F. C. (1979). Facile attachment of transition metal complexes to graphite electrodes coated with polymeric ligands. Observation and control of metal-ligand coordination among reactants confined to electrode surfaces. Journal of the American Chemical Society, 101(3), 739-741.

[116] Oyama, N., & Anson, F. C. (1979). Polymeric ligands as anchoring groups for the attachment of metal complexes to graphite electrode surfaces. Journal of the American Chemical Society, 101(13), 3450-3456.

[117] Samuels, G. J., & Meyer, T. J. (1981). An electrode-supported oxidation catalyst based on ruthenium (IV). pH "encapsulation" in a polymer film. Journal of the American Chemical Society, 103(2), 307-312.

[118] Oyama, N., & Anson, F. C. (1980). Electrostatic binding of metal complexes to electrode surfaces coated with highly charged polymeric films. Journal of the Electrochemical Society, 127(1), 249-250.

[119] Cassidy, H.G. & Kun, K.A. (1965) Oxidation Reduction Polymers (Redox Polymers), Wiley-Interscience, New York.

[120] Katz, E., de Lacey, A. L., & Fernandez, V. M. (1993). Covalent binding of viologen to electrode surfaces coated with poly (acrylic acid) prepared by electropolymerization of acrylate ions: II. Effect of the ionization state of the polymeric coating on the formal potential of viologen. Journal of Electroanalytical Chemistry, 358(1-2), 261-272.

[121] Moulay, S., & Mehdaoui, R. (2004). Hydroquinone/catechol-bearing polyacrylic acid: redox polymer. Reactive and Functional Polymers, 61(2), 265-275.

[122] Hatozaki, O., & Anson, F. C. (1997). Intramolecular electron transfer within a water-soluble, ferrocene-labeled polyacrylate. Journal of Electroanalytical Chemistry, 420(1-2), 195-199.

[123] Paunovic, M. (2000). Modern Electroplating 4th ed. ed M. Schlesinger and M. Paunovic.

[124] Mohler, J. B. (1969). Electroplating and related processes. Chemical Publishing Co., 1969.

[125] Gamburg, Y. D., & Zangari, G. (2011). The structure of the metal-solution interface. In Theory and Practice of Metal Electrodeposition (pp. 27-51). Springer, New York, NY.

[126] Gamburg, Y. D., & Zangari, G. (2011). Technologies for the Electrodeposition of Metals and Alloys: Electrolytes and Processes. In Theory and Practice of Metal Electrodeposition (pp. 265-316). Springer, New York, NY.

[127] Farahi, A., Achak, M., El Gaini, L., El Mhammedi, M. A., & Bakasse, M. (2016). Silver particles-modified carbon paste electrodes for differential pulse voltammetric determination of paraquat in ambient water samples. Journal of the Association of Arab Universities for Basic and Applied Sciences, 19(1), 37-43.

[128] Hammani, H., Boumya, W., Laghrib, F., Farahi, A., Lahrich, S., Aboulkas, A., & El Mhammedi, M. A. (2017). Electro-catalytic effect of Al_2O_3 supported onto activated carbon in oxidizing phenol at graphite electrode. Materials Today Chemistry, 3, 27–36.

[129] Hammani, H., Boumya, W., Laghrib, F., Farahi, A., Lahrich, S., Aboulkas, A., & El Mhammedi, M. A. (2017). Electrocatalytic effect of NiO supported onto activated carbon in oxidizing phenol at graphite electrode: Application in tap water and olive oil samples. Journal of the Association of Arab Universities for Basic and Applied Sciences, 24(1), 26-33.

[130] Boudart, M. (1969). Catalysis by supported metals. In Advances in catalysis, 20, 153-166. Academic Press.

[131] Boudart, M. (1985). Heterogeneous catalysis by metals. Journal of molecular catalysis, 30(1-2), 27-38.

[132] Ertl, G., Knözinger, H., & Weitkamp, J. (Eds.). (1997). Handbook of heterogeneous catalysis, Wiley-VCH: New York.

[133] Cejka, J., Corma, A., & Zones, S. (Eds.). (2010). Zeolites and catalysis: synthesis, reactions and applications. John Wiley & Sons.

[134] Millini, R., Zou, X., Strohmaier, K., Schwieger, W., Eliasova, P., Morris, R. E., & Opanasenko, M. (2017). Zeolites in catalysis: properties and applications. Royal Society of Chemistry.

[135] Somorjai, G. A., & Carrazza, J. (1986). Structure sensitivity of catalytic reactions. Industrial & engineering chemistry fundamentals, 25(1), 63-69.

[136] Che, M., & Bennett, C. O. (1989). The influence of particle size on the catalytic properties of supported metals. In Advances in Catalysis (Vol. 36, pp. 55-172). Academic Press.

[137] Gates, B. C., Guczi, L., & Knözinger, H. (Eds.). (1986). Metal clusters in catalysis (Vol. 29). Amsterdam: Elsevier.

[138] Rycenga, M., Cobley, C. M., Zeng, J., Li, W., Moran, C. H., Zhang, Q., & Xia, Y. (2011). Controlling the synthesis and assembly of silver nanostructures for plasmonic applications. Chemical reviews, 111(6), 3669-3712.

[139] Li, J. F., Yang, Z. L., Ren, B., Liu, G. K., Fang, P. P., Jiang, Y. X., ... & Tian, Z. Q. (2006). Surface-enhanced Raman spectroscopy using gold-core platinum-shell nanoparticle film electrodes: toward a versatile vibrational strategy for electrochemical interfaces. Langmuir, 22(25), 10372-10379.

[140] Frederix, F., Friedt, J. M., Choi, K. H., Laureyn, W., Campitelli, A., Mondelaers, D., & Borghs, G. (2003). Biosensing based on light absorption of nanoscaled gold and silver particles. Analytical chemistry, 75(24), 6894-6900.

[141] Xia, Y., Xiong, Y., Lim, B., & Skrabalak, S. E. (2009). Shape-controlled synthesis of metal nanocrystals: simple chemistry meets complex physics?. Angewandte Chemie International Edition, 48(1), 60-103.

[142] Arinze, E. S., Qiu, B., Nyirjesy, G., & Thon, S. M. (2016). Plasmonic nanoparticle enhancement of solution-processed solar cells: practical limits and opportunities. Acs Photonics, 3(2), 158-173.

[143] Metzger, B., Hentschel, M., & Giessen, H. (2016). Ultrafast nonlinear plasmonic spectroscopy: from dipole nanoantennas to complex hybrid plasmonic structures. ACS Photonics, 3(8), 1336-1350.

[144] Anikeeva, P., & Deisseroth, K. (2012). Photothermal genetic engineering. ACS nano, 6(9), 7548-7552.

[145] Valsecchi, C., & Brolo, A. G. (2013). Periodic metallic nanostructures as plasmonic chemical sensors. Langmuir, 29(19), 5638-5649.

[146] Li, J., Liu, J., & Chen, C. (2017). Remote control and modulation of cellular events by plasmonic gold nanoparticles: implications and opportunities for biomedical applications. ACS nano, 11(3), 2403-2409.

[147] Kim, T., Lee, C. H., Joo, S. W., & Lee, K. (2008). Kinetics of gold nanoparticle aggregation: experiments and modeling. Journal of colloid and interface science, 318(2), 238-243.

[148]   Grillet, N., Manchon, D., Cottancin, E., Bertorelle, F., Bonnet, C., Broyer, M., ... & Pellarin, M. (2013). Photo-oxidation of individual silver nanoparticles: a real-time tracking of optical and morphological changes. The Journal of Physical Chemistry C, 117(5), 2274-2282.

[149]   Ustarroz, J., Kang, M., Bullions, E., & Unwin, P. R. (2017). Impact and oxidation of single silver nanoparticles at electrode surfaces: one shot versus multiple events. Chemical science, 8(3), 1841-1853.

[150]   Zhang, H., Chen, B., & Banfield, J. F. (2010). Particle size and pH effects on nanoparticle dissolution. The Journal of Physical Chemistry C, 114(35), 14876-14884.

[151]   Dai, D., Xu, D., Cheng, X., & He, Y. (2014). Direct imaging of single gold nanoparticle etching: sensitive detection of lead ions. Analytical Methods, 6(13), 4507-4511.

[152]   Daniel, M. C., & Astruc, D. (2004). Gold nanoparticles: assembly, supramolecular chemistry, quantum-size-related properties, and applications toward biology, catalysis, and nanotechnology. Chemical reviews, 104(1), 293-346.

[153]   Faraday, M. (1857). X. The Bakerian Lecture.—Experimental relations of gold (and other metals) to light. Philosophical Transactions of the Royal Society of London, (147), 145-181.

[154]   Turkevich, J., Stevenson, P. C., & Hillier, J. (1951). A study of the nucleation and growth processes in the synthesis of colloidal gold. Discussions of the Faraday Society, 11, 55-75.

[155]   Frens, G. (1973). Controlled nucleation for the regulation of the particle size in monodisperse gold suspensions. Nature physical science, 241(105), 20-22.

[156]   Giersig, M., & Mulvaney, P. (1993). Preparation of ordered colloid monolayers by electrophoretic deposition. Langmuir, 9(12), 3408-3413.

[157]   Brust, M., Walker, M., Bethell, D., Schiffrin, D. J., & Whyman, R. (1994). Synthesis of thiol-derivatised gold nanoparticles in a two-phase liquid–liquid system. Journal of the Chemical Society, Chemical Communications, (7), 801-802.

[158]   Reetz, M. T., & Helbig, W. (1994). Size-selective synthesis of nanostructured transition metal clusters. Journal of the American Chemical Society, 116(16), 7401-7402.

[159]   Cushing, B. L., Kolesnichenko, V. L., & O'Connor, C. J. (2004). Recent advances in the liquid-phase syntheses of inorganic nanoparticles. Chemical reviews, 104(9), 3893-3946.

[160]   Rodriguez-Sanchez, L., Blanco, M. C., & Lopez-Quintela, M. A. (2000). Electrochemical synthesis of silver nanoparticles. The Journal of Physical Chemistry B, 104(41), 9683-9688.

[161]   Huang, C. J., Chiu, P. H., Wang, Y. H., Chen, K. L., Linn, J. J., & Yang, C. F. (2006). Electrochemically controlling the size of gold nanoparticles. Journal of the Electrochemical Society, 153(12), D193-D198.

[162]   Yin, B., Ma, H., Wang, S., & Chen, S. (2003). Electrochemical synthesis of silver nanoparticles under protection of poly (N-vinylpyrrolidone). The Journal of Physical Chemistry B, 107(34), 8898-8904.

[163]   Lapp, A. S., Duan, Z., Marcella, N., Luo, L., Genc, A., Ringnalda, J., & Crooks, R. M. (2018). Experimental and theoretical structural investigation of AuPt nanoparticles synthesized using a direct electrochemical method. Journal of the American Chemical Society, 140(20), 6249-6259.

[164]   Shen, Q., Jiang, L., Zhang, H., Min, Q., Hou, W., & Zhu, J. J. (2008). Three-dimensional dendritic Pt nanostructures: sonoelectrochemical synthesis and electrochemical applications. The Journal of Physical Chemistry C, 112(42), 16385-16392.

[165]   Lee, P. C., & Meisel, D. (1982). Adsorption and surface-enhanced Raman of dyes on silver and gold sols. The Journal of Physical Chemistry, 86(17), 3391-3395.

[166]   Tao, A., Sinsermsuksakul, P., & Yang, P. (2006). Polyhedral silver nanocrystals with distinct scattering signatures. Angewandte Chemie International Edition, 45(28), 4597-4601.

[167]   Wiley, B., Sun, Y., & Xia, Y. (2007). Synthesis of silver nanostructures with controlled shapes and properties. Accounts of Chemical Research, 40(10), 1067-1076.

[168]   Jana, N. R., Gearheart, L., & Murphy, C. J. (2001). Seed-mediated growth approach for shape-controlled synthesis of spheroidal and rod-like gold nanoparticles using a surfactant template. Advanced Materials, 13(18), 1389-1393.

[169]   Pietrobon, B., McEachran, M., & Kitaev, V. (2009). Synthesis of size-controlled faceted pentagonal silver nanorods with tunable plasmonic properties and self-assembly of these nanorods. ACS nano, 3(1), 21-26.

[170]   Pietrobon, B., & Kitaev, V. (2008). Photochemical synthesis of monodisperse size-controlled silver decahedral nanoparticles and their remarkable optical properties. Chemistry of Materials, 20(16), 5186-5190.

[171]   Jin, R., Cao, Y. C., Hao, E., Métraux, G. S., Schatz, G. C., & Mirkin, C. A. (2003). Controlling anisotropic nanoparticle growth through plasmon excitation. Nature, 425(6957), 487-490.

[172]   Tauster, S. J. (1987). Strong metal-support interactions. Accounts of Chemical Research, 20(11), 389-394.

[173]   Campbell, C. T., Parker, S. C., & Starr, D. E. (2002). The effect of size-dependent nanoparticle energetics on catalyst sintering. Science, 298(5594), 811-814.

[174]   Campbell, C. T. (2013). The energetics of supported metal nanoparticles: relationships to sintering rates and catalytic activity. Accounts of chemical research, 46(8), 1712-1719.

[175]   Farmer, J. A., & Campbell, C. T. (2010). Ceria maintains smaller metal catalyst particles by strong metal-support bonding. Science, 329(5994), 933-936.

[176]   Sun, Y., & Xia, Y. (2002). Shape-controlled synthesis of gold and silver nanoparticles. science, 298(5601), 2176-2179.

[177]   Sun, Y., Yin, Y., Mayers, B. T., Herricks, T., & Xia, Y. (2002). Uniform silver nanowires synthesis by reducing AgNO3 with ethylene glycol in the presence of seeds and poly (vinyl pyrrolidone). Chemistry of Materials, 14(11), 4736-4745.

[178]   Im, S. H., Lee, Y. T., Wiley, B., & Xia, Y. (2005). Large-scale synthesis of silver nanocubes: the role of hcl in promoting cube perfection and monodispersity. Angewandte Chemie International Edition, 44(14), 2154-2157.

[179]   Wiley, B., Herricks, T., Sun, Y., & Xia, Y. (2004). Polyol synthesis of silver nanoparticles: use of chloride and oxygen to promote the formation of single-crystal, truncated cubes and tetrahedrons. Nano Letters, 4(9), 1733-1739.

[180]   Wiley, B. J., Im, S. H., Li, Z. Y., McLellan, J., Siekkinen, A., & Xia, Y. (2006). Maneuvering the surface plasmon resonance of silver nanostructures through shape-controlled synthesis.

[181]   Métraux, G. S., & Mirkin, C. A. (2005). Rapid thermal synthesis of silver nanoprisms with chemically tailorable thickness. Advanced Materials, 17(4), 412-415.

[182] Aherne, D., Ledwith, D. M., Gara, M., & Kelly, J. M. (2008). Optical properties and growth aspects of silver nanoprisms produced by a highly reproducible and rapid synthesis at room temperature. Advanced Functional Materials, 18(14), 2005-2016.

[183] Bastys, V., Pastoriza-Santos, I., Rodríguez-González, B., Vaisnoras, R., & Liz-Marzán, L. M. (2006). Formation of silver nanoprisms with surface plasmons at communication wavelengths. Advanced Functional Materials, 16(6), 766-773.

[184] Darmanin, T., Nativo, P., Gilliland, D., Ceccone, G., Pascual, C., De Berardis, B., ... & Rossi, F. (2012). Microwave-assisted synthesis of silver nanoprisms/nanoplates using a "modified polyol process". Colloids and Surfaces A: Physicochemical and Engineering Aspects, 395, 145-151.

[185] Li, K., Jia, X., Tang, A., Zhu, X., Meng, H., & Wang, Y. (2012). Preparation of spherical and triangular silver nanoparticles by a convenient method. Integrated Ferroelectrics, 136(1), 9-14.

[186] Rivas, L., Sanchez-Cortes, S., Garcia-Ramos, J. V., & Morcillo, G. (2001). Growth of silver colloidal particles obtained by citrate reduction to increase the Raman enhancement factor. Langmuir, 17(3), 574-577.

[187] Lee, K. J., Jun, B. H., Kim, T. H., & Joung, J. (2006). Direct synthesis and inkjetting of silver nanocrystals toward printed electronics. Nanotechnology, 17(9), 2424.

[188] Kim, D., Jeong, S., & Moon, J. (2006). Synthesis of silver nanoparticles using the polyol process and the influence of precursor injection. Nanotechnology, 17(16), 4019.

[189] Sato-Berrú, R., Redón, R., Vázquez-Olmos, A., & Saniger, J. M. (2009). Silver nanoparticles synthesized by direct photoreduction of metal salts. Application in surface-enhanced Raman spectroscopy. Journal of Raman Spectroscopy: An International Journal for Original Work in all Aspects of Raman Spectroscopy, Including Higher Order Processes, and also Brillouin and Rayleigh Scattering, 40(4), 376-380.

[190] Zhang, W., Qiao, X., & Chen, J. (2007). Synthesis of nanosilver colloidal particles in water/oil microemulsion. Colloids and Surfaces A: Physicochemical and Engineering Aspects, 299(1-3), 22-28.

[191] Lim, P. Y., Liu, R. S., She, P. L., Hung, C. F., & Shih, H. C. (2006). Synthesis of Ag nanospheres particles in ethylene glycol by electrochemical-assisted polyol process. Chemical physics letters, 420(4-6), 304-308.

[192]   Ashkarran, A. A. (2010). A novel method for synthesis of colloidal silver nanoparticles by arc discharge in liquid. Current Applied Physics, 10(6), 1442-1447.

[193]   Ghosh, S. K., Kundu, S., Mandal, M., Nath, S., & Pal, T. (2003). Studies on the evolution of silver nanoparticles in micelle by UV-photoactivation. Journal of nanoparticle research, 5(5-6), 577-587.

[194]   Pugazhenthiran, N., Anandan, S., Kathiravan, G., Prakash, N. K. U., Crawford, S., & Ashokkumar, M. (2009). Microbial synthesis of silver nanoparticles by Bacillus sp. Journal of Nanoparticle Research, 11(7), 1811.

[195]   Sintubin, L., De Windt, W., Dick, J., Mast, J., Van Der Ha, D., Verstraete, W., & Boon, N. (2009). Lactic acid bacteria as reducing and capping agent for the fast and efficient production of silver nanoparticles. Applied Microbiology and Biotechnology, 84(4), 741-749.

[196]   Suresh, A. K., Pelletier, D. A., Wang, W., Moon, J. W., Gu, B., Mortensen, N. P., & Doktycz, M. J. (2010). Silver nanocrystallites: biofabrication using Shewanella oneidensis, and an evaluation of their comparative toxicity on gram-negative and gram-positive bacteria. Environmental science & technology, 44(13), 5210-5215.

[197]   Fayaz, A. M., Balaji, K., Girilal, M., Yadav, R., Kalaichelvan, P. T., & Venketesan, R. (2010). Biogenic synthesis of silver nanoparticles and their synergistic effect with antibiotics: a study against gram-positive and gram-negative bacteria. Nanomedicine: Nanotechnology, Biology and Medicine, 6(1), 103-109.

[198]   Sagar, G., & Ashok, B. (2012). Green synthesis of silver nanoparticles using Aspergillus niger and its efficacy against human pathogens. European Journal of Experimental Biology, 2(5), 1654-1658.

[199]   Young, K. (2007). Synthesis and galvanic replacement reaction of silver nanocubes in organic medium. Journal of Young Investigators, 16 (4), web publication.

[200]   Huang, L., Zhai, M. L., Long, D. W., Peng, J., Xu, L., Wu, G. Z., ... & Wei, G. S. (2008). UV-induced synthesis, characterization and formation mechanism of silver nanoparticles in alkalic carboxymethylated chitosan solution. Journal of Nanoparticle Research, 10(7), 1193-1202.

[201]   Aslan, K., Leonenko, Z., Lakowicz, J. R., & Geddes, C. D. (2005). Fast and slow deposition of silver nanorods on planar surfaces: application to metal-enhanced fluorescence. The Journal of Physical Chemistry B, 109(8), 3157-3162.

[202]   Gu, X., Nie, C., Lai, Y., & Lin, C. (2006). Synthesis of silver nanorods and nanowires by tartrate-reduced route in aqueous solutions. Materials Chemistry and Physics, 96(2-3), 217-222.

[203]   Zhang, D., Qi, L., Yang, J., Ma, J., Cheng, H., & Huang, L. (2004). Wet chemical synthesis of silver nanowire thin films at ambient temperature. Chemistry of Materials, 16(5), 872-876.

[204]   Nghia, N. V., Truong, N. N., Thong, N. M., & Hung, N. P. (2012). Synthesis of nanowire-shaped silver by polyol process of sodium chloride. Int. J. Mater. Chem, 2(2), 75-78.

[205]   Luther, W. (2004). Technological analysis: Industrial application of nanomaterials—chances and risksFuture Technologies Division of VDI Technologiezentrum GmbH, D€usseldorf, Germany.

[206]   Ghosh Chaudhuri, R., & Paria, S. (2012). Core/shell nanoparticles: classes, properties, synthesis mechanisms, characterization, and applications. Chemical reviews, 112(4), 2373-2433.

[207]   Hu, Z., Escamilla Ramírez, D. J., Heredia Cervera, B. E., Oskam, G., & Searson, P. C. (2005). Synthesis of ZnO nanoparticles in 2-propanol by reaction with water. The Journal of Physical Chemistry B, 109(22), 11209-11214.

[208]   FuÈredi-Milhofer, H., Ivancic, V. B., Brecevic, L., & Filipovic, N. (1990). Vincekovic', D. Kralj, L. Komunjer, M. Marcovic, D. Skrtic. Colloids. Surf, 48, 219.

[209]   Mafuné, F., Kohno, J. Y., Takeda, Y., Kondow, T., & Sawabe, H. (2000). Structure and stability of silver nanoparticles in aqueous solution produced by laser ablation. The Journal of Physical Chemistry B, 104(35), 8333-8337.

[210]   Sugimoto, T., & Shiba, F. (2000). Spontaneous nucleation of monodisperse silver halide particles from homogeneous gelatin solution II: silver bromide. Colloids and Surfaces A: Physicochemical and Engineering Aspects, 164(2-3), 205-215.

[211]   Zhang, W., Qiao, X., & Chen, J. (2008). Formation of silver nanoparticles in SDS inverse microemulsions. Materials Chemistry and Physics, 109(2-3), 411-416.

[212]   Pal, T., Sau, T. K., & Jana, N. R. (1997). Reversible formation and dissolution of silver nanoparticles in aqueous surfactant media. Langmuir, 13(6), 1481-1485.

[213]   Pawar, M. J., & Chaure, S. S. (2009). Synthesis of CdS nanoparticles using glucose as a capping agent. Chalcogenide Lett, 6(12), 689-693.

[214]   Chaudhuri, R. G., & Paria, S. (2010). Synthesis of sulfur nanoparticles in aqueous surfactant solutions. Journal of colloid and interface science, 343(2), 439-446.

[215]   Bahadar, H., Maqbool, F., Niaz, K., & Abdollahi, M. (2016). Toxicity of nanoparticles and an overview of current experimental models. Iranian biomedical journal, 20(1), 1.

[216]   Ibrahim, K. S. (2013). Carbon nanotubes-properties and applications: a review. Carbon letters, 14(3), 131-144.

[217]   Khlebtsov, N., & Dykman, L. (2011). Biodistribution and toxicity of engineered gold nanoparticles: a review of in vitro and in vivo studies. Chemical Society Reviews, 40(3), 1647-1671.

– Chapter 2 –

Preparation and characterization of silver-based materials as carbon paste electrode modifiers

I. Introduction

The preparation and electrochemical characterization of compact and coherent metal deposits are of greatest importance in various fields of engineering and technology such as supercapacitors, corrosion protective coatings, energy conversion, electrosynthesis, electrocatalysis devices, etc. [1–3]. In the latest years, chemically modified electrodes (CMEs) have been used for the quantification of various organic and inorganic species after open-circuit accumulation [4, 5]. Many modifying agents have been used either as coatings on solid electrode surfaces or dispersed within a conductive matrix [6]. Thus, they are widely used in the voltammetric detection of organic compounds by dint of their efficiency and sensitivity. The design of new nanoscale materials has acquired ever-greater importance in recent years owing to their various applications. Among these materials, metallic particles are of great interest due to their numerous properties [7, 8].

The use of carbon paste electrodes (CPEs) in electrochemical studies were initiated by Adams[9] and well investigated by Bauer et *al.* [10, 11] and Lecuire [12, 13]The first works were carried out using ultra pure graphite rods whose surface was renewed after each measurement by simple sintering of the end of the electrode. The non-reproducibility of the measurements, as well as the presence of large residual currents, limits the use of this electrode [14].Furthermore, the carbon paste electrode properties depend on the purity of the compounds used to prepare the paste, the carbon/binder ratio, the graphite particle size, the treatment and the mode of renewal of the surface of the electrode. From the beginning of the 70s, a new approach regarding the design of electrodes was proposed. This approach consists of the fixation of a substance to the surface of the electrode in order to improve the reactivity and selectivity of electrochemical reactions. In fact, an extensive range of materials such as silver [15-17], palladium particles-impregnated sodium montmorillonite [18], NiO supported onto activated carbon [19], Al_2O_3 supported onto activated carbon [20], polymers and enzymes [21-24] were used as carbon paste modifiers. The fields of application of modified electrodes are wide and numerous especially for the control of the environment. They are generally used for the analysis of pesticides [23-25], pharmaceuticals compounds [18], phenolic [19, 20] and aromatic nitrocompounds [25]. Aromatic nitrocompounds are among the most toxic substances and widely used as precursor in chemical synthesis of various azo dyes, antioxidants, pesticides, antiseptic agents, poultry medicines, fuel additives, and corrosion inhibitors [26]. Among these metals, silver species has drawn great scientific interest

because of its wide range of electrochemical applications. In fact, silver finds numerous applications since they impart useful properties to the coated surfaces, such as excellent thermal and electrical conductivity, chemical resistance, catalytic and bactericidal activity [27–29]. As of late, CPE and associated sensors have attracted remarkable attention compared to other solid-state electrodes in electroanalysis due to their practical advantages such as a large potential window, simple preparation, easy and inexpensive modification, etc. [30, 31]. However, the response recorded on the unmodified electrode was the least selective and sensitive. In addition, these electrodes present a very difficult task in the presence of interference, which is probably due to their sluggish electron transport phenomenon [32]. Indeed, variously modified carbon paste electrodes, modification procedures, and methodologies have been described in the literature [33–43].

In electrocatalysis and electroanalysis, there is increasing interest in the development of effective electrochemical methodologies based on innovative and suitable electrode materials in order to improve the catalytic efficiencies and to reduce both cathode and anode overpotentials during the electrosynthesis processes. Thus, one of the dominant themes in electrochemical research has been the attempt to modulate the chemical composition and/or morphological properties of the electrode materials in order to obtain the desired degree of catalytic activity, selectivity, chemical, and physical stability or mechanical properties.

The present chapter was undertaken in order to define in detail the synthesis procedures of the different silver-based modifiers (Impregnation, Electrodeposition, and modification by nanoparticles) as well as the characterization methods we have used.

II. Chemicals and reagents

Sodium hydroxide, acetic acid, and phosphoric acid, and boric acid were obtained from Merck (Darmstadt, Germany), Fluka (St. Gallen, Switzerland), and Riedel de Haen (Seelze, Germany) and were used as received from supplier. 4-nitroaniline, hexacyanoferrate ($\{Fe(CN)6\}^{3-/4-}$) were ordered from Sigma-Aldrich and used without any further purification. Phosphate buffered saline (PBS) with different pH was served as a working medium throughout the experiment, containing 0.1 mol L^{-1} K_2HPO_4, and 0.1 M KH_2PO_4. PNA purchased from Sigma-Aldrich. Sodium borohydride was obtained from Merck (Darmstadt, Germany), Fluka (St. Gallen, Switzerland), and Riedel de Haen (Seelze, Germany) and was used as received from supplier. Paraffin was used

as the pasting liquid for the carbon-paste electrode (CPE). Carbon paste was supplied from Carbone Lorraine (Lorraine, France; ref. 9900). All aqueous solutions used through this thesis were prepared using distilled water. All experiments were unrolled at room temperature.

Silver nitrate ($AgNO_3$) is one of the most widely used salts for the preparation of silver nanoparticles. Despite its degradation in light requiring conservation precautions like most silver salts, it is mainly used in literature, for its accessibility, ease of use (easy and direct reduction without preparation) and price. Tollens reagent, silver sulfate and silver perchlorate have disadvantages compared to a green synthesis process: the first requires purification treatments, the second is poorly soluble in water and the last is explosive. Silver nitrate, of the formula $AgNO_3$, is in the form of odorless white crystals, soluble in water at room temperature with a molar mass of 169.87 g/mol. Silver represents 63.5% of the molar mass. The silver nitrate was purchased from Sigma Aldrich and has been stored in a dark place.

The chitosan flakes >75% deacetylated (Merck (Darmstadt, Germany) stock solution was prepared by dissolving an appropriate amount of commercial chitosan (0.1 g) in 2% acetic acid. Chitosan is a polysaccharide composed of 2-amino-2-deoxy- and 2-acetamido-2-deoxy-D-glucopyranose. It is generated by deacetylation of chitin. The name chitosan was proposed by *Hoppe-Seyler* in 1894. It is now commercially produced from waste from the consumption of crustaceans and the industrial processing of mushrooms. The degree of deacetylation (DDA) of chitosan is defined as the percentage of deacetylated units relative to the total number of units. The term chitosan applies to any copolymer with a deacetylation degree (DDA) greater than 50%. It has been considered as a potential biomaterial because of its distinguished properties, including biodegradability, biocompatibility, and non-toxicity. The presence of reactive amino and hydroxyl groups in the molecule makes chitosan an attractive metal chelating ligand for removal of heavy metal ions from wastewaters. Furthermore, chitosan is a biopolymer often used to enhance the stability of metal nanoparticles

II.2. Experimental analysis techniques

II.2.1. Electrochemical measurements

All electrochemical experiments (Cyclic voltammetry, Linear sweeping voltammetry, AC electrochemical impedance spectroscopy, Chronoamperometry, and differential pulse voltammetry were recorded in this thesis in a classical three electrodes setup using a voltalab

potentiostat/galvanostat/EIS electrochemical analyzer (ZIVE Lab sp1, WonATech, Korea), which was connected to a computer for storage and data acquisition, and a Smart Manager software served as the user interface. A platinum wire was used as a counter electrode; all potentials appointed in this report refer to values against Ag/AgCl/KCl (3M).The bare of CPE was cleaned with cyclic voltammetry by applying a potential between 0 V and + 2 V for several cycles in a solution containing 0.1 M H_2SO_4 and ethanol.

II.2.2. Optical measurements

II.2.2.1. Characterization of silver nanoparticles

The study of optical properties by absorption spectroscopy is an indispensable step in the characterization of synthesized silver nanoparticles. Indeed, metallic nanoparticles (silver, gold, copper) present particular optical properties linked to a classical effect of exaltation of the electric field, often called dielectric confinement.

Nanoparticles have a larger number of atoms, and therefore more free electrons on the surface than macroscopic objects. The excitation of the metal surface by light causes the collective vibration of the surface electrons. The excitation of the electrons induces vibration, a resonance at a certain wavelength. The electrons resonate and the wavelength concerned is thus absorbed.

The wavelength is mainly dependent on the chemical element (Ag, Au, Cu ...). In addition, smaller nanoparticles will have a vibration of higher energy, i.e. of shorter wavelength.

The absorbance bands depend on the shape and size of the nanoparticles [44, 45], so the change in size or shape induces a change in absorbance and wavelength of the absorption band [46-48]. UV-VIS spectroscopy is a spectral technique involving photons with wavelengths in the ultraviolet (200 nm-400 nm), visible, and near infrared (750 nm- 1400 nm) range. The spectra in this region are due to electronic transitions and correspond to emission or absorption spectra. Generally speaking, spherical silver nanoparticles are characterized by an absorbance band around 400 nm [49]. The width and symmetry of the band are characteristic of the size distribution of the nanoparticles. Indeed, wide size distribution of nanoparticles induces a widening of the absorbance band towards long wavelengths. Specifically, an absorption maximum observed between 300 and 330 nm characterizes the presence of nanoprisms. When this maximum is between 400 and 450 nm, the nanoparticles are spherical or near-spherical in geometry. Finally, the presence of an absorption maximum beyond 450 nm indicates the

94

formation of particles larger than 100 nm [50]. UV-Vis spectroscopy can also be used to check the stability of nanoparticles dispersions.

II.2.2.2. Conditions and apparatus

The UV–Visible absorption spectra was carried out using a double-beam scanning spectrophotometer (Shimadzu spectrophotometer, model biochrom) with a variable wavelength between 300 and 700 nm using a quartz cuvette of 1 cm path length and 3.50mL total volume.

II.2.3.Scanning Electron Microscopy (SEM)

II.2.3.1. Characterization

Another method for determining the average particle diameter is based on the use of electron microscopy techniques such as scanning electron microscopy (SEM). In this case, the particles are observed in the solid-state, so the technique does not take into account the possible hydration layer of the particles present in the solution. For this reason, differences of several tens of nanometers between the sizes measured by DLS and electron microscopy are frequently observed [51].

Scanning electron microscopy allows the observation of a sample at magnifications that cannot be achieved with visible light microscopy (from 35 to 100,000), with a large depth of field allowing the observation of rough samples. Microscopy can often confirm the conclusions made in UV-Vis spectroscopy. Silver being a metallic element, is known to be directly observable unlike organic elements sometimes requiring contrast agents as in the field of biology or polymer blends.

II.2.3.2. Conditions and apparatus

SEM observations were carried out using the JOEL JSM-IT100 scanning electron microscopy.

II.2.4. X-ray diffraction (XRD)

II.2.4.1. Characterization

X-ray diffraction is a technique for analyzing the organization of material at great distances. It allows the identification of crystalline compounds by comparison with spectra of compounds referenced in a database.

The structure of silver nanoparticles can be studied by X-ray diffraction (XRD). The technique makes it possible to characterize metallic silver and its diffraction planes. The diffraction planes of metallic silver Ag0 are generally observed at 2θ = 38.0, 44.0, 64.7, and 77.9° (with a copper cathode).These peaks are attributed to planes (1 1 1), (2 0 0), (2 2 0) and (3 1 1) of a face-centered cubic structure [52]. It is generally the most intense diffraction peak at 2θ = 38° that is sought by the authors. Diffraction peaks can also provide indications on the morphology of nanoparticles. A larger and less intense peak is indicative of a smaller size of nanoparticles and sometimes also of wider size distribution.

II.2.4.2. Conditions and apparatus

The phase compositions were observed by XRD (XPERT-PRO, PANalytical's) with X-ray source emitting Cu Kα radiation (k = 1.5406 Å) and scans acquisition at 2θ range from 10° to 80°, scan speed of 1°/min and step size of 0.02^o per second. The operational voltage and current were kept at 30 kV and 25 mA, respectively.

II.2.5. FT-IR Spectroscopy
II.2.5.1. Characterization

Infrared spectrometry is used to confirm the interaction between the silver and chitosan film. The reaction between silver nanoparticles and chitosan can be identified by shifting characteristic bands attributed to different functional groups present in the reagents [53], such as carbonyl and amine groups. The presence of silver nanoparticles in the composite can cause the number of waves to shift to lower values. This is known as "blue-shift", and "red-shift" in the opposite case.

II.2.5.2. Conditions and apparatus

The Fourier transform infrared (FTIR) spectrums were recorded using a (PerkinElmer FTIR 1600, Germany using a KBr method).

III. Electrodes preparation
III.1. Thermal deposition of silver onto carbon paste electrode (Ag$_{Imp}$-CPE)

The modified carbon paste electrode was prepared by thoroughly mixing carbon graphite powder and silver nitrates ($AgNO_3$) by different ratios by weight (w/w) in an agate mortar. The obtained

powder was calcined at temperature of 200 °C for 12 h in the kiln. The resulting powder was mixed with paraffin oil in a mortar by exhaustively hand mixing with a pestle and then incorporated into the electrode cavity (laboratory made, 0.13 cm^2 geometric surface areas) (Figure 1). The external surface of electrode was smoothed on a paper sheet. Electrical contact was established by a bar of carbon. The resulting electrode is hereby denoted as Ag$_{Imp}$-CPE.
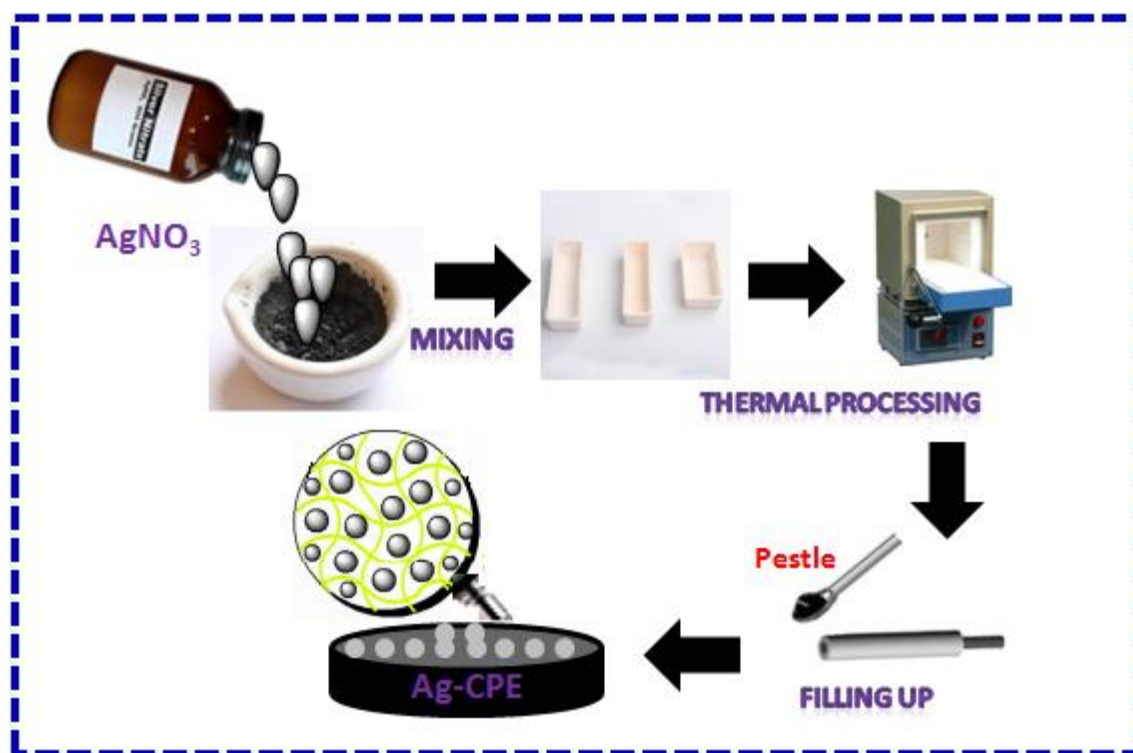

Figure1: *Illustration of the impregnation process of silver on carbon paste electrode*

(Ag$_{Imp}$-CPE)

III.2. Electrochemical deposition of silver onto carbon paste electrode (Ag$_{ED}$-CPE)

CPEs were prepared according to the following procedure [19]. A portion of the homogeneous paste was firmly packed in the electrode cavity (laboratory made, 0.13 cm^2 geometric surface area) and was polished by smooth paper. A carbon bar was used to establish electrical contact. To deposit Ag particles onto CPE, it was soaked in an electrochemical cell containing 0.5 mmol L^{-1} of AgNO$_3$ dissolved in 0.1 mol L^{-1} of potassium nitrates (KNO$_3$) electrolyte solution. The Ag particles were fixed on the surface of the electrode with cyclic voltammetry between potential

ranges from 600 mV to -400 mV for 1.5 cycles (6 segments).The resulting electrode is hereby denoted as Ag_{ED}-CPE. The electrodeposition process schematically illustrated in Figure 2.
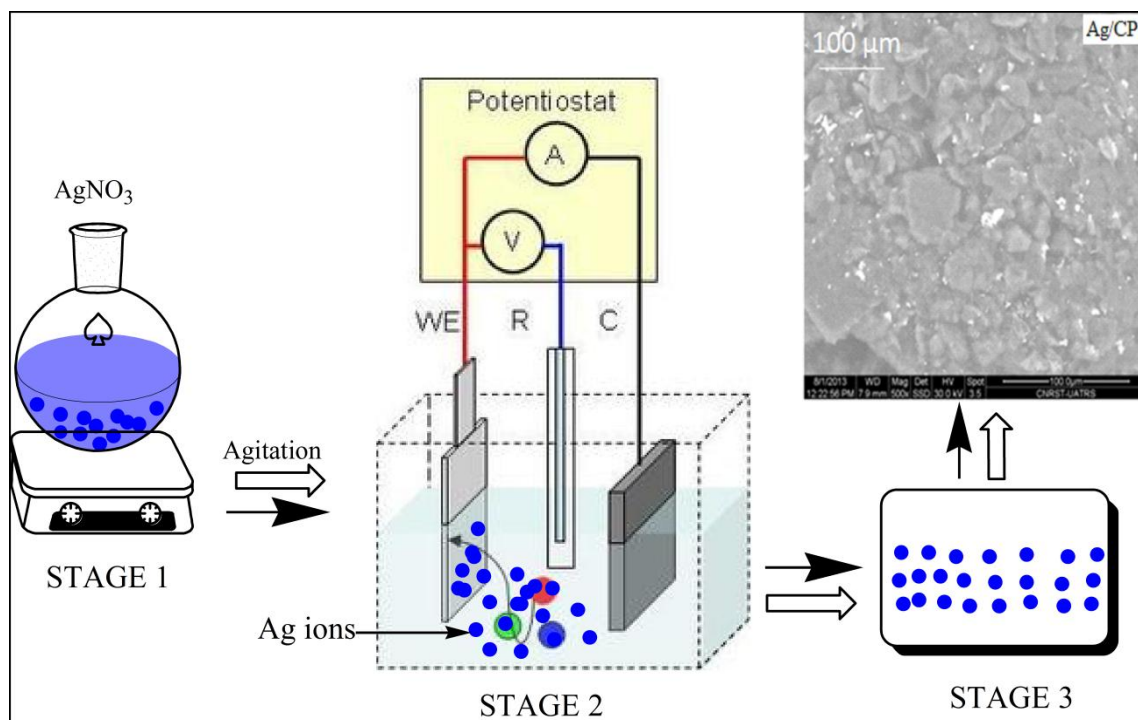

Figure 2: Illustration of the electrodeposition process of silver on carbon paste electrode

III.3. Chitosan gelified modified carbon paste electrodes

Initially, the chitosan gelified solution was prepared by dissolving an appropriate amount of chitosan (0.1 g) in a 2% acetic acid solution by stirring quickly for one night at room temperature until it had completely dispersed. The pH was adjusted to 5.0 with a 1.0 mol L^{-1} NaOH solution under vigorous agitation. A transparent chitosan gel was obtained. Then, carbon paste powder was added to the transparent gelified solution with hand mixing (2:98 w/w). Figure3 depicts the construction process of chitosan modified carbon electrode CS-CPE.
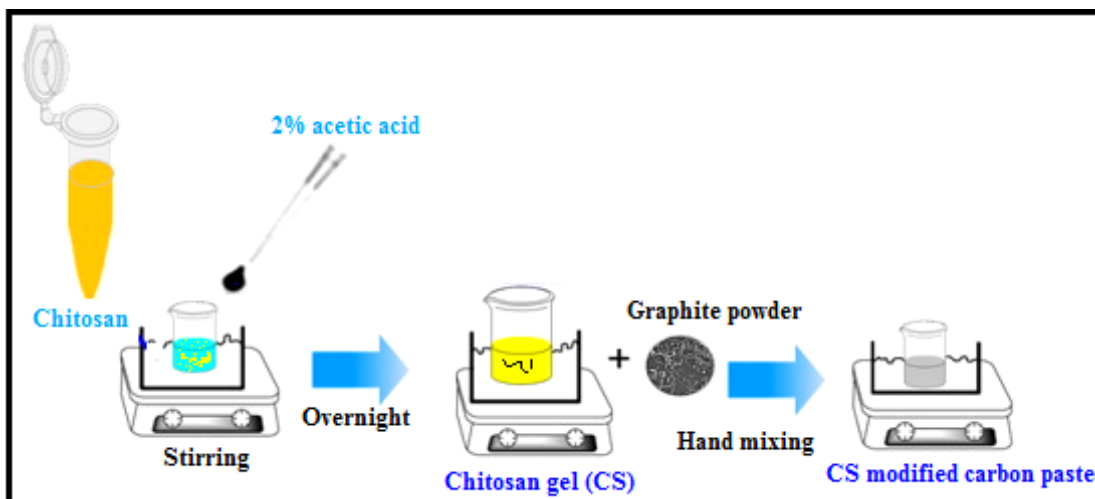
98

Figure3: *Construction process of chitosan modified carbon electrode CS-CPE.*

III.4. Chitosan stabilized silver nanoparticles modified carbon paste electrodes

The chitosan–silver nanoparticles (CS@AgNPs) are manufactured by reduction of silver nitrate ($AgNO_3$) with sodium borohydride ($NaBH_4$) and stabilized with chitosan, which is a polysaccharide biopolymer known by their dispersive properties and stability in an aqueous medium. Silver nanoparticles were modified by chitosan by dint of the presence of $-NH_2$ and $-$OH groups in the chitosan, which can help in possible adsorption interactions between chitosan and heavy metal ions including Ag^+, proteins, and dyes [54]. The suspension of chitosan-AgNPs material was prepared as reported in the literature [55]: 0.10 g of chitosan was dissolved in 10 mL of 2% acetic acid, and then the mixture was stirred overnight to obtain a homogeneous solution. To the above solution, 1 mL of 10 mM $AgNO_3$ was added. After 30 min, 0.8 mg of $NaBH_4$ was then added under vigorous stirring. The sodium borohydride was used as a reducing agent [56]. The solution becomes colored (yellow) denoting the formation of AgNPs (Figure 4).
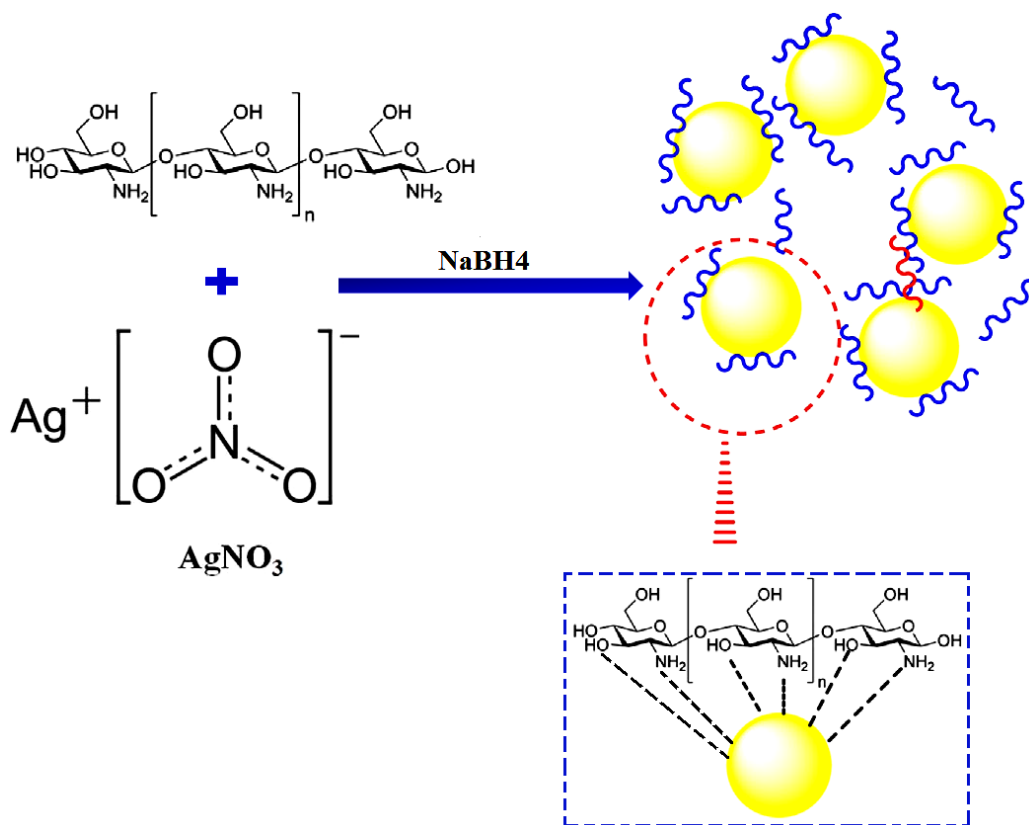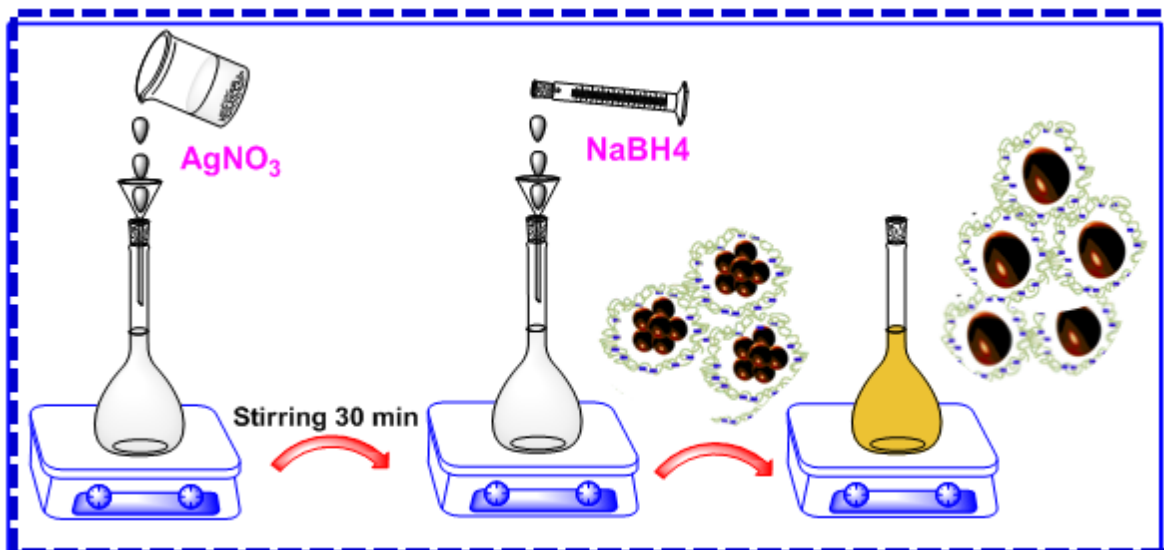
Figure 4: *The mechanism of formation of chitosan-Ag nanoparticles.*

The modified electrodes were prepared by immersing carbon paste electrodes in the homogeneous yellow-brown solution of CS@AgNPs for 15 min with slight agitation. The modification is summarized in Figure 5.

100
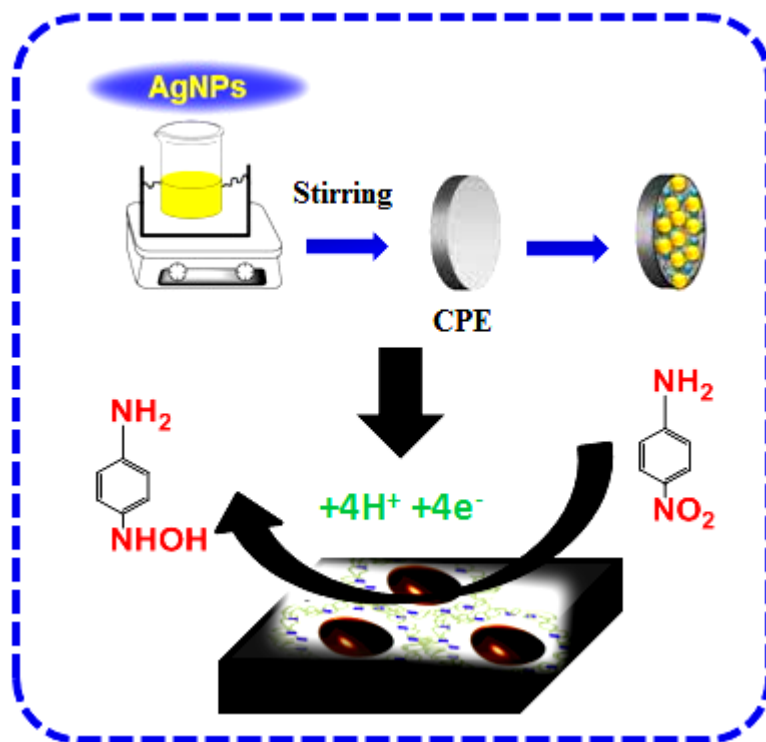
Figure 5: *The modification process of carbon paste electrodes*

References

[1]   Lipkowski, J., & Ross, P. N. (1994). The electrochemistry of novel materials (Vol. 3). VCH Publishers, Inc., Weinheim.

[2]   Masters, J. I. (1970). The Ultraviolet Photovoltaic Effect in Evaporated Silver Bromide Conduction Cells. Journal of The Electrochemical Society, 117(11), 1378.

[3]   Prudenziati, M., Morten, B., Gualtieri, A. F., & Leoni, M. (2004). Dissolution kinetics and diffusivity of silver in glassy layers for hybrid microelectronics. Journal of Materials Science: Materials in Electronics, 15(7), 447-453.

[4]   Kalcher, K., Kauffmann, J. M., Wang, J., Švancara, I., Vytřas, K., Neuhold, C., & Yang, Z. (1995). Sensors based on carbon paste in electrochemical analysis: a review with particular emphasis on the period 1990–1993. Electroanalysis, 7(1), 5-22.

[5]   Li, J., Liu, S., Mao, X., Gao, P., & Yan, Z. (2004). Trace determination of rare earths by adsorption voltammetry at a carbon paste electrode. Journal of Electroanalytical Chemistry, 561, 137-142.

[6]   Laghrib, F., Lahrich, S., Farahi, A., Bakasse, M., & El Mhammedi, M. A. (2018). Impregnation of silver in graphite carbon using solid reaction: Electrocatalysis and detection of 4-nitroaniline. Journal of Electroanalytical Chemistry, 823, 26-31.

[7]   Starowicz, M., Stypuła, B., & Banaś, J. (2006). Electrochemical synthesis of silver nanoparticles. Electrochemistry Communications, 8(2), 227-230.

[8]   Welch, C. M., & Compton, R. G. (2006). The use of nanoparticles in electroanalysis: a review. Analytical and bioanalytical chemistry, 384(3), 601-619.

[9]   Adams, R. N. (1969). Electrochemistry at Solid Electrodes, Marcel Deccer. Inc., New York, 26.

[10]   Bauer, D., & Gaillochet, M. P. (1974). Etude du comportement de la pate de carbone a compose electroactif incorpore. Electrochimica Acta, 19(10), 597-606.

[11]   Lamache, M., & Bauer, D. (1977). Étude, par chronoampérométrie, de l'électrode á pâte de carbone á liant électrolytique et solide électroactif incorporé. Journal of Electroanalytical Chemistry and Interfacial Electrochemistry, 79(2), 359-364.

[12]   Lecuire, J. M. (1975). Réduction électrochimique des oxydes de fer: Application à la mesure de non stoechiométrie. Journal of Electroanalytical Chemistry and Interfacial Electrochemistry, 66(3), 195-205.

[13]   Lecuire, J. M., & Evrard, O. (1977). Reduction electrochimique des oxydes de fer: Confrontation des caracteristiques electrochimiques et crist allographiques. Journal of Electroanalytical Chemistry and Interfacial Electrochemistry, 78(2), 331-339.

[14]   R. N. Adams, Carbon paste electrodes application to anodic voltammetry, Analytical. Chimica Acta, 30 (1958) 1576.

[15]   Farahi, A., Achak, M., El Gaini, L., El Mhammedi, M. A., & Bakasse, M. (2016). Silver particles-modified carbon paste electrodes for differential pulse voltammetric determination of paraquat in ambient water samples. Journal of the Association of Arab Universities for Basic and Applied Sciences, 19(1), 37-43.

[16]   Farahi, A., Achak, M., El Gaini, L., El Mhammedi, M. A., & Bakasse, M. (2015). Electrochemical determination of paraquat in citric fruit based on electrodeposition of silver particles onto carbon paste electrode. journal of food and drug analysis, 23(3), 463-471.

[17]   Lahrich, S., Hammani, H., Boumya, W., Loudiki, A., Farahi, A., Achak, M.,& El Mhammedi, M. A. (2016). Correlation between electrochemical impedance and spectroscopic measurements in adsorbing paraquat on silver: Application in underground water samples. Electroanalysis, 28(5), 1012-1022.

[18]   Loudiki, A., Boumya, W., Hammani, H., Nasrellah, H., El Bouabi, Y., Zeroual, M.,& Bakasse, M. (2016). Ibuprofen analysis in blood samples by palladium particles-impregnated sodium montmorillonite electrodes: Validation using high performance liquid chromatography. Materials Science and Engineering: C, 69, 616-624.

[19]   Hammani, H., Boumya, W., Laghrib, F., Farahi, A., Lahrich, S., Aboulkas, A., & El Mhammedi, M. A. (2017). Electrocatalytic effect of NiO supported onto activated carbon in oxidizing phenol at graphite electrode: Application in tap water and olive oil samples. Journal of the Association of Arab Universities for Basic and Applied Sciences, 24(1), 26-33.

[20]   Hammani, H., Boumya, W., Laghrib, F., Farahi, A., Lahrich, S., Aboulkas, A., & El Mhammedi, M. A. (2017). Electrocatalytic effect of NiO supported onto activated carbon in oxidizing phenol at graphite electrode: Application in tap water and olive oil samples. Journal of the Association of Arab Universities for Basic and Applied Sciences, 24(1), 26-33.

[21]   Laschi, S., Bulukin, E., Palchetti, I., Cristea, C., & Mascini, M. (2008). Disposable electrodes modified with multi-wall carbon nanotubes for biosensor applications. Irbm, 29(2-3), 202-207.

[22]   Antiochia, R., & Gorton, L. (2014). A new osmium-polymer modified screen-printed graphene electrode for fructose detection. Sensors and Actuators B: Chemical, 195, 287-293.

[23]   de Lacey, A. L., Bes, M. T., Gómez-Moreno, C., & Fernández, V. M. (1995). Amperometric enzyme electrode for NADP+ based on a ferrodoxin-NADP+ reductase and viologen-modified glassy carbon electrode. Journal of Electroanalytical Chemistry, 390(1-2), 69-76.

[24]   Ramdane-Terbouche, C. A., Terbouche, A., Djebbar, S., & Hauchard, D. (2014). Electrochemical sensors using modified electrodes based on copper complexes formed with Algerian humic acid modified with ethylenediamine or triethylenetetramine for determination of nitrite in water. Talanta, 119, 214-225.

[25]   El Mhammedi, M. A., Achak, M., Bakasse, M., & Chtaini, A. (2009). Electrochemical determination of para-nitrophenol at apatite-modified carbon paste electrode: Application in river water samples. Journal of Hazardous Materials, 163(1), 323-328.

[26]   Sun, J. H., Sun, S. P., Fan, M. H., Guo, H. Q., Qiao, L. P., & Sun, R. X. (2007). A kinetic study on the degradation of p-nitroaniline by Fenton oxidation process. Journal of hazardous materials, 148(1-2), 172-177.

[27]   Rondinini, S. B., Mussini, P. R., Crippa, F., & Sello, G. (2000). Electrocatalytic potentialities of silver as a cathode for organic halide reductions. Electrochemistry communications, 2(7), 491-496.

[28]   Liu, H. T., Xia, X., & Guo, Z. P. (2002). A novel silver oxide electrode and its charge–discharge performance. Journal of applied electrochemistry, 32(3), 275-279.

[29]   Jana, S., Ghosh, S. K., Nath, S., Pande, S., Praharaj, S., Panigrahi, S., ...& Pal, T. (2006). Synthesis of silver nanoshell-coated cationic polystyrene beads: A solid phase catalyst for the reduction of 4-nitrophenol. Applied Catalysis A: General, 313(1), 41-48.

[30]   Ganesh, P. S., & Swamy, B. K. (2015). Sodium dodecyl sulphate/poly (brilliant blue)/multi walled carbon nanotube modified carbon paste electrode for the voltammetric

resolution of dopamine in the presence of ascorbic acid and uric acid. Journal of Analytical & Bioanalytical Techniques, 6(6), 1.

[31]   Apetrei, C., Apetrei, I. M., Saja, J. A. D., & Rodriguez-Mendez, M. L. (2011). Carbon paste electrodes made from different carbonaceous materials: application in the study of antioxidants. Sensors, 11(2), 1328-1344.

[32]   Ganesh, P. S., & Swamy, B. K. (2016). Voltammetric resolution of catechol and hydroquinone at eosin Y film modified carbon paste electrode. Journal of Molecular Liquids, 220, 208-215.

[33]   Jain, A., Gupta, V., & Singh, L. (1997). Macrocycle based membrane sensors for the determination of cobalt (II) ions. Analyst, 122(6), 583-586.

[34]   Gupta, V. K., Prasad, R., Kumar, P., & Mangla, R. (2000). New nickel (II) selective potentiometric sensor based on 5, 7, 12, 14-tetramethyldibenzotetraazaannulene in a poly (vinyl chloride) matrix. Analytica Chimica Acta, 420(1), 19-27.

[35]   Prasad, R., Gupta, V. K., & Kumar, A. (2004). Metallo-tetraazaporphyrin based anion sensors: regulation of sensor characteristics through central metal ion coordination. Analytica Chimica Acta, 508(1), 61-70.

[36]   Gupta, V. K., Ganjali, M. R., Norouzi, P., Khani, H., Nayak, A., & Agarwal, S. (2011). Electrochemical analysis of some toxic metals by ion–selective electrodes. Critical Reviews in Analytical Chemistry, 41(4), 282-313.

[37]   Goyal, R. N., Gupta, V. K., Oyama, M., & Bachheti, N. (2007). Gold nanoparticles modified indium tin oxide electrode for the simultaneous determination of dopamine and serotonin: application in pharmaceutical formulations and biological fluids. Talanta, 72(3), 976-983.

[38]   Gupta, V. K., Singh, L. P., Singh, R., Upadhyay, N., Kaur, S. P., & Sethi, B. (2012). A novel copper (II) selective sensor based on dimethyl 4, 4′(o-phenylene) bis (3-thioallophanate) in PVC matrix. Journal of Molecular Liquids, 174, 11-16.

[39]   Gupta, V. K., Sethi, B., Sharma, R. A., Agarwal, S., & Bharti, A. (2013). Mercury selective potentiometric sensor based on low rim functionalized thiacalix [4]-arene as a cationic receptor. Journal of Molecular Liquids, 177, 114-118.

[40] Gupta, V. K., Jain, A. K., & Maheshwari, G. (2007). Aluminum (III) selective potentiometric sensor based on morin in poly (vinyl chloride) matrix. Talanta, 72(4), 1469-1473.

[41] Gupta, V. K., Jain, A. K., Agarwal, S., & Maheshwari, G. (2007). An iron (III) ion-selective sensor based on a μ-bis (tridentate) ligand. Talanta, 71(5), 1964-1968.

[42] Goyal, R. N., Gupta, V. K., Bachheti, N., & Sharma, R. A. (2008). Electrochemical sensor for the determination of dopamine in presence of high concentration of ascorbic acid using a Fullerene-C60 coated gold electrode. Electroanalysis: An International Journal Devoted to Fundamental and Practical Aspects of Electroanalysis, 20(7), 757-764.

[43] Jain, R., Gupta, V. K., Jadon, N., & Radhapyari, K. (2010). Voltammetric determination of cefixime in pharmaceuticals and biological fluids. Analytical biochemistry, 407(1), 79-88.

[44] Domingos, J. B. (2013). Preparation of Silver Nanoparticles Stabilized by Dextran and Oligosaccharides-Based Amphiphiles for Application in Catalysis and Sensors (Doctoral dissertation, Université de Grenoble).

[45] Evanoff Jr, D. D., & Chumanov, G. (2005). Synthesis and optical properties of silver nanoparticles and arrays. ChemPhysChem, 6(7), 1221-1231.

[46] Sharma, V. K., Yngard, R. A., & Lin, Y. (2009). Silver nanoparticles: green synthesis and their antimicrobial activities. Advances in colloid and interface science, 145(1-2), 83-96.

[47] Zhao, X., Xia, Y., Li, Q., Ma, X., Quan, F., Geng, C., & Han, Z. (2014). Microwave-assisted synthesis of silver nanoparticles using sodium alginate and their antibacterial activity. Colloids and Surfaces A: Physicochemical and Engineering Aspects, 444, 180-188.

[48] Jovanović, Ž., Radosavljević, A., Šiljegović, M., Bibić, N., Mišković-Stanković, V., & Kačarević-Popović, Z. (2012). Structural and optical characteristics of silver/poly (N-vinyl-2-pyrrolidone) nanosystems synthesized by γ-irradiation. Radiation Physics and Chemistry, 81(11), 1720-1728.

[49] Huang, H., & Yang, X. (2004). Synthesis of polysaccharide-stabilized gold and silver nanoparticles: a green method. Carbohydrate research, 339(15), 2627-2631.

[50]   Luo, C., Zhang, Y., Zeng, X., Zeng, Y., & Wang, Y. (2005). The role of poly (ethylene glycol) in the formation of silver nanoparticles. Journal of colloid and interface science, 288(2), 444-448.

[51]   Seo, S. Y., Lee, G. H., Lee, S. G., Jung, S. Y., Lim, J. O., & Choi, J. H. (2012). Alginate-based composite sponge containing silver nanoparticles synthesized in situ. Carbohydrate polymers, 90(1), 109-115.

[52]   Liu, T. M., Yu, J., Chang, C. A., Chiou, A., Chiang, H. K., Chuang, Y. C., ... & Huang, C. C. (2014). One-step shell polymerization of inorganic nanoparticles and their applications in SERS/nonlinear optical imaging, drug delivery and catalysis. Scientific reports, 4(1), 1-10.

[53]   Bin Ahmad, M., Lim, J. J., Shameli, K., Ibrahim, N. A., & Tay, M. Y. (2011). Synthesis of silver nanoparticles in chitosan, gelatin and chitosan/gelatin bionanocomposites by a chemical reducing agent and their characterization. Molecules, 16(9), 7237-7248.

[54]   Chen, Z., Zhang, X., Cao, H., & Huang, Y. (2013). Chitosan-capped silver nanoparticles as a highly selective colorimetric probe for visual detection of aromatic ortho-trihydroxy phenols. Analyst, 138(8), 2343-2349.

[55]   de Lima, C. A., da Silva, P. S., & Spinelli, A. (2014). Chitosan-stabilized silver nanoparticles for voltammetric detection of nitrocompounds. Sensors and Actuators B: Chemical, 196, 39-45.

[56]   Tolaymat, T. M., El Badawy, A. M., Genaidy, A., Scheckel, K. G., Luxton, T. P., & Suidan, M. (2010). An evidence-based environmental perspective of manufactured silver nanoparticle in syntheses and applications: a systematic review and critical appraisal of peer-reviewed scientific papers. Science of the total environment, 408(5), 999-1006.

– Chapter 3 –

Electrochemical evaluation of catalytic effect of metallic silver electrode towards the reduction of p-nitroaniline

I. Introduction

The performance of the voltammetric procedure is strongly influenced by the working-electrode material. The working electrode should provide high signal to-noise characteristics, as well as a reproducible response. Thus, its selection depends primarily on two factors: the redox behavior of the target analyte and the background current over the potential region required for the measurement. Other considerations include the potential window, electrical conductivity, surface reproducibility, mechanical properties, cost, availability, and toxicity. A range of materials have found application as working electrodes for electroanalysis. The most popular are those involving mercury, carbon, or noble metals.

The fields of electroanalytic and electrocatalytic chemistry are as vibrant as ever today. New platforms for detection and sensing are being developed for a wide variety of chemically, biologically, and environmentally important analytes and many of these involve some sort of electrochemical signal transduction. At the heart of any electroanalytical method is the working or indicator electrode. These methods are made possible by the unique nature of the specific working electrode material, namely the electronic, structural, and chemical properties. Due to their unusual physical and chemical properties [1, 2], metal electrodes have attracted much more attention in recent years and generally exhibit high electrocatalytic activity towards aromatic nitro compounds, whose redox process is slow on bare electrodes. A series of studies on the catalytic conversion of nitroaromatics have been extended using various metals, including Au, Ag and Cu particles, as catalysts. These materials have superior electrochemical properties for the study of the electrochemical behavior of nitroaromatics and their determination.

In recent years, increasing attention has been paid to the field of conversion of nitroaromatics into NH_2-containing aromatics, not only because of the toxicity to humans, fish, algae, and invertebrates but also because of the explosive nature of some nitroaromatics resulting from nitro groups as explosophores [3–6].They attract much attention in relation to pollutions, toxicity, mutagenesis, carcinogenesis, therapeutic action and as intermediates in the synthesis of important organic compounds [7, 8]. As a member of aniline compounds, PNA is an important compound used as an intermediate or precursor in the manufacture of organics, such as p-phenylenediamine, azo dyes, antioxidants, pesticides, antiseptic agents and medicines for poultry. The release of PNA in its production or utilization will cause serious eco-environmental problems due to its high toxicity, carcinogenic and mutagenic effects [9–12]. It may induce central nervous, cardiovascular system and other organ damage even if a

small amount of PNA is ingested by human body. PNA-containing wastewater discharged into water will result in the death of aquatic organisms and the long-term damage to the environment.

This chapter described the electrocatalytic effect of metallic silver electrode towards the reduction of PNA and their sensitive determination in aqueous medium using cyclic voltammetry (CV), chronoamperometry, linear scan voltammetry, electrochemical impedance spectroscopy (EIS), and differential pulse voltammetry (DPV). Specifically, this chapter focuses on the comparison of the performances of silver electrode with different other electrodes including gold, graphite, and glassy carbon.

II. p-nitroaniline an overview

p-nitroaniline is an aromatic amine extensively used as an intermediate in the production of several industrial and high-volume chemicals including pesticides [13,14], and thus it has been found as a contaminant in agricultural biosolid generated from industrial wastewater sludge [15]. PNA is a ubiquitous contaminant in the environment up to 100 mg L^{-1} [16] especially in agricultural soil from the application of such biosolid as a part of fertilizer [15] and from pesticide natural transformation [13, 17]. It has been enlisted as one of the major priority pollutants and subjected to treatment [14] due to its chemical stability and persistence [18–20] as well as toxicological effects to living organisms and human health even at low concentrations [21, 22]. Its unique chemical structure containing an electron withdrawing nitro group and an electron donating amino group in para position in the aromatic ring has attracted attention due to its non-linear optical properties, such as non-linear susceptibility [23]. The chemical treatment of PNA using advanced oxidation process or photocatalytic degradation has been used [14, 24–26], but they are costly and usually cause secondary pollution. Thus, there is a growing interest in an easy, time efficiency, stable, and high selectivity and sensitive determination of harmful chemicals using electrochemical methods. Previous works have explored its determination using voltammetric methods which exhibit low cost per analysis, the possibility of multi analyte detection, easy miniaturization and high sensitivity when compared to other methods of determination [27–29]. Shikata and Taguchi were the first to determine the reduction potential of the isomers of nitroaniline. Their study revealed that since nitroanilines are weak bases, the reduction potential of ionic and molecular forms of this compound could be detected using polarographic method with the dropping mercury electrode [30]. Maistrenko et al. used carbon paste electrode (CPE) with adsorption-

stripping voltammetry (ASV) for determination of nitroaniline. This study reveals that the range of the reduction potential in acid pH is from 0.48 to 0.52 V, depending on the nature and the position of the substituents. The sensibility of detection of para isomers with CPE is lower than for meta and ortho isomers in all cases studied [31]. Lin et *al*. made a simultaneous determination of the noxious nitroaniline isomers, by cyclic voltammetry (CV) and DPV, with the electro-polymerization of 7-[(2,4-dihydroxy-5-carboxybenzene)azo]-8-hydroxyquinoline-5-sulfonic acid (DHCBAQS) at a graphene-nafion-modified GCE, denoted at this work as, DHCBAQS/graphene nafion/GCE. The obtained LD was about 0.14l mol dm^{-3} for all the compounds [32]. Maistrenko et *al*. studied the preconcentration and voltammetric behavior of nitro organic compounds on carbon paste electrodes modified by chromatographic stationary phases (CSP/CPE). The ortho and para isomers of nitrophenol, nitroaniline, and nitro benzoic acid can be detected selectively, but for all substances, the LQ and LD are not available [33]. Abdel Asis Jbarah and Rudolf Holze reported a complete spectro-electrochemical redox mechanism for nitroanilines isomers using gold and platinum working electrodes [34]. The authors pointed out that PNA could be electrochemically detected either by reduction of the nitro group and formation of p-phenylenediamine (p-PDA) or by oxidation of the amine group. Passivation of the working electrode was noticed for the oxidation reaction and pretreatment of the electrode is necessary to eliminate this passivation.

Rizk presented an alternative way for the detection of PNA by potentiometric methods with apoly(vinyl chloride) membrane sensor [35]. Chen et *al*. reported the simultaneous detection of nitroaniline isomers using beta-cyclodextrin (beta-CD)/silver nanoparticles (AgNP) composite modified indium titanium oxide (ITO) electrodes (beta-CD/AgNPs/ITOE) [36]. Kodari et *al*. reported a simultaneous detection of 4-nitrobenzoic acid, PNA, and 4-nitrobenzaldehyde using voltammetric methods at a commercial GCE [37].

Zhao et *al*. made the electrochemical quantification of PNA can be based on DPV reduction at modified glassy carbon electrode using ionic liquid–single-walled carbon nanotube (SWNT) gel [38]. The author's report that PNA can exhibit a sensitive cathodic peak at 0.70 V (vs.SCE) in pH 7.0 phosphate buffer solution on the electrode, resulting from the irreversible reduction of PNA. Another paper uses as working electrode a CPE modified with 6,7,9,10,17,18,19,20,21,22-decahydrodibenzo [h,r][1,4,7,11,15] trioxadiazacyclonanodecine-16,23-dione (DTD)/silver nanoparticles (AgNPs) [39]. Wushuang Bai et *al*. developed a new method of production of silver nanoparticles (AgNPs)modified with hydrophobic polyhedral oligomeric silsesquioxane (POSS) and graphene oxide (GO) nanocomposites.GCE modified

by this nanocomposite (AgNPs/POSS/rGO/GCE) was used as a working electrode for an electrochemical sensor to detect and quantify nitrobenzene, PNA, and 4-nitrobenzoic acid detection and quantification [40]. Ahmad et *al.* developed a binder-free high-sensitive chemical sensor based on directly grown ZnO NRs on pre-seeded FTO electrodes via low-temperature solution route for PNA determination. Laghrib et *al.* developed based-silver sensors for the electrocatalytic reduction of PNA and there sensitive determination in real samples [41-47].

III. Electrochemistry of p-nitroaniline

III.1. Electrochemical procedure

Several supporting electrolytes were tested such as phosphate, acetate, and Britton Robinson buffer solutions. The best electrochemical response measured was obtained using Britton Robinson buffer solution (pH 2.0). A known concentration of PNA solution was prepared in 0.1 mol L^{-1} Britton Robinson buffer solution (pH 2.0) and thereafter, 20 mL of prepared solution was transferred into an electrochemical cell. The cyclic and differential voltammograms were recorded between 0.2 and -1 V at scan rate of 50 mV s^{-1}. For chronoamperometry, the potential was scanned from 0.4 to -1.2 V at scan rate of 0.10 V s^{-1}. The linear voltammetry polarization was carried out from 0.2 to -0.7 at a scan rate 50 mV s^{-1}. The EIS measurements were performed in frequency range as follows: first frequency (10^3 Hz), middle frequency (10^6) Hz and last one (10 mHz) with amplitude of 10^3 V.

III.2. Electrochemical behavior of PNA

The electrochemical behavior of PNA was evaluated using cyclic voltammetry (CV) at GC, Au, Gr and Ag electrodes in BR buffer (pH: 2.0) containing 1.0×10^{-3} mol L^{-1} of PNA in the range from 0.2 to -1 V at a scan rate of 100 mV s^{-1}. As shown in Fig. 1A the cathodic peak potential for PNA on glassy carbon (GC), gold (Au), and graphite carbon Gr electrodes appeared at about -0.8 V, while on metallic silver (Ag) electrode, it appears approximately at -0.26 V. No oxidation peak was observed in the cyclic voltammograms at all electrodes in the range from -1 V to 0.2 V, indicating that the electrochemical process is totally irreversible. The meanwhile peak potential of metallic silver electrode (curve a) shifted toward positive direction compared to other used electrodes which indicated a greatly decreased over-potential on the metallic silver electrode. This demonstrates that silver facilitates the reduction of PNA. In addition, the metallic silver electrode may also aid in the detection of PNA.

Indeed, it has an excellent anti-interference property since it allows the potential peak to shift between PNA and other compounds [48].

In order to properly evaluate the catalytic capacity of the Ag electrode, amperometric experiments were also carried out in BR buffer 0.1 mol L^{-1} (pH 2.0) using the above-mentioned electrodes. The results (Fig. 1B) show that silver electrode has higher current densities than other metal electrodes.
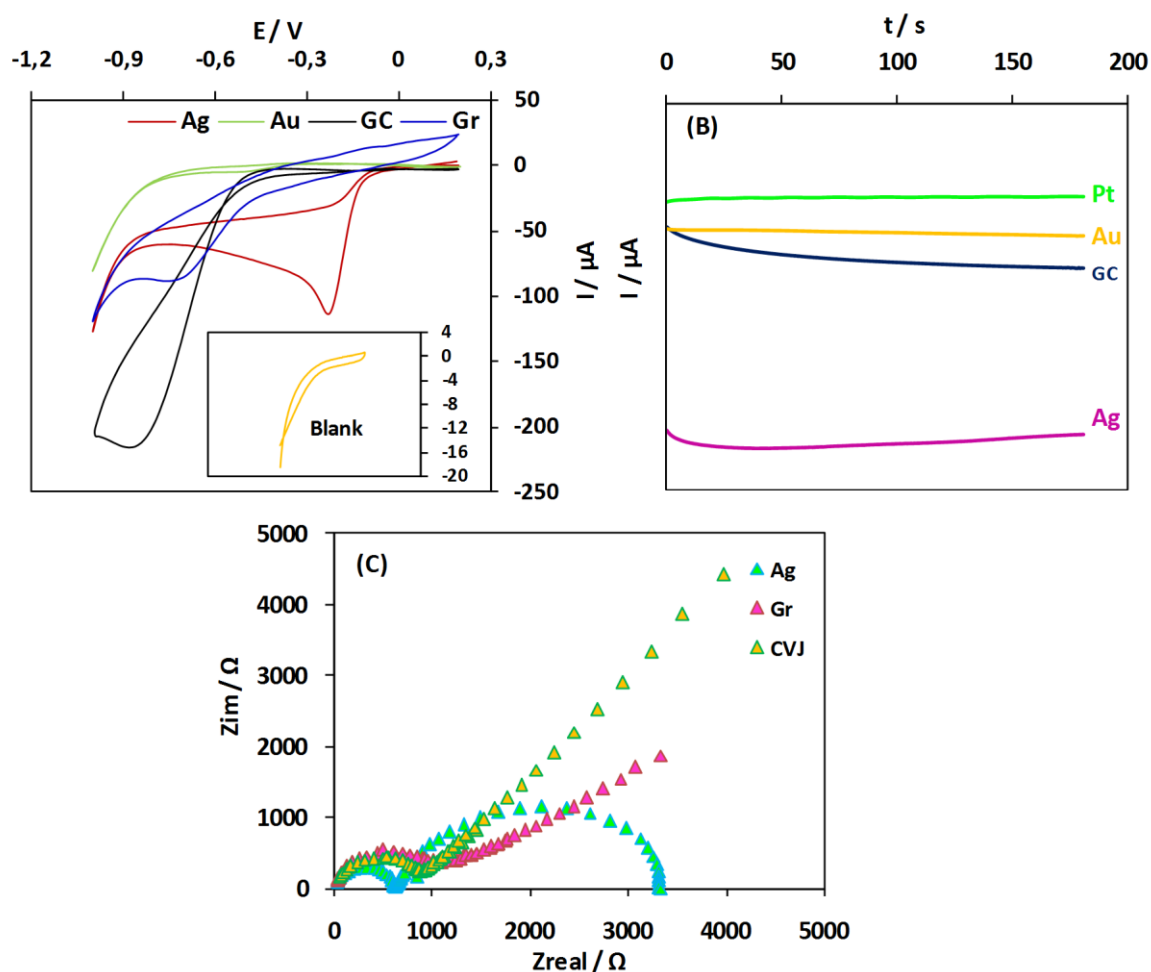

Figure 1: *(A) CV of 1.0×10^{-3} mol L^{-1} PNA for Ag, Gr, GC and Au at scan rate 100 mV s^{-1} in 1.0×10^{-1} mol L^{-1} BR buffer (pH 2.0). Inset blank solution. (B) Chronoamperograms obtained in 0.1 mol L^{-1} BR buffer (pH 2) of PNA at reduction potential (-0.3 V) using different electrodes. (C) EIS Nyquist plots obtained for Ag, GC and Gr in 0.1 mol L^{-1} BR buffer containing 1.0×10^{-3} mol L^{-1} of PNA.*

Moreover, electrochemical impedance spectroscopy (EIS) was also recorded to further investigate and to confirm the electrocatalytic effect of silver in reducing PNA with regard to the other electrodes. The experiments were carried out in a solution containing 0.1 mol L^{-1} BR

buffer and 1.0×10^{-3} mol L^{-1} of PNA. As can be seen in the Fig. 1C, the plots are composed of semi-circles and straight-line portions, representing charge transfer and diffusion-controlled processes, respectively.

In Nyquist plots, the charge transfer resistance (Rct) on metallic surface electrodes is related to the diameter of semicircle. It is seen that the charge transfer resistance (Rct) was 1380.90 kΩ of bare GCE, 1411.60 kΩ of Au and 45.70 kΩ of Gr. While, when using the metallic silver electrode, the scale of the semicircle dramatically decreased and the Rct value was 2.10 kΩ. This lowest Rct value can be attributed to the lowest charge transfer resistance and corresponding superior electrochemical kinetics at the surface of this electrode. This result was also confirmed by calculating k (the heterogeneous electron transfer rate constant) in the case of the various electrodes according to the following equation (Eq. 1) [49-51]:

$$K = \frac{RT}{(nF)^2 C_0 A R_{ct}} \quad (1)$$

where "Rct" is the charge transfer resistance, "T" is the temperature, "R" is the gas constant, "F" is the Faraday constant, "C$_0$" is the concentration of the solution and "A" is the area of the electrode. In particular, the Ag electrode displayed higher constant k value (4.02×10^{-5} cm² s^{-1}) compared to all other electrodes (5.99×10^{-8} cm² s^{-1} for Au, 1.85×10^{-6} cm² s^{-1} for Gr and 6.13×10^{-8} cm² s^{-1} for GC). The observed boucle of low frequency charge transfer can be attributed to the relaxation process, resulting in the adsorption of PNA on the surface of the Ag electrode. All these results confirm the best catalytic properties of the metallic silver electrode for the reduction of PNA. Based on these results, a mechanistic and kinetic study of PNA on metallic silver electrode is carried out in the next sections.

III.3. Electrocatalytic study

III.3.1. Scan rate and pH effect

To further investigate the PNA characteristics at the metallic silver electrode, the effect of scan rates on the PNA voltammetric behavior was studied. Fig. 2A shows a series of cyclic voltammograms of PNA (1.0×10^{-3} mol L^{-1}) in Britton Robinson buffer at metallic silver electrode with increasing scan rates from 1 to 400 mV s^{-1}. The peak current (Ip) is directly proportional to the square root of scan rate ($v^{1/2}$) of Ag electrode (Fig. 2B). The correlation coefficient was 0.997 and high value of slope (-17.44 μA mV s$^{-1/2}$) was obtained. This

phenomenon suggested a diffusion-controlled process at this electrode surface. In this case, for irreversible diffusion-controlled processes [52], the number of electrons in the overall reaction is obtained from the slope of (Ip) versus ($v^{1/2}$) plot (Eq. 2):

$$I_p = 3.01 \times 10^5\, n[(1-\alpha)n_\alpha]^{1/2}\, AC_b\, v^{1/2}\, D^{1/2} \quad (2)$$

Considering $(1-\alpha)n_\alpha = 0.72$ (as calculated below), $D = 5.44 \times 10^{-4}\,\text{cm}^2\,\text{S}^{-1}$(that was obtained by chronoamperometry), $A = 0.2\,\text{cm}^2$, the total number of electrons (n) corresponding to PNA reduction is calculated ($n \approx 4$). This founding is in good agreement with the results reported in the literature [53, 54]. The electrocatalytic reduction mechanism of PNA was studied using the plot of the scan rate normalized current (Ip $v^{-1/2}$) versus the scan rate (v) (Fig. 2C),which exhibits a characteristic shape typical of an EC' catalytic mechanism.
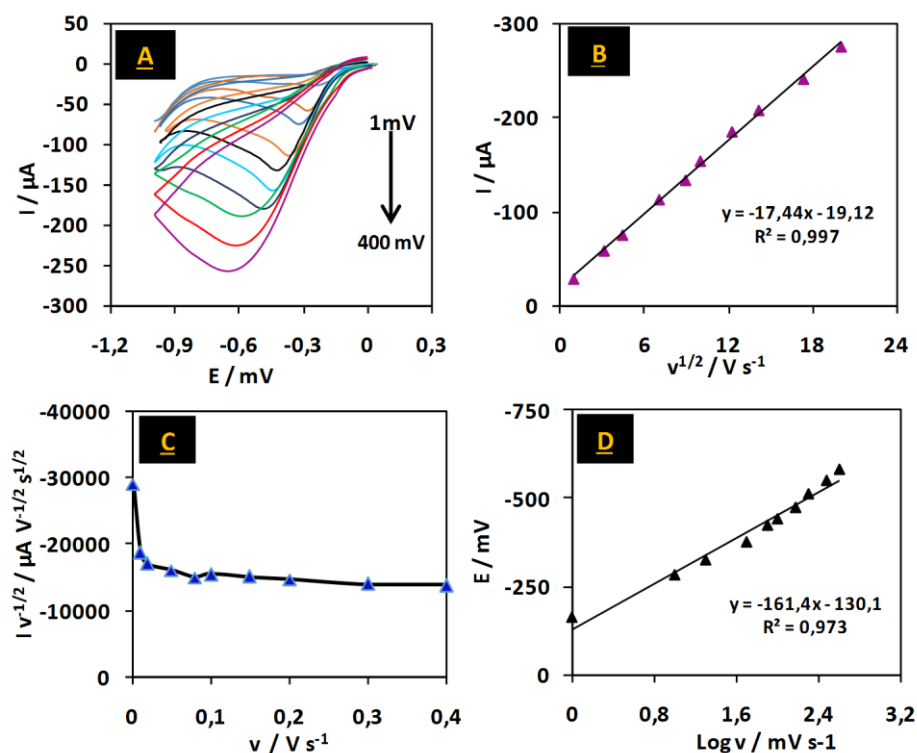

Figure 2: CVs of 1.0×10^{-3} mol L^{-1} PNA in 0.1 mol L^{-1} BR buffer (pH 2); (A) CVs at scan rates of 1, 10, 20, 50, 80, 100, 150, 200, 300, 400 mV s^{-1}; (B) Variations of Ip with root of scan rate;(C) variation of the scan rate normalized peak current (Ip $v^{-1/2}$) versus scan rate; (D) Variations ofEp with logarithm of scan rate.

115

In the case of a slow scan rate (υ), the catalytic rate constant (k') can be calculated using the developed theoretical model [55] for EC' catalytic mechanism and derived a relationship between the peak current and the concentration of analyte (Eq. 3):

$$I_{cat} = 0.496 \, nFAC_s \, D^{1/2} \, \upsilon^{1/2} \, (RT/nF)^{1/2} \quad (3)$$

Where C_s is the bulk concentration (mol cm^{-3}) of the analyte (in this case; PNA) and other symbols have their conventional meanings. According to the approach of Andrieux and Saveant in their theoretical paper [55], the average value of k' was calculated to be 7.38×10^{-5} cm^2 s^{-1}. The electrochemical behavior of silver electrode was carefully investigated in BR buffer by cyclic voltammetry. The effect of buffer pH on cyclic voltammetric responses of the silver electrode was further investigated in the pH range from 1.07 to 11.8 and well-defined cyclic voltammetric curves were observed (Fig. 3A). With the decrease of buffer pH bellow 2.0, the reduction peak potential shifted to the positive direction, implying that protons were involved in the electrode process. Once the pH of the solution exceeds pH 2.48, the peak potential of PNA reduction returns to its initial position obtained by the conventional electrodes, approximately at -0.8 V. Consequently, pH ≤ 2.48 represents the best range of electrocatalytic activity of the working electrode toward PNA reduction.

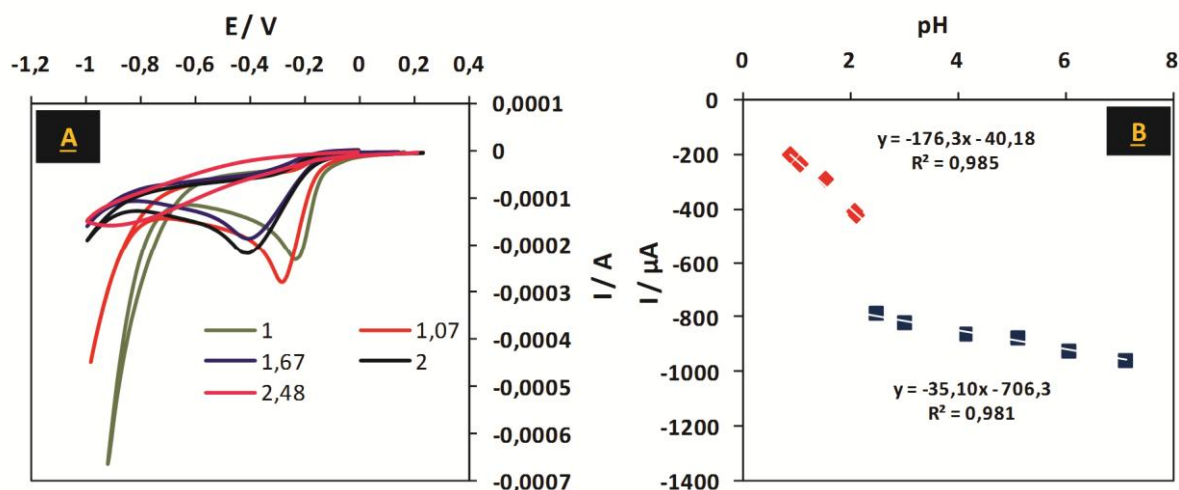**Figure 3:** *(A) CVs (at 50 mV s^{-1}) of 1.0×10^{-3} mol L^{-1} PNA at different values of buffered pH. (B) Plot of Ep versus pH.*

Moreover, the pH dependence of peak current and peak potential shows that the number of electrons transferred is not equal to that of the hydrogen ions, since the slopes of the equations

Ep *vs.* pH (Fig. 3B) over the studied pH range which are not close to the expected theoretical value of 59 mV/pH [56].

III.3.2. Amperometric studies

Chronoamperometry is a time-dependent technique where a square-wave potential is applied to the working electrode. The current of the electrode, measured as a function of time, fluctuates according to the diffusion of an analyte from the bulk solution toward the sensor surface. Chronoamperometry can therefore be used to measure current–time dependence for the diffusion-controlled process occurring at an electrode. This varies with analyte concentration. Chronoamperometry experiments were carried out for various concentrations of PNA to examine the electrochemical activity and stability of the electrocatalysts by setting the working electrode at a potential of -500 mV at a fixed time of 180s.The resulting current–time dependence is monitored and typical profiles are shown in fig. 4A.

The shape of this can be explained by the changes in concentration distance profiles of the target analyte in a similar manner as described for cyclic voltammetry. The characteristic shape of the resulting chronoamperograms can be represented by the Cottrell equation (Eq. 4) [57]:

$$Ip = \frac{nFAC * \sqrt{D}}{\sqrt{\pi}\sqrt{t}} \qquad (4)$$

where, n is the moles of electrons involved in the reaction, F is the Faraday constant, A is the area of the electrode (cm^2), C* the concentration of the analyte in the bulk solution (mol / cm^3), D is the diffusion coefficient (cm^2/s) and t is time(s). Consequently, *i* will be proportional to $t^{-1/2}$ for each concentration of PNA (Fig. 4B).

By substituting the slopes of the Cottrell plots (Fig. 4C) and other parameters in Cottrell equation, the mean value of D for PNA was found to be $5.44 \times 10^{-4} cm^2 s^{-1}$.

The rate constant of the electro-catalytic PNA reduction was also calculated using the obtained chronoamperograms and the following equation (Eq. 5) [58]:

$$I_C/I_L = \Upsilon^{1/2}[\pi^{1/2} erf (\Upsilon^{1/2}) + exp (\Upsilon) /\Upsilon^{1/2}] \qquad (5)$$

Where, I_L and I_C are the currents in the absence and presence of 4-NA, respectively. $\Upsilon = kC_0t$ is the argument of error function. C_0, k, and t are the concentration of PNA in bulk solution,

the catalytic rate constant and elapsed time, respectively. When Υ exceeds 2, the error function is almost equal to 1 and the equation can be reduced to (Eq. 6):

$$I_C / I_L = \pi^{1/2} \cdot \Upsilon^{1/2} = \pi^{1/2} (kC_0 t)^{1/2} \quad (6)$$

Therefore, from the slope of the I_C/I_L versus $t^{1/2}$ plot (Fig. 4D) and the above equation, the mean value of k was found to be approximately 5.24×10^{-3} mol L^{-1} s^{-1}.
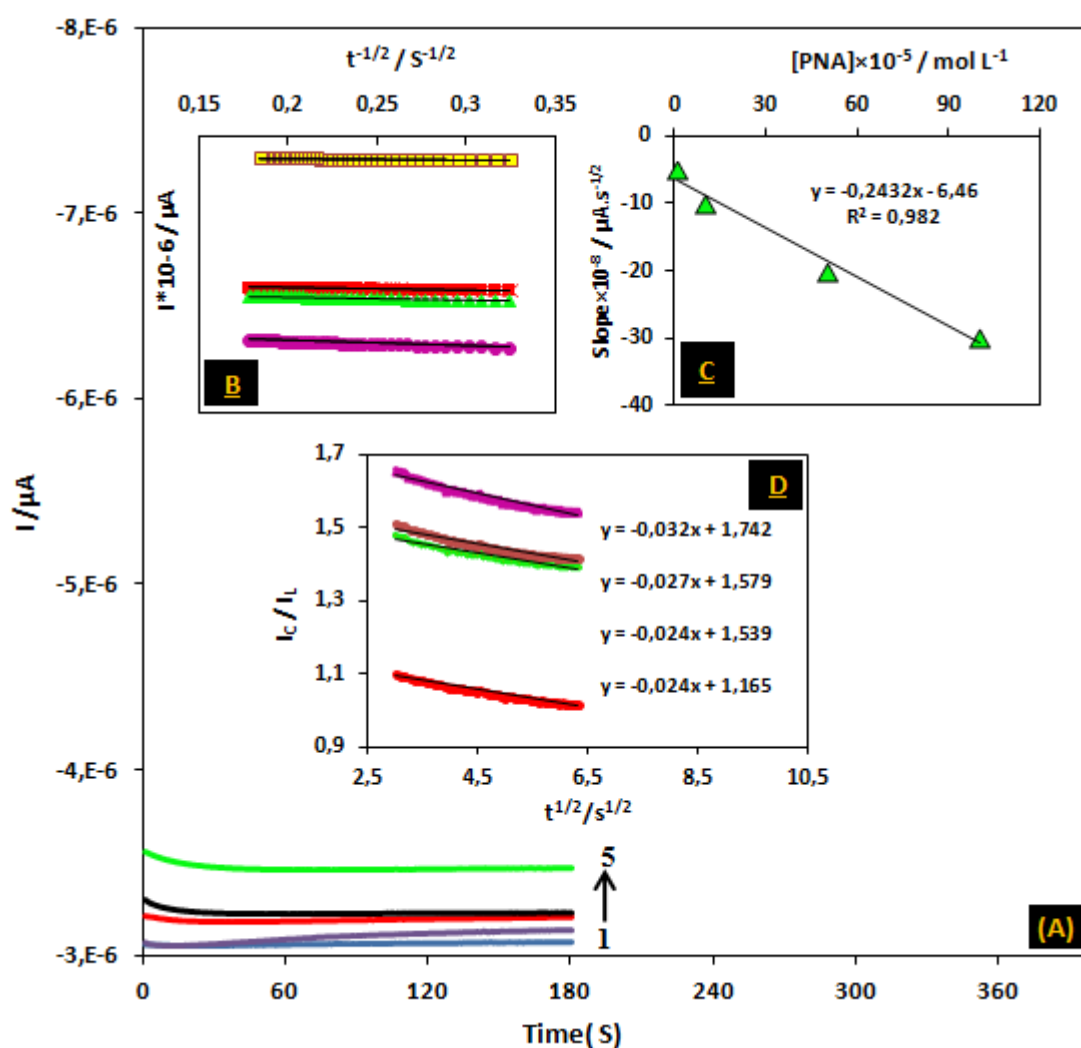

Figure 4:(A) Chronoamperograms obtained for PNA concentrations at Ag electrode of 1 (1), 0.5 (2), 0.1 (3), 0.05 (4) and 0.01 (5) mmol L^{-1}. (B) Plots of I versus $t^{-1/2}$ obtained from chronoamperograms (1) to (5). (C) Plot of slopes of straight lines against PNA concentration and (D) dependence of I_C/I_L on $t^{1/2}$.

III.3.3. Tafel polarization plot

In order to obtain information about the rate determining step, a Tafel plot was recorded (Fig. 5) using the data derived from the raising part of the current–voltage curve at scan rate of 50 mV s^{-1}. The value of Tafel slope, 0.54 V/ decade, indicates that for n ≈ 4electron transfer process in the rate determining step, a transfer coefficient α of about 0.57 can be calculated which shows a highly parallel kinetic curve[57]. Moreover, the value of the exchange current density (j$_0$), which was calculated from the intercept of Tafel plot [57], is equal to 381.15 μA/cm^2.
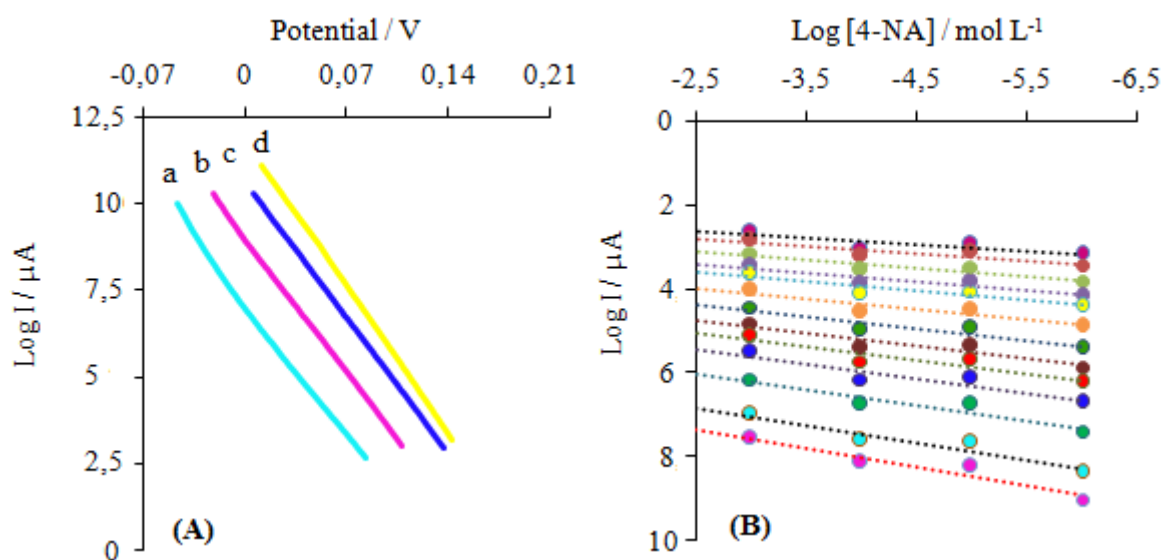

Figure 5: *(A) Tafel plots at various PNA concentrations (a: 1.0×10^{-3}; b: 5.0×10^{-4}; c: 1.0×10^{-4} and d: 1.0×10^{-5} mol L^{-1}) in B-R buffer solution (pH 2.0) with scan rate 50 mV s^{-1}. (B) Double logarithmic plot of current as a function of PNA concentrations at constant potential.*

III.4. Electroanalytic study

III.4.1. Optimization of parameters

More than their electrocatalytical properties, the silver electrode demonstrates a higher capacity for analysis of PNA. This electroanalytical study was carried out using DPV method. Firstly, all electrochemical parameters were optimized in BR solution (pH 2.0) containing 1.0×10^{-5} mol L^{-1} of PNA. After the experimental study, the optimal electrochemical parameters to perform the PNA determination are 8mV s^{-1}, 130 ms, 430 mV, and 500 ms for the step, pulse, width and period, respectively. The choice of optimum values was made

taking into account the peak current intensity, the symmetry of voltammograms and the signal/noise ratio.

The effect of pH solution on cathodic current intensity of PNA was also evaluated. The results show that the current intensity of PNA reduction increased when decreasing the value of pH solution. Therefore, the maximum intensity is obtained with pH=1.32, which was used for further work.

III.4.2. Calibration curve

The effect of 4-NA concentration was studied under the optimized conditions using DPV method at silver electrode. Fig. 6 shows the calibration curve for PNA reduction. The cathodic current peak height of PNA increases linearly with the concentration in the range from 8.0×10^{-9} to 1.0×10^{-3} mol L^{-1} of PNA. The minimum concentration calculated that can be detected by the proposed electrode is 4.0×10^{-9} mol L^{-1} in term of limit of detection (LOD). The repeatability of our method was also evaluated as relative standard deviation (RSD). Consequently, the RSD obtained is 1.97 % after eight measurements in solutions of 1.0×10^{-4} mol L^{-1} PNA. Consequently, the silver electrode revealed a high efficiency to reduce PNA with good repeatability.
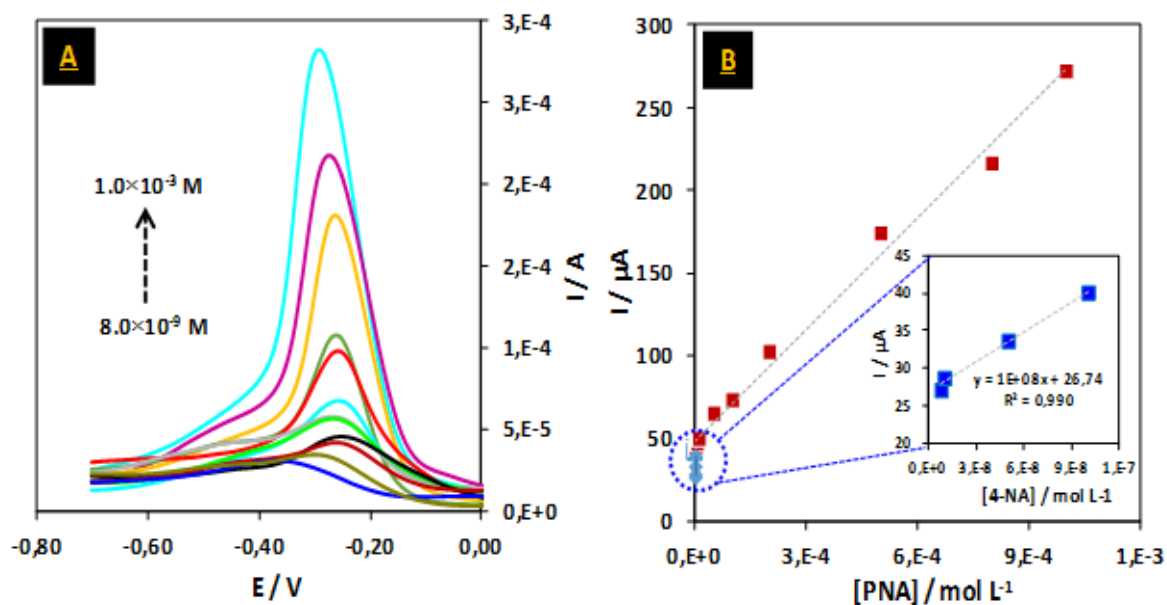
Figure 6: *DPVs of PNA in 0.1 mol L^{-1} B-R (pH 2) 1.0×10^{-3}; 8.0×10^{-4}; 5.0×10^{-4}; 2.0×10^{-4}; 1.0×10^{-4}; 5.0×10^{-5}; 1.0×10^{-5}; 5.0×10^{-6}; 8.0×10^{-7}; 4.0×10^{-7}; 2.0×10^{-7}; 1.0×10^{-7}; 5.0×10^{-8}; 1.0×10^{-8} and 8.0×10^{-9} mol L^{-1}. Inset: plots of electrocatalytic peak current as a function of PNA concentration.*

III.4.3. Interference effect

The influence of interfering agents was also probed to examine the selectivity of the designed sensor. These organic compounds are dopamine, ascorbic acid, paracetamol, 4-nitrophenol, 2-nitrophenol, 4-aminophenol and 2-nitroaniline into solution containing 1.0×10^{-5} mol L^{-1} of PNA. The measurements were evaluated in order to investigate the influence of interfering compounds on the signals of reduction currents of the analyte examined (Table 1).

Table 1: *Influence of coexisting substances on the determination of 1.0×10^{-5} mol L^{-1} of PNA (n = 3).*

Interfering agent	Concentration (1.0×10^{-5} mol L^{-1})	Recovery (%)
Dopamine	0.1	98 ±1.49
	1.0	101 ±1.27
	5.0	101 ±0.49
	10.0	105 ±1.89
Ascorbic acid	0.1	111 ±1.69
	1.0	109 ±0.34
	5.0	79 ±1.43
	10.0	65 ±2.12
Paracetamol	0.1	95 ±1.35
	1.0	109 ±0.70
	5.0	108 ±0.08
	10.0	102.6 ±0.83
4-nitrophenol	0.1	99 ±0.21
	1.0	100 ±0.16
	5.0	99.64 ±0.008
	10.0	101.13 ±0.03
2-nitroaniline	0.1	104 ±1.85
	1.0	106 ±0.25
	5.0	134 ±2.85
	10.0	172 ±1.43
2-nitrophenol	0.1	105 ±0.18
	1.0	119 ±1.12
	5.0	142 ±2.83
	10.0	174 ±1.88
4-aminophenol	0.1	101 ±1.42
	1.0	103 ±0.5
	5.0	100 ±0.88
	10.0	105 ±0.27

The results show that the presence of dopamine, paracetamol, 4-nitrophenol and 4-aminophenol in solution containing PNA has no effect on the peak current. However, 2-nitroaniline and 2-nitrophenol increase the signal of PNA reduction due to the overlap

between potentials. Moreover, the presence of ascorbic acid decreases the current peak of PNA reduction when presents at higher concentration of PNA (5-fold or more).

III.4.4. Analysis of PNA in water samples

The electrode was also successfully applied to the direct determination of PNA in drinking water and wastewater samples. The tap water solutions were performed without any pretreatment, while the wastewater samples were used after filtration. Consequently, the calibration plots of the samples under optimized conditions are linear with a higher correlation coefficient (R^2>0.98). After the experimental study, the concentration of the PNA was found to be lower than the LOD. The recovery test was carried out by adding a known concentration of PNA into water samples to confirm the practicability of this method. Therefore, the statistical results are listed in Table 2. All measurements were performed in triplicate. This shows the possibility to detect PNA in drinking water and wastewater samples.

Table 2: Obtained results for the determination of PNA in drinking and wastewater samples.

Samples	LOD (mol L^{-1})	RSD (%)	Recovery (%)
Drinking water	1.0×10^{-5}	3.68	91.96
Wastewater	2.5×10^{-6}	1.57	81.27

IV. Conclusion

In summary, given that silver is known to be a powerful catalyst for the reduction of aromatic nitro compounds. The present study is devoted to a first step to study the electro-catalytic performance of the metallic silver electrode in reducing PNA compared to other solid electrodes including gold, graphite, and glassy electrodes. Indeed, metallic silver electrode showed high electrocatalytic activity in 0.1 M Britton-Robinson buffer solution (pH: 2.0) with a remarkable decrease in over-potential compared to other electrodes. Thereafter, the kinetics of PNA reduction has been investigated.

The catalytic effect was investigated using cyclic voltammetry, electrochemical impedance spectroscopy, and chronoamperometry. The cathodic transfer coefficient electron transfer rate

constant, and diffusion coefficient were evaluated to be 0.57, 7.38×10^{-5} cm^2 s^{-1} and 5.44×10^{-4} cm^2 s^{-1} respectively. In addition, the sensitivity of the proposed electrode is achieved using differential pulse voltammetry after pH optimization and other electrochemical parameters. The results showed that the reduction peak current for PNA at the Ag electrode increased significantly compared with conventionally used electrodes. The relationship between the reduction peak current and the PNA concentration was linear in the range from 8.0×10^{-9} to 1.0×10^{-3} mol L^{-1}. The limit of detection was found to be 4.0×10^{-9} mol L^{-1}. Moreover, the results indicated the feasibility to determine PNA in real samples such as drinking water and wastewater.

References

[1] Hernández-Santos, D., González-García, M. B., & García, A. C. (2002). Metal-nanoparticles based electroanalysis. Electroanalysis: An International Journal Devoted to Fundamental and Practical Aspects of Electroanalysis, 14(18), 1225-1235.

[2] Katz, E., Willner, I., & Wang, J. (2004). Electroanalytical and bioelectroanalytical systems based on metal and semiconductor nanoparticles. Electroanalysis: An International Journal Devoted to Fundamental and Practical Aspects of Electroanalysis, 16(1-2), 19-44.

[3] Madaj, R., Kalinowska, H., & Sobiecka, E. (2016). Biodegradation of nitrocompounds. Biotechnol Food Sci, 80, 63-73.

[4] Claus, H., Bausinger, T., Lehmler, I., Perret, N., Fels, G., Dehner, U., ... & König, H. (2007). Transformation of 2, 4, 6-trinitrotoluene (TNT) by Raoultella terrigena. Biodegradation, 18(1), 27-35.

[5] Brown, G. I. (1999). Scientist, Soldier, Statesman, Spy: Count Rumford: the Extraordinary Life of a Scientific Genius. Sutton Pub Limited.

[6] Booth, G. (2000). Nitro compounds, aromatic. Ullmann's Encyclopedia of Industrial Chemistry, Weinheim, 2005.

[7] Kovacic, P., & Somanathan, R. (2014). Nitroaromatic compounds: Environmental toxicity, carcinogenicity, mutagenicity, therapy and mechanism. Journal of Applied Toxicology, 34(8), 810-824.

[8] Viswanathan, P., & Ramaraj, R. (2016). Polyelectrolyte assisted synthesis and enhanced catalysis of silver nanoparticles: Electrocatalytic reduction of hydrogen peroxide and catalytic reduction of 4-nitroaniline. Journal of Molecular Catalysis A: Chemical, 424, 128-134.

[9] Khalid, A., Arshad, M., & Crowley, D. E. (2009). Biodegradation potential of pure and mixed bacterial cultures for removal of 4-nitroaniline from textile dye wastewater. Water research, 43(4), 1110-1116.

[10] Sun, J. H., Sun, S. P., Fan, M. H., Guo, H. Q., Lee, Y. F., & Sun, R. X. (2008). Oxidative decomposition of p-nitroaniline in water by solar photo-Fenton advanced oxidation process. Journal of hazardous materials, 153(1-2), 187-193.

[11]   Ma, H., Wang, M., Pu, C., Zhang, J., Zhao, S., Yao, S., & Xiong, J. (2009). Transient and steady-state photolysis of p-nitroaniline in aqueous solution. Journal of hazardous materials, 165(1-3), 867-873.

[12]   Saupe, A. (1999). High-rate biodegradation of 3-and 4-nitroaniline. Chemosphere, 39(13), 2325-2346.

[13]   Khan, F., Pandey, J., Vikram, S., Pal, D., & Cameotra, S. S. (2013). RETRACTED: Aerobic degradation of 4-nitroaniline (4-NA) via novel degradation intermediates by Rhodococcus sp. strain FK48.

[14]   Sun, J. H., Sun, S. P., Fan, M. H., Guo, H. Q., Qiao, L. P., & Sun, R. X. (2007). A kinetic study on the degradation of p-nitroaniline by Fenton oxidation process. Journal of hazardous materials, 148(1-2), 172-177.

[15]   Smith, S. R. (2009). Organic contaminants in sewage sludge (biosolids) and their significance for agricultural recycling. Philosophical Transactions of the Royal Society A: Mathematical, Physical and Engineering Sciences, 367(1904), 4005-4041.

[16]   Smith, S. R., & Riddell-Black, D. (2007). Sources and impacts of past, current and future contamination of soil, in: Research Project Final Report for Defra Project code SP 0547, Imperial College London, pp. 1–247.

[17]   Haderlein, S. B., Weissmahr, K. W., & Schwarzenbach, R. P. (1996). Specific adsorption of nitroaromatic explosives and pesticides to clay minerals. Environmental Science & Technology, 30(2), 612-622.

[18]   Khalid, A., Arshad, M., & Crowley, D. E. (2009). Biodegradation potential of pure and mixed bacterial cultures for removal of 4-nitroaniline from textile dye wastewater. Water research, 43(4), 1110-1116.

[19]   Kutty, R., Purohit, H. J., & Khanna, P. (2000). Isolation and characterization of a Pseudomonas sp. strain PH1 utilizing meta-aminophenol. Canadian journal of microbiology, 46(3), 211-217.

[20]   Saupe, A. (1999). High-rate biodegradation of 3-and 4-nitroaniline. Chemosphere, 39(13), 2325-2346.

[21]   Bhunia, F., Saha, N. C., & Kaviraj, A. (2003). Effects of Aniline–an aromatic amine to some freshwater organisms. Ecotoxicology, 12(5), 397-404.

[22]   Chung, K. T., Chen, S. C., Zhu, Y. Y., Wong, T. Y., & Stevens Jr, S. E. (1997). Toxic effects of some benzamines on the growth of Azotobacter vinelandii and other bacteria. Environmental Toxicology and Chemistry: An International Journal, 16(7), 1366-1369.

[23]   Clays, K. (2003). Molecular nonlinear optics: From para-nitroaniline to electrochemical switching of the hyper polarizability. Journal of Nonlinear Optical Physics & Materials, 12(04), 475-494.

[24]   Gautam, S., Kamble, S. P., Sawant, S. B., & Pangarkar, V. G. (2005). Photocatalytic degradation of 4-nitroaniline using solar and artificial UV radiation. Chemical Engineering Journal, 110(1-3), 129-137.

[25]   Lee, D. S., Park, K. S., Nam, Y. W., Kim, Y. C., & Lee, C. H. (1997). Hydrothermal decomposition and oxidation of p-nitroaniline in supercritical water. Journal of hazardous materials, 56(3), 247-256.

[26]   Shen, L. R., Yang, P. Z., & Shen, L. Y. (1997). Treatment of waste water containing p-nitrophenylamine with emulsion liquid membrane processes. Tec. Water Tr.(Chinease), 23, 45-49.

[27]   Tarley, C. R. T., & Kubota, L. T. (2005). Molecularly-imprinted solid phase extraction of catechol from aqueous effluents for its selective determination by differential pulse voltammetry. Analytica chimica acta, 548(1-2), 11-19.

[28]   Shkumbatiuk, R., Bazel, Y. R., Andruch, V., & Török, M. (2005). Investigation of 2-[(E)-2-(4-diethylaminophenyl)-1-ethenyl]-1, 3, 3-trimethyl-3H-indolium as a new highly sensitive reagent for the spectrophotometric determination of nitrophenols. Analytical and bioanalytical chemistry, 382(6), 1431-1437.

[29]   Wang, S. P., & Chen, H. J. (2002). Separation and determination of nitrobenzenes by micellar electrokinetic chromatography and high-performance liquid chromatography. Journal of Chromatography A, 979(1-2), 439-446.

[30]   Shikata, M., & Tachi, I. (1932). Researches on the Electrolytic Reduction Potentials of Organic Compounds, Part XVI. Bulletin of the Agricultural Chemical Society of Japan, 8(10-12), 154-155.

[31]   Maistrenko, V. N., Sapel'nikova, S. V., Kudasheva, F. K., & Amirkhanova, F. A. (2000). Isomer-selective carbon-paste electrodes for the determination of nitrophenol,

nitroaniline, and nitrobenzoic acid by adsorption-stripping voltammetry. Journal of Analytical Chemistry, 55(6), 586-589.

[32]   Lin, X., Ni, Y., & Kokot, S. (2012). Voltammetric analysis with the use of a novel electro-polymerised graphene-nafion film modified glassy carbon electrode: Simultaneous analysis of noxious nitroaniline isomers. Journal of hazardous materials, 243, 232-241.

[33]   Maistrenko, V. N., Sapel'nikova, S. V., & Kudasheva, F. K. (1999). Preconcentration and voltammetric determination of nitro compounds on carbon pasted electrodes modified by chromatographic stationary phases. Journal of analytical chemistry (New York, NY), 54(5), 434-437.

[34]   Jbarah, A. A., & Holze, R. (2006). A comparative spectro electrochemical study of the redox electrochemistry of nitroanilines. Journal of Solid State Electrochemistry, 10(6), 360-372.

[35]   Rizk, N. M. (2011). Potentiometric behavior of p-nitroaniline and its quantification in environmental samples. Asian Journal of Chemistry, 23(12), 5323-5326.

[36]   Chen, X., Cheng, X., & Gooding, J. J. (2012). Detection of trace nitroaromatic isomers using indium tin oxide electrodes modified using β-cyclodextrin and silver nanoparticles. Analytical chemistry, 84(20), 8557-8563.

[37]   Khodari M, Rabie E, Fahmy O (2013) XXXIII moderni elektrochemicke metody, book of abstracts. BEST Service, Usti nad Labem, p 92.

[38]   Zhao, F., Liu, L., Xiao, F., Li, J., Yan, R., Fan, S., & Zeng, B. (2007). Sensitive Voltammetric Response of p-Nitroaniline on Single-Wall Carbon Nanotube-Ionic Liquid Gel Modified Glassy Carbon Electrodes. Electroanalysis: An International Journal Devoted to Fundamental and Practical Aspects of Electroanalysis, 19(13), 1387-1393.

[39]   Zavar, M. H. A., Heydari, S., Rounaghi, G. H., Eshghi, H., & Azizi-Toupkanloo, H. (2012). Electrochemical behavior of para-nitroaniline at a new synthetic crown ether-silver nanoparticle modified carbon paste electrode. Analytical Methods, 4(4), 953-958.

[40]   Bai, W., Sheng, Q., Ma, X., & Zheng, J. (2015). Synthesis of silver nanoparticles based on hydrophobic interface regulation and its application of electrochemical catalysis. ACS Sustainable Chemistry & Engineering, 3(7), 1600-1609.

[41]   Laghrib, F., Boumya, W., Lahrich, S., Farahi, A., El Haimouti, A., & El Mhammedi, M. A. (2017). Electrochemical evaluation of catalytic effect of silver in reducing 4-nitroaniline: Analytical application. Journal of Electroanalytical Chemistry, 807, 82-87.

[42]   Laghrib, F., Lahrich, S., Farahi, A., Bakasse, M., & El Mhammedi, M. A. (2018). Impregnation of silver in graphite carbon using solid reaction: Electrocatalysis and detection of 4-nitroaniline. Journal of Electroanalytical Chemistry, 823, 26-31.

[43]   Laghrib, F., Ajermoun, N., Hrioua, A., Lahrich, S., Farahi, A., El Haimouti, A., & El Mhammedi, M. A. (2019). Investigation of voltammetric behavior of 4-nitroaniline based on electrodeposition of silver particles onto graphite electrode. Ionics, 25(6), 2813-2821.

[44]   Laghrib, F., Farahi, A., Bakasse, M., Lahrich, S., & El Mhammedi, M. A. (2019). Voltammetric determination of nitro compound 4-nitroaniline in aqueous medium at chitosan gelified modified carbon paste electrode (CS@ CPE). International journal of biological macromolecules, 131, 1155-1161.

[45]   Laghrib, F., Farahi, A., Bakasse, M., Lahrich, S., & El Mhammedi, M. A. (2019). Chemical synthesis of nanosilver on chitosan and electroanalysis activity against the p-nitroaniline reduction. Journal of Electroanalytical Chemistry, 845, 111-118.

[46]   Laghrib, F., Ajermoun, N., Bakasse, M., Lahrich, S., & El Mhammedi, M. A. (2019). Synthesis of silver nanoparticles assisted by chitosan and its application to catalyze the reduction of 4-nitroaniline. International journal of biological macromolecules, 135, 752-759.

[47]   Laghrib, F., Ajermoun, N., Bakasse, M., Lahrich, S., & El Mhammedi, M. A. (2019). Catalytic effect of silver particles supported on chitosan surface for the electrochemical sensing para nitroaniline at graphite electrode. International Journal of Environmental Analytical Chemistry, 1-16.

[48]   Rameshkumar, P., & Ramaraj, R. (2014). Electroanalysis of nitrobenzene derivatives and nitrite ions using silver nanoparticles deposited silica spheres modified electrode. Journal of Electroanalytical Chemistry, 731, 72-77.

[49]   Nandini, S., Nalini, S., Sanetuntikul, J., Shanmugam, S., Niranjana, P., Melo, J. S., & Suresh, G. S. (2014). Development of a simple bioelectrode for the electrochemical detection of hydrogen peroxide using Pichia pastoris catalase immobilized on gold nanoparticle nanotubes and polythiophene hybrid. Analyst, 139(22), 5800-5812.

[50] Rastogi, P. K., Ganesan, V., & Krishnamoorthi, S. (2014). Palladium nanoparticles incorporated polymer-silica nanocomposite based electrochemical sensing platform for nitrobenzene detection. Electrochimica Acta, 147, 442-450.

[51] Gupta, R., Rastogi, P. K., Ganesan, V., Yadav, D. K., & Sonkar, P. K. (2017). Gold nanoparticles decorated mesoporous silica microspheres: a proficient electrochemical sensing scaffold for hydrazine and nitrobenzene. Sensors and Actuators B: Chemical, 239, 970-978.

[52] Antoniadou, S., Jannakoudakis, A. D., & Theodoridou, E. (1989). Electrocatalytic reactions on carbon fibre electrodes modified by hemine II. Electro-oxidation of hydrazine. Synthetic metals, 30(3), 295-304.

[53] Zhao, F., Liu, L., Xiao, F., Li, J., Yan, R., Fan, S., & Zeng, B. (2007). Sensitive Voltammetric Response of p-Nitroaniline on Single-Wall Carbon Nanotube-Ionic Liquid Gel Modified Glassy Carbon Electrodes. Electroanalysis: An International Journal Devoted to Fundamental and Practical Aspects of Electroanalysis, 19(13), 1387-1393.

[54] Zavar, M. H. A., Heydari, S., Rounaghi, G. H., Eshghi, H., & Azizi-Toupkanloo, H. (2012). Electrochemical behavior of para-nitroaniline at a new synthetic crown ether-silver nanoparticle modified carbon paste electrode. Analytical Methods, 4(4), 953-958.

[55] Andrieux, C. P., & Saveant, J. M. (1978). Heterogeneous (chemically modified electrodes, polymer electrodes) vs. homogeneous catalysis of electrochemical reactions. Journal of Electroanalytical Chemistry and Interfacial Electrochemistry, 93(2), 163-168.

[56] Martins, I., Carreira, F. C., Canaes, L. S., Junior, F. A. D. S. C., da Silva Cruz, L. M., & Rath, S. (2011). Determination of parabens in shampoo using high performance liquid chromatography with amperometric detection on a boron-doped diamond electrode. Talanta, 85(1), 1-7.

[57] Bard, A. J., & Faulkner, L. R. (2001). Fundamentals and applications. Electrochemical Methods, John Wiley & Sons, New York, 2(482), 580-632.

[58] Prathap, M. A., Anuraj, V., Satpati, B., & Srivastava, R. (2013). Facile preparation of Ni (OH) 2–MnO2 hybrid material and its application in the electrocatalytic oxidation of hydrazine. Journal of hazardous materials, 262, 766-774.

– Chapter 4 –

Thermal and electrochemical deposition of Ag catalysts for the electrochemical reduction of p-nitroaniline

I. Introduction

Carbon-based electrode materials have long been used in electrochemistry and have outperformed traditional noble metals in many important areas, allowing them to be at the forefront of innovation in this field [1]. This diversity and sustainable success are due to the structural polymorphism of carbons, chemical stability, and low cost, large windows of exploitable potential, relatively inert electrochemistry, rich surface chemistry, and electro-catalytic activities for a variety of redox reactions [1, 2]. Graphite surfaces are heterogeneous (anisotropic) in nature, with a very different chemical and electrochemical reactivity between two of the structural contributions that are fundamental to the behavior of the electrodes, namely the edge and base planes [1].Carbon materials have significantly more complex surface chemistry than metals, not only because the underlying microstructure varies with carbon type, but also because carbon forms a wider variety of surface bonds and functional groups. Since electrochemistry is based fundamentally on interfacial phenomena, the nature of the carbon electrode surface is of obvious importance.

Not surprisingly, carbon electrodes are subject to unintentional or unknown adsorption of impurities during electrode preparation. Intentional or not, these adsorbates can dramatically affect the electron transfer rates and electrocatalytic activity of carbon electrodes, possibly subverting their intended electrochemical applications [1]. There is a long history of "activation" procedures for carbon electrodes, including polishing, heat treatment, solvent treatment, laser activation, ultrasonication, and others [3, 4]. These procedures improve electrode performance in part by removing adventitious adsorbates from the electrode surface. The tendency of carbon to adsorb molecules from the solution and the presence of surface oxides allow electrocatalytic reactions on carbon electrodes that are weaker or absent on metal electrodes. In addition, the history and preparation of carbon electrodes can have profound effects on the coverage and activity of catalytic sites, so it is important to understand the electrocatalytic effects. Several methods defining the synthesis of silver particles in solution as well as by deposition on solid surfaces have been presented. These include chemical synthesis through the use of different reducing agents [5], electron beam irradiation or UV light [6], and electrochemical methods [7–10]. The latter methods provide an easy and rapid alternative for the synthesis of metallic particles.

Deposition is a well-known conventional surface modification method to improve the surface characteristics, decorative and functional, of a wide variety of materials. Works done in this direction are discussed in this chapter. The electrodeposition method, also known as electroplating, is a method of electrical current deposition that allows precise control of the coating of species on a conductive target material. To date, three different electrodeposition methods, including potentiostatic technique, galvanostatic techniques, and pulse-plating techniques, were experimentally designated. In the potentiostatic technique, current density is changed under constant potential. In galvanostatic technique, electrode potential is varied with a constant current. In pulse-plating technique, the variation of pulse amplitude (e.g., 5V, 10V) and/or pulse width (from ns to μs) could be studied. When studying with electrodeposition methods, it is also common to refer to the method depending on the forms of the voltammetry. Potential-step electrolysis method [11, 8] and cyclic voltammetric technique are such examples used to deposit gold and silver on substrates having a low electrical resistance, such as glassy carbon, and carbon paste electrodes [12-14].

Impregnation and drying is a frequently used preparation method among others due to its simple execution and low waste streams. The first step is contacting a metal precursor with porous support. Common precursors include inorganic metal salts, such as metal sulfates, carbonates, chlorides, nitrates, or acetates, and organic metal complexes, such as metal acetylacetonates [15]. In this chapter, silver microparticles modified carbon paste electrodes by electrodeposition (Ag_{ED}-CPE) and impregnation using solid reaction following by thermal treatment (Ag_{Imp}-CPE) were constructed and used for the electrocatalytic reduction of PNA and their determination.

II. Physical characterization of Ag_{Imp}-CPE and Ag_{ED}-CPE

II.1. XRD characterization of Ag_{Imp}-CPE and Ag_{ED}-CPE

After the preparation of electrodes (see chapter 2), Different percentages of silver-impregnated onto carbon paste treated at 200°C were studied by X-ray diffraction. A sharper and stronger peaks indexed at the angle $2\theta = 38.2°$, 44.0, 64.5° as can be seen in (Fig. 1A). These peaks are attributed to the crystal planes of (111), (200) and (220) respectively. However, it is notable that in the case of 10% Ag-CP, the peak observed at $2\theta = 38.2°$ is the most intense compared to other percentage. This result is comparable to that found in literature [16]. Moreover, the X-ray

diffraction analysis of silver deposited on carbon paste (Fig. 1B) shows the formation of silver particles. In fact, the presence of three peaks of metallic silver at 2θ of 38.18, 46.62, and 66.42 affirms the metallic state of the coated silver.
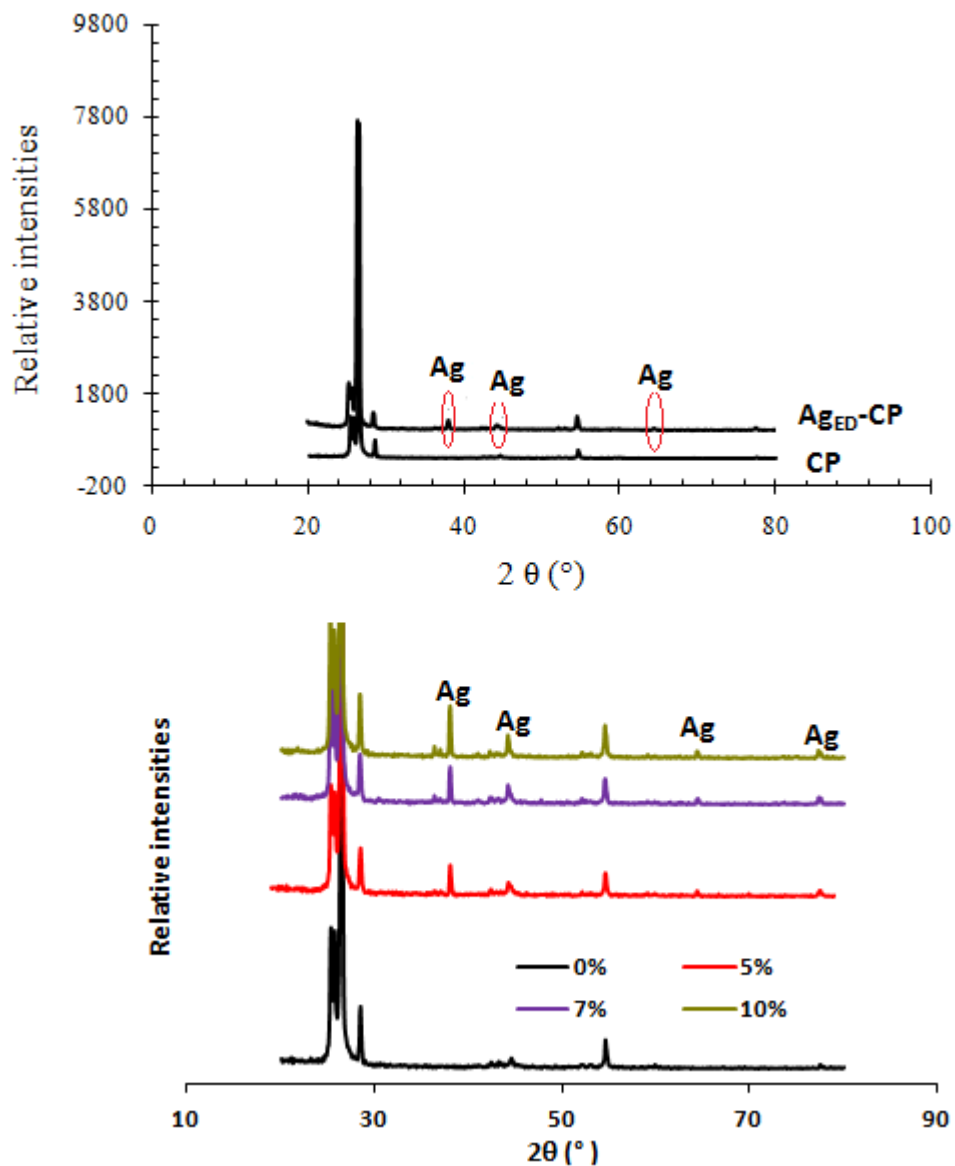

Figure 1:*X-ray diffraction (XRD) patterns of (A) carbon paste and Ag$_{ED}$CP after electrodeposition step. (B) Silver microparticles impregnated onto CPE heated at 200°C at different percentages of AgNO$_3$*

II.2. SEM images of Ag$_{Imp}$-CPE and Ag$_{ED}$-CPE

SEM images for both electrodes Ag$_{Imp}$-CPE and Ag$_{ED}$-CPE were obtained to illustrate the differences in the surface morphology and distribution of silver. The SEM image of Ag$_{Imp}$-CPE (Fig. 2A) shows a significantly greater roughness, high-density, polydispersed, spherical microparticles. On the other hand, the electrodeposition of silver (Fig. 2B) showed particle size smaller compared to impregnation with a uniform distribution on the surface of graphite carbon.
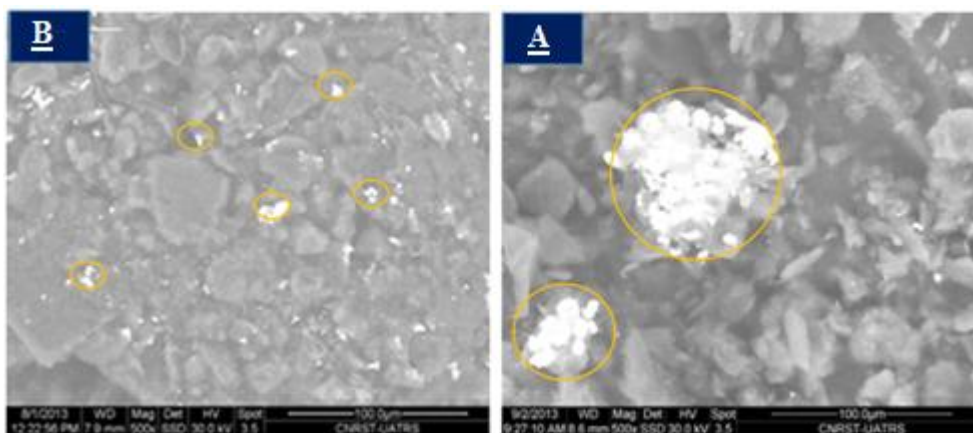

Figure 2: SEM images of (A) Ag$_{Imp}$-CPE, and (B) Ag$_{ED}$-CPE

II.3. Electrochemical surface properties of Ag$_{Imp}$-CPE and Ag$_{ED}$-CPE

Electrochemical impedance spectroscopy (EIS) measurements were used to evaluate the conductivity of modified electrodes (Ag$_{Imp}$-CPE). EIS is an effective technique for probing the kinetics at interfaces and measuring the dielectric and transport properties of materials. Before starting the EIS experiments, cyclic voltammograms curves of the $[Fe(CN)_6]^{3-/4-}$ redox probe in 0.1M KCl have been performed and serve as initial insights into the electron transfer processes at the modified electrodes. The cyclic voltammograms of the modified CPEs by different amounts of silver, 2%, 9%, 10%, and 15% were shown in Fig. 3A. The cathodic peak current appeared at modified carbon paste electrode (10% silver, w/w) was enhanced and well presented than that shown by the other electrodes. These results exhibit that the 10 % of silver seems the better redox mediators by increasing the electronic communication between the CPE and $[Fe(CN)_6]^{3-/4-}$ species. For further insight into the electron transfer at Ag$_{Imp}$-CPEs, EIS experiments were carried out with potential fixed at $E_{1/2} = 0.124$ V versus Ag/AgCl. The Nyquist plots (Z_{im} versus Z_{real}) (Fig. 3B) were exhibited the characteristics of semicircles at high frequencies and a straight

line at low frequencies. The EIS data (R_s, R_{ct}, and Q) were extracted from the Nyquist plots by modeling the spectra following the circuit equivalent shown using the ZMAN software (Fig. 3B inset). Where R_s is the cell-electrolyte resistance, R_{et} is the electron-transfer resistance (the domain of kinetic control) and Q is the constant phase angle (CPE) element, in which it replaces the double layer capacitance in the Randles' model [17]. As shown in the Nyquist plots, the equivalent circuit is in good agreement with the experimental results. Therefore, the obtained parameters are listed in Table 1.

Table 1: Summary of calculated EIS parameters obtained for the different electrodes

Electrodes	R_s (Ω)	R_{ct} ($K\Omega$)	K_{app} (cm s^{-1})
(2%) Ag-CPE	66. 55	10.186	2.61×10^{-5}
(9%) Ag-CPE	82. 328	11.245	2.37×10^{-5}
(10%) Ag-CPE	68. 68	3.178	8.37×10^{-5}
(15%) Ag-CPE	82. 348	30.439	8.74×10^{-6}

Ideally, R_s should not be affected by modification of the electrode surface [18]. The increase observed in the percentage of 15 and 25% compared to that of Ag_{Imp}-CPE (10% w/w) may be due to the resistance induced by the film formed on the electrode surface and possible making the [Fe $(CN)_6]^{3-/4-}$ redox species more difficult to diffuse to the electrode [19]. The apparent electron transfer rate constant k_{app} was obtained from the following equation (Eq. 1) [20]:

$$K = \frac{RT}{F^2 R_{ct} C} \quad (1)$$

Where R is the gas constant (8.314 J mol^{-1} K^{-1}), T is the absolute temperature of the system (298 K), F is the Faraday constant (96,485 C mol^{-1}), and C is the concentration of the [Fe(CN)$_6$]$^{3-}$ and [Fe (CN)$_6$]$^{4-}$ (equimolar) (mol L^{-1}). The K_{app} and R_{et} values expressed as 8.37×10^{-5} cm s^{-1} and 3.178 KΩ respectively show that the Ag-CPE (10% w/w) exhibits faster and easier electron transfer processes for [Fe(CN)$_6$]$^{3-/4-}$ compared to other electrodes. From the Bode plots (θ (phase

135

angle) vs log f (frequency)), it is shown that on Ag_{Imp}-CPE (10% w/w), relaxation process shifts to different phase angles and at lower frequencies (Fig. 3C). This shift indicate that the reaction takes place at the surface of the Ag_{Imp}-CPE (10% w/w) rather than the other electrodes.
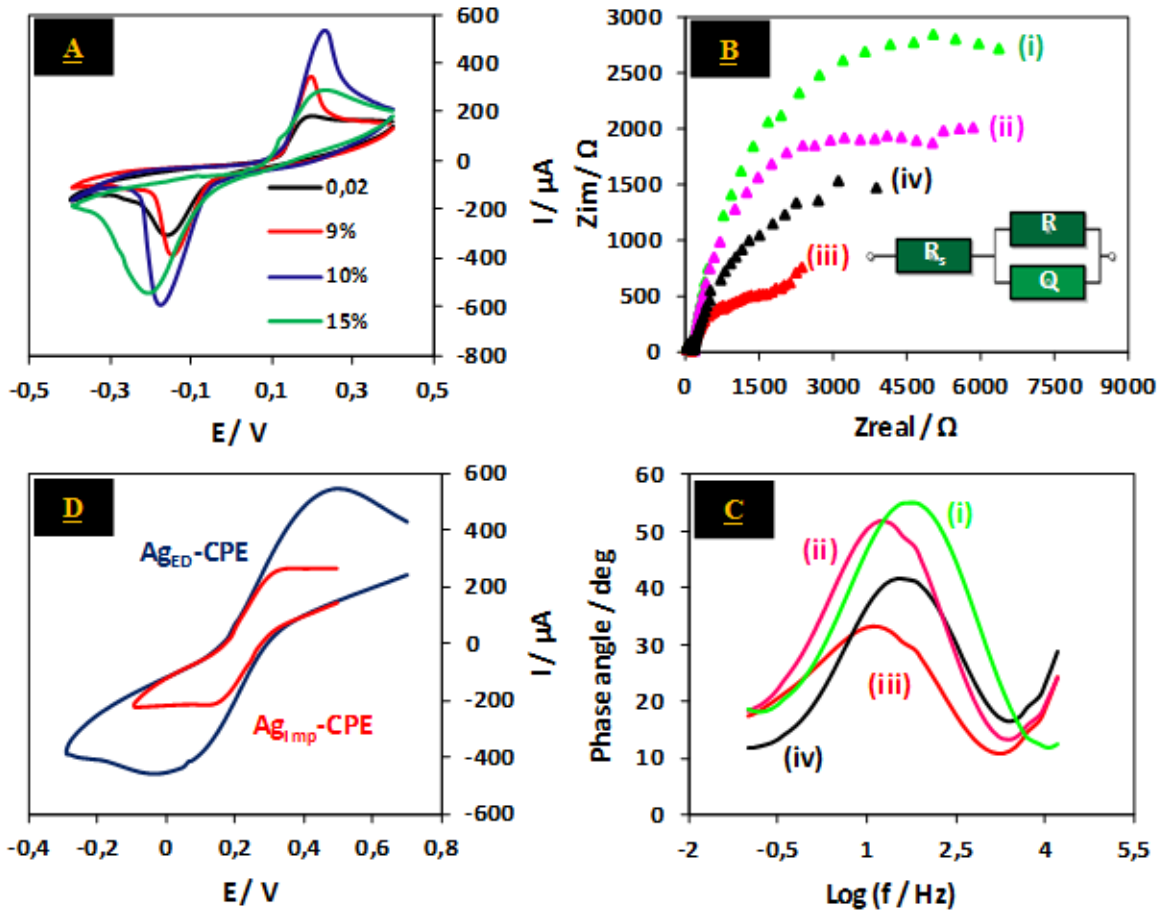

Figure3: (A) CV profile resulting from CPEs modified with different amounts of silver in 0.1 KCl containing 1mM of $K_4Fe(CN)_6$ and 1mM $K_3Fe(CN)_6$ (1:1) at dE/dt = 100 mV s^{-1}. (B) Nyquist plots of $[Fe(CN)_6]^{3-/4-}$ species resulting from CPEs modified by different amount of silver, 2% (i), 9% (ii), 10% (iii) and 15% (iv). Inset represent Simple equivalent circuit model. (C) Bode plots of phase angle vs. logarithm of frequency for the CPEs modified by different amount of silver, 2% (i), 9% (ii), 10% (iii) and 15% (iv)performed between 100 mHz and 1 kHz using amplitude of 10 mV in 0.1 KCl containing 1mM of $K_4Fe(CN)_6$ and 1mM $K_3Fe(CN)_6$. (D) CV profile of Ag_{Imp}-CPE and Ag_{ED}-CPE in 0.1M KCl containing 1mM $[Fe(CN)_6]^{3-/4-}$. (dE/dt) = 50 mV s^{-1}.

Although the same geometric surface area is utilized for both electrodes, the $[Fe(CN)_6]^{3-/4-}$ in 0.1 M KCl redox was used as the first overview of the electronic transfer process, to estimate the electro-active surface area and to detect the integrity of silver in the electrodes. As shown in Fig. 3D well defined characteristic waves of $[Fe(CN)_6]^{3-/4-}$ for Ag_{ED}-CPE is observed as well as for Ag_{Imp}-CPE. Thus, the faradaic current measured for the latest seems to be very small than that of Ag_{ED}-CPE, this decreasing current may result from increasing the particle size of silver or formation of silver oxide during treatment which can effectively insulate the graphite carbon electrode surface and undergo to decreasing the conductivity of the electrode. Furthermore, according to Randles– Sevick equation (Eq. 2) [21, 22]:

$$Ip = 2.99 \times 10^5 \; nACD^{1/2} v^{1/2} \qquad (2)$$

where Ip, n, A, C, D, and υ are the peak current, the number of the electrons involved in the reaction, the electroactive surface area, the concentration of the reactant, the diffusion coefficient of the target species and the potential sweeping rate, respectively, the corresponding active surface area was calculated to be 0.095 cm² and 0.06 cm² for Ag_{ED}-CPE and Ag_{Imp}-CPE respectively.

III. Electrochemical determination of PNA at Ag_{Imp}-CPE and Ag_{ED}-CPE

III.1. Electrochemical determination of PNA at Ag_{Imp}-CPE

III.1.1. Voltammetric characteristic of p-nitroaniline at Ag_{Imp}-CPE

Cyclic voltammetry is the most extensively used technique for acquiring qualitative information about electrochemical reactions. It tenders the rapid identification of redox potentials distinctive to the electroactive species under investigation, providing considerable information about the thermodynamics of a redox process, kinetics of heterogeneous electron-transfer reactions and analysis of coupled electrochemical reactions or adsorption processes. The voltammetric diagnosis that the electrochemical process is undergoing a reversible or irreversible heterogeneous charge transfer process.

Therefore, in the first instance, it was used to investigate the effect of the silver modifier on the peak potential of PNA in 0.1 mol L^{-1} B-R solution (pH 2.0) for different percentages (5%, 7%, 9%, 10%, 12%, 15%, 25%, 35%, and 50%). When the content of the modifier was 10% in the

carbon paste, significant shift of the reduction peak potential of PNA have been obtained. However, for silver amounts greater than 10%, the reduction peak of PNA appears at a more negative potential close to that obtained by CPE. This is due to the formation of a partial silver film on the CPE electrode [23], which is in good agreement with XRD.

To further investigate the electrocatalytic effect of silver microparticles toward the reduction of PNA, different cyclic voltammograms were compared. This comparison was made without and with PNA (1.0×10^{-3} mol L^{-1} in 0.1 mol L^{-1} B-R), and even in the absence and presence of silver modifier (Fig. 4). Moreover, a, b, and c voltammograms corresponding to the Ag_{Imp}-CPE in blank solution, PNA at carbon paste and PNA at silver modified carbon paste electrodes respectively. The modifying agent exhibits excellent electrocatalytic activity of PNA versus the bare of carbon paste electrode with shift in peak potential towards more positive side by $\simeq 300$ mV. The shift of the reduction peak, which was observed on voltammograms of PNA at Ag_{Imp}-CPE, proves that there is an interaction between silver and PNA.
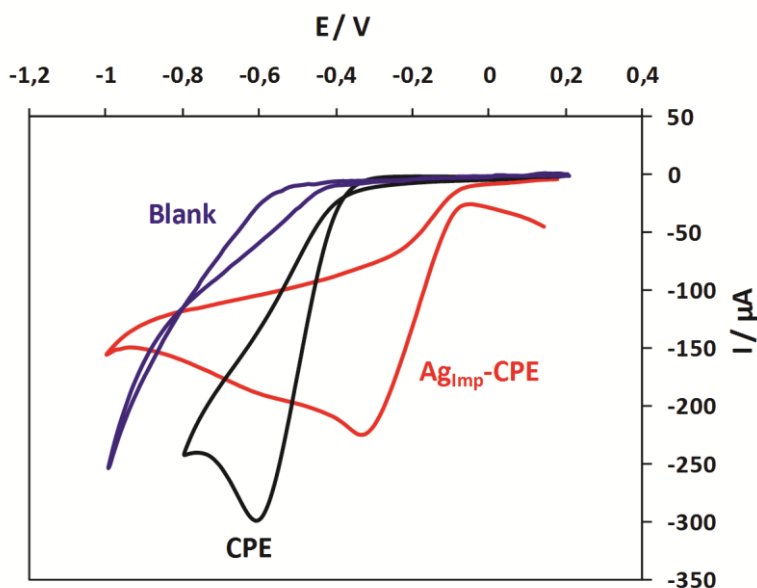

Figure 4: *Blank for AgImp-CPE, 1.0×10^{-3} mol L^{-1} PNA for CPE and for AgImp-CPE at scan rate of 100 mV s^{-1} in 1.0×10^{-1} mol L^{-1} B-R (pH 2.0).*

A key diagnostic is a scan rate study. (Fig. 5A) depicts typical voltammetric profiles resulting from applying a range of scan rates (1-400 mV s^{-1}). The Randles–Ševick equation as follows in the light of IUPAC recommendations (Eq. 3) [24]:

138

$$Ip = (2.99 \times 10^5)\ AD^{0.5}\ C\ \upsilon^{0.5}\ n\ (n' + \alpha_{RDS})^{0.5} \quad (3)$$

where Ip is the peak current of PNA, n is the total number of electrons transferred per molecule in the electrochemical process, A is the geometric area of the electrode (cm^2), C is the concentration of PNA species in solution (moles L^{-1}), D is the diffusion coefficient of PNA ($cm^2\ s^{-1}$), υ is the scan rate (V s^{-1}), n' is the number of electrons transferred per mole before the rate-determining step (RDS), and α RDS is the transfer coefficient for the RDS is given by (Eq. 4) [25,26].

$$\alpha = \pm\ (RT/nF)\ (dln\ |j|\ /dE) \quad (4)$$

Where j the current density has been corrected for any changes in the reactant concentration at the electrode surface with respect to its bulk value, E is the applied electric potential, and R, T, and F have their usual significance. The $\pm$ sign is used for mounting if oxidation or reduction is involved.
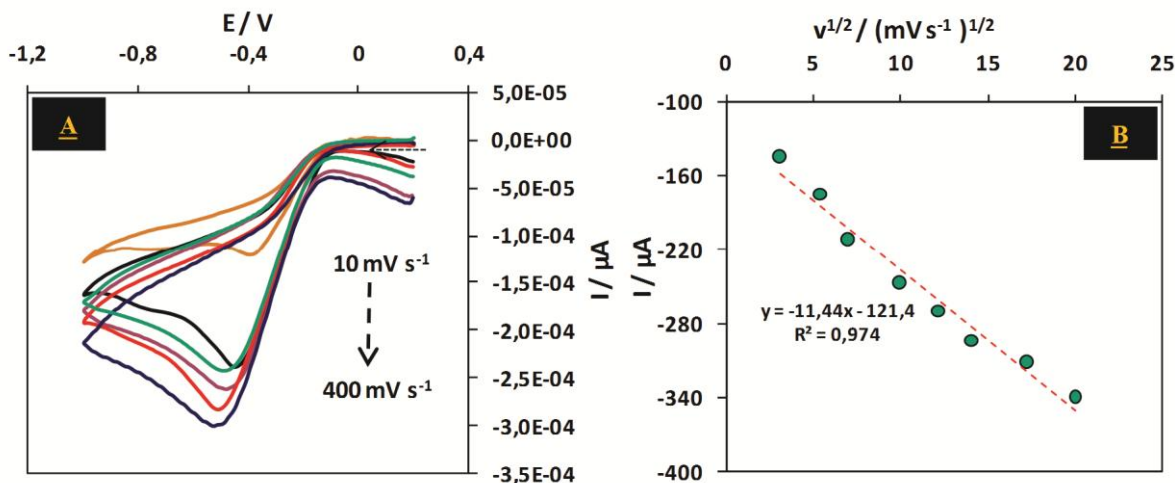

Figure 5: *CVs of 1.0×10^{-3} mol L^{-1} PNA in 0.1 mol L^{-1} B-R buffer (pH 2); (A) CVs at scan rates of 10, 30, 50, 100, 150, 200, 300, 400 mVs^{-1}. (B) Variations of Ip vs. square root of scan rate.*

As shown in (Fig. 5B), the peak height (I_p) of PNA is proportional to the applied voltammetric scan rate and a plot of I_p against $\upsilon^{1/2}$ is linear. The position of the current maximum of PNA at the

surface of Ag-CPE occurs at the different potential; this peak maximum, which does shift in potential with scan rate, is characteristic of electrode reactions which exhibit slow electron transfer kinetics, usually termed irreversible electron transfer reaction. Since the electrochemical process, that is, reversible or irreversible, reflects the competition between the electrode kinetics and mass transport, ($k^o << m_T$) indicating electrochemical irreversibility. Where m_T is the rate of mass transport and given by (Eq. 5):

$$m_{T=} \sqrt{D(RT/F\upsilon)} \quad (5)$$

Theory of Nicholson is used to estimate the observed standard heterogeneous electron transfer rate constant (k^o, cm s^{-1}) using the following equation (Eq. 6) [27]:

$$\Psi = K^{\circ} [\pi Dn \, \upsilon F \, / \, (RT)]^{-1/2} \quad (6)$$

Where Ψ is a kinetic parameter, D is the diffusion coefficient of PNA system, n is the number of electrons involved in the process, F is the Faraday constant, R is the gas constant and T is the temperature (K). The kinetic parameter (Ψ) is tabulated as a function of peak-to-peak separation ($\Delta Epc \times n$) at a temperature (298 K) for a one electron process (where the charge transfer coefficient, $\alpha = 0.5$). A plot of Ψ against $[\pi Dn\upsilon F \, / \, (RT)]^{-1/2}$ allows the standard heterogeneous rate transfer constant, k^o to be readily deduced. The kinetic parameter was deduced as a function of ΔEpc by utilizing the Nicholson method. The empirical equation (Eq. 7) [28];

$$\Psi = (-0.6288 + 0.021X) \, / \, (1 - 0.017X) \quad (7)$$

Where X = ΔEp in mV used to determine the Ψ as a function of ΔEp.
This CV experiment was conducted in PNA for scan rate from 10 to 400 mV s^{-1} and the ΔEp is ranging from 236 to 353 mV. The calculated k^o value corresponding to 0.22×10^2 cm s^{-1}. Karikalan et al used bare SPCE (screen printed carbon electrodes) and GR/SPCE (screen printed carbon electrode modified by graphite) for electrocatalytic reduction of nitroaromatic compounds, the calculated values of k^o are 1.18×10^2, 3.34×10^2 and 5.02×10^2 cm s^{-1} respectively [29], which is in good agreement with that found by our electrode (Ag$_{Imp}$-CPE). This value

suggested that the Ag_{Imp}-CPE has highest electron transfer rate constant, which provides excellent electrochemical behavior towards PNA.

The effect of buffer pH on cyclic voltammetric responses of the silver-impregnated onto carbon paste electrode was further investigated. The effect of pH on the reduction properties of the modified electrode (Ag_{Imp}-CPE) was determined in solutions of different pH over the range from 1 to 12 by cyclic voltammetry in the presence of 1.0×10^{-3} mol L^{-1} PNA (Fig. 6A). The PNA reduction was shifted to the negative value with increasing pH. The insert in (Fig. 6B) shows a plot of potential of the PNA molecule as a function of pH. It is evident that there is a deviation from the linearity probably due to the pKa of the PNA analyte. The slope of 52.17 mV/ pH was found, which is very close to the anticipated Nernstian value for the same number of electron and proton transfer processes.
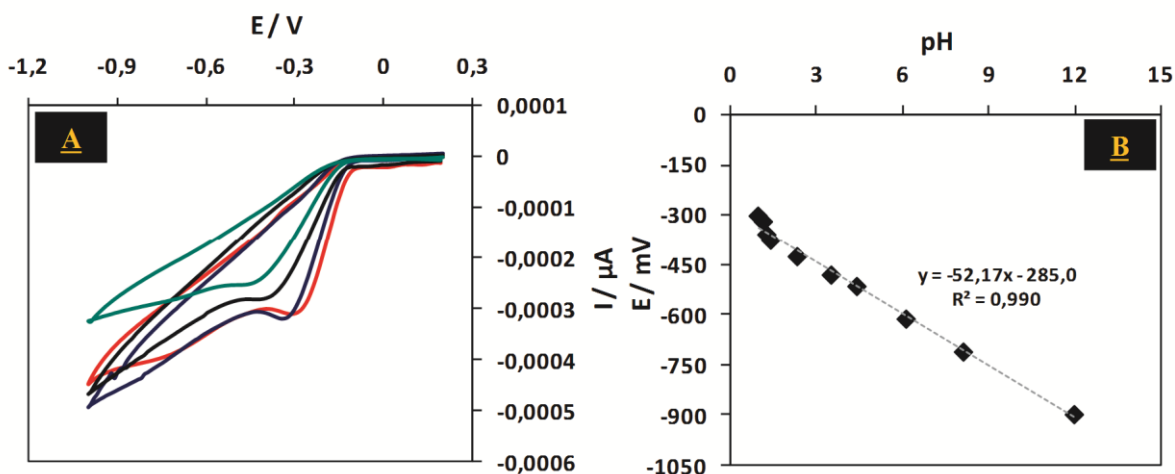

Figure 6: *(A) CVs (at 50 mV s^{-1}) of 1.0×10^{-3} mol L^{-1} PNA at different values of buffered pH. (B) Plot of E versus pH.*

III.1.2. Chronoamperometric studies

Catalytic reduction of PNA onto modified electrode was also studied by chronoamperometry. (Fig. 7A) shows the chronoamperometric measurements for PNA. The figure represents the current-time profiles obtained by setting the working electrode potential at -0.5 V for various PNA concentrations. For an electroactive material with a diffusion coefficient of D, the current response under diffusion control is described by the Cottrell equation (Eq. 8) [30]:

$$Ip = nFACD^{1/2}\pi^{1/2}t^{-1/2} \quad (8)$$

Where D and C are the diffusion coefficient ($cm^2 s^{-1}$) and bulk concentration of PNA (mol cm^{-3}), respectively; A is the electrode area (cm^2), and I is the current controlled by the diffusion of PNA from the bulk solution to the electrode/solution interface.
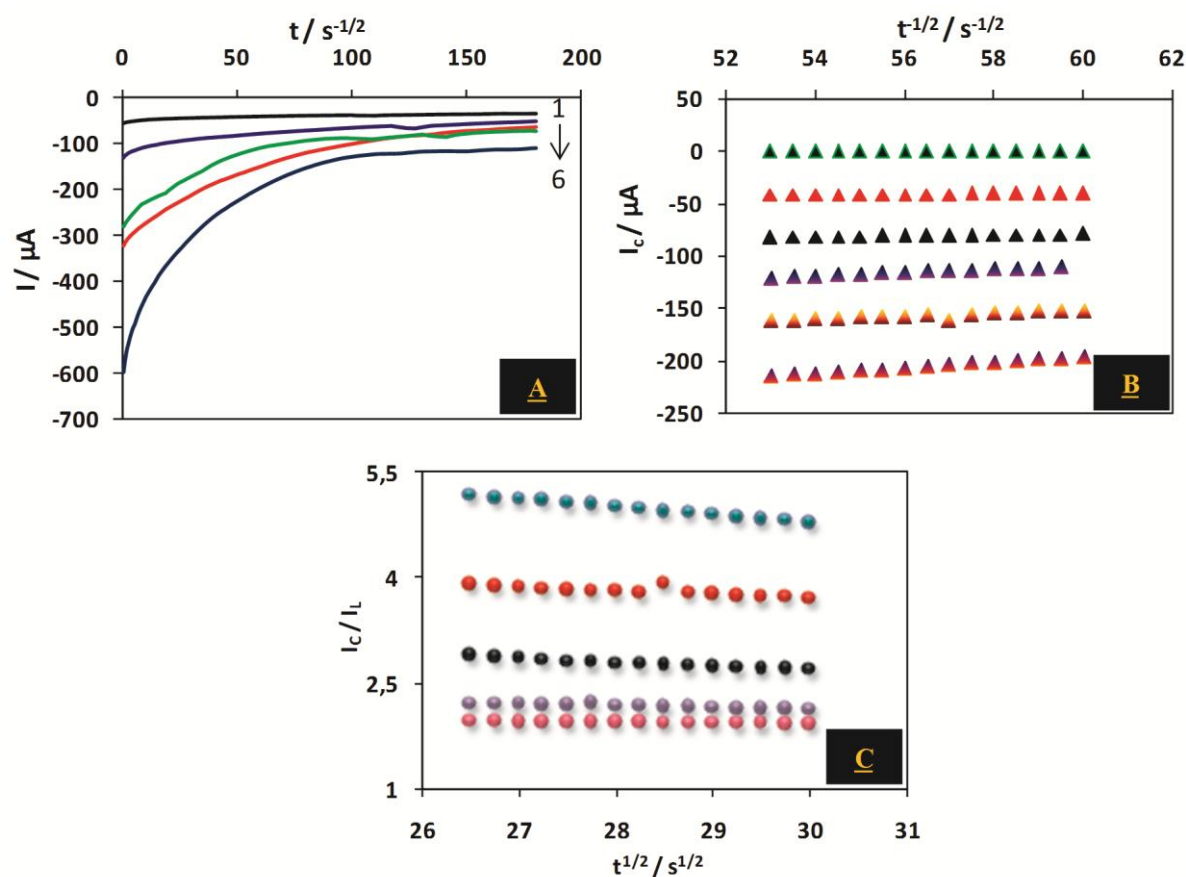

Figure 7: (A) Chronoamperograms obtained for PNA concentrations at Ag_{Imp}-CPE of 1 (1), 0.1 (2), 0.05 (3), 0.01 (4) and 0.001(5) mmol L^{-1} at reduction potential (-0.5 V). (B) Insets; plots of I versus $t^{-1/2}$ obtained from chronoamperograms (A) and (C) dependence of I_C/I_L on $t^{1/2}$.

The plot of I vs. $t^{-1/2}$ at various PNA concentrations were linear as shown in (Fig. 7B). From the slopes of the resulting straight lines and the PNA concentrations, the average value of D was calculated to be $3.35 \times 10^{-6} cm^2 s^{-1}$.

In addition to that, we also investigated the catalytic rate constant (K_{cat}) associated to PNA system, when the catalytic current is dominated by the rate of the electro catalyzed reduction of PNA at intermediate times.

The catalytic rate constant K_{cat} has been determined according to the method described earlier [22] from the following relation (Eq. 9):

$$I_{Cat}/I_L = \pi^{1/2} \cdot \Upsilon^{1/2} = \pi^{1/2} (kC_0t)^{1/2} \quad (9)$$

Where I_{cat} and I_L are the currents of the Ag_{Imp}-CPE modified electrode in the presence and absence of PNA, respectively. K_{cat} was calculated from the slope of the I_{cat}/I_L vs. $t^{1/2}$ plot constructed from the chronoamperograms (Fig.7C), and value for K_{cat} was found to be 1.36×10^{-2} mol^{-1} L s^{-1}.

III.2. Electrochemical determination of PNA at Ag_{ED}-CPE

III.2.1. Electrochemical behavior of PNA

The same phenomenon is observed using Ag_{ED}-CPE for the reduction of PNA. Indeed, the cathodic peak potential of PNA was positively shifted to -230 mV. More than this potential shift of 370 mV, the reduction peak current was also increased at the Ag_{ED}-CPE electrode at low concentrations.

III.2.2. Effect of Ag electrodeposition conditions on PNA responses

The influence of the experimental conditions of Ag electrodeposition (scan rate, sweeping potential range, number of cycles and concentration of silver in KNO_3 solution) on the potential and intensity of the PNA reduction peak were studied.

Scan rate is one of the most important parameters. Their influence on the electrodeposition of silver particles onto CPE to reduce PNA was studied. The experiments were carried out in a solution of 0.1 mol L^{-1} KNO_3 containing 5.0×10^{-4} mol L^{-1} of $AgNO_3$ in the range from 1 mV s^{-1} to 30 mV s^{-1}. It was found that the high intensity with positively shifted cathodic peak potentials was obtained at a scan rate of 10 mV s^{-1}. Moreover, the range of electrodeposition potential was studied by testing a variety of sweeping potential ranges and the result demonstrates that the

Ag$_{ED}$-CPE electrode prepared in a sweeping potential range of 600 mV to -400 mV is efficient for the detection of PNA. Similarly, the highest response was also improved when the electrode prepared for the total segments of 6. The deposition process also depends on the concentration of reacting (electroactive) ions. Therefore, the effect of the latter on the response of PNA was studied in a concentration range from 1.0×10^{-5} to 1.0×10^{-3} mol L^{-1} of AgNO$_3$ dissolved in cell containing 0.1 mol L^{-1} KNO$_3$. The highest response was reached for 0.5 mmol L^{-1} AgNO$_3$, above this concentration; a poor response for PNA is obtained. This behavior was attributed to the formation of a partial silver film on CPE [31]. Hence, for all succeeding experiments, 0.5 mmol L^{-1} AgNO$_3$ under the scan rate of 10 mV s^{-1} with a total segment number of 6 in the sweeping potential range from 600 mV to -400 mV was used to deposit silver particles onto CPE surface.

III.2.3. Catalytic studies

In order to evaluate the electrocatalytic effect of Ag$_{ED}$-CPE for the reduction of PNA, a series of electrochemical analyses are performed. The product Ag$_{ED}$-CPE exhibits excellent electrocatalytic activity towards the reduction of PNA. The catalytic effect was investigated using cyclic voltammetry and chronoamperometry techniques. Indeed, the diffusion coefficient (D) was 2.91×10^{-6} cm^2 s^{-1} and catalytic rate constant K$_{cat}$ was evaluated to be 6.43×10^{-4} mol^{-1} L s^{-1}.

III.2.4. Calibration data

Firstly, the electrochemical reduction of PNA was performed at both Ag$_{Imp}$-CPE and Ag$_{ED}$-CPE using differential pulse voltammetry (DPV). It was found that at concentrations below 10^{-5} M PNA, no peaks were detected on Ag$_{Imp}$-CPE. While the current height of the PNA reduction peak has decreased for Ag$_{Imp}$-CPE may be confirming the formation of silver oxide on the surface of CPE, all of this is in good agreement with the previously reported observation.

Before establishing the calibration curve, we were interested in optimizing the various electrochemical variables (step, pulse, width and period) that influence the determination of PNA at Ag$_{ED}$-CPE using DPV method. From the obtained results, it was found that the best response to PNA was recorded with 10 mVs^{-1}, 140 ms, 470 mV and 500 ms for step, pulse, width and period, respectively. On the other hand, the pH effect on cathodic current intensity of PNA was also evaluated. The results show that the peak intensity of PNA reduction increased when decreasing

the value of pH solution. Therefore, the maximum intensity is obtained with pH=1.34, which was used for further work. Finally, in order to observe the effect of accumulation time, Ag_{ED}-CPE was inserted into a cell containing 20 mL of the PNA at open-potential for different times (0, 60, 120, 180, 240, 300, 360, 420, 600 and 900 sec), and then the resulting responses of the prepared electrodes were evaluated to determine the optimum value. The increase of peak current with increase of accumulation time indicated that PNA can be accumulated at the surface of CPE electrode probably due to its increase surface activity. According to our findings, the most convenient value was obtained with an accumulation time of 180 sec.

Calibration data were obtained for PNA solutions under optimum experimental conditions described obviously. (Fig. 8) shows some of the typical DPV voltammograms recorded on the Ag_{ED}-CPE in two linear dynamic ranges of $8.0\times10^{-8}-1.0\times10^{-6}$ and $5.0\times10^{-6}-1.0\times10^{-4}$ mol L^{-1} of PNA. The calibration plot is required for quantitative measurements of the PNA concentration at a given potential. The intensity of cathodic current increase with concentration of PNA with a coefficient of determination of $R^2 = 0.994$. The electrochemical sensing showed a detection limit (S/N = 3) of 4.18×10^{-8} mol L^{-1}. The relative standard deviation (R.S.D.) for eight measurements was calculated as 2.44 % for PNA concentration of 1.0×10^{-4} mol L^{-1}.

Table 2 shows the comparison of some of the reported electrochemical sensors for the detection of PNA derivatives with the present sensor.
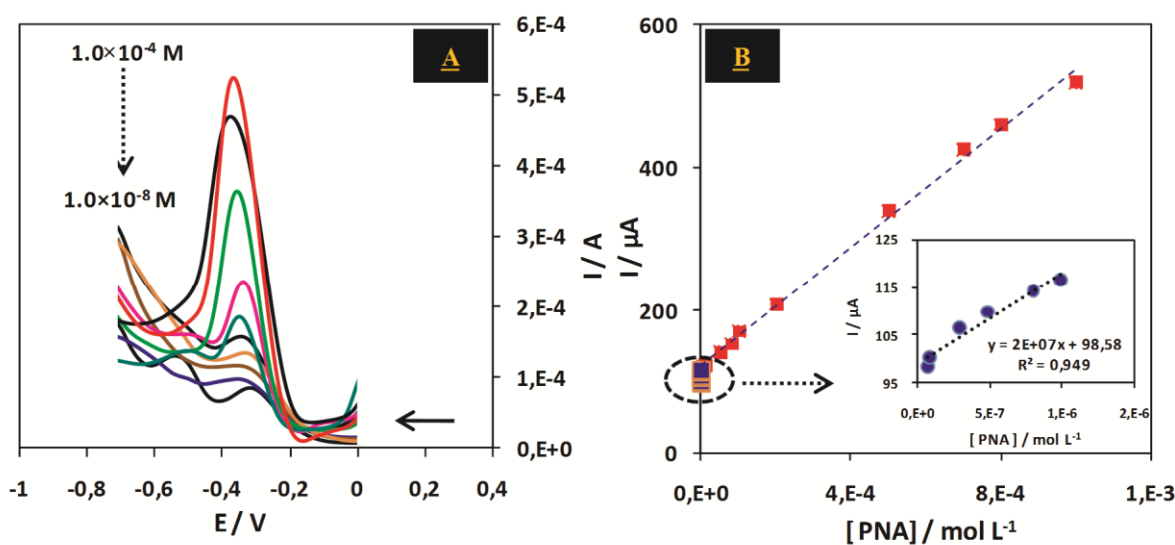

Figure 8: *(A) DPVs for different PNA concentrations in 0.1 mol L^{-1} B-R buffer (pH 2). (B)Plot of electrocatalytic peak current as a function of PNA concentration.*

Table 2: *Some of the reported electrochemical sensors for PNA detection.*

Modified electrode	Analytical technique	Detection limit	E_{pc} (mV)	References
CPE/DTD/Ag NPs	DPV[a]	0.23 µM	-320	[32]
GC/TPDT–SiO2/Ag NPs	SWV[b]	0.50 µM	-800	[33]
BMIMPF6-SWNT/GCE	LSV[c]	8.0 nM	-750	[34]
Metallic silver electrode	DPV	4.74 nM	-260	[35]
Silver/CPE	CV[d]	--------	-300	[36]
ZnO NRs/FTO	Amperometry	0.5 µM	___	[37]
AgED-CPE	DPV	0.418 nM	-230	Present work

The abbreviations of the modified electrodes can be referred from the corresponding references
[a]Differential pulse voltammetry.
[b]Square wave voltammetry.
[c]Linear sweep voltammetry.
[d]Cyclic voltammetry

III.2.5. Interference effect

In order to evaluate the effect of several species frequently found with PNA on the electrode response, a study involving these compounds was performed. The selectivity of the suggested sensor was investigated in electrolytic solution containing 1.0×10^{-5} mol L^{-1} of PANA spiked with different concentrations of dopamine, ascorbic acid, paracetamol, 4-nitrophenol, 2-nitrophenol, 4-aminophenol and 2-nitroaniline.

The effect of representative potential interference on the determination of PNA was investigated, which were expressed as the recovery relating to the responses with and without interference compounds. The different concentrations of 4-nitrophenol were investigated and significantly interfered especially by the addition of 10-fold leading to an increase in the peak current of PNA. The increase of current signal is probably due to the overlap of the PNA and 4-nitrophenol reduction peaks. It was too observed that the peak current of PNA was decreased by the addition of dopamine, ascorbic acid and paracetamol. This decrease may be due to the paracetamol/

dopamine/ ascorbic acid adsorption on the surface of Ag electrode, which is blocking the surface sites. Therefore, the potential range from 0.0 mV to -600 mV was recommended to remove the effect of these interferences. However, 2-nitrophenol, 2-nitroaniline and 4-aminophenol did not interfere with PNA detection, where the recovery rates were greater than 97%.

III.2.6. DPV measurements of PNA in water samples

In order to evaluate the practical application of the proposed electrode Ag_{ED}-CPE, it was used to detect PNA in drinking water samples. No signal for PNA was observed when the sample was analyzed. Hence, the proposed method was applied to analyze water samples contaminated with PNA at different concentrations. The reduction peak of PNA was clearly displayed. The linear calibration curve of PNA was obtained in the concentration range of 1.0×10^{-6} mol L^{-1} to 1.0×10^{-5} mol L^{-1} for drinking water samples (Fig. 7). The coefficient of determination of the curve was ($R^2 = 0.981$). The limit of detection (LOD) was found to be 1.38×10^{-7} mol L^{-1} with RSD of 2.2 % and satisfactory recovery that exceeds 95 %.

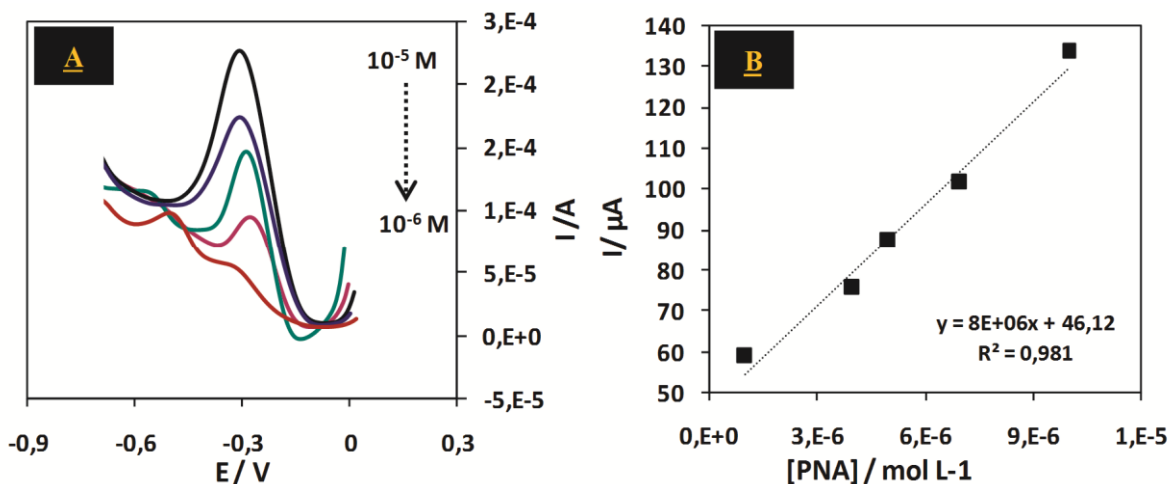***Figure 9:*** *(A) Calibration curve of PNA in drinking water in the concentration range of 1.0×10^{-6} mol L^{-1} to 1.0×10^{-5} mol L^{-1} using DPV method at Ag_{ED}-CPE. (B) Plot of peak current as a function of PNA concentration.*

147

IV. Conclusion

As a conclusion, this study is devoted to the development of simple and easy methods for the deposition of silver on carbon paste electrodes such as impregnation using solid reaction and electrodeposition for the determination of PNA. The morphology and the distribution of silver on the electrode surface were evaluated by XRD, and Scanning electron microscopy. The electro-active surface area of the as prepared electrodes were estimated using $[Fe(CN)_6]^{3-/4-}$ as redox probe by cyclic voltammetry. The electrochemical reduction of PNP was followed by cyclic voltammetry in the first time with determination of kinetic parameters. This study has demonstrated that both electrodes exhibit excellent electrocatalytic activity toward PNA reduction in B-R buffer solution (pH 2.0). The electrocatalytic activity of silver based electrodes is discussed on the basis of the real electro-active surface area and particle size which results from varying modification modes.

In addition, the analytical determination of PNA was performed for both Ag_{Imp}-CPE and Ag_{ED}-CPE using differential pulse voltammetry (DPV). It was found that the current height of the PNA reduction peak at Ag_{Imp}-CPE is very low than at Ag_{ED}-CPE, this may confirm the formation of silver oxide on the surface of CPE. Finally, the Ag_{ED}-CPE has been successfully applied for the determination of PNA in drinking water samples. Simplicity of preparation, good reproducibility and low cost of the modified electrode, high active surface area as well as wide linear concentration range, low detection limit and good repeatability for PNA determination are the important advantages of Ag_{ED}-CPE.

References

[1]   Mc Creery, R. L. (2008). Advanced carbon electrode materials for molecular electrochemistry. Chemical reviews, 108(7), 2646-2687.

[2]   Brownson, D. A., & Banks, C. E. (2010). Graphene electrochemistry: an overview of potential applications. Analyst, 135(11), 2768-2778.

[3]   Mc Creery, R. L. (1991). In Electroanalytical Chemistry; Bard, A. J., Ed.; Dekker, New York, 17.

[4]   Mc Creery, R. L., Cline, K. K., McDermott, C. A., & McDermott, M. T. (1994). Control of reactivity at carbon electrode surfaces. Colloids and Surfaces A: Physicochemical and Engineering Aspects, 93, 211-219.

[5]   Sun, L., Zhang, Z., & Dang, H. (2003). A novel method for preparation of silver nanoparticles. Materials letters, 57(24-25), 3874-3879.

[6]   Fukushima, M., Yanagi, H., Hayashi, S., Suganuma, N., & Taniguchi, Y. (2003). Fabrication of gold nanoparticles and their influence on optical properties of dye-doped sol-gel films. Thin Solid Films, 438, 39-43.

[7]   Dai, X., Nekrassova, O., Hyde, M. E., & Compton, R. G. (2004). Anodic stripping voltammetry of arsenic (III) using gold nanoparticle-modified electrodes. Analytical chemistry, 76(19), 5924-5929.

[8]   El-Deab, M. S., Okajima, T., & Ohsaka, T. (2003). Electrochemical reduction of oxygen on gold nanoparticle-electrodeposited glassy carbon electrodes. Journal of the electrochemical society, 150(7), A851-A857.

[9]   Welch, C. M., Banks, C. E., Simm, A. O., & Compton, R. G. (2005). Silver nanoparticle assemblies supported on glassy-carbon electrodes for the electro-analytical detection of hydrogen peroxide. Analytical and bioanalytical chemistry, 382(1), 12-21.

[10]   Yin, B., Ma, H., Wang, S., & Chen, S. (2003). Electrochemical synthesis of silver nanoparticles under protection of poly (N-vinylpyrrolidone). The Journal of Physical Chemistry B, 107(34), 8898-8904.

[11]   El-Deab, M. S. (2009). On the preferential crystallographic orientation of Au nanoparticles: effect of electrodeposition time. Electrochimica Acta, 54(14), 3720-3725.

[12]   Ma, Y., Di, J., Yan, X., Zhao, M., Lu, Z., & Tu, Y. (2009). Direct electrodeposition of gold nanoparticles on indium tin oxide surface and its application. Biosensors and Bioelectronics, 24(5), 1480-1483.

[13]   Farahi, A., Achak, M., El Gaini, L., El Mhammedi, M. A., & Bakasse, M. (2015). Electrochemical determination of paraquat in citric fruit based on electrodeposition of silver particles onto carbon paste electrode. Journal of food and drug analysis, 23(3), 463-471.

[14]   Laghrib, F., Ajermoun, N., Hrioua, A., Lahrich, S., Farahi, A., El Haimouti, A., & El Mhammedi, M. A. (2019). Investigation of voltammetric behavior of 4-nitroaniline based on electrodeposition of silver particles onto graphite electrode. Ionics, 25(6), 2813-2821.

[15]   Munnik, P., de Jongh, P. E., & de Jong, K. P. (2015). Recent Developments in the Synthesis of Supported Catalysts. Chemical Reviews, 115(14), 6687–6718.

[16]   A. Farahi, M. Achak, L. El Gaini, M.A. El Mhammedi, M. Bakasse, Silver particles-modified carbon paste electrodes for differential pulse voltammetric determination of paraquat in ambient water samples, J. Assoc. Arab Univ. Basic Appl. Sci. 19 (2016) 37-43.

[17]   Macdonald, D. D. (2006). Reflections on the history of electrochemical impedance spectroscopy. Electrochimica Acta, 51(8-9), 1376-1388.

[18]   Yang, L., & Li, Y. (2005). AFM and impedance spectroscopy characterization of the immobilization of antibodies on indium–tin oxide electrode through self-assembled monolayer of epoxysilane and their capture of Escherichia coli O157: H7. Biosensors and Bioelectronics, 20(7), 1407-1416.

[19]   Pillay, J., & Ozoemena, K. I. (2007). Electrochemical properties of surface-confined films of single-walled carbon nanotubes functionalised with cobalt (II) tetra-aminophthalocyanine: Electrocatalysis of sulfhydryl degradation products of V-type nerve agents. Electrochimica acta, 52(11), 3630-3640.

[20]   Sabatani, E., & Rubinstein, I. (1987). Organized self-assembling monolayers on electrodes. 2. Monolayer-based ultramicroelectrodes for the study of very rapid electrode kinetics. Journal of Physical Chemistry, 91(27), 6663-6669.

[21]   Viswanathan, S., Radecka, H., & Radecki, J. (2009). Electrochemical biosensor for pesticides based on acetylcholinesterase immobilized on polyaniline deposited on

vertically assembled carbon nanotubes wrapped with ssDNA. Biosensors and Bioelectronics, 24(9), 2772-2777.

[22] Sun, W., Guo, C. X., Zhu, Z., & Li, C. M. (2009). Ionic liquid/mesoporous carbon/protein composite microelectrode and its biosensing application. Electrochemistry communications, 11(11), 2105-2108.

[23] Calvo, M. E. B., Renedo, O. D., & Martínez, M. J. A. (2007). Determination of lamotrigine by adsorptive stripping voltammetry using silver nanoparticle-modified carbon screen-printed electrodes. Talanta, 74(1), 59-64.

[24] Batchelor-McAuley, C., & Compton, R. G. (2012). Voltammetry of multi-electron electrode processes of organic species. Journal of Electroanalytical Chemistry, 669, 73-81.

[25] Guidelli, R., Compton, R. G., Feliu, J. M., Gileadi, E., Lipkowski, J., Schmickler, W., & Trasatti, S. (2014). Defining the transfer coefficient in electrochemistry: An assessment (IUPAC Technical Report). Pure and Applied Chemistry, 86(2), 245-258.

[26] Guidelli, R., Compton, R. G., Feliu, J. M., Gileadi, E., Lipkowski, J., Schmickler, W., & Trasatti, S. (2014). Definition of the transfer coefficient in electrochemistry (IUPAC Recommendations 2014). Pure and Applied Chemistry, 86(2), 259-262.

[27] Nicholson, R. S. (1965). Theory and application of cyclic voltammetry for measurement of electrode reaction kinetics. Analytical chemistry, 37(11), 1351-1355.

[28] I. Lavagnini, R. Antiochia, F. Magno, An extended method for the practical evaluation of the standard rate constant from cyclic voltammetric data, Electroanalysis 16 (2004) 505-506.

[29] Karikalan, N., Kubendhiran, S., Chen, S. M., Sundaresan, P., & Karthik, R. (2017). Electrocatalytic reduction of nitroaromatic compounds by activated graphite sheets in the presence of atmospheric oxygen molecules. Journal of Catalysis, 356, 43-52.

[30] ABard, A. J., & Faulkner, L. R. (2001). Fundamentals and applications. Electrochemical Methods, 2(482), 580-632.

[31] Galus, Z. (1976). Fundamentals of electrochemical analysis. Halsted Press.

[32] Zavar, M. H. A., Heydari, S., Rounaghi, G. H., Eshghi, H., & Azizi-Toupkanloo, H. (2012). Electrochemical behavior of para-nitroaniline at a new synthetic crown ether-silver nanoparticle modified carbon paste electrode. Analytical Methods, 4(4), 953-958.

151

[33]   Rameshkumar, P., & Ramaraj, R. (2014). Electroanalysis of nitrobenzene derivatives and nitrite ions using silver nanoparticles deposited silica spheres modified electrode. Journal of Electroanalytical Chemistry, 731, 72-77.

[34]   Zhao, F., Liu, L., Xiao, F., Li, J., Yan, R., Fan, S., & Zeng, B. (2007). Sensitive Voltammetric Response of p-Nitroaniline on Single-Wall Carbon Nanotube-Ionic Liquid Gel Modified Glassy Carbon Electrodes. Electroanalysis: An International Journal Devoted to Fundamental and Practical Aspects of Electroanalysis, 19(13), 1387-1393.

[35]   Laghrib, F., Boumya, W., Lahrich, S., Farahi, A., El Haimouti, A., & El Mhammedi, M. A. (2017). Electrochemical evaluation of catalytic effect of silver in reducing 4-nitroaniline: Analytical application. Journal of Electroanalytical Chemistry, 807, 82-87.

[36]   Laghrib, F., Lahrich, S., Farahi, A., Bakasse, M., & El Mhammedi, M. A. (2018). Impregnation of silver in graphite carbon using solid reaction: Electrocatalysis and detection of 4-nitroaniline. Journal of Electroanalytical Chemistry, 823, 26-31.

[37]   Ahmad, R., Tripathy, N., Ahn, M. S., & Hahn, Y. B. (2017). Development of highly-stable binder-free chemical sensor electrodes for p-nitroaniline detection. Journal of colloid and interface science, 494, 300-306.

– Chapter 5 –

Silver nanostructured electrodes for direct electrocatalysis and electroanalysis of p-nitroaniline

I. Introduction

Nanomaterials have, by definition, one or more dimensions in the nanometer scale (≤100 nm) and then exhibit new properties from their base materials. The synthesis, characterization, and applications of nanoparticles are among the most important sections of the wide range of nanotechnology fields falling under the general category of "nanotechnology". In recent years, nanoparticles have been the focus of attention for researchers in this field, as it has been found that the transition from microparticles to nanoparticles leads to immense changes in the physical and chemical properties of a material. The most important characteristics, among many others, at the nanoscale are the following: Firstly, the small particle size, which leads to an increase in the surface-to-volume ratio and therefore the one in which quantum effects predominate. Second, the increase in the surface/volume ratio results in an increase in the predominance of the surface atoms of the nanoparticle over those in its interior. Nanoparticles are of great scientific interest as they bridge the gap between bulk materials and atomic or molecular structures [1]. Among various nanoparticles, metal nanoparticles are the most promising ones and this is due to their anti-bacterial properties which, occur because of the high surface to volume ratio. Change in the size or surface of the composition can change the physical and chemical properties of the nanoparticles [2, 3]. In recent decades, the application of metal nanoparticles is very common due to their wide applications in various industries [4]. The synthesis of nanoparticles (NPs) with control over particle size, shape, and crystalline nature has been one of the main objectives in chemistry that could be used for potential applications, such as bio-medical, biosensor, catalyst, and lower cost electrode [5-7].

Metallic nanoparticles exhibit size and shape-dependent properties that are of interest for applications ranging from catalysis and sensing to optics, antibacterial activity and data storage [8-13]. For example, the antibacterial activity of different metal nanoparticles such as silver colloids is closely related to their size; that is, the smaller the silver nuclei, the higher the antibacterial activity. In addition, the catalytic activity of these nanoparticles also depends on their size as well as their structure, shape, size distribution and physicochemical environment.

A series of investigations on the catalytic conversion of aromatic nitro-compounds have been reported using a variety of nanostructures, including silver [14-18], copper [19], iron [20], iron oxide [21], gold [22], platinum, and palladium [23-25] nanoparticles as nanocatalysts. Silver

nanoparticles (AgNPs), for example, tender great performance and attracted particular attention in catalysis for numerous types of chemical reactions by dint of their low cost [26].

Generally, various techniques are used for the metallic nanoparticles synthesis, including high-temperature methods (e.g. laser ablation), often expensive and complicated to implement. Other techniques such as chemical reduction of silver ions in aqueous [27, 28] or non-aqueous [29, 30] solutions, the template method [31], electrochemical [32], photocatalytic [33] or biochemical [34] methods are more commonly used. According to the synthesis method, the nanoparticles obtained have different shapes (spherical, cubic, tetrahedral, threads, etc.) and sizes [35-39]. The chemical methods for the synthesis of metallic nanoparticles are quite successful and have been well studied [40–42] because it's a simple and inexpensive technique. However, this type of process requires in particular, the use of various chemical agents: reducers, stabilizers and, accelerants. Thus, the silver salt is reduced to give metal atoms that enter into collision in solution with ions, atoms or clusters to form a stable nucleus irreversible [43]. Commonly used reducers are borohydride, citrate, ascorbate, and elemental hydrogen [44–52]. The stage of growth is influenced by the presence of stabilizers which are surfactants, hydrogels or polymers such as chitosan. They have the effect of stopping the growth of nanoparticles that begins after nucleation, but also of preventing agglomeration of the nanoparticles already formed. The name chitosan was proposed by *Hoppe-Seyler* in 1894. It is now commercially produced from waste from the consumption of crustaceans and the industrial processing of mushrooms [53]. It can be used as an efficient adsorbent due to the presence of amino ($-NH_2$) and hydroxyl groups (-OH), which can serve as active sites [54]. Amino groups of chitosan can be cationized, after which they strongly adsorb anionic dyes by electrostatic attraction [55]. Chitosan also exhibits a large range of applications, for example, as microcapsule implants for controlled release in drug delivery [56, 57], in water treatment [58], membrane component [59], food additive [60], and catalyst support [61], for biomedical devices and processes [62], and analytical applications [63]. Chitosan has been employed in electroanalysis, for example, to immobilize proteins in carbon structures [64], for the electroanalysis of paracetamol [65].

In this chapter, a chemical method for the synthesis of silver nanoparticles and there electrocatalytic activity for the reduction of PNA was presented. The silver ions are stabilized by chitosan so the nanoparticles could be kept from agglomerating during the synthesis, and reduced by $NaBH_4$. The characterization of samples was performed using UV–Visible spectroscopy, X-

ray diffraction analyses (XRD), Fourier transform infrared spectroscopy (FT-IR), cyclic voltammetry (CV), and electrochemical impedance spectroscopy (EIS). Finally, the electroanalytic activity of synthesis material was investigated against the PNA reduction using differential pulse voltammetry (DPV).

II. Characterization

To better understand the formation process of silver nanoparticles as previously discussed in chapter 2, a series of control experiments and measurements was performed.

II.1. UV-Vis spectroscopy

The colloidal solution sample obtained was subjected to UV-Visible spectroscopy. The study of optical properties by absorption spectroscopy is an essential step in the characterization of synthesized silver nanoparticles. Indeed, the metallic nanoparticles absorption present optical properties specific issues related to a classic effect of exaltation of the electric field often called dielectric confinement. Nanoparticles have a larger number of atoms, and therefore free electrons at the surface compared to macroscopic objects. The excitation of the metal surface by light causes the collective vibration of the electrons on the surface and thus a resonance at a certain wavelength. Generally, silver nanoparticles are characterized by an absorbance band of around 400–420 nm [23]. As shown in Fig. 1A, the surface plasmon resonance (SPR) of silver at $\lambda_{max} =$ 420 nm confirms the formation of colloïdal CS@AgNPs with particle size between (35-45 nm) [66, 67].Otherwise, the peak was sharp and symmetric indicating a narrow size distribution of AgNPs [68]. When the experiment begins, all the silver is in the form of Ag^+ ions. The formation of nanoparticles germs will be possible when these ions reduced to Ag^0. Thus, the concentration of Ag^+ ions decreases very strongly during the reaction which results in a magnification of the particles. As the particle size increases, there are less of ions in solution and, therefore, the growth rate decreases until it reaches a level of total reduction. The color change of the solution is rapid during the synthesis and confirms the hypothesis of rapid reaction kinetics Fig. 1B.The kinetics of the reaction, as it depends on the concentration of the Ag^+ ion, also depends on $NaBH_4$.Thus, reaction kinetics is more rapid when the concentration of silver nitrate is high. The maximum absorption wavelength (plasmon band) increases very slightly with the concentration of silver nitrate (Fig. 1C).
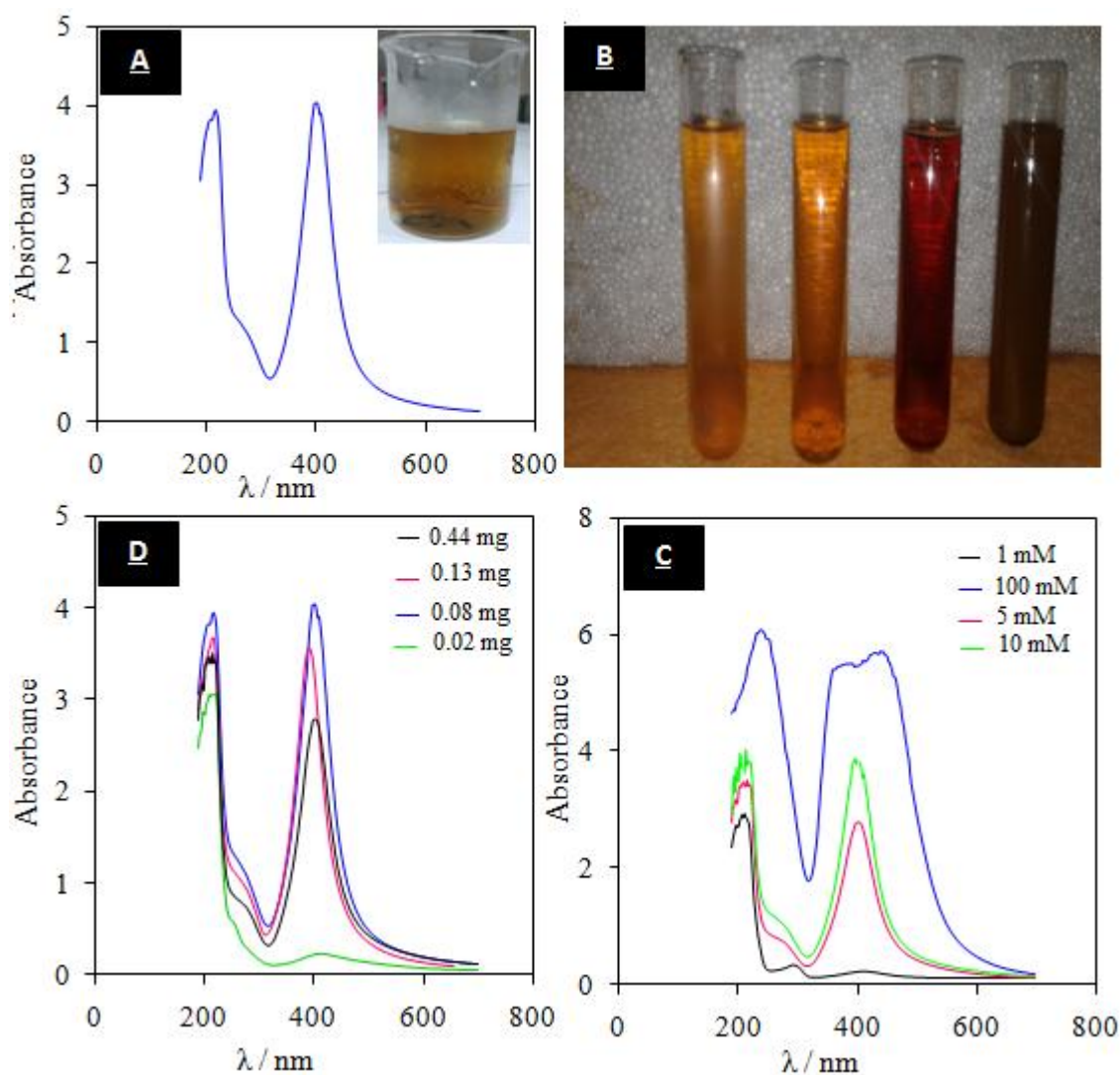
Figure 1: *(A) UV-Vis absorption spectra of freshly prepared CS@AgNPs solution. Inset photographic images. (B) Photographic images of CS@Ag NPs solution at different amount of NaBH₄. (C) UV-Vis absorption spectra of freshly prepared CS@AgNPs solution at different concentration of AgNO₃ and (D) UV-Vis absorption spectra of freshly prepared CS@AgNPs solution at different quantity of NaBH₄.*

The resistance to aggregation seems to evolve similarly to the size of particles. It is indeed possible to think that more the nanoparticles are small, the resistance to aggregation is important. This can be explained by the fact that nanoparticles of larger sizes due to their weight will tend to settle more easily. Increasing the amount of silver nitrate is also observed to enlarge the plasmon band of the absorption spectra resulting from the presence of nanoparticles of polydisperse sizes.

Furthermore, to find a suitable quantity of NaBH₄, the effect of different amounts of this reducer on the absorbance in the presence of 0.10 g of chitosan dissolved in 10 mL of 2% acetic acid and 10 mmol L^{-1} AgNO₃ was tested. The results indicated that the values of absorbance increased strongly within 0.4 mg of NaBH₄. It is also noted that for the absorbance whose amount of NaBH₄ less than 0.8 mg is very low (Fig. 1D). This is mainly due to the aggregation of nanoparticles, because of the lack of NaBH₄ to reduce silver nitrate. On the other hand, for quantities greater than 0.8 mg, a slight decrease in the absorption intensity was observed, which due to a decrease in the quantity of nanoparticles formed. In addition, the absorption bands of the solutions are much thinner, thus reflecting a lower dispersity in size.

II.2. XRD, SEM, and FT-IR analysis

The synthesized CS@AgNPs were separated by centrifugation at 4000 rpm for 10 min followed by dispersion in distilled water three times. The solid was then dried at 40°C. The dried powder was used for X-ray diffraction (XRD) analysis. A typical XRD pattern of the synthesized CS@AgNPs was found to possess a face-centered cubic (fcc) lattice, [69] as shown in Fig. 2A. Four Bragg reflections at 2θ = 37.36, 44.47, 64.80 and 77.44 are corresponding to the (1 1 1), (2 0 0), (2 2 0) and (3 1 1) plans respectively, confirmed the presence of AgNPs. These results pointed out apparently that the NPs were formed of extremely crystalline nanostructures [70]. XRD analysis was also applied to further calculate the particle size using Scherrer's formula (Eq. 1):

$$d = \frac{K\lambda}{B.\cos\theta_{max}} \quad (1)$$

Where d is the average crystal size, k is the X-ray wavelength (0.1541 nm), B is the full-width at half-maximum (FWHM) and θ is the diffraction angle [71]. The size of the AgNPs by calculating the FWHM of the most intense reflection (1 1 1) peak from the XRD data revealed a size of 51.54 nm. The presence of chitosan peaks is observed from the XRD pattern. The chitosan peaks that extended from 15.5 to 24° showed the amorphous region of the film. Moreover, SEM observations were carried out.
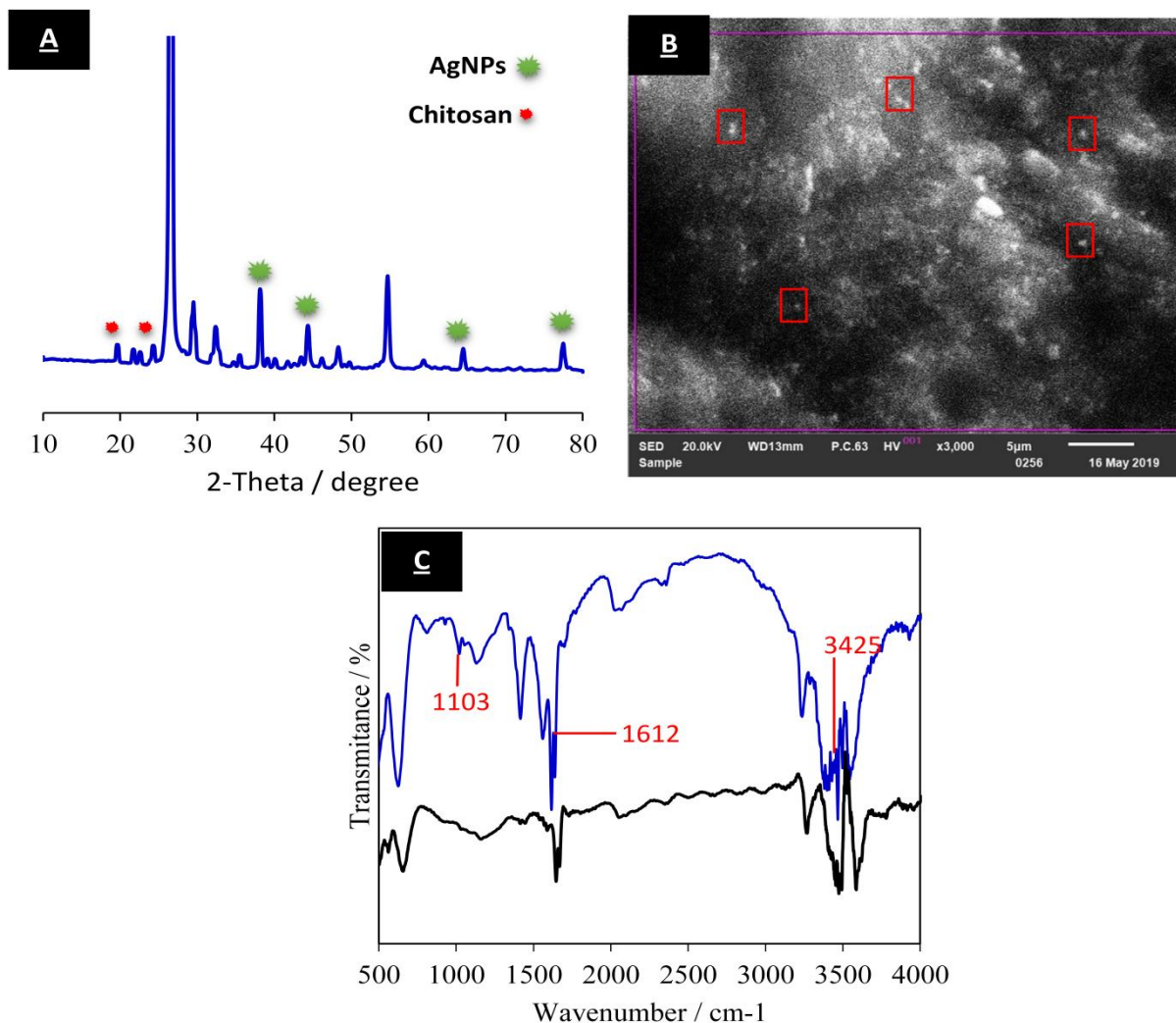
Figure 2: *(A) XRD pattern of synthesized CS@Ag NPs (B) SEM images of synthesized chitosan-Ag NPs and (C) The FTIR spectra of synthesized CS@AgNPs.*

Fig. 2B shows the SEM images of CS@AgNPs synthesized. It seems that the sample consisted of a large quantity of dispersive nanoparticles. As it is clear in the SEM image, the nanoparticles are relatively uniform and seemed like quasi-spheres. Infrared spectrometry is used to confirm the interaction between silver and chitosan. Fig. 2C shows the FTIR spectra of synthesized CS@AgNPs. As compared with some IR spectra of chitosan reported in the literature [72], the result revealed some degree shift in the chitosan stabilized silver nanoparticles. This suggests that the formation of AgNPs was promoted by N-H bond (*Wei et al. 2009*) [73]. The observed peaks at 3425, 1612, and 1103 cm^{-1} may be originated from the -OH stretching vibration N-H vibration, and C=O asymmetric stretch in chitosan molecule [74, 75].

Bands at 2925 cm^{-1} arising from C-H stretching of aromatic compound. The band at 1741 cm^{-1} was assigned for C-C stretching. The band 1660 cm^{-1} developed for C-N and C-C. The bands at 1450 cm^{-1} and 1100 cm^{-1} arising from N-H stretch vibration. These functional groups indicating an important role in stability/capping of silver nanoparticles [76, 77].

II.3. Electrochemical impedance characterization

Electrochemical impedance spectroscopy (EIS) can provide useful information about the surface features during the fabrication process. The EIS curve includes a semicircular part and a linear part. The semicircular part at higher frequencies corresponds to the electron-transfer limited process and its diameter is equal to the charge transfer resistance (Rct), which controls the electron transfer kinetics of the redox probe at the electrode interface. Meanwhile, the linear part at lower frequencies corresponds to the diffusion process.

Fig. 3 displays the EIS of the electrodes at different stages. Carbon paste electrode CPE (i), chitosan modified carbon paste electrode CS-CPE (ii), and chitosan stabilized silver nanoparticles modified carbon paste electrode CS@AgNPs-CPE (iii) in 1.0 mmol L^{-1} K$_3$[Fe(CN)$_6$] / K$_4$[Fe(CN)$_6$] (1:1) with 0.1 mol L^{-1} KCl. For the bare CPE, the EIS curve consists of only a linear part with a R$_{et}$ value of 36.310 Kohm indicating a diffusion-controlled redox process at the electrode. In the case of CS-CPE and CS@AgNPs-CPE, both curves consist of a semicircular part and a linear part, and the diameter of the semicircle is much less for the former than for the latter with interfacial electron transfer resistance of 0.5298 Kohm and 0.1821 Kohm respectively. This can explain that the AgNPs could generate a conductivity-increased surface that enhanced the Fe(CN)$_6^{3-}$/Fe(CN)$_6^{4-}$ probe to access the modified CS@AgNPs-CPE. Thus, the CS@AgNPs-CPE can more effectively promote the transportation and accessibility of target molecules and facilitate the transfer of electrons, which is the key to its much-enhanced sensitivity and reduced non-faradaic behavior [78].
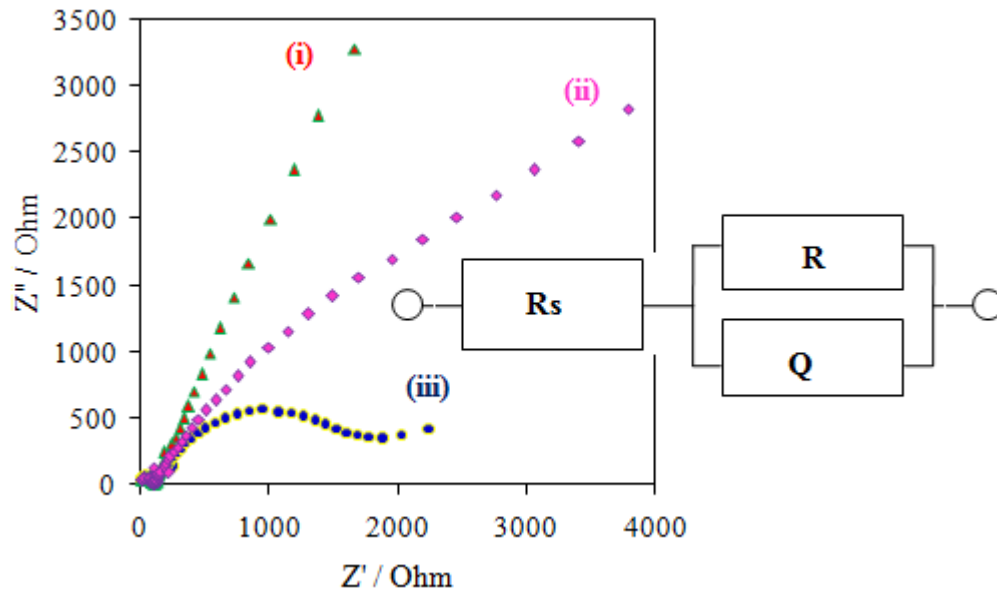
Figure 3: *EIS spectra of unmodified (**i**), chitosan modified carbon CS-CPE (**ii**) and CS@AgNPs-CPE (**iii**) in 0.1M KCl containing 5mM [Fe(CN)$_6$]$^{3-/4}$ performed between 100 MHz and 1 kHz using amplitude of 10 mV.*

II.4. Cyclic voltammetry characterization

Cyclic voltammetry (CV) was carried out to evaluate the electrochemistry of the bare CPE, CS-CPE and CS@AgNPs-CPE in 0.1 M KCl solution containing 5 mM Fe(CN)$_6^{3-}$ / Fe(CN)$_6^{4-}$ probe at a scan rate of 50 mVs^{-1} as shown in Fig. 4. The well-defined redox behavior was observed for all the electrodes that attributed to the redox reaction of Fe(CN)$_6^{3-}$/Fe(CN)$_6^{4-}$. Among all, the CS@AgNPs-CPE (Fig. 4C) exhibited an excellent redox peak current when compared with the CPE (Fig. 4A) and CS-CPE (Fig. 4B). The peak current of Fe(CN)6^{3-}/Fe(CN)$_6^{4-}$ at various electrodes are fall in the order CS@AgNPs-CPE (|Ipc|: 300 μA) > CS-CPE (|Ipc|: 174 μA) > CPE (|Ipc|: 130 μA). The enhanced peak current response designates enriched active surface area, which could be attributed to the nano-silver that boosts the redox reaction of Fe(CN)$_6^{3-}$/Fe(CN)$_6^{4-}$. These findings indicate that the CS@AgNPs-CPE holds excellent electron transfer capability and enriched active surface area than that of CS-CPE and CPE.
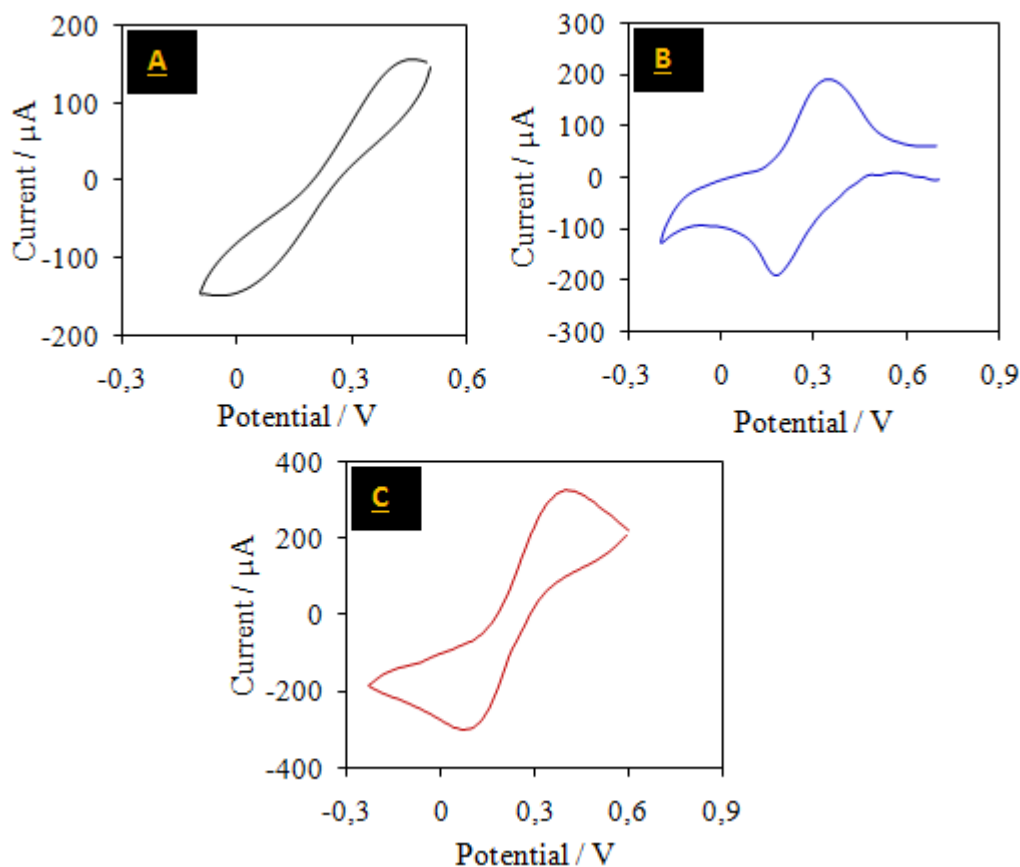
Figure 4: *CVs voltammograms of CPE (A), chitosan modified carbon CS/CPE (B) and CS@AgNPs-CPE(C) in 0.1M KCl containing 5mM [Fe(CN)$_6$]$^{3-/4-}$ at scan rate 50 mV s^{-1}.*

III. Determination of PNA at CS-CPE

The working electrode CS-CPE was placed in appropriate PBS, with suitable pH: 7.0 when the peak current is maximum, containing desired concentrations of PNA before starting the scan. DPV voltammograms of PNA were registered at CPE bare and CS-CPE for direct comparison (Fig. 5). A sensitive and well-defined reduction peak appears at all two tested the working electrodes indicate a reduction of four electrons from the nitro group to the hydroxyamino group after exposure to a 1 mM PNA in PBS pH 7.0. It is obvious that an enhancement of current peak of PNA at CS-CPE compared to CPE. This phenomenon should be attributed to the porous area of chitosan, which improves the absorbance amount of PNA onto the electrode surface and increases the electrochemical reduction response.
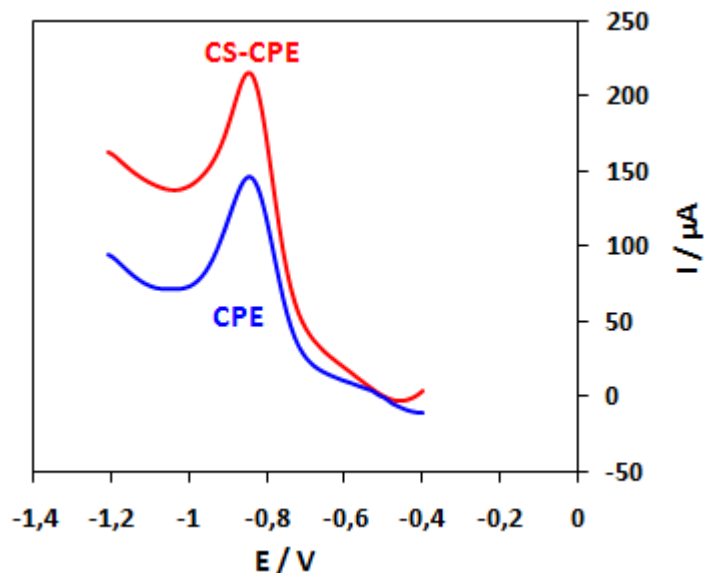
Figure 5: *DPV voltammograms of unmodified CPE and CS-CPE at 0.1 mM PNA containing 0.1 M PBS pH 7.0.*

The effect of CS amount on the cathodic peak current of 10 μM PNA in 0.1 M PBS pH 7was investigated as can be seen in Fig. 6A.It is notable that the reduction peak current increases with increasing the amount of CS from 0 to 2 %. However, a significant decrease in the peak current was recorded when the amount was greater than 2% (w/w) due to the decrease in conductivity of the modified electrode. At 2% (w/w) the current reached the maximum, and then it was chosen throughout this work.

The response of CS-CPE was strongly accumulation time-dependent. The peak current of PNA increases greatly with the first 1 min (Fig. 6B). Further, the peak current decreases remarkably when increasing the accumulation time. Considering sensitivity and efficiency, the accumulation time chosen for the following experiments was 1 min.

The effect of solution pH on the peak current of 10 μM PNA was further investigated using DPV within the range from 2 to 12 and the results shown in Fig. 6C. It is evident that the peak current varied remarkably with pH and attained its maximum at pH 7.0. Thus, the pH for further study is chosen at 7.0.
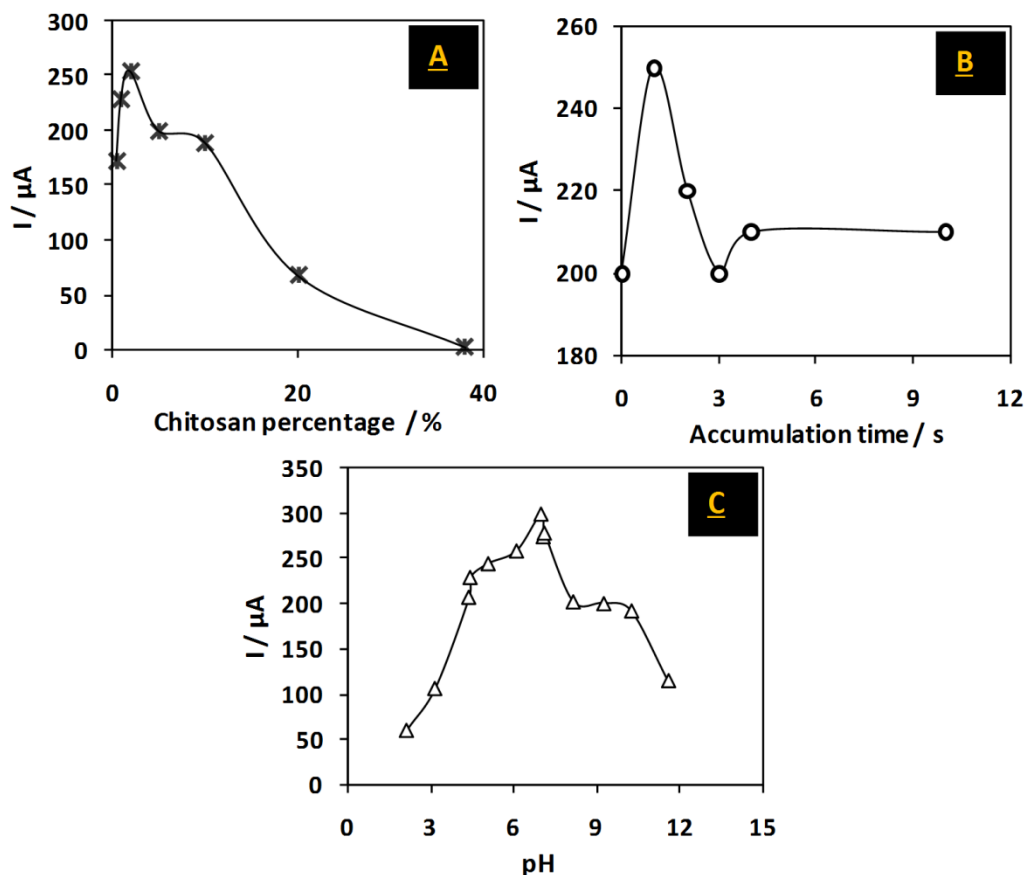
***Figure 6:** Optimization of the experimental parameters(A) Chitosan percentage (%), (B) Accumulation time, and (C) pH of buffer solution recorded by DPV technique in 55 μM PNA containing 0.1 M PBS pH 7.0.*

Under all these optional parameters, the relationship between current and concentration was studied in the range of 0.1 μM to 0.1 mM PNA(Fig. 7).The calibration curve as indicated in Fig. 7B,C presents two linear ranges of current versus PNA concentration from 1.0 μM to 0.1 mM(Fig. 7B) and from 0.1μM to 1.0 μM (Inset Fig. 7B).These relationships can be described through the following linear regression equations: (I) Ipc/μA $= 2.0 \times 10^{-6}$ [PNA] + 230.7 ($R^2 =$ 0.984) and (II) Ipc/μA $= 8.0 \times 10^{-7}$ [PNA] + 138.1 ($R^2 =$ 0.996). The limit of detection (LD) was calculated according to the equation: LD = 3sb/B, where sb is the standard deviation of the y-coordinate obtained from the line of best fit (linear coefficient) and B is the slope (angular coefficient) of this straight line. The LD calculated was 93.4 nM.
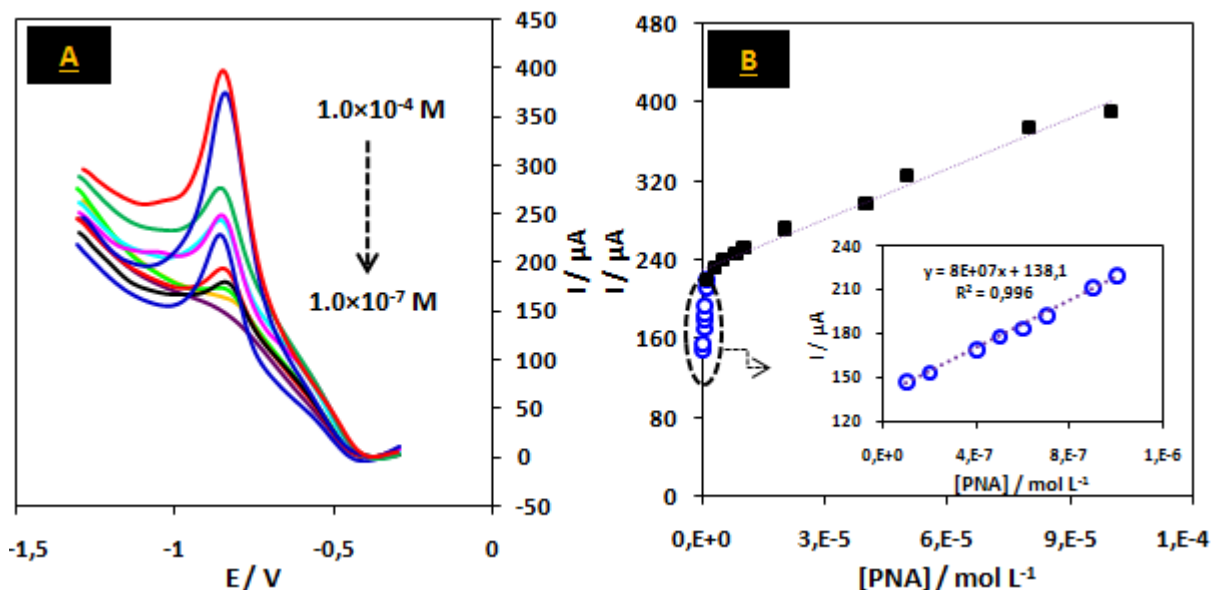
Figure 7: (A) DPV voltammograms obtained at CS@CPE for different concentrations of PNA. (B) Calibration curve and (Inset B) Zoom of calibration curve at lower concentration. Experimental conditions: 0.1 M PBS pH 7.0; 10 mVs⁻¹, 170 ms, 450 mV and 500 ms for step, pulse, width and period, respectively.

Compared to our transducers previously discussed, chitosan gelified modified carbon paste electrode facilitates a higher surface coverage for the binding of PNA and presents some advantages as being cost-effective, and easy to use. Knowing that polymeric matrices have been extensively utilized as solid support for numerous metal nanoparticles, we are interested in developing nanostructured electrodes based on silver nanoparticles using chitosan as a stabilizing agent due to its flexibility regarding morphology, dimension, mechanical properties, and hydrophobic/hydrophilic balance. The use of such a stabilizing agent is encouraged since it has a large number of amino ($-NH_2$) and hydroxyl ($-OH$) groups. In our studies silver has a promising role as catalyst in the reduction of PNA (Chapters 3 and 4), and that chitosan exhibits enhanced electroanalytical properties towards PNA. That's where the idea of developing this nanostructured electrode came from.

IV. Determination of PNA at CS@AgNPs-CPE

IV.1. Catalytic studies

As discussed above, silver nanoparticles are well-known catalyst for the reduction of aromatic nitrocompounds. In this context, PNA was used as representative analyte to evaluate the electrocatalytic efficiency of the prepared electrode CS@AgNPs-CPE.

In the beginning, the reduction of PNA at the suggested sensor was evaluated in various supporting medium such as Britton Robinson (B-R), acetate, and phosphate buffers. The results showed that the best potential shift was obtained with the B-R buffer. However, PBS causes a great increase in the peak current.

Furthermore, the effect of B–R buffers on the catalytic electro-reduction of PNA was then investigated over the pH range from 1.0 to 6.0 in 1.0 mM PNA. The reduction peak potential (E_{pr}) shifted to more positive potentials as the solution pH lowers than 2.0. However, E_{pr} was shifted to a negative direction when the pH values exceed2 up to a value that reaches 3. Beyond this value, the cathodic peak no longer appeared. This may have been due to the deprotonation of the solution. In the acidic condition, $R–NH_2$ reacts with H^+ to form $R–NH_3^+$,when a further amount of NaOH is added, the amino groups are saturated with OH^-, and the decrease in conductance was observed. The deprotonation of the medium makes links easier between OH^- ions and amino groups [79].

Cyclic voltammetry was employed to evaluate the comportment of PNA detection on CPE and CS@AgNPs modified electrode under the same conditions with 1 mM PNA in 0.1 M B-R buffer solution at a scan rate of 50 mV s^{-1}as shown in Fig. 8.

The meanwhile peak potential of CS@AgNPs modified electrode (curve a) shifted toward positive direction by 422 mV compared to the bare CPE (curve b), which indicated a greatly decreased over-potential on the CS@AgNPs.
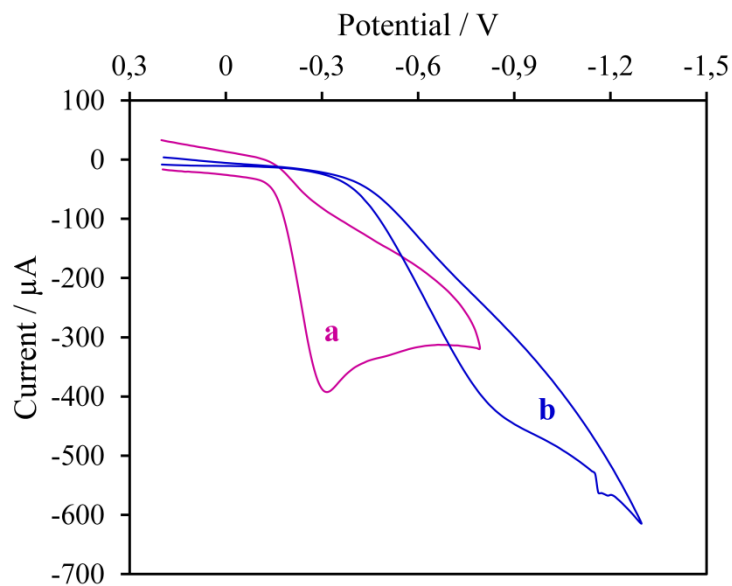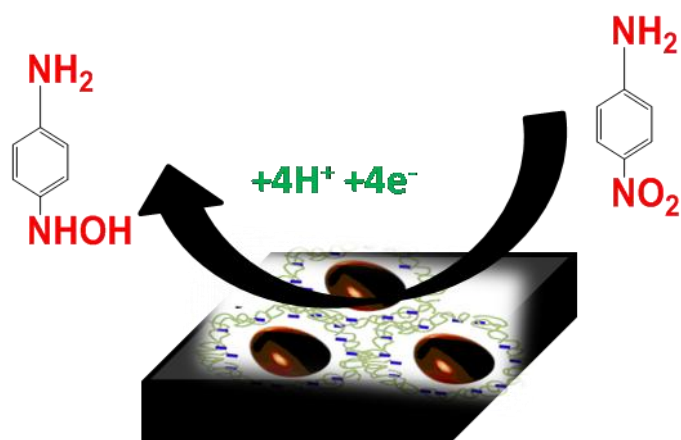
Figure 8: *CV voltammograms of CS@AgNPs-CPE (a) and CPE (b) at 1.0 mM PNA containing 0.1 M B-R pH 2.0.*

This demonstrates that CS@AgNPs facilitate the reduction of PNA. The cathodic peak is owing to the reduction of nitro group (NO_2) to 4-hydroxylaminophenol (NHOH) via a $4e^-/4H^+$ transfer electrochemical process.

Scheme 1: *Electron transfer reaction of PNA.*

IV.1.1. Scan rate effect

The CV showing the catalytic performance of CS@AgNPs modified electrode at different scan rates between 5 mV s^{-1} and 500 mV s^{-1} for 1 mM PNA in 0.1 M B–R buffer solution (pH 2.0).
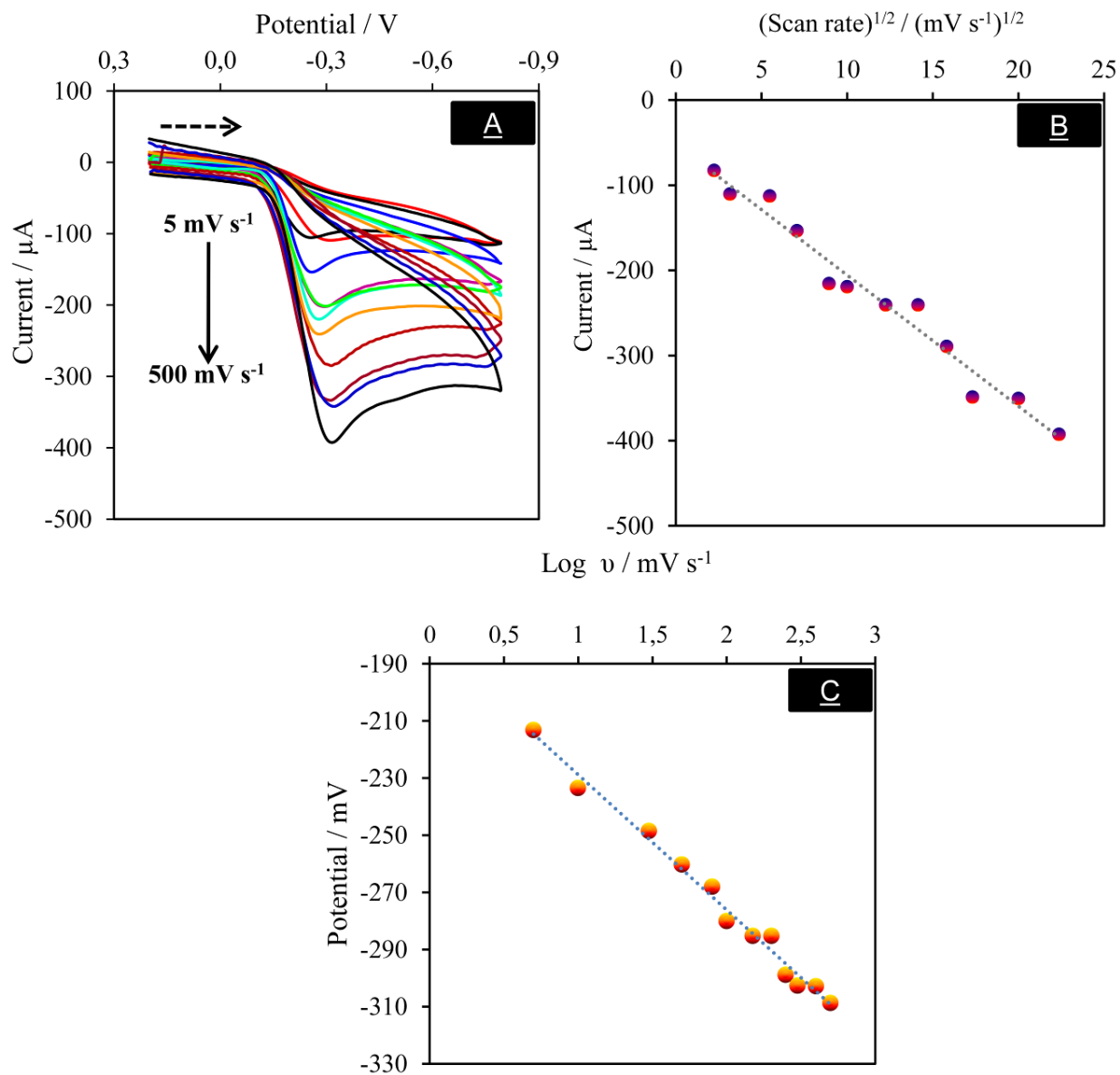

Figure 9: *(A) CVs of CS@AgNPs in 0.1 M B-R pH 2 containing 1.0 mM PNA different scan rates between 5 mV s^{-1} and 500 mV s^{-1}. (B) Plot of the linear relationship between current and square root of scan rate and (C) Plot between peak potential (Ep) and log v.*

As demonstrated in Fig. 9A as the scan rate (υ) increased, the peak potential moved to more negative potentials, reaching -308.78 mV at 500 mV s^{-1}. A good dependence between current and the square root of the scan rate, as seen in Fig. 9B which suggests that the electrocatalytic reduction of PNA at the CS@AgNPs modified electrode is a diffusion-controlled and irreversible process (Ip = 15.38 υ – 51.88 (mV$^{1/2}$s$^{1/2}$), R^2= 0.969) [80].

Plot between peak potential (Ep) and log v (Fig. 9C) was linear in the range of 5 mV s^{-1} and 500 mV s^{-1} according to the equation E$_p$/V = -1.65 - 0.0302 log υ. For a completely irreversible electrode process, the dependence between the potential (Epa) and scan rate (v) is (Eq. 2) [81]:

$$E_p = E^\circ + \left(\frac{RT}{\alpha nF}\right) + \ln\left(\frac{RTK_s}{\alpha nF}\right) + \left(\frac{RT}{\alpha nF}\right)lnv \quad (2)$$

Type, α is the cathodic electron transfer coefficient, n is the electron transfer number, ks is the standard rate constant of the surface reaction, and R, T, and F have their usual meanings. The αn value calculated from the slope of the aforementioned equation was 1.95, which provides n = 3.8, α is assumed to be 0.5 for a completely irreversible electrode process [82] and consequently, the value for the electron numbers (n) involved in the electrode reaction of PNA is (n = 4). Thus, four electrons are involved in the reduction of PNA.

The results are consistent with those published in the literature [83]. The surface coverage concentration of CS@AgNPs-CPE was predicted by applying Laviron's equation (Eq. 3) [84]:

$$I_p = \frac{n^2 F^2 A \Gamma v}{4RT} \quad (3)$$

Herein, 'n' is the number of electrons involved, 'F' is the Faraday constant (96,485 C mol^{-1}), 'Γ' is the surface coverage concentration (mole/cm^2), 'A' is the surface area of the electrode (0.1265 cm^2), 'v' is the scan rate (V s^{-1}), 'R' is the gas constant (8.314 Jmol^{-1} K^{-1}) and 'T' is the absolute temperature (298 K). The value of the surface coverage concentration (Γ) on the electrode was found to be as 1.21 × 10^{-3} mol cm^{-2}.

IV.1.2. Amperometric studies

Owing to its relative simplicity, chronoamperometry is one of the most frequently employed techniques. The technique is performed with a stationary electrode in solution at rest, initially in open circuit or at potential, where the target analyte undergoes no electrochemical reaction. The potential is then raised to a point beyond that necessary for the target analyte to be oxidized or electrochemically reduced. Here its surface concentration effectively becomes zero. Chronoamperometric experiments employed to get more information about the electrocatalytic process of numerous concentrations of PNA at CS@AgNPs-CPE by setting the working electrode at a potential of -300 mV at fixed times of 180 s. Thus, the current corresponding to the electrochemical reaction obeys Cottrell's law (Eq. 4) [85]:

$$I_p = \frac{nFACD^{\frac{1}{2}}}{\pi^{1/2}t^{1/2}} \quad (4)$$

Type, n is the moles of electrons involved in the reaction, F is the Faraday constant, A is the area of the electrode (cm^2), C the concentration of the analyte in the bulk solution (mol /cm^3), D is the diffusion coefficient ($cm^2 s^{-1}$) and t is time(s). The plot of I vs. $t^{-1/2}$ at various PNA concentrations is linear (Fig. 10A) and the slope of such lines can be used to estimate the diffusion coefficient of PNA (Inset Fig. 10A). The mean value of D is found to be 2.20×10^{-6} cm^2 s^{-1}.

Chronoamperometry can also be used for the prediction of the catalytic rate constant (K_{cat}) between 4-NA and the sites of the surface CS@AgNPs according to Galus equation [86]:

$$\frac{I_{cat}}{I_l} = \pi^{1/2}(K_{cat}C^{\circ}t)^{1/2}$$

Herein, I_L is the current of the CS@AgNPs-CPE in the absence of PNA, and I_{cat} is the catalytic current in the presence of PNA. k_{cat}, C°, and t are the catalytic rate constant (M^{-1} s^{-1}), the bulk concentration of PNA and time elapsed (s), respectively. One such plot, as shown in Fig. 10B, the average value of k_{cat} is found to be 0.125×10^{-3} M^{-1} s^{-1}.
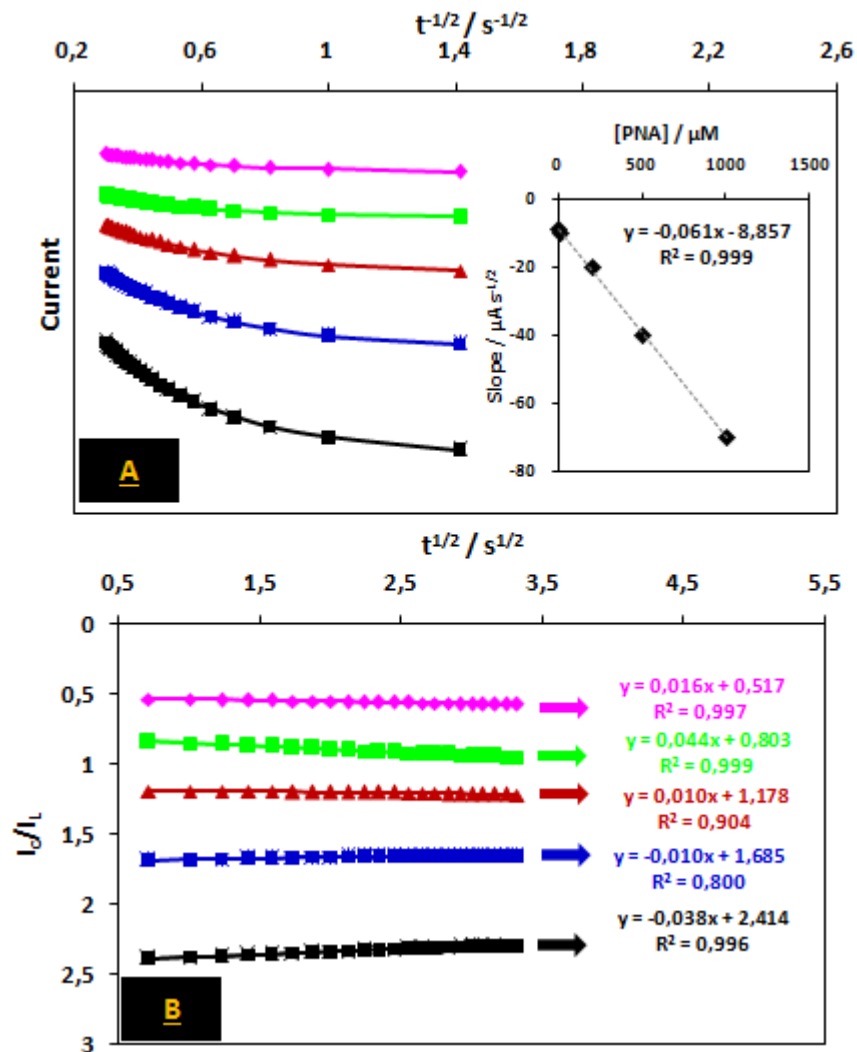
Figure 10: *(A) Plot of I vs. t*$^{-1/2}$ *of CS@AgNPs-CPE obtained from chronoamperogrammes at various PNA concentrations by setting reduction potential at -300 mV. Slopes of straight lines against PNA concentration showed in insert. (B) Plot of current vs. t*$^{-1/2}$ *of CS@AgNPs-CPE derived from the data chronoamperogrammes at various PNA concentrations.*

IV.2. Electroanalytical studies

The optimum conditions for the electrochemical response were established by measuring the peak current in dependence on all parameters. The reduction peak of p-NA is depending on the concentration of the Ag^{+} ions (Figure 11A).

The peak current increases greatly within the concentration of Ag^{+} ions and at 10 mM AgNO$_3$ it achieved a maximum. However, the continuous increase of the concentration of Ag^{+} causes a

remarkable decrease in peak current, due to the decrease of the conductivity of the modified electrode and the presence of nanoparticles of polydisperse sizes. This result confirms that found with UV-Visible absorption spectra. As the particle size increases, there are less of ions in solution and, therefore, the growth rate decreases until it reaches a level of total reduction and it is indeed possible to think that more the nanoparticles are small, the resistance to aggregation is important. Increasing the amount of silver nitrate is also observed to enlarge the plasmon band of the absorption spectra. Taking account of sensitivity and efficiency, the concentration of 10 mM $AgNO_3$ is fixed in the following experiments.
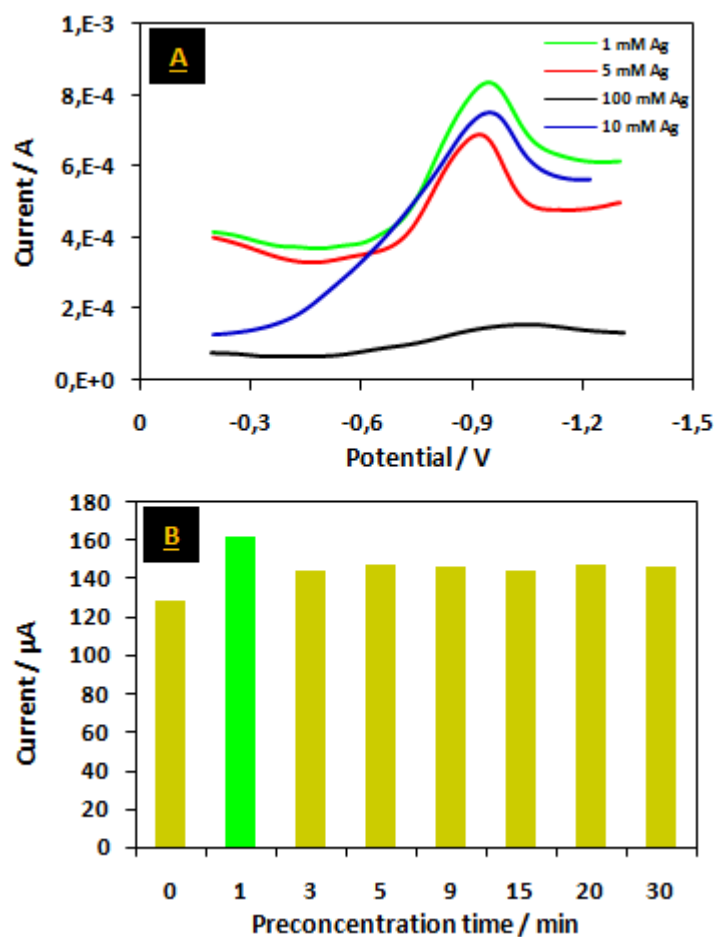

Figure 11: (A) DPV voltammograms of the concentration of the Ag^+ ions on the reduction peak of PNA. (B) Preconcentration time effect on the reduction peak of PNA.

The peak current increases greatly within the concentration of Ag^+ ions and at 10 mM $AgNO_3$ it achieved a maximum. However, the continuous increase of the concentration of Ag^+ causes a

remarkable decrease in peak current, due to the decrease of the conductivity of the modified electrode and the presence of nanoparticles of polydisperse sizes. This result confirms that found with UV-Visible absorption spectra. As the particle size increases, there are less of ions in solution and, therefore, the growth rate decreases until it reaches a level of total reduction and it is indeed possible to think that more the nanoparticles are small, the resistance to aggregation is important. Increasing the amount of silver nitrate is also observed to enlarge the plasmon band of the absorption spectra. Taking account of sensitivity and efficiency, the concentration of 10 mM $AgNO_3$ is fixed in the following experiments.

The effect of the accumulation time is investigated (Figure 11B).The peak current of 10 µM PNA increases greatly within the first 1 min and then enhances slowly. Further increase in accumulation time does not increase the amount of PNA at the electrode surface owing to surface saturation, and the peak current remains constant. Taking account of sensitivity, the accumulation time of 1 min was chosen for the following experiments.

Furthermore, it is important to study the electrochemical activity at different pH value for the detection of PNA. Therefore, the DPV response of 10 µM PNA in 0.1 M PBS buffer solution at CS@AgNPs-CPE shows that the PNA sensing was observed with higher reduction peak current at pH 7.0. The electrochemical parameters of the (DPV) techniques were also investigated, thus, the better response was registered at 10 mVs^{-1}, 170 ms, 450 mV and 500 ms for step, pulse, width and period, respectively.

Differential pulse voltammetry (DPV) plays a vital role in the electrochemical study due to high sensitivity when compared to the other voltammetry techniques. Figure 12A shows DPV response attained at a low-level concentration of PNA in the range from7 nM to 1 µM. It's shown that the reduction peak current was found to increase with increasing the PNA concentration.

Figure 12B shows the reduction peak current plotted against the concentration of PNA. It exhibits a good linear relationship in the range from 7 nM to 1 µM with a correlation coefficient of 0.986. The detection limit is calculated from the slope of linear calibration, it was found to be 5.0 nM according to the equation (3*sb/m).
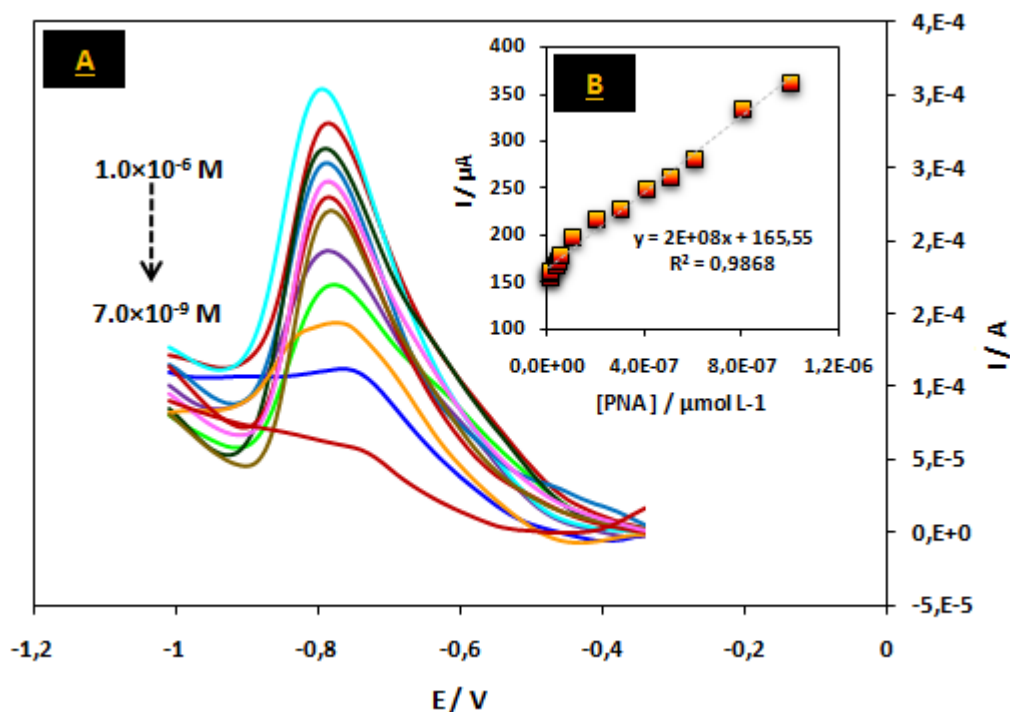
Figure 12: (A) DPV voltammograms obtained at CS@AgNPs-CPE for different concentrations of PNA in the range from 7.0×10^{-9} to 7.0×10^{-6}. (B) Calibration curve. Experimental conditions: 0.1 M PBS pH 7; 12 mVs^{-1}, 170 ms, 450 mV and 500 ms for step, pulse, width and period, respectively.

V. Interferences studies

The selectivity of CS-CPE and CS@AgNPs-CPE towards the detection of PNA was recorded by using DPV technique under the same experimental conditions. It is advisable to study the feasibility of identifying the PNA in the presence of possible chemical species that may interfere with their detection. This has been assessed by deliberately embeddings diverse solutions of organic nitro-compounds, such as 4-nitrophenol, 2, 4-dinitrophenylhydrazine (DNPH), and 2-nitroaniline along the accumulation step.

At CS-CPE the reduction peak of 10.0 μM PNA was separately measured in the presence of different concentrations of the common interferents, and then the peak current variation was checked. It's obviously discovered that 10-folder 2-NA, 4-NP, and DNPH, Practically have no impact on the signal of PNA. However, in the case of CS@AgNPs-CPE the basal PNA concentration is very low, while the concentration of the other nitro-compounds is normally higher (10 μM). There is an additional peak reduction observed for DNPH for one hundred

174

folders. However, for other interferents, no effect on the cathodic peak current of PNA has been observed for one hundred folders. Wherein the proposed sensor CS@AgNPs-CPE would be selectively reduced PNA in the presence of other interfering compounds.

VI. Determination of PNA in water samples

The applicability of CS-CPE and CS@AgNPs-CPE electrodes was investigated ethically by performing conventional real sample experimentation. The real sample such as wastewater was acquired from wastewater treatment plant (STEP Khouribga) and then used directly after filtration in a filter paper for the determination of PNA according to the method of standard addition. The recovered ratio on the basis of this method was investigated using formula (R = (found / Added) × 100) and the values are between 94.5 % and 100.9 %. Table 1 presents the estimated results obtained which are in good agreement with the spiked concentrations.

Table 1: *Results of PNA determination at CS-CPE and CS@AgNPs-CPE in wastewater samples.*

Electrode	Added (µM)	Detected (µM)	Recovery (%)
CS-CPE	0.1	0.094	94.5
	1.0	0.95	95.0
	10.0	10.09	100.9
CS@AgNPs-CPE	0.1	0.097	97.0
	1.0	0.93	98.0
	10.0	9.89	98.9

This finding indicating that the quantitative determination of PNA in wastewater samples using CS-CPE and CS@AgNPs-CPE modified electrode is effective and accurate.

Moreover, Differential pulse voltammetric experiments were recorded as shown in Fig. 13A. A good linear relationship was found between peak current and PNA concentrations with a correlation coefficient of (R^2 = 0.997). The increase of peak currents of PNA fit the linear equation of Ip/µA = 61.01 + 3×10^7 [PNA] when the concentrations of PNA were in the range

0.1–10 µM (Figure 13B). The detection limit calculated was found to be 8.80 nM. The decrease in the sensitivity of the as-prepared electrode CS@AgNPs-CPE towards the PNA reduction can be probably attributed to the adsorption of other species on the electrode surface.
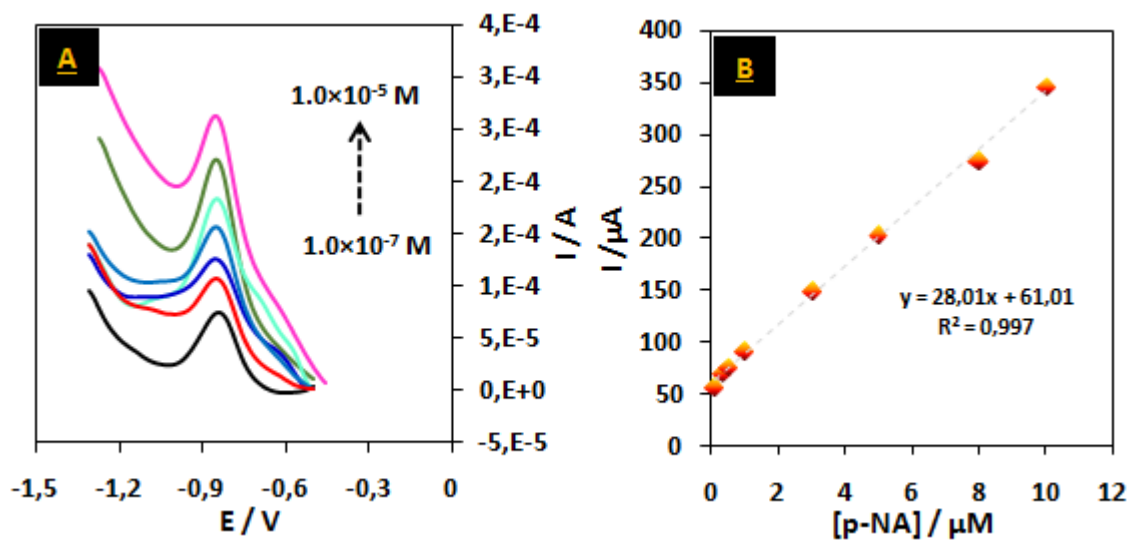

Figure 13: (A) DPV voltammograms obtained at CS-AgNPs-CPE for different concentrations of PNA in wastewater within the range 0.1µM – 10 µM. (B) Calibration curves. Experimental conditions: 12 mVs^{-1}, 170 ms, 450 mV and 500 ms for step, pulse, width and period, respectively.

V. Conclusions

This chapter seeks to emphasize how the modification of carbon paste electrodes with silver nanoparticles offers the possibility of gaining higher electrocatalytic activities, sensitivities, and selectivities in reducing PNA. Eventually, a chemical process has been used to synthesis silver nanoparticles. Thus, the silver salt was reduced to give metal atoms that enter in collision with ions, atoms or clusters to form stable nucleus irreversible. Through this chapter, we have demonstrated that the kinetics of the reaction as it depends on the concentration of the Ag$^+$ ions also depends on the concentration of NaBH$_4$. The enhanced electrocatalytic ability of the nanostructured electrode in B-R buffer solution was attributed to the silver nanoparticles acting as electron antennae, which efficiently funnel electrons between the electrode and electrolyte. In the

simplest cases, this has been to increase the surface area for enhanced sensitivity or to provide electrocatalytic properties to the electrodes.

The Ag nanostructured electrodes also showed linear current response with increasing PNA concentrations, selectivity to PNA and detection limits of 5 nM PNA, making the use of such electrodes for PNA quantification very attractive in neutral medium (PBS Ph 7.0). In all the cases, the comparison between CS@AgNPs electrodes and CS-CPE shows an enhancement of peak current, providing evidence of the electroanalytic properties of silver nanoparticles on electrodes.

References

[1]   Thakkar, K. N., Mhatre, S. S., & Parikh, R. Y. (2010). Biological synthesis of metallic nanoparticles. Nanomedicine: nanotechnology, biology and medicine, 6(2), 257-262.

[2]   Kouvaris, P., Delimitis, A., Zaspalis, V., Papadopoulos, D., Tsipas, S. A., & Michailidis, N. (2012). Green synthesis and characterization of silver nanoparticles produced using Arbutus Unedo leaf extract. Materials Letters, 76, 18-20.

[3]   Shameli, K., Bin Ahmad, M., Jaffar Al-Mulla, E. A., Ibrahim, N. A., Shabanzadeh, P., Rustaiyan, A., & Zidan, M. (2012). Green biosynthesis of silver nanoparticles using Callicarpa maingayi stem bark extraction. Molecules, 17(7), 8506-8517.

[4]   Sahoo, S. K., Misra, R., & Parveen, S. (2017). Nanoparticles: a boon to drug delivery, therapeutics, diagnostics and imaging. In Nanomedicine in cancer (pp. 73-124). Pan Stanford.

[5]   Antonyraj, C. A., Jeong, J., Kim, B., Shin, S., Kim, S., Lee, K. Y., & Cho, J. K. (2013). Selective oxidation of HMF to DFF using Ru/γ-alumina catalyst in moderate boiling solvents toward industrial production. Journal of Industrial and Engineering Chemistry, 19(3), 1056-1059.

[6]   Neville, F., Pchelintsev, N. A., Broderick, M. J., Gibson, T., & Millner, P. A. (2009). Novel one-pot synthesis and characterization of bioactive thiol-silicate nanoparticles for biocatalytic and biosensor applications. Nanotechnology, 20(5), 055612.

[7]   Staniland, S. S. (2007). Magnetosomes: Bacterial biosynthesis of magnetic nanoparticles and potential biomedical applications. Nanotechnologies for the Life Sciences: Willey Online Library.

[8]   Choi, Y., Ho, N. H., & Tung, C. H. (2007). Sensing phosphatase activity by using gold nanoparticles. Angewandte chemie international edition, 46(5), 707-709.

[9]   Hutter, E., & Fendler, J. H. (2004). Exploitation of localized surface plasmon resonance. Advanced materials, 16(19), 1685-1706.

[10]   Sudrik, S. G., Chaki, N. K., Chavan, V. B., Chavan, S. P., Chavan, S. P., Sonawane, H. R., & Vijayamohanan, K. (2006). Silver nanocluster redox-couple-promoted nonclassical electron transfer: an efficient electrochemical Wolff rearrangement of α-diazoketones. Chemistry–A European Journal, 12(3), 859-864.

[11]   Sun, S., Murray, C. B., Weller, D., Folks, L., & Moser, A. (2000). Monodisperse FePt nanoparticles and ferromagnetic FePt nanocrystal superlattices. science, 287(5460), 1989-1992.

[12]   Vilchis-Nestor, A. R., Sánchez-Mendieta, V., Camacho-López, M. A., Gómez-Espinosa, R. M., Camacho-López, M. A., & Arenas-Alatorre, J. A. (2008). Solventless synthesis and optical properties of Au and Ag nanoparticles using Camellia sinensis extract. Materials Letters, 62(17-18), 3103-3105.

[13]   Yoosaf, K., Ipe, B., Suresh, C. H., & Thomas, K. G. (2007). Silver nanoparticles: synthesis and size control by electron irradiation. The Journal of Physical Chemistry C, 1287, 111.

[14]   Yoksan, R., & Chirachanchai, S. (2009). Silver nanoparticles dispersing in chitosan solution: Preparation by γ-ray irradiation and their antimicrobial activities. Materials Chemistry and Physics, 115(1), 296-302.

[15]   Dong, Z., Le, X., Li, X., Zhang, W., Dong, C., & Ma, J. (2014). Silver nanoparticles immobilized on fibrous nano-silica as highly efficient and recyclable heterogeneous catalyst for reduction of 4-nitrophenol and 2-nitroaniline. Applied Catalysis B: Environmental, 158, 129-135.

[16]   Edison, T. N. J. I., Sethuraman, M. G., & Lee, Y. R. (2016). $NaBH_4$ reduction of ortho and para-nitroaniline catalyzed by silver nanoparticles synthesized using Tamarindus indica seed coat extract. Research on Chemical Intermediates, 42(2), 713-724.

[17]   Edison, T. J. I., & Sethuraman, M. G. (2013). Biogenic robust synthesis of silver nanoparticles using Punica granatum peel and its application as a green catalyst for the reduction of an anthropogenic pollutant 4-nitrophenol. Spectrochimica Acta Part A: Molecular and Biomolecular Spectroscopy, 104, 262-264.

[18]   Jebakumar Immanuel Edison, T. N., & Sethuraman, M. G. (2013). Electrocatalytic reduction of benzyl chloride by green synthesized silver nanoparticles using pod extract of Acacia nilotica. ACS Sustainable Chemistry & Engineering, 1(10), 1326-1332.

[19]   Tiwari, A. D., Mishra, A. K., Mishra, S. B., Kuvarega, A. T., & Mamba, B. B. (2013). Stabilisation of silver and copper nanoparticles in a chemically modified chitosan matrix. Carbohydrate polymers, 92(2), 1402-1407.

[20]   Geng, B., Jin, Z., Li, T., & Qi, X. (2009). Preparation of chitosan-stabilized Fe0 nanoparticles for removal of hexavalent chromium in water. Science of the Total Environment, 407(18), 4994-5000.

[21]   Bhattarai, S. R., KC, R. B., Aryal, S., Khil, M. S., & Kim, H. Y. (2007). N-Acylated chitosan stabilized iron oxide nanoparticles as a novel nano-matrix and ceramic modification. Carbohydrate polymers, 69(3), 467-477.

[22]   Guan, H., Yu, J., & Chi, D. (2013). Label-free colorimetric sensing of melamine based on chitosan-stabilized gold nanoparticles probes. Food Control, 32(1), 35-41.

[23]   Huang, H., Yuan, Q., & Yang, X. (2004). Preparation and characterization of metal–chitosan nanocomposites. Colloids and surfaces B: Biointerfaces, 39(1-2), 31-37.

[24]   Yang, J., Yuan, M., Xu, D., Zhao, H., Zhu, Y., Fan, M., & Dong, Z. (2018). Highly dispersed ultrafine palladium nanoparticles encapsulated in a triazinyl functionalized porous organic polymer as a highly efficient catalyst for transfer hydrogenation of aldehydes. Journal of Materials Chemistry A, 6(37), 18242-18251.

[25]   Zhao, H., Yu, G., Yuan, M., Yang, J., Xu, D., & Dong, Z. (2018). Ultrafine and highly dispersed platinum nanoparticles confined in a triazinyl-containing porous organic polymer for catalytic applications. Nanoscale, 10(45), 21466-21474.

[26]   Ai, L., & Jiang, J. (2013). Catalytic reduction of 4-nitrophenol by silver nanoparticles stabilized on environmentally benign macroscopic biopolymer hydrogel. Bioresource technology, 132, 374-377.

[27]   Abkhalimov, E. V., Ershov, V. A., & Ershov, B. G. (2017). An aqueous colloidal silver solution stabilized with carbonate ions. Colloid Journal, 79(6), 735-739.

[28]   Shankar, R., Groven, L., Amert, A., Whites, K. W., & Kellar, J. J. (2011). Non-aqueous synthesis of silver nanoparticles using tin acetate as a reducing agent for the conductive ink formulation in printed electronics. Journal of Materials Chemistry, 21(29), 10871-10877.

[29]   Pastoriza-Santos, I., & Liz-Marzán, L. M. (2002). Synthesis of silver nanoprisms in DMF. Nano letters, 2(8), 903-905.

[30]   Faure, C., Derré, A., & Neri, W. (2003). Spontaneous formation of silver nanoparticles in multilamellar vesicles. The Journal of Physical Chemistry B, 107(20), 4738-4746.

[31]   Nasretdinova, G. R., Fazleeva, R. R., Mukhitova, R. K., Nizameev, I. R., Kadirov, M. K., Ziganshina, A. Y., & Yanilkin, V. V. (2015). Electrochemical synthesis of silver nanoparticles in solution. Electrochemistry Communications, 50, 69-72.

[32]   Q. F. Zhou, Z. Xu, J. Mater. Sci. 392 (2004) 487–2491.

[33]   V. Karunagaran, S. Sen, Int. J. Pharm. Sci. Res. 2 (2011) 2781-2785.

[34]   Remita, S., Fontaine, P., Lacaze, E., Borensztein, Y., Sellame, H., Farha, R., & Goldmann, M. (2007). X-ray radiolysis induced formation of silver nano-particles: A SAXS and UV–visible absorption spectroscopy study. Nuclear Instruments and Methods in Physics Research Section B: Beam Interactions with Materials and Atoms, 263(2), 436-440.

[35]   Huang, L., Zhai, M. L., Long, D. W., Peng, J., Xu, L., Wu, G. Z., &Wei, G. S. (2008). UV-induced synthesis, characterization and formation mechanism of silver nanoparticles in alkalic carboxymethylated chitosan solution. Journal of Nanoparticle Research, 10(7), 1193-1202.

[36]   Aslan, K., Leonenko, Z., Lakowicz, J. R., & Geddes, C. D. (2005). Fast and slow deposition of silver nanorods on planar surfaces: application to metal-enhanced fluorescence. The Journal of Physical Chemistry B, 109(8), 3157-3162.

[37]   Darmanin, T., Nativo, P., Gilliland, D., Ceccone, G., Pascual, C., De Berardis, B., & Rossi, F. (2012). Microwave-assisted synthesis of silver nanoprisms/nanoplates using a "modified polyol process". Colloids and Surfaces A: Physicochemical and Engineering Aspects, 395, 145-151.

[38]   Kelly, J., Keegan, G., & Brennan-Fournet, M. (2012). Triangular silver nanoparticles: their preparation, functionalisation and properties. Acta Physica Polonica A, 122(2), 337-345.

[39]   Sun, Y., & Xia, Y. (2002). Shape-controlled synthesis of gold and silver nanoparticles. science, 298(5601), 2176-2179.

[40]   Mallick, K., Witcomb, M. J., & Scurrell, M. S. (2004). Polymer stabilized silver nanoparticles: a photochemical synthesis route. Journal of Materials Science, 39(14), 4459-4463.

[41] Schultz, S., Smith, D. R., Mock, J. J., & Schultz, D. A. (2000). Single-target molecule detection with nonbleaching multicolor optical immunolabels. Proceedings of the National Academy of Sciences, 97(3), 996-1001.

[42] Handzhiyski, Y. (2011). Ivaylo Hinkov*, Svetlomir Diankov, Maria Karsheva, Veska Lasheva 2, Ivan Ivanov 3. Revue de génie industriel, 6, 16-22.

[43] S. V Bannea, M. S. Patilb .R. M. Kulkarnic, S. J. Patil, Mate.r Today. Proc. 4 (2017) 12054–12060.

[44] Shirtcliffe, N., Nickel, U., & Schneider, S. (1999). Reproducible preparation of silver sols with small particle size using borohydride reduction: for use as nuclei for preparation of larger particles. Journal of colloid and interface science, 211(1), 122-129.

[45] Nickel, U., zu Castell, A., Pöppl, K., & Schneider, S. (2000). A silver colloid produced by reduction with hydrazine as support for highly sensitive surface-enhanced Raman spectroscopy. Langmuir, 16(23), 9087-9091.

[46] Chang, Y. K., Byung, M. K., Jeong, S. H., & Yi, S. (2006). Effect of sodium carbonate on the formation of colloidal silver particles by a reduction reaction of silver ions with PVP. Journal of Ceramic Processing Research, 7(3), 241-244.

[47] Evanoff, D. D., & Chumanov, G. (2004). Size-controlled synthesis of nanoparticles. 1."Silver-only" aqueous suspensions via hydrogen reduction. The Journal of Physical Chemistry B, 108(37), 13948-13956.

[48] Sondi, I., Goia, D. V., & Matijević, E. (2003). Preparation of highly concentrated stable dispersions of uniform silver nanoparticles. Journal of colloid and interface science, 260(1), 75-81.

[49] Merga, G., Wilson, R., Lynn, G., Milosavljevic, B. H., & Meisel, D. (2007). Redox catalysis on "naked" silver nanoparticles. The Journal of Physical Chemistry C, 111(33), 12220-12226.

[50] Kim, D., Jeong, S., & Moon, J. (2006). Synthesis of silver nanoparticles using the polyol process and the influence of precursor injection. Nanotechnology, 17(16), 4019.

[51] Zhang, Y., Peng, H., Huang, W., Zhou, Y., & Yan, D. (2008). Facile preparation and characterization of highly antimicrobial colloid Ag or Au nanoparticles. Journal of colloid and interface science, 325(2), 371-376.

[52]   Ngah, W. W., & Isa, I. M. (1998). Comparison study of copper ion adsorption on chitosan, Dowex A-1, and Zerolit 225. Journal of Applied Polymer Science, 67(6), 1067-1070.

[53]   Wu, F. C., Tseng, R. L., & Juang, R. S. (2001). Enhanced abilities of highly swollen chitosan beads for color removal and tyrosinase immobilization. Journal of hazardous materials, 81(1-2), 167-177.

[54]   Kumar, M. N. R. (2000). A review of chitin and chitosan applications. Reactive and functional polymers, 46(1), 1-27.

[55]   Park, J., Ye, M., & Park, K. (2005). Biodegradable polymers for microencapsulation of drugs. Molecules, 10(1), 146-161.

[56]   Singla, A. K., & Chawla, M. (2001). Chitosan: Some pharmaceutical and biological aspects-an update. Journal of Pharmacy and Pharmacology, 53(8), 1047-1067.

[57]   Gerente, C., Lee, V. K. C., Cloirec, P. L., & McKay, G. (2007). Application of chitosan for the removal of metals from wastewaters by adsorption—mechanisms and models review. Critical reviews in environmental science and technology, 37(1), 41-127.

[58]   Sridhar, S., Smitha, B., & Shaik, A. (2005). Pervaporation-based separation of methanol/MTBE mixtures—A review. Separation and Purification Reviews, 34(1), 1-33.

[59]   No, H. K., Meyers, S. P., Prinyawiwatkul, W., & Xu, Z. (2007). Applications of chitosan for improvement of quality and shelf life of foods: a review. Journal of food science, 72(5), R87-R100.

[60]   Guibal, E. (2005). Heterogeneous catalysis on chitosan-based materials: a review. Progress in Polymer Science, 30(1), 71-109.

[61]   Rinaudo, M. (2006). Chitin and chitosan: properties and applications. Progress in polymer science, 31(7), 603-632.

[62]   Varma, A. J., Deshpande, S. V., & Kennedy, J. F. (2004). Metal complexation by chitosan and its derivatives: a review. Carbohydrate Polymers, 55(1), 77-93.

[63]   Tsai, Y. C., Chen, S. Y., & Liaw, H. W. (2007). Immobilization of lactate dehydrogenase within multiwalled carbon nanotube-chitosan nanocomposite for application to lactate biosensors. Sensors and Actuators B: Chemical, 125(2), 474-481.

[64]   Bouabi, Y. E., Farahi, A., Labjar, N., El Hajjaji, S., Bakasse, M., & El Mhammedi, M. A. (2016). Square wave voltammetric determination of paracetamol at chitosan modified

carbon paste electrode: application in natural water samples, commercial tablets and human urines. Materials Science and Engineering: C, 58, 70-77.

[65]   Porchezhiyan, V., & Noorjahan, S. E. (2016). Fabrication of a versatile chitosan nanocomposite hydrogel impregnated with biosynthesized silver nanoparticles using Sapindus mukorossi: characterization and applications. RSC advances, 6(98), 95564-95573.

[66]   Agnihotri, S., Mukherji, S., & Mukherji, S. (2014). Size-controlled silver nanoparticles synthesized over the range 5–100 nm using the same protocol and their antibacterial efficacy. Rsc Advances, 4(8), 3974-3983.

[67]   Sharma, S., Sanpui, P., Chattopadhyay, A., & Ghosh, S. S. (2012). Fabrication of antibacterial silver nanoparticle—sodium alginate–chitosan composite films. RSC Advances, 2(13), 5837.

[68]   Rani, P. U., & Rajasekharreddy, P. (2011). Green synthesis of silver-protein (core–shell) nanoparticles using Piper betle L. leaf extract and its ecotoxicological studies on Daphnia magna. Colloids and Surfaces A: Physicochemical and Engineering Aspects, 389(1-3), 188-194.

[69]   Vigneshwaran, N., Kathe, A. A., Varadarajan, P. V., Nachane, R. P., & Balasubramanya, R. H. (2007). Silver− protein (core− shell) nanoparticle production using spent mushroom substrate. Langmuir, 23(13), 7113-7117.

[70]   Cullity, B. D. (1978). Answers to problems: elements of X-ray diffraction. Addison-Wesley Publishing Company.

[71]   Zheng, X. F., Lian, Q., Yang, H., & Wang, X. (2016). Surface molecularly imprinted polymer of chitosan grafted poly (methyl methacrylate) for 5-fluorouracil and controlled release. Scientific reports, 6, 21409.

[72]   Wei, D., Sun, W., Qian, W., Ye, Y., & Ma, X. (2009). The synthesis of chitosan-based silver nanoparticles and their antibacterial activity. Carbohydrate research, 344(17), 2375-2382.

[73]   Zang, L., Qiu, J., Wu, X., Zhang, W., Sakai, E., & Wei, Y. (2014). Preparation of magnetic chitosan nanoparticles as support for cellulase immobilization. Industrial & engineering chemistry research, 53(9), 3448-3454.

[74]   Stuart, B. H. (2004). Spectral analysis. Infrared spectroscopy: fundamentals and applications, 45-70.

[75]   Niraimathi, K. L., Sudha, V., Lavanya, R., & Brindha, P. (2013). Biosynthesis of silver nanoparticles using Alternanthera sessilis (Linn.) extract and their antimicrobial, antioxidant activities. Colloids and Surfaces B: Biointerfaces, 102, 288-291.

[76]   Prakash, P., Gnanaprakasam, P., Emmanuel, R., Arokiyaraj, S., & Saravanan, M. (2013). Green synthesis of silver nanoparticles from leaf extract of Mimusops elengi, Linn. for enhanced antibacterial activity against multi drug resistant clinical isolates. Colloids and Surfaces B: Biointerfaces, 108, 255-259.

[77]   Liu, L., Wang, N., Cao, X., & Guo, L. (2010). Direct electrochemistry of cytochrome c at a hierarchically nanostructured TiO 2 quantum electrode. Nano Research, 3(5), 369-378.

[78]   Bhumkar, D. R., & Pokharkar, V. B. (2006). Studies on effect of pH on cross-linking of chitosan with sodium tripolyphosphate: a technical note. Aaps Pharmscitech, 7(2), E138-E143.

[79]   Zhang, H. X., Cao, A. M., Hu, J. S., Wan, L. J., & Lee, S. T. (2006). Electrochemical sensor for detecting ultratrace nitroaromatic compounds using mesoporous SiO2-modified electrode. Analytical Chemistry, 78(6), 1967-1971.

[80]   Laviron, E. (1979). General expression of the linear potential sweep voltammogram in the case of diffusionless electrochemical systems. Journal of Electroanalytical Chemistry and Interfacial Electrochemistry, 101(1), 19-28.

[81]   Yin, H., Zhou, Y., Ma, Q., Ai, S., Chen, Q., & Zhu, L. (2010). Electrocatalytic oxidation behavior of guanosine at graphene, chitosan and Fe3O4 nanoparticles modified glassy carbon electrode and its determination. Talanta, 82(4), 1193-1199.

[82]   Laghrib, F., Boumya, W., Lahrich, S., Farahi, A., El Haimouti, A., & El Mhammedi, M. A. (2017). Electrochemical evaluation of catalytic effect of silver in reducing 4-nitroaniline: Analytical application. Journal of Electroanalytical Chemistry, 807, 82-87.

[83]   Laviron, E. (1979). The use of linear potential sweep voltammetry and of ac voltammetry for the study of the surface electrochemical reaction of strongly adsorbed systems and of redox modified electrodes. Journal of Electroanalytical Chemistry and Interfacial Electrochemistry, 100(1-2), 263-270.

[84]   Bard, A. J., Faulkner, L. R., Leddy, J., & Zoski, C. G. (1980). Electrochemical methods: fundamentals and applications (Vol. 2, p. 1). New York: wiley.

[85]   Galus, Z. (1976). Fundamentals of Electrochemical Analysis, Ellis Horwood Press, New York, p. 313 (Chapter 10).

– Conclusion –

The natural quality of water can be altered by human activity. Deterioration of water quality is due to the presence of large quantities of mineral salts and/or organic matter that must be reduced or eliminated completely.PNA is one of the most hazardous products, entering the environment through wastewater and agricultural water. Moreover, it is soluble, stable in water so it can affect soils. It has a harmful effect on public health. In order to overcome this problem, the researchers have thought of water treatment techniques such as extraction, adsorption on activated carbon, advanced oxidation processes, and electrochemical techniques.

The aim of the work carried out in this thesis was the elimination of the hazardous aromatic nitro compound (PNA) via the reduction of the nitro group to the amino group as it is considered to be the most efficient, ecological and economical approach, and the reduction products, namely 4-aminophenol (4-AP) and o-phenylenediamine (o-PDA) can be reused as they are important intermediates for the synthesis of drugs and dyestuffs via the use of silver-based electrodes.

PNA reduction was evaluated using electrochemical techniques. As the first tests, silver exhibits excellent catalytic activity as well as a tremendous amplification of the current intensity compared to several electrodes including graphite, glassy carbon, and gold. The study carried out with these electrodes, whose initial results are promising, has yet to be finalized. The catalytic and analytical performance of the metallic silver electrode has begun to be investigated for the determination of PNA in aqueous media. The kinetics of PNA reduction were investigated using cyclic voltammetry, electrochemical impedance spectroscopy, and chronoamperometry. Moreover, the sensitivity was also achieved using differential pulse voltammetry after pH optimization and other electrochemical parameters. However, the results showed that metallic silver electrode offers high background contribution and high cost. In fact, silver-based carbon paste electrodes were used for subsequent works because of their broad potential window, low background current, rich surface chemistry, low cost, chemical inertness, and suitability for various sensing and detection applications.

Hence, thermal and electrochemical deposition has been used for the modification of carbon paste electrode using silver as a dopant. We were able to evaluate the morphology and distribution of silver on the electrode surfaces by XRD and scanning electron microscopy as well as the electroactive surface of the prepared electrodes was also estimated using $[Fe(CN)_6]^{3-/4-}$ as a

redox probe. The founds showed that electrochemical deposition offer high catalytic properties and enhanced sensitivity in reducing PNA compared to thermal deposition process indicating the formation of a silver oxide film during the thermal modification process involving reduced electron flow or charge transfer process between the electrode surface and solution

Modifying carbon paste electrode surface with solid nanoparticles of a different chemical identity can impart additional chemical functionality to the electrode such as electrocatalytic activity. Modifying electrodes with nanoparticles to act as electro-catalysts has the following advantages: i) nanoparticles have a high surface area to volume ratio, hence ii) nanoparticles experience a greater rate of mass transport than bulk materials, iii) the surface properties of the nanoparticles are different to their bulk form and in some cases exhibit enhanced catalytic activity, iv) gives specific control over the electrode environment, and v) can be a more economical method of utilizing catalyst materials.

Chemical processing methods have been adjusted to tune the diameter of silver nanoparticles and this has been found to have significant impact on its activity. Optimization of nanoparticle sizes and its chemical interaction with the carbon paste has been proven to dramatically increase the activity of the electrode. The distribution of nanoparticles is also important; to fully benefit from increased mass transport from its nano-scaled structures, each nanoparticle must be separated by enough distance such that its neighbor.

Modification with silver nanoparticles dramatically improves the electron transfer kinetics of PNA reduction into 4-AP, such that much faster rates of conversion (observable as an increase in reductive current) are possible. A related factor is the size of the nanoparticles; along with the effects of surface area (per given mass), the diameter of nanoparticles affects its surface electron energy, such that its electrochemistry and reactivity can be tuned by varying its size. Tuning the size of the nanoparticles with precision can be technically challenging, but can be done to optimize electro-catalytic activity.